

**Collapse Assessment and Performance-Based Evaluation Techniques  
for Concentrically Braced Frames Designed in Seismic Regions**

**By**

**Emre Karamanci**



**McGill**

**Department of Civil Engineering and Applied Mechanics**

**McGill University, Montreal, Canada**

**February 2013**

**A thesis submitted to McGill University in partial fulfillment of the requirements of  
the degree of Master of Engineering**

**©Emre Karamanci, 2013**



# Abstract

---

Performance-Based Earthquake Engineering necessitates the development of simulation models that can predict the nonlinear behavior of structural components as part of a building subjected to seismic loading. For reliable seismic assessment of buildings, these models need to be calibrated with large sets of experimental data. This thesis advances the state-of-knowledge on the collapse assessment of concentrically braced frames (CBFs) designed in seismic regions.

The thesis discusses the development of a database that includes extensive information from more than 300 tests of steel braces that have been conducted worldwide over the past 40 years. Statistical information of various properties of steel braces that can be used for quantification of modeling uncertainties is summarized and implications regarding the expected yield properties of various steel types as part of current design provisions are discussed. The steel brace database is utilized to develop drift-based and dual-parameter fragility curves for different damage states of steel braces. These curves can be used as tools for rapid estimation of earthquake damage towards the next generation of performance-based evaluation methods for new and existing buildings. Through extensive calibrations of an inelastic fiber-based steel brace cyclic model, modeling recommendations for the post-buckling behaviour and fracture of steel braces due to low-cycle fatigue are developed for three different brace shapes. The effectiveness of these recommendations is demonstrated through two case studies including concentrically

braced frames (CBFs) subjected to earthquake loading. The emphasis is on the accurate assessment of the collapse capacity of concentrically braced frames with the explicit consideration of strength and stiffness deterioration of various structural components that are part of local story mechanisms that develop in CBFs after the steel braces fracture. The influence of modeling classical damping on the collapse capacity of CBFs is also discussed.

# Résumé

---

Le génie parasismique basé sur la performance des structures nécessite le développement des modèles de simulation qui peuvent estimer le comportement non-linéaire des composantes structurales faisant partie d'un bâtiment sujet à des efforts sismiques. Afin d'avoir une évaluation sismique fiable, les modèles doivent être étalonnés avec un grand inventaire de données obtenues expérimentalement. Cette thèse avance l'état des connaissances sur l'évaluation de l'effondrement des contreventements en treillis concentrique conçus dans les régions sismiques.

Cette thèse adresse le développement d'une banque de données qui inclut plus de 300 essais effectués autour du monde sur des contreventements en acier depuis plus de 40 ans. Les données statistiques de plusieurs propriétés du contreventement en acier qui peuvent être utilisées pour la quantification des incertitudes de la modélisation sont résumées. Également les implications liées aux propriétés limitées d'élasticité qui sont attendues selon le type d'acier sont présentées en fonction des règles d'actuelles de conception. La banque de données des contreventements en acier est utilisée afin de développer des drift-based et dual-parameter fragility curves courbes de fragilité à deux paramètres en fonction du déplacement horizontal relatif de l'étage pour différents degrés de dommage. Ces courbes servant à estimer efficacement et rapidement les dommages sismiques, amènent vers la prochaine génération des méthodes d'évaluation de la performance des structures. À travers une vérification approfondie de l'étalonnage du modèle non-

linéaire cyclique à fibres du contreventement en acier des recommandations de modélisation du postflambement et de la rupture en fatigue oligocyclique sont développées pour trois différents types de contreventement. L'efficacité de ces recommandations est démontrée à travers des études de cas incluant des contreventements concentriques qui reprisent des efforts sismiques. L'accent est mis sur l'évaluation précise de la capacité de l'effondrement des contreventements en treillis concentriques en prenant en compte explicitement le processus de dégradation de la capacité et de la rigidité des plusieurs composants structuraux qui font partie des mécanismes du dommage local qui s'évoluent dans différents étages d'une structure en contreventements concentriques en acier une fois que le contreventement s'est fracturé. L'effet de la modélisation de l'amortissement de la structure sur la capacité à l'effondrement des contreventements concentriques en acier est également considéré.

# Acknowledgements

---

First and foremost I would like express my deep gratitude to my advisor, professor and good friend Professor Dimitrios G. Lignos for his support and help throughout the last two years. This thesis wouldn't be possible if it weren't for your help throughout everything. I will miss our long meetings, especially the soccer discussions. Thank you for making my graduate degree much more enjoyable than I expected it to be. Ευχαριστώ πολύ!

I would also like to thank Gabriel Martin and Samy Al-Bardaweel for helping develop the steel brace database. Your help is greatly appreciated.

I would like to thank Dr. P. Uriz (Exponent Failure Analysis), Professor S. Mahin (University of California, Berkeley) and Professor B. Fell (California State University, Sacramento) for taking their time to provide us with important experimental data.

I won't forget the good times that I've spent at McGill in the last two years especially with my buddies Alain, Dino and Xavier. Also thanks for all of my friends in McGill, Montreal and Istanbul for their support through the harder times. Thanks guys!

I also would like to thank my research colleagues and good friends Ahmed, Evalina, Nasser, Sarven, Omar and Yusuke for their help with my research and their companionship.

Last, but not least, I would like to thank my family for their endless support through everything. None of this would be possible if it weren't for you.



# Table of Contents

---

<b>Abstract</b> .....	<b>i</b>
<b>Résumé</b> .....	<b>iii</b>
<b>Acknowledgements</b> .....	<b>v</b>
<b>List of Tables</b> .....	<b>xi</b>
<b>List of Figures</b> .....	<b>xiii</b>
<b>1 Introduction</b> .....	<b>1</b>
1.1 General Overview .....	1
1.2 Research Objectives.....	2
1.3 Scope.....	2
1.4 Outline.....	4
<b>2 Literature Review</b> .....	<b>9</b>
2.1 Introduction.....	9
2.2 Analytical Research .....	9
2.2.1 Analytical Models to Simulate the Hysteretic Behaviour of Steel Braces .....	9
2.2.2 Analytical Studies on Steel Braced Frames .....	16
2.3 Experimental Research .....	23
2.3.1 Component Experimental Studies.....	23
2.3.2 Experimental Studies on Braced Frame Systems .....	30
2.4 Summary .....	35
<b>3 Development of a Steel Brace Database</b> .....	<b>37</b>

---

3.1 Purpose and Scope .....	37
3.2 Database Development .....	38
3.3 Steel Braces Contained in the Database.....	40
3.3.1 Loading Protocols .....	42
3.4 Steel Brace Database Evaluation .....	43
3.4.1 Statistical Evaluation of Material Properties of Various Grades.....	43
3.4.2 Ductility Classes of the Steel Braces .....	45
3.4.3 Maximum Brace Compressive Strength Requirements.....	47
3.5 Summary .....	51
<b>4 Drift-Based Fragility Curves for Rapid Earthquake Damage Assessment... of Centrally Braced Frames.....</b>	<b>63</b>
4.1 Purpose and Scope .....	63
4.2 Definition of Damage States.....	64
4.2.1 DS1 Brace Flexural Buckling .....	64
4.2.2 DS2 Brace Local Buckling .....	65
4.2.3 DS3 Brace Strength Loss – Loss of Force Capacity.....	65
4.3 Drift-Based Fragility Curves for Steel Braces.....	66
4.4 Incorporating Other Sources of Uncertainty.....	68
4.4.1 Influence of the Material Type on the Fragility Curves .....	71
4.4.2 Influence of the Global Slenderness Ratio on the Fragility Curves.....	72
4.5 Summary .....	74
<b>5 Relationships for Modelling Post-Buckling Behaviour and Fracture of... Steel Braces.....</b>	<b>89</b>

5.1 Introduction and Scope .....	89
5.2 Description of the Steel Brace Component Model .....	89
5.3 Calibrated Case Studies .....	94
5.4 Calibration Process .....	95
5.5 Modelling Recommendations for Rectangular HSS Braces .....	98
5.6 Modelling Recommendations for Round HSS Braces.....	102
5.7 Modelling Recommendations for W-Shape Braces.....	106
5.8 Effect of End Conditions on the Hysteretic Behaviour of Steel Braces .....	110
5.9 Effect of the Material Hardening Parameters on the Hysteretic Behaviour of. Steel Braces.....	113
5.10 Summary.....	115
<b>6 Case Studies.....</b>	<b>139</b>
6.1 Introduction.....	139
6.2 Description of the Benchmark 2-Story SCBF .....	140
6.3 Summary of the Experimental Results .....	141
6.4 Analytical Model for the Concentrically Braced Frame.....	142
6.5 Results and Discussion .....	145
6.5.1 Static-cyclic analysis.....	145
6.5.2 Pushover Analysis.....	147
6.5.3 Collapse Assessment of CBFs through Incremental Dynamic Analysis: Rayleigh Damping with Initial Stiffness Proportional Damping Assumption .....	148
6.5.4 Collapse Assessment of CBFs through Incremental Dynamic Analysis: Rayleigh Damping with Current Stiffness Proportional Damping Assumption.....	152

6.6 Description of the 12-Story SCBF.....	153
6.7 Analytical model of the 12-Story SCBF .....	154
6.8 Performance Evaluation.....	155
6.9 Mean Annual Frequency of Collapse .....	158
6.10 Summary.....	160
<b>7 Conclusions.....</b>	<b>183</b>
7.1 Development of a Steel Brace Database.....	183
7.2 Development of Drift-Based and Dual-Parameter Fragility Curves for Discrete.. Damage States of Steel Braces .....	184
7.3 Modelling Guidelines for Inelastic Buckling and Fracture of Steel Braces .....	186
7.4 Collapse Assessment of Concentrically Braced Frames.....	187
7.5 Suggestions for Future Work.....	188
<b>List of References.....</b>	<b>191</b>
<b>A Steel Brace Database.....</b>	<b>205</b>

# List of Tables

---

Table 3.1	Statistics of material yield stress from coupon tests .....	53
Table 3.2	Statistics of material ultimate stress from coupon tests .....	53
Table 3.3	Statistics of expected to measured yield strength .....	54
Table 3.4	Statistics of expected to measured ultimate strength .....	54
Table 3.5	Ultimate-to-yield stress ratios .....	55
Table 3.6	Ductility and section classes of the specimens in the database .....	55
Table 4.1.	Statistical parameters for fragility curves for HSS braces .....	76
Table 4.2.	Statistical parameters for fragility curves for round HSS braces.....	76
Table 4.3.	Statistical parameters for fragility curves for W-shape braces .....	76
Table 4.4.	Statistical parameters for fragility curves for L-shape braces .....	76
Table 4.5.	Statistical parameters for HSS braces considering all sources of epistemic uncertainty .....	77
Table 4.6.	Statistical parameters for round HSS braces considering all sources of epistemic uncertainty .....	77
Table 4.7.	Statistical parameters for W-shape braces considering all sources of epistemic uncertainty .....	77
Table 4.8.	Statistical parameters for L-shape braces considering all sources of epistemic uncertainty .....	77
Table 5.1	Calibrated rectangular HSS specimens.....	116
Table 5.2	Calibrated round HSS specimens .....	119
Table 5.3	Calibrated W- specimens .....	120
Table 5.4	Regression statistics for rectangular HSS braces.....	121
Table 5.5	Statistics for the coefficients of the regression analysis for rectangular HSS braces .....	121
Table 5.6	Summary of modelling guidelines for rectangular HSS braces.....	121
Table 5.7	Fracture parameter $\varepsilon_0$ for various HSS braces based on Equation 5.3 .....	121

Table 5.8	Regression statistics for round HSS braces .....	122
Table 5.9	Statistics for the coefficients of the regression analysis for round HSS braces.....	122
Table 5.10	Summary of modelling guidelines for round HSS braces .....	122
Table 5.11	Fracture parameter $\varepsilon_0$ for various round HSS braces based on Equation 5.5 .....	122
Table 5.12	Regression statistics for W- braces.....	123
Table 5.13	Statistics for the coefficients of the regression analysis for W- braces .....	123
Table 5.14	Summary of modelling guidelines for W- braces .....	123
Table 5.15	Fracture parameter $\varepsilon_0$ for various W- braces based on Equation 5.6.....	123
Table 6.1	Section properties of the various members of the 2-story SCBF .....	161
Table 6.2	Material properties of the various members of the 2-story SCBF.....	161
Table 6.3	Selected ground motions for collapse assessment of the 2-story SCBF.....	162
Table 6.4	Member sizes of the various members of the 12-story SCBF .....	163
Table 6.5	Material properties of the various members of the 12-story SCBF.....	163
Table 6.6	Specified gravity loads of the 12-story SCBF .....	163
Table A.1.	Steel brace database .....	207

# List of Figures

---

Figure 1.1	Examples of Concentrically Braced Frames (CBFs).....	7
Figure 1.2	Discrete damage states observed in bracing members .....	7
Figure 3.1	Sample hysteretic brace axial load displacement history .....	56
Figure 3.2	Steel brace configurations considered in the steel brace database .....	57
Figure 3.3	Loading protocols.....	58
Figure 3.4	Normalized buckling load vs slenderness based on measured yield stress .....	59
Figure 3.5	Normalized buckling load vs slenderness based on measured yield stress categorized by ductility classes.....	59
Figure 3.6	Normalized buckling load vs slenderness based on the nominal yield stress .....	60
Figure 3.7	Normalized buckling load vs slenderness based on the probable yield stress as defined in CSA-S16-09 .....	60
Figure 3.8	Normalized buckling load vs slenderness based on the expected yield stress as defined in AISC-341-10 .....	61
Figure 4.1	Damage stages for steel .....	78
Figure 4.2	Definition of damage states for a typical steel brace.....	78
Figure 4.3	Drift-based fragility curves for damage state DS1 for HSS, round HSS, W- and L-shape steel braces .....	79
Figure 4.4	Drift-based fragility curves for damage state DS2 for HSS, round HSS, W- and L-shape steel braces .....	80
Figure 4.5	Drift-based fragility curves for damage state DS3 for HSS, round HSS, W- and L-shape steel braces .....	81
Figure 4.6	Drift-based fragility curves for damage state DS3 for HSS, round HSS, W- and L-shape steel braces including the envelope of epistemic uncertainties on the fragility curves .....	82
Figure 4.7	Material influence on the drift-based fragility curves for damage state DS1 for HSS, round HSS and W- shape steel braces .....	83

Figure 4.8	Material influence on the drift-based fragility curves for damage state DS2 for HSS, round HSS and W- shape steel braces .....	84
Figure 4.9	Material influence on the drift-based fragility curves for damage state DS3 for HSS, round HSS and W- shape steel braces .....	85
Figure 4.10	Dual parameter fragility curves for damage state DS1 for HSS, round HSS, W- and L-shape steel braces.....	86
Figure 4.11	Dual parameter fragility curves for damage state DS2 for HSS, round HSS, W- and L-shape steel braces.....	87
Figure 4.12	Dual parameter fragility curves for damage state DS3 for HSS, round HSS, W- and L-shape steel braces.....	88
Figure 5.1	Description of the steel brace component model .....	124
Figure 5.2	Effect of $kL/r$ and $w/t$ on the parameter $m$ .....	125
Figure 5.3	Sample calibrated rectangular HSS specimens .....	126
Figure 5.4	Sample calibrated round HSS specimens .....	127
Figure 5.5	Sample calibrated W-shape specimens .....	128
Figure 5.6	Individual trends and regression equations for rectangular HSS sections ...	129
Figure 5.7	Effect of geometric parameters on the normalized axial displacement at fracture for rectangular HSS sections .....	130
Figure 5.8	Stress-strain curves of carbon steel and stainless steel.....	130
Figure 5.9	Individual trends and regression equations for round HSS braces.....	131
Figure 5.10	Effect of geometric parameters on the normalized axial displacement at fracture for round HSS sections .....	132
Figure 5.11	Individual trends and regression equations for W- sections.....	133
Figure 5.12	Effect of geometric parameters on the normalized axial displacement at fracture for round W- sections .....	134
Figure 5.13	Effect of modelling gusset plates on the hysteretic behaviour of steel braces .....	135
Figure 5.14	Effect of $a_1$ , $a_3$ and $R_0$ on the hysteretic behaviour of a steel brace .....	136
Figure 5.15	Effect of $a_1$ , $a_3$ , $R_0$ on the fracture parameter $\epsilon_0$ of steel braces .....	137
Figure 6.1	Geometry and the member sizes of the 2-story SCBF .....	164
Figure 6.2	Photograph of the 2-story SCBF as built.....	164

Figure 6.3 Loading protocol of the experimental study.....	165
Figure 6.4 Base shear versus first story drift ratio of the 2-story SCBF.....	165
Figure 6.5 Axial force versus axial deformation of the lower story braces of the 2-story SCBF .....	166
Figure 6.6 Ductile tearing of the north lower story column of the 2-story SCBF .....	166
Figure 6.7 Overview of the analytical model of the 2-story SCBF .....	167
Figure 6.8 Calibration of the IMK deterioration model for steel beams .....	168
Figure 6.9 Calibration of the IMK deterioration model for steel columns .....	168
Figure 6.10 Typical hysteretic behaviour of the modified IMK model with pinching hysteretic response.....	169
Figure 6.11 Moment - rotation diagram for the south lower story column of the 2-story SCBF .....	169
Figure 6.12 Base shear versus roof drift ratio of the 2-story SCBF based on pushover analysis.....	170
Figure 6.13 Base shear versus first story SDR of the 2-story SCBF based on pushover analysis.....	170
Figure 6.14 IDA curves of the 2-story SCBF (Rayleigh damping using initial stiffness approximation).....	171
Figure 6.15 Collapse fragility curve of the 2-story SCBF (Rayleigh damping using initial stiffness approximation).....	171
Figure 6.16 Story drift ratio histories of the 2-story SCBF during the Canoga Park record from the Northridge 1994 earthquake (Rayleigh damping using initial stiffness approximation).....	172
Figure 6.17 Base shear versus first story SDR of the 2-story SCBF during the Canoga Park record from the Northridge 1994 earthquake (Rayleigh damping using initial stiffness approximation).....	172
Figure 6.18 Brace hysteretic response of the 2-story SCBF during the Canoga Park record from the Northridge 1994 earthquake (Rayleigh damping using initial stiffness approximation).....	173
Figure 6.19 Story drift histories of the 2-story SCBF during the Canoga Park record from the Northridge 1994 earthquake (Rayleigh damping using current	

stiffness approximation).....	174
Figure 6.20 Base shear versus first story SDR of the 2-story SCBF during the Canoga Park record from the Northridge 1994 earthquake (Rayleigh damping using current stiffness approximation).....	174
Figure 6.21 Brace hysteretic response of the 2-story SCBF during the Canoga Park record from the Northridge 1994 earthquake (Rayleigh damping using current stiffness approximation).....	175
Figure 6.22 IDA curves of the 2-story SCBF (Rayleigh damping using current stiffness approximation).....	176
Figure 6.23 Collapse fragility curve of the 2-story SCBF (Rayleigh damping using current stiffness approximation).....	176
Figure 6.24 Plan view of the 12-story SCBF.....	177
Figure 6.25 Elevation view of the 12-story SCBF.....	177
Figure 6.26 Typical corner gusset plate design of the 12-story SCBF.....	178
Figure 6.27 Typical middle gusset plate design of the 12-story SCBF.....	178
Figure 6.28 Pushover curves for 12-storey SCBF based on a triangular lateral load pattern.....	179
Figure 6.29 IDA curves of the 12-story SCBF (Rayleigh damping using current stiffness approximation).....	180
Figure 6.30 Collapse fragility curve of the 12-story SCBF (Rayleigh damping using current stiffness approximation).....	180
Figure 6.31 Seismic hazard curve for Bulk Mail Center, downtown Los Angeles, CA.....	181
Figure 6.32 Fitted seismic hazard curve for Bulk Mail Center, downtown Los Angeles, CA.....	181

# Chapter 1

## Introduction

---

### 1.1 General Overview

Concentrically Braced Frames (CBFs) are one of the most common lateral load resisting systems that are used in steel buildings in North America due to their economical advantages and ease of construction. Figure 1.1 displays examples of steel buildings employing CBFs as their primary lateral load resisting system. The diagonal bracing members help increase the lateral stiffness of the steel building to resist lateral loads from wind and earthquakes and limit lateral deformations due to these loading conditions. In a lateral load resisting system it is required that the forces generated from earthquakes to safely be transferred from the upper stories of a building to its foundations. Modern design of CBFs in seismic regions also requires a ductile behaviour of the lateral load resisting system, where brittle fracture modes such as the fracture at the brace ends in a CBF are to be avoided.

However past earthquakes such as the 1994 Northridge Earthquake in the United States of America and 1995 Kobe Earthquake in Japan displayed some of the shortcomings of CBFs. In particular, CBFs are prone to local story mechanisms that might induce collapse of the building once the bracing members of the lateral resisting structural system are severally damaged (Tremblay et al. 1995, Nakashima et al. 2000). Some of the typical

failure modes associated with brace damage are shown in Figure 1.2. For example, Figure 1.2a illustrates a W-shape brace member that buckled globally during the Kobe earthquake. Figures 1.2b and 1.2c show local buckling and fracture due to low cycle fatigue at mid-length of a hollow square section brace during the Northridge earthquake. Therefore it is important to be able to assess the structural damage of the bracing members in CBFs and to evaluate the collapse capacity of these systems when subjected to earthquakes.

## **1.2 Research Objectives**

The main focus of this thesis is to (1) develop performance-based assessment techniques for rapid estimation of structural damage (associated with global buckling, local buckling and fracture) observed in CBFs after an earthquake and (2) to develop modelling guidelines for different brace shapes for inelastic buckling and fracture of braces towards the development of a computational framework for reliable collapse assessment of CBFs subjected to earthquake loading.

## **1.3 Scope**

Rapid estimation of structural damage is an effective way in estimating damage in a structure, without the use of detailed analytical models, after an earthquake. In this research, rapid estimation of earthquake damage in CBFs designed in seismic regions is evaluated through drift-based and dual parameter fragility curves that are developed for four main steel brace shapes and for three discrete damage states (global buckling, local buckling and brace fracture). This is in line with the next generation of performance-

based evaluation techniques for post-earthquake functionality of new and existing building (ATC-58, 2012a,b). The rapid estimation techniques developed in this thesis may be used in earthquake risk management to effectively allocate resources after a earthquake disaster in an urban area. The developed fragility curves allow performing a quick assessment of earthquake damage of instrumented buildings in a city-wide scale without the need for comprehensive analytical models that take months to be built and verified.

The seismic performance assessment of buildings subjected to earthquakes from the onset of damage through collapse necessitates the use of reliable hysteretic models that describe the cyclic response of various structural components for different damage states. In the context of Performance-Based Earthquake Engineering (PBEE), specific damage states are associated with large deformations in which strength and stiffness deterioration of structural components in combination with P-Delta effects trigger dynamic collapse of a building. A key issue to trace the collapse capacity of steel braced frames subjected to severe ground motions is to simulate the post-buckling behaviour and fracture of steel braces. The main challenge to reliably predict the strength and stiffness deterioration of steel braces and subsequently the post-fracture dynamic behaviour of steel braced frames is to accurately represent the input model parameters that control global/local instabilities and ultimately fracture due to low cycle fatigue. Another challenge is the treatment of the modelling uncertainties of steel braces and their effect on the seismic performance of steel frame buildings through collapse. This thesis advances the state-of-knowledge on the collapse assessment of concentrically braced frames. The emphasis is on a certain

collapse mode associated with sidesway instability in which a story or a number of stories displaces sufficiently and collapse occurs due to P-Delta effects accelerated by component deterioration in strength and stiffness.

To be able to reach these research goals it is essential to have a large set of experimental data on steel braces. Therefore a steel brace database is developed that includes information from more than 300 steel brace experiments. This database is employed to achieve the research scope of this thesis.

## **1.4 Outline**

A literature review of the main experimental and analytical studies conducted on individual braces and on braced frames over the past 40 years is discussed in Chapter 2. Emphasis is placed on the main improvements in analytical models and experimental testing of various shapes and configurations of steel braces in relation to this research.

Chapter 3 focuses on the development of a steel brace database that is later used to develop the drift-based fragility curves discussed in Chapter 4 and to derive the modelling guidelines for the non-linear hysteretic behaviour and fracture due to low-cycle fatigue of steel braces (see Chapter 5). Several aspects of the steel brace database are also evaluated to assess some of the uncertainties in modelling the material strength and maximum compressive strength of braces as discussed in present seismic provisions in North America.

The development of the drift-based and dual parameter fragility curves for three discrete damage states observed in steel braces are discussed in Chapter 4. These fragility curves are developed based on a maximum likelihood approach. The effect of geometric and material uncertainties on the fragility curves is also discussed. These uncertainties are reflected on the fragility curves based on robust statistical procedures.

Chapter 5 summarizes the modelling guidelines to accurately simulate the inelastic buckling and fracture of steel braces based on a state-of-the-art fibre based steel brace model. The development of predictive relationships that associate the geometric and material properties of steel braces with a fracture index of the numerical model is extensively discussed. These relationships are based on a multivariate regression analysis, taking advantage of the large database of steel braces that was developed and discussed in Chapter 3. The predictive relationships for inelastic buckling and fracture of steel braces are developed for steel rectangular Hollow Structural Sections (HSS), round HSS and W-shape braces.

The modelling guidelines for modelling the inelastic buckling and fracture of steel braces are evaluated at the system level through an array of case studies of a 2-story and a 12-story CBFs (see Chapter 6). This chapter presents a framework for modelling the strength and stiffness deterioration of various structural components in CBFs. This framework is employed for the reliable collapse assessment of CBFs. This assessment is conducted through the use of collapse fragility curves that are developed from a set of 40 ground motions that are scaled incrementally based on incremental dynamic analysis. Special

emphasis is made on the damping assumption used in the dynamic analyses of CBFs and in particular in cases where the lateral stiffness of the CBF becomes negative due to severe strength and stiffness deterioration after steel brace fracture occurs.

Chapter 7 provides a summary of the major findings of this research in support of the performance-based evaluation techniques and the collapse assessment of CBFs. An appendix (Appendix A) is attached at the end of this thesis that summarizes the main information that is recorded in the steel brace database.



Figure 1.1 Examples of Concentrically Braced Frames (CBFs)



(c) Global buckling (AIJ 1995)



(b) Local buckling  
(Courtesy of Peter Maranian)



(a) Brace fracture  
(Courtesy of Peter Maranian)

Figure 1.2 Discrete damage states observed in bracing members



# Chapter 2

## Literature Review

---

### **2.1 Introduction**

This chapter summarizes the major research studies that discuss analytical and experimental research related to the seismic behaviour of steel braced frames designed in seismic regions over the past 40 years. The literature review presented in the subsequent sections is categorized in analytical and experimental research.

### **2.2 Analytical Research**

This section discusses the major analytical studies and numerical models that have been developed worldwide to simulate the nonlinear behaviour of steel braced frames subjected to cyclic loading. This section is divided into two parts. The first one summarizes analytical studies and models that focus on the cyclic behaviour of individual steel braces and (2) analytical studies that investigate the cyclic behaviour of steel braced frames at the system level.

#### **2.2.1 Analytical Models to Simulate the Hysteretic Behaviour of Steel Braces**

Over the last four decades a number of analytical models were developed to simulate the hysteretic behaviour of steel braces under cyclic loading. These models can be summarized in four categories; (1) phenomenological models; (2) physical theory brace

models; (3) fibre-based models and (4) detailed Finite Element Models (FEMs). Phenomenological models employ springs that force a brace to follow a pre-defined load-displacement path with empirical hysteretic rules. Physical theory brace models also employ springs to model the hysteretic behaviour of steel braces; however the spring behaviour is characterized by a closed-form analytical solution that depends on the geometric and material properties of the brace. With increasing computational power and need for more accurate models to simulate the hysteretic behaviour of steel braces, fibre-based and finite element models have been developed. These models discretize the brace component into smaller segments with appropriate material and geometrical properties. The main difference between the fibre-based and detailed finite element models for brace components is that the latter are able to simulate local buckling whereas the former fail to do so.

One of the first component models developed for inelastic cyclic behaviour of axially-loaded steel members were developed by Higginbotham (1973). To determine the post-buckling force-deformation behaviour, Higginbotham (1973) employed a physical theory and a phenomenological model. The physical theory model that was developed proved to be far too complex and inefficient for computation purposes at that time. The phenomenological model employed second order polynomial equations to curve-fit the brace response. This model offered a great improvement in computational time over the physical theory model. Both models were tested with small-scale specimens and it was found that they were able to predict well the early stages of the cyclic load-displacement of a steel brace.

Based on the research work by Higginbotham (1973), Singh (1977) proposed an analytical model using an energy approach to determine the axial force-axial deformation relationship to simulate the post-buckling behaviour of steel braces. This proved to be computationally a more efficient model than the earlier analytical model by Higginbotham. A phenomenological model was also developed, which was similar to Higginbotham's (1973) using piecewise linear curve-fitting for computational efficiency. As part of the same study, this component model was utilized to analyze a single story K-braced frame and it was proved to be an improved hysteretic model to capture the nonlinear behaviour of steel braces.

Shibata (1982) developed a physical theory model based on a closed-formed solution for an ideal bar of a W-section under cyclic axial loading. He used a bilinear stress-strain material relationship that employed an elastic-plastic spring and two non-flexural straight segments. The closed formed solution, which determined the axial displacement response of the brace when an incremental axial load is applied, included polynomial functions, which had a great advantage over some of the earlier physical models that included exponential or trigonometric functions in processing time (e.g., Nonaka 1973). Based on a comparison with the analytical model that was developed by Wakabayashi et al. (1973), Shibata's (1982) model proved to be very accurate in determining the post-buckling behaviour prior to brace fracture.

Ikeda et al. (1984) performed a series of experimental testing on steel braces to determine empirical parameters needed for the phenomenological model they proposed to simulate the cyclic behaviour of a steel brace. However this model failed to simulate the Bauschinger effect, local buckling and the gradual plastification along the length of the brace. Few years later, Ikeda and Mahin (1986) developed a comprehensive physical theory model and argued the advantages of such models over phenomenological and finite element models. The authors also demonstrated the improvements of the proposed model over a number of other models (e.g., Gugerli and Goel 1982, Ikeda et al. 1984). The Ikeda and Mahin (1986) model is able to simulate phenomena such as the Bauschinger effect and the reduction of post-buckling compressive load carrying capacity of a steel brace.

Mamaghani et al. (1996) developed finite element models for pin connected and cantilever steel compression members using an elastoplastic material behaviour model and beam-column elements. These models were employed to simulate bridge piers under cyclic loading. The emphasis of this model was put on the accuracy in the large displacement range, where most models of the time failed to address. This model was able to simulate the Bauschinger effect, cyclic hardening and the spread of plasticity across the brace member. The suggested models complied very well with experimental data.

More recently, Jin and El-Tawil (2003) developed a beam-column model that can also be used to simulate the cyclic behaviour of steel braces. The proposed model is able to

model deterioration of the cross-section stiffness that occurs after the local buckling of the brace component forms. This model is also able to simulate the spread of plasticity throughout the cross section of a brace component by using a bounding surface plasticity model. The authors validated successfully this analytical model with the component tests performed by Black et al. (1980) and with available experimental data from a three story braced frame test conducted by Ghanaat (1980).

Haddad (2004) developed a finite element model to simulate fracture due to low-cycle fatigue of braces subjected to cyclic loading. This model is also able to simulate local buckling of a steel brace cross section. A cumulative plastic strain approach was adopted to assess damage and fracture of the brace component. It was concluded that accumulated plastic strain is the principle reason for brace fracture due to cyclic loading. Local buckling of the brace cross section increased the plastic strain accumulation.

More recently, Uriz (2005) proposed a fibre-based hysteretic model to simulate the cyclic behaviour of steel braces and Buckling Restrained Braces (BRBs). This model is able to simulate the effects of low cycle fatigue of steel braces and is implemented in the Open System for Earthquake Engineering Simulation (OpenSees) platform (McKenna, 1997). This model has been employed to investigate analytically the cyclic behaviour of large-scale steel braced frames that were tested experimentally as part of the same research study. More details about this model can be found in Uriz (2005) and Uriz et al. (2008). Chapter 5 of this thesis also includes specific details about the Uriz et al. model since it is extensively used as part of this research. Similar to the Uriz (2005) study, Agüero et al.

(2006) performed an analysis of braced frames using a fibre brace element that was implemented in the OpenSees simulation platform. The authors also provided guidelines on how to use the brace element, such as number of fibers and integration points.

Calik (2007) formulated a new physical theory brace model that is simpler and more efficient compared to earlier physical theory models. The brace component is idealized as a pin-connected member with a plastic hinge at the center of the brace where local buckling is expected to occur. The authors employed semi-empirical formulas that were based on experimental tests on steel braces to represent the hysteretic response of the brace component. This allowed the model to simulate strength degradation of the compressive load carrying capacity.

Remennikov and Walpole (1997) developed a physical-based model that focused on the plastic hinge behaviour at the mid-span of a brace component. The model used empirical formulas based on experimental data to derive the load displacement relationship of a steel brace. This model was utilized with end conditions other than pin-connection by using the brace effective length factor as discussed in CISC (2010). The same investigators ran experiments on two-story braced frames with V and X-configurations to validate the proposed numerical model. They provided design recommendations for the estimation of maximum story drift ratios for concentrically braced steel frames (CBFs) subjected to earthquake loading. Davaran and Adalzadeh (2009) improved the original model proposed by Remennikov and Walpole (1997) by refining the work hardening formulas of the brace component model. This resulted to a better match between the

analytical and the experimental work conducted by Leowardi and Walpole (1996) and Popov et al. (1980). It is noted that the model is not able to simulate local buckling and fracture due to low cycle fatigue.

Davaran and Far (2009) developed an analytical model to predict fracture of steel braces due to low cycle fatigue. The authors employed a simplification of the linear cumulative damage theory to simulate low cycle fatigue and compared the simulated hysteretic response with experimental tests performed by Black et al. (1980). The model predicts fairly well the tension side of the loading history of a steel brace. However, the same model typically overestimates the buckling load of the brace in compression. This model is not able to capture local buckling of the brace cross section. In addition, the authors pointed out that the low cycle fatigue rule has to be further developed.

Krishnan (2003, 2009) proposed a modified elastofiber element model for slender columns and braces. This model is able to simulate any end condition of such members. A geometric imperfection needs to be included in the model in order to simulate flexural buckling of a steel component (Krishnan, 2010). The author also proposed a probability-based low cycle fatigue model to simulate fracture initiation due to low-cycle fatigue. Since this model employs fibre elements, fracture is defined as the probability of fracture of the entire member given that rupture occurs in some of the fibers that are used to discretize the brace cross section. This model was validated successfully with experimental results from a full-scale six-story braced frame as discussed in Krishnan (2010).

More recently, Hsiao et al. (2012) proposed a fibre-based element model to simulate the hysteretic behaviour of HSS steel braces including the flexibility and flexural strength of gusset plate connections. Fracture of the steel brace is modeled with a maximum strain range in the extreme fibre of the cross section. This model was calibrated with experimental tests that were mostly performed by Lehman and Roeder (2008) on HSS steel braces.

### **2.2.2 Analytical Studies on Steel Braced Frames**

While it is important to have an accurate component model to mimic the behaviour of braces subjected to cyclic loading, it is equally important to analyze steel braced frames as a system. This section summarizes the major analytical studies that have been conducted worldwide to investigate the seismic behaviour of steel braced frames over the past four decades.

Popov et al. (1976) performed one of the earliest analytical studies related to the seismic performance of steel braced frames subjected to cyclic loading. This study focused on the inelastic behaviour of braced frames subjected to severe ground motions. Based on this study, the pinching of the force-displacement hysteretic behaviour of steel braces was attributed to the decrease of compressive resistance of braces after the occurrence of flexural buckling. As part of the same study, the effect of such component behaviour on the seismic behaviour of braced frames was investigated and a set of design recommendations for braced frames were proposed in order to ensure acceptable seismic performance.

Singh (1977) proposed a simplified brace component model that is used to conduct nonlinear response history analysis of a single story and a six-story K-braced frame. According to the results of this study it was concluded that a more efficient brace performance may be obtained if steel braced frames are designed to have a controlled uplift. Since this study was conducted with a simple analytical model in order to simulate the brace component behaviour, the importance of efficient modelling of post-buckling behaviour of steel braces was emphasized.

Ballio and Perotti (1987) proposed a brace component model and performed analytical studies of one-story braced frames with alternative configurations. The same researchers tested the same frames experimentally with a quasi-static loading protocol. This research was primarily conducted to propose a new analytical model for braced frames and to evaluate the importance factors, implemented in the European seismic design guidelines Eurocode 8 (1998). Perotti and Scarlassara (1991) extended the same study and evaluated analytically the effect of slenderness of brace components on the nonlinear behaviour of single-story braced frames with X-configuration through an extensive analytical research.

In order to address issues related to soft story mechanisms that have been observed on steel braced frames after fracture of their brace components, Khatib et al. (1988) performed extensive analytical studies to identify parameters that lead to these failure modes. The analysis on chevron-braced frames concluded that the brace slenderness, the steel beam design approach and the proportioning of columns and connections are found

to be critical in influencing such failure mechanisms in braced frames. As part of the same study, the importance of the beam-to-column strength ratio on the seismic performance of steel braced frames was emphasized. The authors analyzed various braced frame configurations such as double story X-braced framing, V-braced framing and the addition of a secondary moment resisting frame and discussed the advantages, along with the disadvantages, of each configuration. Finally, the use of tie bars in braced frames or the use of zipper frames, which is discussed later in this chapter, were proposed as alternative structural system configurations.

Tang and Goel (1989) employed a steel brace hysteretic model that was originally developed by Jain et al. (1978) to investigate the seismic performance of steel braced frames. They included a fracture criterion in the steel brace model. This study served as the basis for the improvement of the seismic design provisions for steel braced frames in the early 90s. The authors analyzed four concentrically braced frames and three moment resisting frames. One of the main design recommendations given by the authors was to increase ductility of bracing members instead of increased strength, which was a common design approach of that time as discussed in AISC (1989).

More recently, Gan (1996) compared some of the existing steel brace configurations to each other and to a steel frame that utilized BRBs. This analytical study concluded that the global frame load carrying capacity deterioration due to brace buckling could be avoided by using BRBs. The same study also compared existing widely used braced frame configurations, conventional chevron braced frames and conventional X-braced

frames. The effect of several phenomena such as the brace component end conditions on the seismic behaviour of steel braced frames was investigated. Finally, several design guidelines for braced frames were provided such as the use of fixed ended bracing members and, if possible, employing BRBFs to ensure better braced frame behaviour.

Bara (2007) investigated analytically the behaviour of multi-story braced frames designed in accordance with NBCC (2005) and CSA-S16-S1-05 provisions (CSA 2005). These frames were analyzed in the OpenSees platform. Rigorous 3-D models were developed for five different building heights ranging from 2 to 16 stories. These models were subjected to a set of twenty ground motions. Based on the results from these analyses it was concluded that steel braced frames designed in accordance with the aforementioned seismic provisions performed satisfactorily during design level ground motions. A numerical database was also developed in order to investigate what loading protocols are suitable for experimental testing of bracing members.

Chen et al. (2008) analyzed a number of three-story steel buildings that were modeled in the OpenSees platform. These buildings utilized steel braced frames as the primary lateral resisting system and they were designed in accordance with NEHRP (1997) and ASCE-7-05 (ASCE 2005) guidelines. The scope of this investigation was to develop improved design guidelines towards performance-based design of steel braced frames. An emphasis was put on the response modification factor,  $R$ , as defined in ASCE-7 (2005). It was found that structures designed with a low  $R$  factor tend to decrease seismic demands on the braces. The tendency for a soft story failure mode is also decreased with the same

design philosophy. However, absolute floor accelerations are increased and this could have an important effect on the non-structural components as part of the same buildings. The authors performed a parametric study to design four large-scale two-story braced frames of various brace types and configurations to be tested experimentally. The results of this study are discussed in the experimental research section of this chapter.

Richard (2009) investigated the adequacy of the seismic provisions of NBCC (2005) and CSA S16-01 (CSA 2001) towards the design of steel industrial buildings that utilize braced frames as their primary lateral resisting system. These design provisions are heavily targeted for the design of regular residential and office buildings and do not represent a typical design of industrial buildings that might have irregular geometry, mass and stiffness distribution. Nonlinear response history analyses of two different industrial buildings were performed using a set of 90 ground motions. It was concluded that one of the industrial buildings that was designed with the above seismic provisions might yield limited plastic deformation capacity, due to buckling of the lower column segment. The same analytical study also provided design guidelines for crane-supporting structures in seismic regions.

In order to assess the seismic demands in columns of ductile braced frames, Richards (2009) performed an analytical study on buckling restrained braced frames (BRBFs), special concentrically braced frames (SCBFs), and eccentrically braced frames (EBFs) of various building heights (3, 9 and 18-stories). Based on nonlinear response history analysis, Richards (2009) concluded that SCBFs, especially low-rise frames, can

experience a significantly larger seismic demand in columns when compared to other braced frame configurations. This is attributed to the force redistribution that occurs after flexural buckling of the braces within a story.

While evaluating the possible use of partially buckling restrained braced frame (PBRB) elements, Eckert (2009) tested a number of braced frames that employ braces of different slenderness ratios. Several six story braced frames of different brace slenderness ratios  $kL/r$  ranging from 40 to 120, were analyzed with pushover and nonlinear response history analyses. Based on this study an improvement in structural behaviour of braced frames is observed when the brace slenderness is changed from slender to compact.

Huang and Mahin (2010) conducted a detailed finite element study to investigate the effect of fracture due to low cycle fatigue on braced frames. They used the finite element software LS-DYNA (LSTC 1988). The authors proposed a new material model that simulates low cycle fatigue in steel braces. The analysis results of the finite element models that were developed as part of this study were compared with experiments of beam-to-column connections, braced components and steel braced frames. The authors also provided guidelines for analyzing and detailing SCBFs.

While researching the reliability of the capacity based design philosophy in braced frames subjected to ground motions, Victorsson (2011) performed an extensive analytical study to determine the expected demand on components designed according to the capacity-based design philosophy and to assess the effect of the  $R$  factor as defined

before. Models for 1, 6 and 16-story buildings that utilize SCBFs as their primary lateral resisting system were developed. Analysis results helped to explain some of the connection failures observed in braced frames. Based on the same study, a correlation between the  $R$  factor and spectral accelerations where brace yielding was observed and reported.

More recently, Aboosaber and Hines (2011) employed and further analyzed the braced frame models developed by Hines et al. (2009) that predicted the collapse of chevron-braced frames. Due to lack of experimental data on collapse of braced frames, they compared their analysis to the experimental work on the sideways collapse of moment frames that was conducted by Lignos (2008) and Lignos et al. (2011). Furthermore, the authors performed an Incremental Dynamic Analysis (IDA) (Vamvatsikos and Cornell, 2002) using three different ground motions on a one-story chevron braced frame and a nine-story braced frame to assess their collapse capacity. The research study concluded that collapse assessment of braced frames is feasible. However more experimental studies are required to validate the proposed numerical models discussed in the study by Aboosaber and Hines (2011).

Stoakes (2012) performed a comprehensive study on the reserved capacity of low ductility braced frames including the flexural behaviour of the gusset plate beam-to-column connections. In order to model the flexural behaviour of such connections, large-scale experiments on gusset plate beam-to-column connections were performed (Stoakes and Fahnestock 2012). As part of the same study, the authors assessed the reserved

capacity of braced frames designed in moderate seismic regions through incremental dynamic analysis. Stoakes (2012) simulated the contribution of the gusset plate shear connections on low ductility braced frames to resist lateral loads in a seismic event. The authors provided recommendations for gusset plate detailing and braced frame design to insure that the gusset plates could provide enough lateral resistance to resist collapse of the frame after the fracture of the braces.

## **2.3 Experimental Research**

This section discusses the major experimental studies that have been conducted worldwide to investigate the cyclic behaviour and design of steel braces as parts of steel braced frames in seismic regions. This review is organized in two major parts; (1) experimental studies that focus on the behaviour of individual steel brace components and (2) experimental studies that investigate the system behaviour of braced frames during earthquake loading.

### **2.3.1 Component Experimental Studies**

One of the first experimental studies on steel brace components was conducted by Wakabayashi et al. (1977). They tested 24 W-section braces with different orientations, slenderness ratios and single and double bracing configurations under cyclic loading. This study was a very important one in the field of earthquake engineering as it was a pioneering study in component testing. The study concluded that the boundary conditions of braces are more complex than it is previously assumed and that the local buckling of braces have an important influence on the fracture of braces. Wakabayashi et al. (1980a)

expanded his research on the component behaviour of steel braces with other section types such as pipes, angles and flat bars.

Jain et al. (1978) conducted a large experimental study on rectangular Hollow Structural Steel (HSS) and L-shape braces. The study employed 32 small-scale braces with and without gusset plates to address the issue that was brought up by Wakabayashi et al. (1977). Based on this work a new hysteresis model was proposed to model the hysteretic behaviour of brace components, which included the compressive strength reduction and the elongation of the brace members when subjected to cyclic loading.

Black et al. (1980) conducted tests on a large number of large-scale struts of different cross sectional shapes and sizes. They concluded that the slenderness and the width-to-thickness ratios have an important influence on the hysteretic behaviour of axially loaded members. Around the same time, Zayas et al. (1980) conducted an experimental study that focused on the buckling of a small set of round HSS (pipe), sections when subjected to cyclic loading. They examined the importance of boundary conditions and the width-to-thickness ratios on the hysteretic behaviour of round HSS specimens. Based on the same study, a numerical model was proposed to capture the reduction of the buckling loads in pipe sections during cyclic loading.

Lee and Goel (1987) examined the differences in steel hollow structural section braces and concrete filled steel hollow structural section braces in full-scale specimens. According to this study, the concrete filled HSS braces perform significantly better than

hollow HSS braces under cyclic loading due to the fact that the concrete filling provides a better resistance to global buckling. This was an important finding because the study provided an easy and an effective improvement on the performance of braces with high width-to-thickness ratios. Around the same time a pioneering study in the area was conducted by Aslani et al. (1987). This study investigated the effect of stitch spacing in double angle or channel sections on their hysteretic behaviour. According to the same study, a new configuration to employ double angle sections was proposed. This configuration places the angle sections toe to toe, which would address a number of issues related to plastic hinge formation in the gusset plates and early local buckling, which were observed in conventional double angle braces of the time.

Walpole (1996) and Leowardi and Walpole (1996) conducted experimental studies on cold-formed HSS and W- sections of different slenderness ratios. Even though the set of specimens was not as large as some of the earlier experimental studies that were discussed, the study confirmed the same observations of the effect of slenderness ratios on the hysteretic behaviour of steel braces subjected to cyclic loading.

Shaback (2001) performed cyclic tests on rectangular HSS members of different slenderness, width-to-thickness ( $w/t$ ) ratios and end connections. This study concluded that steel brace slenderness among all of the other geometric and material parameters has the biggest effect on the hysteretic behaviour of steel braces.

Elchalakani et al. (2003) conducted an experimental study on a large set of pipe-sectioned braces of different width-to-thickness ratios but similar slenderness. The aim of the study was to investigate the effect of three different loading protocols on this set of braces. The main finding was that in addition to previously discussed geometric parameters of a steel brace member; the loading protocol has an important effect on the inelastic hysteresis behaviour of steel braces that was originally discussed by Tremblay (2002).

Haddad (2004) investigated 10 rectangular HSS members of different gusset plate dimensions, slenderness, width-to-thickness ratios and displacement histories. This study also stressed the importance of the loading histories on the hysteretic behaviour of a steel brace. An important outcome of this study was the development of maximum lateral displacement, fracture and absorbed energy equations for HSS braces. The maximum out-of-plane displacement relationship was compared to those suggested by Tremblay (2002) and Shaback and Brown (2003) and the relationship suggested by Haddad (2004) found to be an improvement. The suggested fracture and energy life relationships demonstrated that these parameters are inversely proportional to width-to-thickness ratio of the brace components and directly proportional to brace slenderness. The proposed fracture life relationship can be found in Equation 2.1, where  $\Delta_f$  is the sum of the absolute axial displacements of the brace component,  $\lambda$  is the slenderness term and  $b/t$  is the width-to-thickness ratio of the steel brace. It should be noted that this equation is applicable to HSS braces of slenderness ratio,  $kL/r$ , between 50 and 68.

$$\Delta_f = 378(\lambda^{0.19})(b/t)^{-0.94} \quad (2.1)$$

Similar to the study conducted by Walpole (1996) and Leowardi and Walpole (1996), Goggins (2004) tested a large number of cold-formed HSS sections of different slenderness ratios. Small-scale sections were employed as part of this study. The experimental data that was provided as part of this study served for calibration and validation of analytical models for steel braces, especially to display the effect of cold forming on the hysteretic behaviour of the braces.

More recently, Yang and Mahin (2005) conducted an experimental study to reduce the net-section fractures that are commonly observed in braced frames, especially those designed with no reinforcement of the net-section at the ends of a steel brace. They employed several different loading histories on different net section designs to improve the seismic code provisions for detailing of such connections. They found that especially in rectangular HSS members, reinforcement of the net section significantly improves the hysteretic behaviour of steel braces. The brittle fracture that seemed to occur near the gusset plates is shifted to a more ductile fracture at the mid length of the brace where a plastic hinge occurs first due to local buckling at the same location.

Han et al. (2007) extended the original work by Lee and Goel (1987) and Shaback and Brown (2003) and examined the effect of  $w/t$  ratio of rectangular HSS bracing members on their hysteretic response. This study concluded that for braces that fracture at their mid-length, the smaller the  $w/t$  ratio, the larger their energy dissipation is.

Tremblay et al. (2008) tested 34 large-scale brace specimens with rectangular HSS, round HSS and W- shape braces with various section depths reaching 305mm. This experimental program confirmed that the effect of slenderness,  $w/t$  and the shape of cross section have a significant effect on the fracture life of steel braces that are currently utilized in seismic design practice. Specimens with smaller  $w/t$  ratios and specimens of W-shape braces displayed a better performance towards fracture life.

In an effort of improving the connection of the pipe sectioned braces to gusset plates, which is still an important issue, Christopoulos et al. (2008) performed cyclic tests on four specimens to assess the feasibility of using cast steel elements to connect pipe sectioned braces to gusset plates in steel braced frames. Even though the study was limited only to four specimens, the suggested connectors contributed for the braces to achieve a desirable ductile hysteretic behaviour.

Fell et al. (2009, 2010) extended the work that was conducted by Tremblay et al. (2008) and tested 19 large-scale steel braces with various cross sections including rectangular HSS, round HSS and W-shapes. In addition to the parameters tested by Tremblay et al. (2008), Fell et al. (2009, 2010) also examined the effect of the loading history, loading rate and grout fill on the hysteretic performance of steel braces. The study also confirmed that the most important parameters that affect the hysteretic behaviour of steel braces are the slenderness and  $w/t$  ratios. They also suggested detailed FEM models to trace fracture of steel braces. A micromechanics-based model was employed for this purpose. This

model is a modified Void-Growth model that was suggested by Kanvinde and Deierlein (2004).

Nip et al. (2009) evaluated the effect of the material used to fabricate a steel brace on its hysteretic behaviour under cyclic loading. They employed hot-rolled, cold-formed carbon steel and stainless steel brace specimens as part of their experimental program. The effect of the material was investigated as well as most of the geometric parameters that were evaluated in earlier experimental studies presented above. This study concluded that the existing models that predict the buckling resistance, post-buckling capacity and mid-length out-of-plane deflections work well on carbon steel and stainless steel specimens, however they are not applicable to cold-formed steel specimens. Thus, the authors suggested new empirical relationships for cold-formed steel specimens.

More recently, Takeuchi and Matsui (2011) conducted an experimental program that involved nine pipe specimens of different slenderness and  $w/t$  ratios. Based on this experimental series the authors proposed a new method to estimate the cumulative cyclic deformation capacity of a steel brace after flexural buckling.

Most of the experimental studies that were summarized above are a part of the steel brace database that is discussed in Chapter 3.

### **2.3.2 Experimental Studies on Braced Frame Systems**

This section discusses the main experimental studies that have been conducted at the system level in which steel braces behave as part of a structural system and gusset plates interact with the actual brace members and beam-to-column connections as part of the braced frame.

Chen and Clough (1980) tested a one-third scale model of a 9-story K-braced steel frame was tested on a shake table. The main objective of this study was to investigate braced frames under uplift forces introduced from strong earthquakes. The effect of the uplift was usually ignored in the design and analysis of structures of the time. Therefore the authors controlled the uplift of columns in their design of the experimental set-up of the braced frame. The behaviour of the braced frame where uplift was allowed, was compared to the case where fixed base conditions were applied to the frame through free vibration testing and ground motions. More than 70 shaking table tests were carried out to obtain engineering demand parameters such as story displacements, shears and overturning moments as well as brace axial forces. These parameters were used to compare the performance of the two scenarios and it was found that the frame in which the uplift was allowed performed better under shake table tests than the frame with fixed base conditions.

Wakabayashi et al. (1980b) tested several one-story braced frames of different configurations to derive relationships to obtain a better estimation of the effective

slenderness ratio of the brace components. Useful information about hysteretic behaviour of braces and columns in a braced frame were also obtained from this experimental study.

In the same year, Ghanaat (1980) tested four 3-story frames with X-bracing configuration primarily designed to resist wind loading. Each of the test frames utilized steel braces of different cross sections. A frame without braces was also tested in order to investigate how effective the numerical models suggested for braced frames were during that time. Since most of the braces in the study stayed in the linear or slightly non-linear range, the analytical techniques employed predicted the response very accurately. The study also concluded that the braced frames that are designed for wind loading could provide reasonable lateral resistance for a moderate earthquake. Two years after this study Ghanaat and Clough (1982) performed a test on a similar frame to the 3-story frame tested by Ghanaat (1980), which employed pipe sectioned braces, that was designed for an offshore platform. The performance of the frame was similar to the 3-story frame test by Ghanaat (1980) in terms of energy dissipation and progression of plastic hinges in the braced frame. It was an important study for offshore oil industry because it was the first test done to investigate the effects of cyclic loading on offshore platforms.

As part of the US-Japan Cooperative Earthquake Research Program, Yamanouchi et al. (1985) tested a full-scale 6-story frame with an eccentric-K brace configuration at the Building Research Institute (BRI) in Japan. This study concluded that the eccentric-K braced frame configuration has a remarkable energy absorption capacity. Since this was one of the first full-scale tests that were conducted using the large strong wall-strong

floor facility, it served as a benchmark study later on. Fukuta et al. (1989) tested a half scale of a 3-story steel braced frame that employed the design of the Yamanouchi et al. (1985) steel braced frame. The half scale 3-story test frame was used to propose an accurate mathematical model to predict the lateral shear force versus story drift ratios of steel braced frames subjected to earthquake loading. Tang and Goel (1989) also investigated and further analyzed the Yamanouchi et al. (1985) frame to develop an empirical model to predict the fracture life of HSS braces. This model was implemented in the structural analysis software DRAIN-2D (Powell, 1973).

Tsuji and Nishino (1988) performed tests on two small-scale single-story braced frames to assess the effects of the inverted chevron brace and the single diagonal brace configurations on the global performance of braced frames. It was found that the braces that were part of the inverted chevron configuration fractured at larger story drift ratios than those of the single brace configuration. This was attributed to the increased vertical deflection of the beams in the inverted chevron configuration.

To further investigate the seismic performance of steel braced frames, Archambault (1995) tested seventeen full-scale frames of single and diagonal brace configurations. They concluded that the effective slenderness is the parameter that affects the most the energy dissipation of steel braces and that the current fracture life equations for slender braces do not predict fracture accurately. As part of the same study, new equations for predicting the fracture life of slender braces were proposed.

Filiatrault and Tremblay (1998) tested a half scale 2-story tension-only CBF to develop more comprehensive design provisions against the phenomena of impact load induced from strong earthquakes that was commonly observed in tension-only CBFs.

More recently, Roeder et al. (2004) tested more than forty single diagonal braced frames with different gusset plate designs to improve the existing code provisions for these elements. After the first set of experiments of thirteen frames, Lehman et al. (2008) proposed a balanced design method to improve gusset plate performance, i.e., to eliminate gusset plate fractures. The balanced designed method is an improvement of the capacity-based design discussed in AISC (2005) since it achieves to maximize the system ductility, while ensuring the capacity demands. The authors came up with several parameters, provisions and requirements, which were tuned as the number of tests increased. The new design provisions also allowed the gusset plates to be lighter and more economical compared to the traditional gusset plate design by AISC (2005).

Uriz (2005) tested a 2-story steel braced frame that was nearly full scale under static cyclic loading. The gusset plates and the braces were designed based on AISC (1993,1997) provisions. Most of the inelastic deformation of the test frame was concentrated in the first story, where both braces fractured. Uriz (2005) used the experimental data of this model to validate the proposed fiber-based fatigue model that is used to trace initiation of fracture of steel braces. The details of this experimental study are discussed in Chapter 6.

Yang (2006) tested a zipper-braced frame to demonstrate the advantage of using zipper frames over traditional inverted-V braced frames. The additional columns used in the zipper frames help resist the unbalanced forces that are generated in the beams and the braces after the occurrence of buckling of the braces. The coordinated analytical and experimental study that was conducted by Yang (2006) verified the suggested frame behaviour and concluded that up to 25% of material costs could be saved if zipper braced frames are employed compared to traditional inverted-V braced frames.

In an effort to improve the seismic performance of braced frames through innovative seismic design techniques Clark (2009) and Lumpkin (2009) tested in total four large-scale braced frames of two and three stories. The effect of improved gusset plate design and different brace shapes on the seismic performance of the braced frames are emphasized. The research showed that proper detailing of SCBF connections can help achieve improved seismic performance at large drifts.

More recently, Lai et al. (2010) tested four large-scale CBFs and two BRBFs. These tests demonstrated that steel braced frames that utilize pipe sections as braces exhibit a better ductile behaviour compared to CBFs that utilize rectangular HSS sections, under similar base shear capacities and loading protocols.

Okazaki et al. (2011, 2012) tested a nearly full-scale single story, single bay chevron braced frame at the world's largest shake table at E-Defense. A number of shake tests were performed with the same frame that was subjected to the North-South component of

the JR Takatori ground motion that was recorded during the 1995 Kobe earthquake in Japan. The gusset plates of the test-specimen were designed according the balanced design method that was proposed by Lehman et al. (2008). The gusset plates proved to work very well and an elliptical fold line was fold on the gusset plates, which was expected from the employed design approach. Both braces fractured at their mid-length, which is a ductile fracture mechanism. The authors employed the modelling approach discussed in Chapter 5 of this thesis and they concluded that post-buckling behaviour and fracture of steel braced frames could be predicted fairly accurately provided that fracture takes place at the mid-length of the braces.

To address the 3-Dimensional (3-D) effects on the seismic response of steel braced frames, Palmer et al. (2011) conducted two 3-D tests of two-story steel buildings with braced frames as their primary lateral resisting system. The first test utilized an X-brace configuration. The second test utilized single diagonal BRBFs. The two-story steel buildings were subjected to bidirectional cyclic loading. The authors also employed the balanced gusset plate design method (Lehman et al. 2008) on the X-braced frame. The frame with BRB braces outperformed the traditional HSS braces as anticipated. However the major finding of this study was that the traditional braced frame fractured at a consistent story drift that is observed in 2-D testing.

## **2.4 Summary**

In this chapter the major findings of experimental and analytical studies conducted on individual braces and braced frames over the last 40 years are presented. All of the steel

brace experiments listed in the steel brace database of this thesis are discussed. Emphasis is made on the relevant findings in all of these studies in relation to the scope of this thesis.

# Chapter 3

## Development of a Steel Brace Database

---

### 3.1 Purpose and Scope

Performance-Based Earthquake Engineering (PBEE) necessitates the use of advanced simulation models to compute engineering demand parameters (EDPs) of buildings subjected to earthquakes. The input parameters of such models need to be calibrated with large sets of experimental data for reliable computed response predictions. In the case of braced frames, the need for a comprehensive set of data that will allow to realistically model the post-buckling behaviour and fracture due to low cycle fatigue of various shapes of steel braces is evident. In addition to that, the tools required to perform a rapid earthquake damage assessment in braced frames also necessitate the use of extensive set of experimental data. This chapter discusses the development of a steel brace database that serves for both purposes.

Tremblay (2002) and Lee and Bruneau (2005) compiled a partial dataset of 76 and 66 specimens, respectively. However, these datasets were primarily used (1) to assess the expected post-buckling compressive resistance of steel braces at different compression ductility levels, (2) to quantify the extent of hysteretic energy dissipation achieved by braces in compression and (3) to develop regression equations that estimate the out-of-plane rotation of rectangular Hollow Structural Section (HSS) braces to fracture. None of

these datasets includes digitized axial load-displacement hysteresis diagrams, which are critical for the development of modelling parameters that control post-buckling behaviour and fracture initiation due to low cycle fatigue. More recently, Hsiao et al. (2012) compiled a dataset of 44 rectangular HSS sections. Based on this data, they developed a strain-based analytical model in the OpenSees platform (McKenna 1997) that is able to simulate the buckling capacity and post-buckling response of Special Concentrically Braced Frames (SCBFs). More information about this model is discussed in Chapter 5.

Chapter 2 discusses the major experimental studies that investigated the behaviour of steel braces subjected to cyclic and/or monotonic loading over the past several decades (see Section 2.3). Based on these studies, a steel brace database is assembled herein. The database includes 317 braces from 22 different experimental programs that were conducted worldwide during the past 40 years. The main features of the database are summarized in the following sections.

## **3.2 Database Development**

The steel brace database that is discussed in this chapter is organized in two main components:

1. Metadata, which includes information regarding the testing configuration, the geometry, the shape and the material properties of the steel brace and its gusset plates (if applicable). Information about the loading protocols that were used as part of each testing program is also provided in the metadata.

2. Reported data, which includes fully digitized histories of the axial force-displacement and the lateral load-story drift ratio hysteresis diagrams of each one of the steel braces.

The complete set of experiments included in the steel brace database together with basic information regarding the steel brace member, material and slenderness ratios can be found in Appendix A (see Table A.1).

More recently, the performance assessment of buildings subjected to earthquakes in terms of losses necessitates the development of deformation-based fragility curves of various structural and non-structural components (ATC-58, 2012a,b). These curves are associated with discrete damage states that have been observed from past earthquakes and/or from structural component testing. Therefore, the steel brace database discussed in this chapter serves for this purpose. This is accomplished by storing the maximum story drift ratios at which discrete brace damage states occurred during the imposed loading history of a steel brace. In this research, these damage states are associated with global buckling, local buckling and complete strength loss due to fracture at the mid-length of a steel brace. These damage states are illustrated in Figure 3.1 that displays a sample hysteretic response of a steel brace subjected to a symmetric loading history. More information regarding the drift-based fragility curves developed as part of this research is discussed in Chapter 4.

Most of the axial force-displacement hysteretic diagrams of the steel braces that serve for the calibration of the component model that is discussed in Chapter 5 are fully digitized

manually from the experimental reports. A digitization software called Digitizer (Lignos and Krawinkler, 2007, 2011, 2012), which is written in JAVA – programming language was employed for this purpose. This program has been successfully used for a similar purpose to obtain digitally the hysteretic behaviour in terms of lateral load-displacement of more than 500 steel and reinforced concrete beams (Lignos and Krawinkler 2011, 2012).

### **3.3 Steel Braces Contained in the Database**

The developed database includes 317 steel braces of different geometries, materials and testing procedures. A total of 158 rectangular hollow structural section (HSS) members, 65 W-shape members, 55 round HSS (noted as pipes) members, 37 angle (L) and channel (C) sections and 2 T sections cut from W-shaped sections (WT) are included in the database. These braces have been fabricated from 14 different material grades that are used for steel fabrication purposes in the U.S., Canada, Japan, Australia and Europe. Statistical information regarding these material properties is presented in Section 3.4.1.

A number of steel brace testing configurations were employed in the experimental studies that are a part of the steel brace database. These include braces that were only tested as a single component and braces that were tested as part of an actual steel brace system. Several different end conditions, such as pin-ended, pin-fixed, fixed-fixed and with gusset plates were employed for the brace testing. The effect of boundary conditions on the hysteretic response of a steel brace is discussed in Chapter 5. The steel brace configurations considered in the steel brace database are shown in Figure 3.2. In this

figure,  $L_B$ , is the clear length of the steel brace and  $L_H$ , is the distance between the expected plastic hinge locations at the ends of the braces (i.e., the effective length of a steel brace).

The effective brace slenderness ratios,  $kL/r$ , where  $k$  is the effective length factor,  $L$  is the centerline length of the brace and  $r$  is the radius of gyration of the steel brace cross section in the plane of buckling varied from 22.4 to 218. Only one steel brace had a  $kL/r > 200$ , which is the limit for compression members by CISC (2010) provisions. The slenderness parameter  $\lambda_C$  as defined in Equation 3.1 varied from 0.26 to 3.09. In this equation,  $k$  is the effective length factor with respect to the axis of buckling,  $L$  is the centerline length of the brace,  $r$  is the radius of gyration with respect to the axis of buckling,  $F_y$  is the measured yield stress and  $E$  is the modulus of elasticity for steel. The brace length  $L_B$  for the specimens ranged from 410mm to 6230mm and the tensile yield force  $A_gF_y$  ranged from 12kN to 6430kN.

$$\lambda_C = \frac{kL}{r} \sqrt{\frac{F_y}{\pi^2 E}} \quad (3.1)$$

The majority of the steel braces in the database did not experience net section failures; Only 34 of the collected braces failed at the net section (Lee and Goel, 1987, Haddad et al. 2004, Goggins et al. 2004, Yang and Mahin, 2005, Han et al. 2007, Lehman et al. 2008, Fell et al. 2010 and Nip et al. 2009). These braces were not considered for the development of the drift-based fragility curves and the calibration of the brace component model discussed in Chapters 4 and 5, respectively.

According to the AISC 360-10 (2010) seismic requirements, 220 of the steel braces are

classified as Highly Ductile, 42 as Moderately Ductile and 52 as Low Ductility braces. Due to the different definitions of the ductility classes, the same braces are classified slightly differently according to the CSA-S16-09 (2009) requirements for Ductile Braced Frames. In particular, 279 steel braces are classified as Class 1, whereas 12 braces are classified as Class 2, 10 braces as Class 3 and 11 braces as Class 4 according to the classification limits per CSA-S16-09 (2009). More details regarding the classification limits are presented in Section 3.4.2.

### **3.3.1 Loading Protocols**

The vast majority of the steel braces included in the database were tested with a symmetric cyclic loading protocol. In summary, 221 steel braces were tested with a standard symmetric cyclic loading protocol (Krawinkler et al. 2000), where the brace is subjected to an increasing amplitude axial displacement both in compression and tension (see Figure 3.3a). Another common loading protocol that has been employed is the near field loading protocol (Krawinkler et al. 2000). This loading protocol is used to mimic the effect of an earthquake load where a structure is near the epicenter of the fault line. Typically, when a structure is subjected to a near-fault ground motion, it is pushed to either a displacement that subjects the steel brace in a large tension or compression force in the early cycles. The displacement amplitude diminishes in latter cycles (see Fell et al. 2009). An example of such protocols is shown in Figures 3.3b,c. A total of 18 steel braces were subjected to a near-field loading protocol. Thirteen steel braces were subjected to a far field loading protocol. This protocol is different compared to the near field loading protocol since the high amplitude displacements are exerted on the brace at the latter stages of the loading history (see Figure 3.3d). Three members were subjected

to earthquake loading protocol. During these tests the steel braces were tested dynamically on a shake table at a rate similar to what a brace would experience during an earthquake as part of a steel structure. Jain et al. (1973) conducted 37 tests with two different loading protocols; increasing asymmetrical and unsymmetrical sine loading protocols (see Figures 3.3e and 3.3f). The increasing asymmetrical loading protocol employs a displacement history that is not symmetrical in the tension and compression zone, whereas the unsymmetrical sine loading protocol employs a displacement history that can be characterized with a sine curve that has different amplitude on the compression side than the tension side. In total, 27 steel braces were tested with an asymmetric loading protocol and 10 with an unsymmetrical sine protocol. As part of the experimental program that was conducted by Lai (2012), four HSS braces were tested in a frame using hybrid simulation that was conducted at a slow rate. Lastly 27 steel braces that are included in the database were subjected to monotonic loading. In this case, the steel braces were pushed to a pre-defined displacement in either compression or tension.

## **3.4 Steel Brace Database Evaluation**

### **3.4.1 Statistical Evaluation of Material Properties of Various Grades**

This section discusses the statistical evaluation of the material properties of steel braces in terms of their yield and ultimate stresses based on counted statistics. The material properties for most of the steel braces discussed in the database are obtained from coupon tests in accordance to the ASTM A370 specification (ASTM, 2012). For most of the specimens, the yield stress is defined as the stress at which the coupons experience at 0.2% strain. The counted statistics for the yield and ultimate stress,  $F_y$  and  $F_u$ ,

respectively, in terms of mean ( $\mu$ ), standard deviation ( $\beta$ ) and coefficient of variation (COV) are summarized in Tables 3.1 and 3.2. From these tables, it is found that all of the steel grades in the database have higher mean measured yield stresses than the nominal yield stresses, as expected. Except for the steel grade AISI 1020 all of the mean measured ultimate stresses are higher than the nominal ultimate stresses. The reason why the AISI 1020 grade has a lower than expected ultimate stress is that the steel material used is annealed. This process typically decreases the ultimate stress of the material (Fadare et al. 2011). It should be noted that the difference between the measured and nominal ultimate stresses is less than the difference observed between the measured and nominal yield stresses. This in part is attributed to the fact that residual stresses due to the manufacturing process affect much more the yield stress compared to the ultimate stress of steel (Huber and Ketter, 1952, Huber 1956).

The statistical evaluation allows the calculation of expected yield and ultimate strength that can be directly compared with various values that are currently used for design purposes depending on the material grade. The measured-to-nominal yield and ultimate strength ratios can be directly compared with the  $R_y$  and  $R_t$  values that are summarized in AISC 360-10 (2010) and CSA-S16-09 (2009) for the most common steel grades that are used in steel construction. Tables 3.3 and 3.4 summarize the counted statistics of the measured-to-nominal yield ( $F_{y,m}/F_{y,n}$ ) and measured-to-nominal ultimate ( $F_{u,m}/F_{u,n}$ ) ratios, respectively. From Table 3.3 it can be seen that for A500 Gr. B steel, which is commonly used for the fabrication of HSS steel braces in the U.S. and Canada the  $F_{y,m}/F_{y,n}$  ratio agrees with the recommended  $R_y$  value by the AISC-360-10 seismic provisions. This

information is particularly important since it can be employed to assess the modelling uncertainties and their effects on the global performance of steel braced frames subjected to earthquakes (see Victorsson 2011). Note that for SS400 steel (typical older type of Japanese steel) a recommended  $R_y = 1.36$  may be used based on the information that was collected. Note that the  $R_y$  and  $R_t$  values listed in AISC 360-10 (2010) are found to be conservative for some materials such as A992 and A501. However, it is found that the currently used  $R_y$  values for steel grades A36, A53 and A500 Gr.C are overestimated. The same observations apply for the  $R_t$  ratios. When the calculated measured-to-nominal yield stresses are compared with  $R_y$  ratios suggested by the CSA-S16-09 guidelines, it is found that for the braces in the database these guidelines do not represent the yield stresses adequately. This will be discussed in Section 3.4.3 in more detail. Table 3.5 displays the measured ultimate-to-yield stress ratios for all braces in the database. This table can be used to estimate the ultimate yield stress of steel braces based on measured yield stresses. The observed differences between the calculated measured-to-nominal yield and ultimate stress ratios and the  $R_y$  and the  $R_t$  ratios suggested by the AISC and CSA guidelines may be attributed in part to (1) the finite sample uncertainty in the collected datasets, (2) the differences between the structural shapes and (3) the fabrication processes during time and region. Tremblay et al. (2002) concluded the same based on a similar study that they conducted with 76 steel braces.

### **3.4.2 Ductility Classes of the Steel Braces**

The ductility classes and the brace slenderness ratios of the steel braces are found to have an important impact on the non-linear behaviour of steel braces (Tremblay, 2002, Fell et

al. 2009 and Nip et al. 2009). Tremblay (2002) concluded that braces with low width to thickness,  $w/t$ , ratios could undergo larger deformations compared to more slender ones. Therefore, to get a better understanding of the steel braces in the database in terms of plastic deformation capacity, the ductility limits per AISC and the class limits per CISC are compared and the steel braces that were collected as part of this research are classified according to the aforementioned limits. Table 3.6 displays a classification of all the steel braces in the database based on the AISC and CISC limits. From this table, it can be seen that 279 braces included in the database are classified as Class 1. Twelve (12) braces are classified as Class 2 according to the section classification limits per CISC (2010). Therefore, the collected braces comply with the CSA-S16-09 (2009) requirements for Ductile Braced Frames, where Class 2 or better sections are required for bracing members in seismic regions. Ten braces are classified as Class 3 and eleven braces as Class 4. Most of the braces that belong to Class 3 and Class 4 are from older experimental studies (Wakayabashi et al. 1980a, Aslani et al. 1987). This is due to the fact that the importance of local slenderness ratios to the hysteretic behaviour of braces wasn't a part of seismic design codes until the early 1990s.

Per AISC 360-10 (2010) seismic compactness requirements, the steel brace classification is slightly different as shown in Table 3.6. The performance requirements of ductility class of Highly Ductile of AISC (2010) overlaps with the requirements of Class 1 in CISC (2010), so does Moderately Ductile with Class 2. If a section fails to qualify for one of these classes it is regarded as Low Ductility, which corresponds to Class 3 or higher in the Canadian codes. However as Table 3.6 displays, there is a difference in the

classification limits of the sections according to these two design codes. The CISC (2010) requirements tend to be less conservative than the AISC (2010) requirements for ductility classes. However in addition to the class checks, CSA-S16-09 (2009) may require sections more compact than the Class 1 limits for bracing elements, depending on the brace slenderness ratio, to be used in order to achieve the desired ductile braced frame behaviour. According to the AISC-360-10 (2010) requirements, 220 steel braces are classified as Highly Ductile, 42 as Moderately Ductile and 52 as Low Ductility braces. In addition to these section class requirements, the brace slenderness ratio limit,  $kL/r < 200$ , as suggested by AISC-360-10 (2010) and CISC (2010) for axially loaded members were checked. Only one brace was found to exceed that ratio. Most of the braces, 266 of them, in the database have a brace slenderness ratio,  $kL/r < 100$  which is in compliance with the CISC (2010) guidelines for bracing members in seismic regions. The steel braces that were found to be of Class 4, Low Ductility or fail the slenderness limits were not considered as part of the development of drift-based fragility curves (see Chapter 4) and the development of modelling recommendations for post-buckling behaviour and fracture of steel braces (see Chapter 5). Note that steel brace sections that are classified as Class 2 and 3 or to the moderate ductility class are not expected to achieve the axial deformation that Class 1 or High Ductility sections can achieve prior to fracture.

### **3.4.3 Maximum Brace Compressive Strength Requirements**

This section discusses the maximum brace compressive strength requirements of the steel braces in the database. For this evaluation, the measured buckling loads of the individual braces were collected and compared with the equivalent buckling loads based on the

current design provisions (CSA-S16-09, 2009). The load corresponding to global buckling is the maximum compressive load that a steel brace can resist and it is noted as  $C_u$ . In order to be able to compare all the specimens in the database, the compressive load is normalized to the yield load, which is the product of the brace cross-section area,  $A_g$  multiplied by its yield stress (measured or nominal),  $F_y$ . This load is plotted against the slenderness parameter  $\lambda$ , as defined in Equation 3.1. Figure 3.5 shows the normalized compressive load at buckling with respect to the slenderness parameter  $\lambda$  based on the measured material properties of the individual steel braces (noted as  $\lambda_m$ ). In the same figure, we have superimposed the Euler buckling load versus slenderness curve and the design load as computed from Equations 3.2 and 3.3 based on CSA-S16-09 (2009) for  $n = 1.34$  and  $2.24$ . In these equations  $E$  is the Young's modulus,  $I$  is the moment of inertia about the buckling axis,  $kL$  is the term for the effective length of the brace,  $A_g$  is the cross sectional area,  $F_y$  is the nominal yield stress,  $\lambda$  is the slenderness term and  $n$  is an empirical coefficient defined by the CSA-S16-09 (2009). The parameter  $n$  in this equation depends on whether the steel material used is of hot-rolled ( $n = 1.34$ ) or cold-formed steel material ( $n = 2.24$ ). The Euler buckling load is used to predict the maximum compressive load for an ideal column, whereas the CSA design code is a semi-empirical formula based on experimental data. The coefficient  $n$  is used as an adjustment factor for Class 4 sections and cold-formed steel members since it is found that they buckle at lower loads than other steel sections. The loads obtained from these equations are also normalized by  $A_g F_y$  for comparison purposes.

$$C_u = \frac{EI\pi^2}{kL^2} \quad (3.2)$$

$$C_u = A_g F_y (1 + \lambda^{2n})^{-1/n} \quad (3.3)$$

From Figure 3.4, the majority of the steel braces are distributed well within the design buckling loads as suggested by CSA-S16-09 (2009). However, some of the members buckled at smaller loads than the expected design loads. This in part is attributed to the fact that the database includes a number of steel braces with open channel shapes. From Figure 3.4 it can be seen that the majority of the buckling load of these braces are distributed below the CSA-S16-09 design curves. These braces in general buckle at compressive loads less than the expected buckling loads due to the fact that they are susceptible to other buckling mechanisms such as lateral torsional buckling or elastic local buckling (Black et al. 1980, CISC 2010). Sectional ductility classes have an effect on the buckling load of the individual steel braces. Sections of classes higher than Class 3, tend to buckle at lower compressive loads compared to sections of Class 1. According to Yu and LaBoube (2010), Class 4 sections are subject to elastic local buckling due to compression that decreases the full resistance of the section. This is the primary reason for lower than expected buckling loads. To display this effect of ductility classes on buckling loads, the cross sectional shapes and ductility classes are separately marked in Figure 3.5. This figure shows the normalized  $C_u$  versus slenderness parameter  $\lambda_m$  (based on measured material properties) for Class 1 through 4 sections. Most of the W-shapes that buckled at a lower compressive load than expected by the design curves tend to be of Class 3 or higher. Another reason for decreased buckling loads is that the steel braces that first experience yielding in tension prior to flexural buckling have a decreased buckling load due to the elongated effective length in tension compared to the undeformed one. However, it should also be acknowledged that tension yield prior to compression can

correct local and global imperfections in a steel brace; therefore, this could be beneficial in the buckling strength of a steel brace.

Figure 3.6 shows the normalized buckling loads of the steel braces in the database versus the nominal slenderness parameter,  $\lambda_n$ . In this case, the normalized buckling load of each brace was normalized with respect to their nominal yield strength. From this figure, most of the normalized buckling loads are much higher than expected by the design curves, due to the fact that the measured material yield stresses are higher than the nominal yield stresses, as discussed in Section 3.4.1. This implies that the computed  $C_u$  and  $\lambda$  values would be better represented if they were computed based on the expected material properties of the same steel materials. This is consistent with both CSA-S16-09 (Clause 27.5.3.4) and AISC-341-10 requirements that for compressive members the expected (or probable) yield strength ( $R_y F_{y,n}$ ) should be used in lieu of  $F_{y,n}$  in the absence of measured material properties. Figure 3.7 shows the normalized buckling loads of the steel braces in the database versus the slenderness parameter using expected yield stresses (noted as  $\lambda_{exp}$ ). The buckling load is normalized with the expected yield strength ( $R_y F_{y,n}$ ) and with an additional factor of 1.2 that the CSA-S16-09 requires for the estimation of buckling loads in braced frames. From this figure, the expected (probable) material properties suggested by CSA-S16-09 do not accurately estimate the buckling loads. This is due to the fact that the minimum  $F_y$  value of 350MPa specified by the CSA-S16-09 for bracing members is higher than that of every steel grade in the database other than CSA-G40.21-350W. Moreover, the suggested  $R_y$  ratio in CSA-S16-09 is constant, except for a reference to AISC-341-10 for the grade ASTM A53, for all material grades whereas

Table 3.3 and AISC-341-10 display a different measured-to-nominal yield stress ratio per steel grade. Braces designed using the CSA-S16-09 guidelines generally buckle at lower loads than design loads (see Figure 3.7). In the absence of measured material properties, Table 3.3 can provide a better estimate of the expected yield stresses of various steel braces depending on the steel material compared to the current CSA-S16 provisions. Figure 3.8 shows the normalized buckling loads of the steel braces in the database versus the slenderness parameter using expected yield stresses (noted as  $\lambda_{exp}$ ) described by AISC-341-10 guidelines. For the grades that are not included in the AISC-341-10 Table I-6-1, the  $R_y$  values calculated in Table 3.3 are used to compute the expected yield stresses. After comparing Figures 3.7 and 3.8, it is observed that the AISC provisions provide more reliable estimates of the buckling loads of most of the steel braces included in the database than the current CSA-S16-09 guidelines. This is due to the fact that the AISC provisions have a more comprehensive set of  $R_y$  values that address the variability of measured-to-nominal yield stresses in different steel grades.

### 3.5 Summary

This chapter discusses the development of a steel brace database to be utilized for the development of drift-based fragility curves in Chapter 4 and modelling guidelines for simulating the post-buckling behaviour and fracture due to low-cycle fatigue of steel braces (see Chapter 5). In total, 317 experimental data were collected from 24 experimental programs that have been conducted worldwide over the past 40 years. After an evaluation of the steel braces collected in the database, it was found that most of the braces qualify to be used in modern seismic design of concentrically braced frames.

Statistical information gathered from the coupon tests of the brace specimens showed that the CSA-S16-09 guidelines do not represent well the probable yield stresses of the braces. The AISC-341-10 guidelines do a better representation of the expected yield stresses because these guidelines take into account the material grade distinction when calculating the expected yield stress of the braces. Similar observations are made when the measured compressive strength of the braces in the database are compared to those computed by CSA-S16-09 and AISC-341-10 guidelines.

Table 3.1 Statistics of material yield stress from coupon tests

Steel Grade	Shapes	N	$F_{y,m}$		
			$\mu$ [MPa]	$\beta$ [MPa]	COV
ASTM A36/A36M	W, WT, L	25	298	30	0.10
ASTM A500 Gr. B	HSS, P	68	441	41	0.09
ASTM A53/A53M	P	12	314	70	0.22
A992/A992M	W	9	397	24	0.06
AISI 1020	P	6	333	189	0.57
ASTM A500 Gr. C	HSS, P	14	400	59	0.15
ASTM A501	HSS	3	513	93	0.18
ASTM A570-Gr. C	HSS	24	278	44	0.16
S235JRH	HSS	16	374	103	0.28
CSA-G40.21-350W	HSS	53	420	39	0.09
SS400 (SS 41)	P, W, L	63	320	59	0.19
M1020	L	8	364	8	0.02
STK400 (STK 41)	P	9	355	7	0.02
AS3679.1-300	W	3	312	0	0.00

Table 3.2 Statistics of material ultimate stress from coupon tests

Steel Grade	Shapes	N	$F_{u,m}$		
			$\mu$ [MPa]	$\beta$ [MPa]	COV
ASTM A36/A36M	W, WT, L	*	-	-	-
ASTM A500 Gr. B	HSS	65	488	40	0.09
ASTM A53/A53M	P	8	444	25	0.05
A992/A992M	W	5	522	27	0.06
AISI 1020	P	4	359	0	0.00
ASTM A500 Gr. C	HSS, P	11	485	47	0.10
ASTM A501	HSS	*	-	-	-
ASTM A570-Gr. C	HSS	24	374	29	0.07
S235JRH	HSS	13	483	52	0.10
CSA-G40.21-350W	HSS	34	482	0	0.00
SS400 (SS 41)	P, W, L	63	444	48	0.10
M1020	L	8	521	23	0.04
STK400 (STK 41)	P	9	412	8	0.02
AS3679.1-300	W	*	-	-	-

\* No available coupon tests

Table 3.3 Statistics of expected to measured yield strength

Steel Grade	Shapes	N	$F_{y,n}$ [MPa]	$R_y$ (based on AISC-341-10, Table A3.1)*	$F_{y,m}/F_{y,n}$		
					$\mu$	$\beta$	COV
ASTM A36/A36M	W, WT, L	25	250	1.5	1.19	0.12	0.10
ASTM A500 Gr. B	HSS, P	68	315	1.4	1.40	0.13	0.09
ASTM A53/A53M	P	12	240	1.6	1.31	0.29	0.22
A992/A992M	W	9	345	1.1	1.15	0.07	0.06
AISI 1020	P	6	295	-	1.13	0.64	0.57
ASTM A500 Gr. C	HSS, P	14	345	1.4	1.16	0.17	0.15
ASTM A501	HSS	3	250	1.4	2.05	0.37	0.18
ASTM A570-Gr. C	HSS	24	230	-	1.21	0.19	0.16
S235JRH	HSS	16	235	-	1.59	0.44	0.28
CSA-G40.21-350W	HSS	53	350	-	1.20	0.11	0.09
SS400 (SS 41)	P, W, L	63	235	-	1.36	0.25	0.19
M1020	L	8	200	-	1.82	0.04	0.02
STK400 (STK 41)	P	9	235	-	1.51	0.03	0.02
AS3679.1-300	W	3	300	-	1.04	0.00	0.00

\* Clause 27.1.7 of CSA-S16-09: The probable yield stress shall be taken as  $R_y F_y$ . The value of  $R_y$  shall be taken as 1.1, and the product  $R_y F_y$  as not less than 460 MPa for HSS sections or 385 for other sections, unless the probable yield stress, taken as an average yield stress, is obtained in accordance with CSA G40.20

Table 3.4 Statistics of expected to measured ultimate strength

Steel Grade	Shapes	N	$F_{u,n}$ [MPa]	$R_t$ (based on AISC-341-10, Table A3.1)	$F_{u,m}/F_{u,n}$		
					$\mu$	$\beta$	COV
ASTM A36/A36M	W, WT, L	*	400	1.2	-	-	-
ASTM A500 Gr. B	HSS	65	400	1.3	1.22	0.10	0.09
ASTM A53/A53M	P	8	415	1.2	1.07	0.06	0.05
A992/A992M	W	5	450	1.1	1.16	0.06	0.06
AISI 1020	P	4	395	-	0.91	0.00	0.00
ASTM A500 Gr. C	HSS, P	11	425	1.3	1.14	0.11	0.10
ASTM A501	HSS	*	400	1.3	-	-	-
ASTM A570-Gr. C	HSS	24	360	-	1.04	0.08	0.07
S235JRH	HSS	13	435	-	1.11	0.12	0.10
CSA-G40.21-350W	HSS	34	450	-	1.07	0.00	0.00
SS400 (SS 41)	P, W, L	63	400	-	1.11	0.12	0.10
M1020	L	8	380	-	1.37	0.06	0.04
STK400 (STK 41)	P	9	400	-	1.03	0.02	0.02
AS3679.1-300	W	*	440	-	-	-	-

\* No available coupon tests

Table 3.5 Ultimate-to-yield stress ratios

Steel Grade	Shapes	N	$F_{u,n}/F_{y,n}$ [MPa]	$F_{u,m}/F_{y,m}$		
				$\mu$	$\beta$	COV
ASTM A36/A36M	W, WT, L	*	1.60	-	-	-
ASTM A500 Gr. B	HSS	65	1.27	1.12	0.05	0.04
ASTM A53/A53M	P	8	1.73	1.29	0.02	0.02
A992/A992M	W	5	1.30	1.32	0.01	0.01
AISI 1020	P	4	1.34	1.13	0.00	0.00
ASTM A500 Gr. C	HSS, P	11	1.23	1.21	0.07	0.06
ASTM A501	HSS	*	1.60	-	-	-
ASTM A570-Gr. C	HSS	24	1.57	1.35	0.05	0.4
S235JRH	HSS	13	1.85	1.20	0.10	0.08
CSA-G40.21-350W	HSS	34	1.29	1.22	0.03	0.02
SS400 (SS 41)	P, W, L	63	1.70	1.41	0.07	0.05
M1020	L	8	1.90	1.43	0.03	0.02
STK400 (STK 41)	P	9	1.70	1.16	0.02	0.02
AS3679.1-300	W	3	1.47	-	-	-

\* No available coupon tests

Table 3.6 Ductility and section classes of the specimens in the database

Shape	Number of Specimens						
	AISC			CISC			
	Highly Ductile	Moderately Ductile	Low Ductility	Class 1	Class 2	Class 3	Class 4
HSS	109	16	30	150	5	-	-
Pipe	43	12	-	55	-	-	-
W	57	6	2	61	2		
Angle	4	8	20	6	5	10	11
Channel	5	-	-	5	-	-	-
WT	2	-	-	2	-	-	-

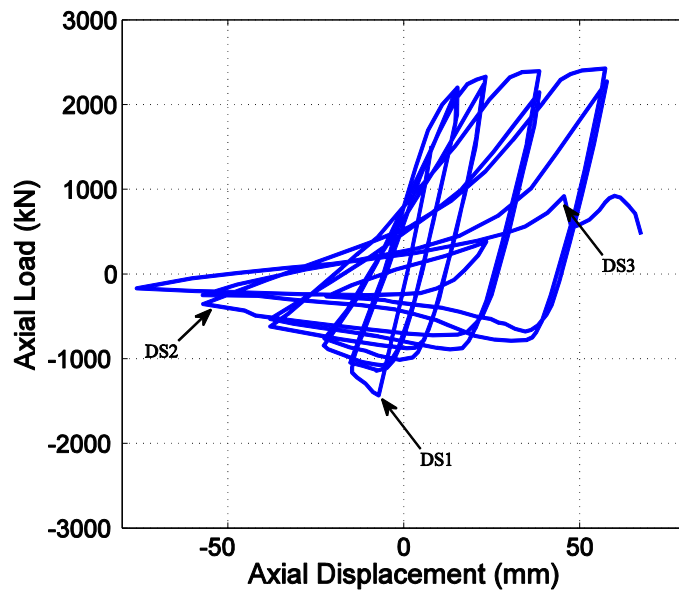


Figure 3.1 Sample hysteretic brace axial load displacement history

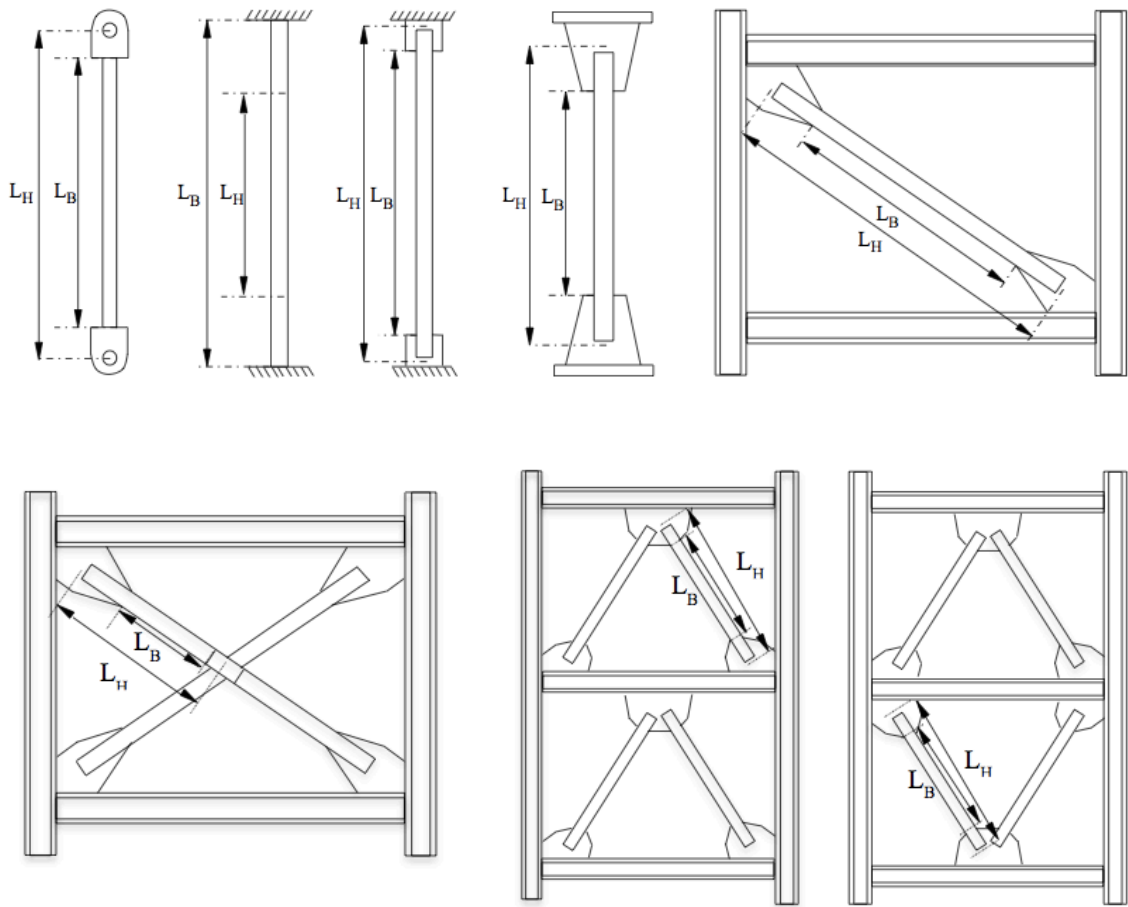
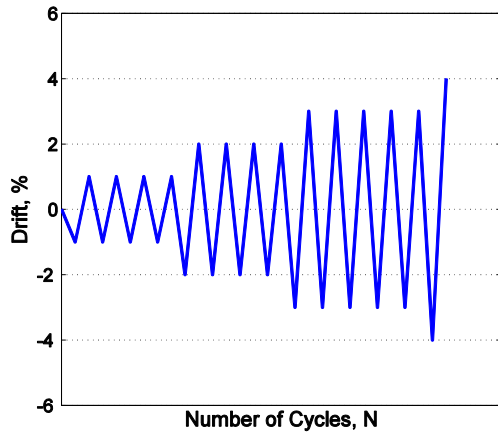
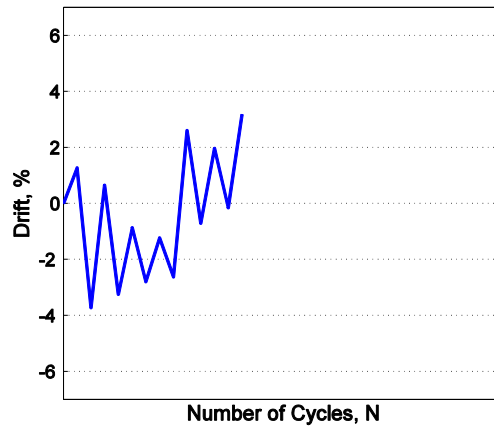


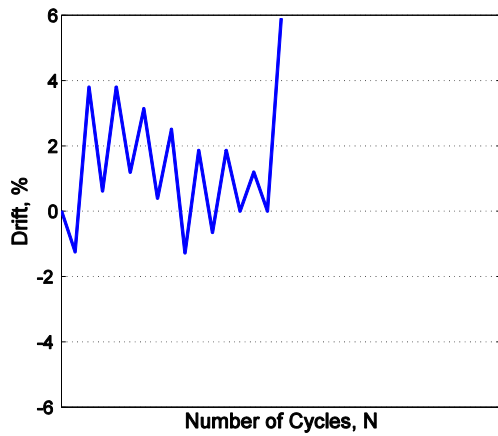
Figure 3.2 Steel brace configurations considered in the steel brace database



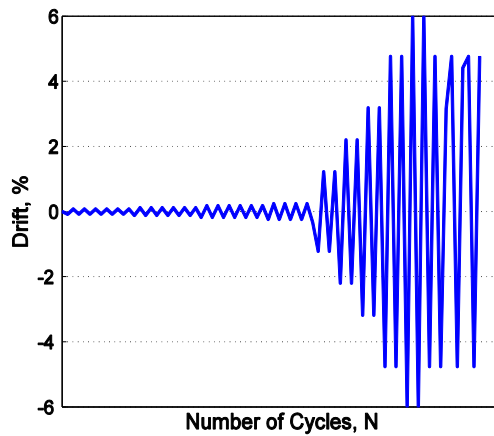
(a)



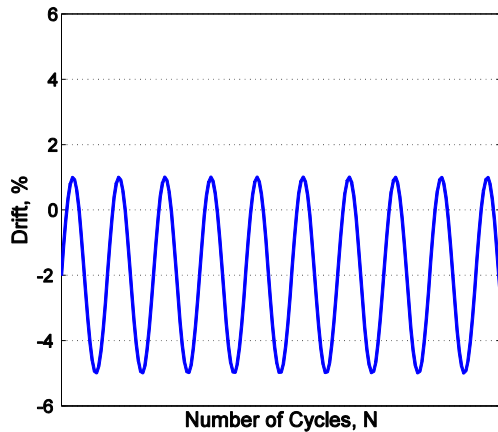
(b)



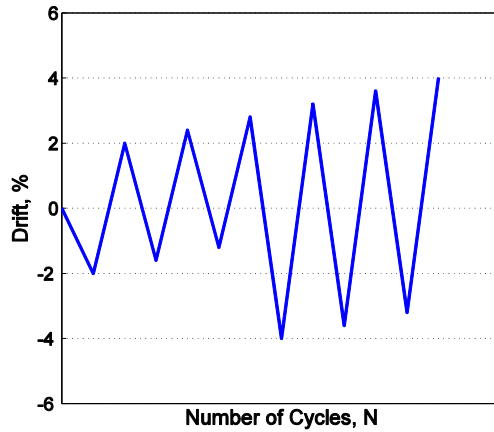
(c)



(d)



(e)



(f)

Figure 3.3 Loading protocols: (a) Symmetric Cyclic, (b) Far End, (c) Near Fault Compression, (d) Near Fault Tension, (e) Unsymmetrical Sine, (f) Increasing Asymmetric

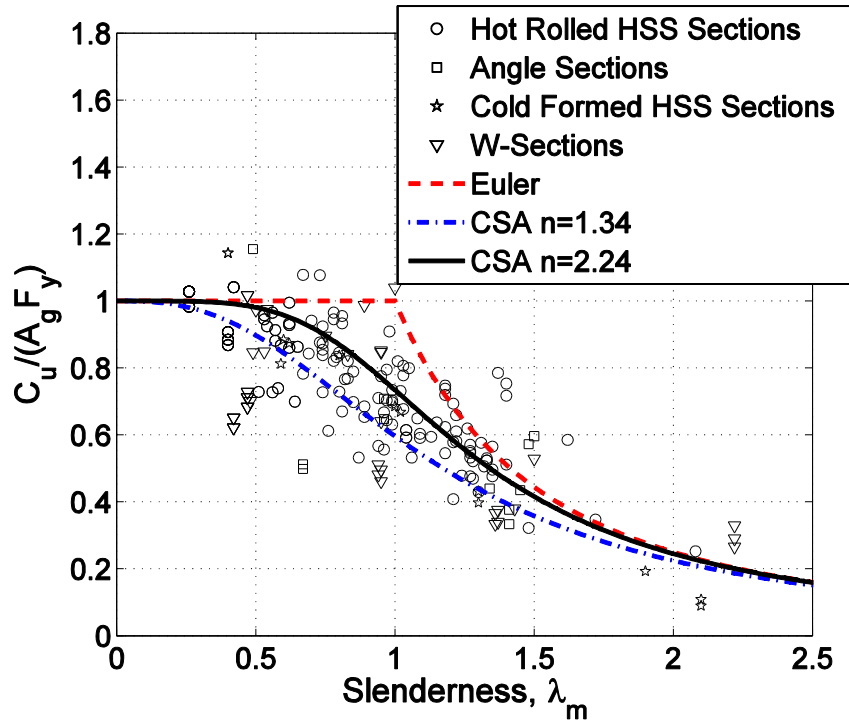


Figure 3.4 Normalized buckling load vs slenderness based on measured yield stress

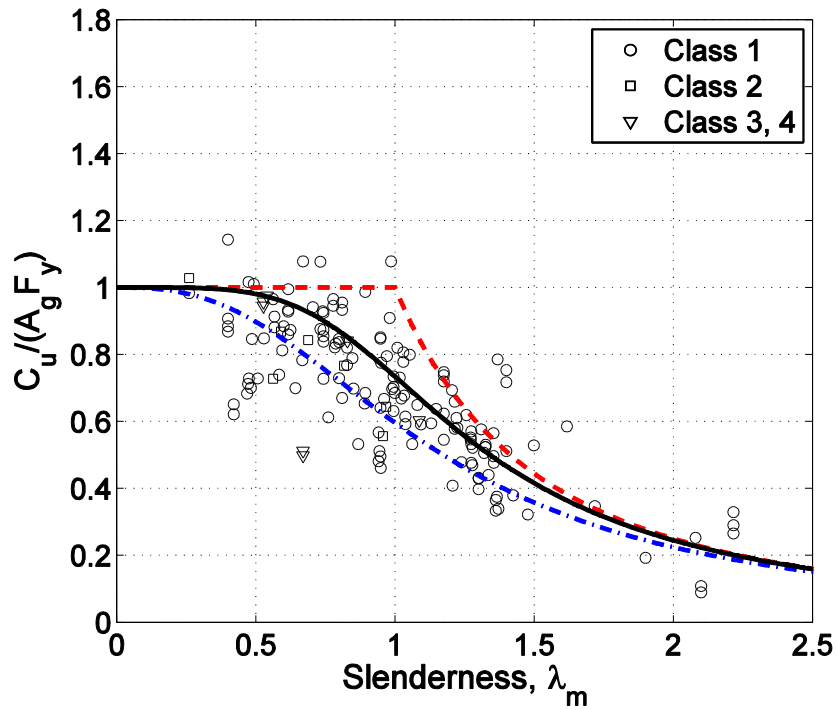


Figure 3.5 Normalized buckling load vs slenderness based on measured yield stress categorized by ductility classes

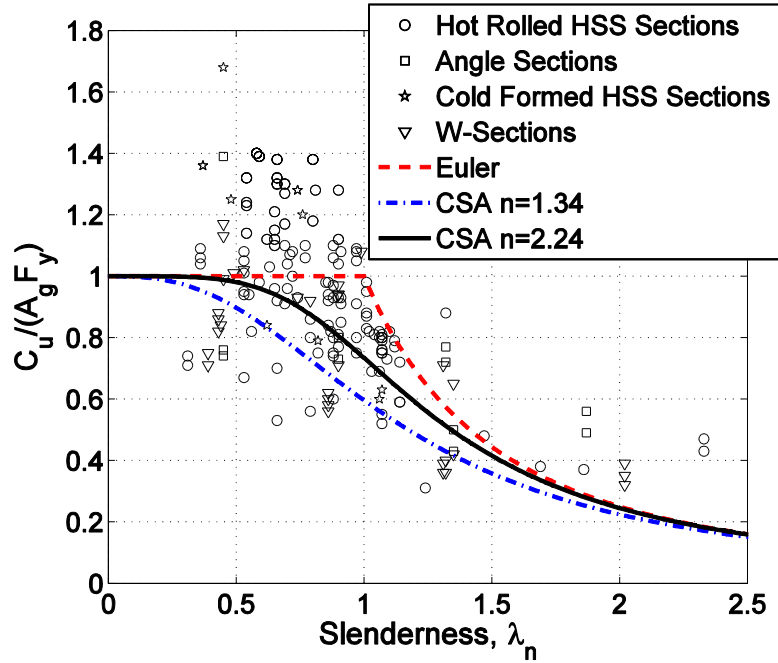


Figure 3.6 Normalized buckling load vs slenderness based on the nominal yield stress

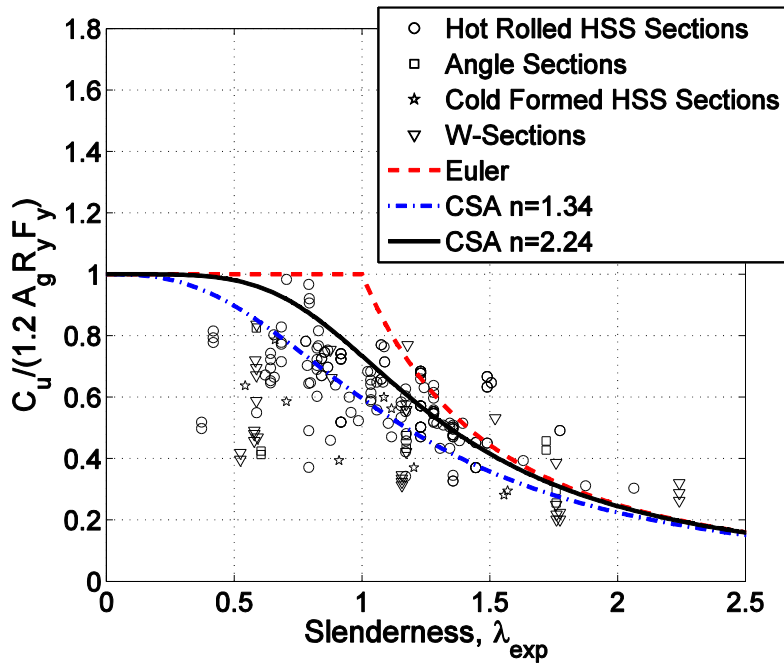


Figure 3.7 Normalized buckling load vs slenderness based on the probable yield stress as defined in CSA-S16-09

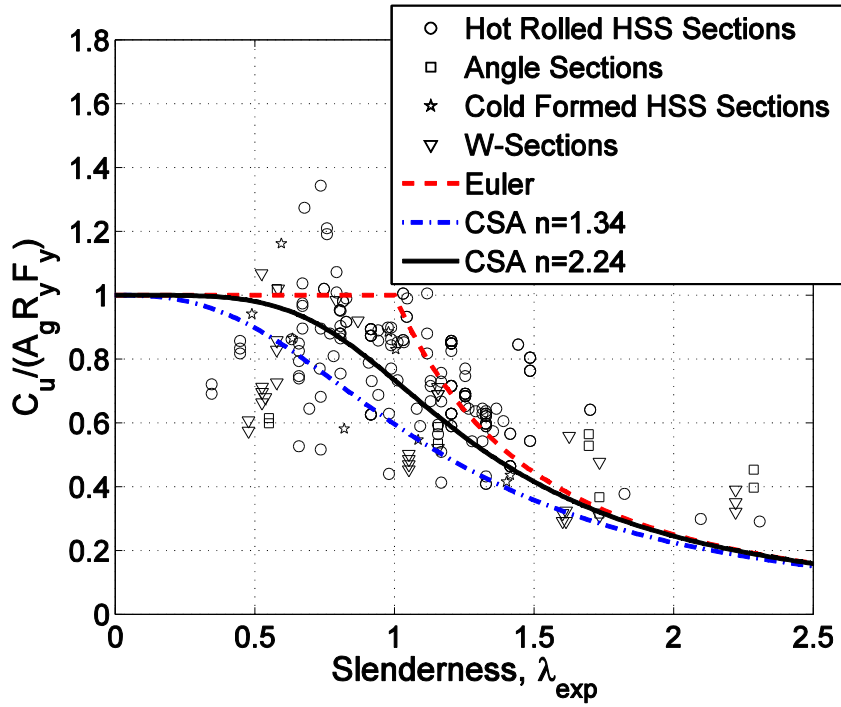


Figure 3.8 Normalized buckling load vs slenderness based on the expected yield stress as defined in AISC-341-10



# Chapter 4

## Drift-Based Fragility Curves for Rapid Earthquake Damage Assessment of Concentrically Braced Frames

---

### 4.1 Purpose and Scope

The next generation of Performance-Based seismic design procedures for new and existing buildings necessitate the development of tools for rapid earthquake damage assessment of buildings. These procedures should assess the earthquake performance of individual buildings based on their unique site, structural, non-structural and occupancy characteristics (ATC-58, 2012a,b). In the case of steel braced frames the general framework for their performance-based assessment should be able to characterize earthquake damage of the steel braces. This chapter discusses the development of fragility curves that characterize three discrete damage states that are associated with steel brace earthquake damage in concentrically braced frames. These fragility curves have been developed for different steel brace shapes that are commonly used in steel construction practice. Dual parameter fragility curves are also developed that associated the three discrete damage states of a steel brace with its global slenderness ratio and the story drift ratio that the individual damage states occur.

## 4.2 Definition of Damage States

Several discrete damage states (*DS*) should be considered in order to describe earthquake damage in steel braced frames. These damage states should describe failure modes associated with the steel brace component, gusset plates and the associated steel frame (ATC-58, 2012a,b). The investigation presented in this thesis is only concerned with three key damage states associated with steel brace components. These damage states were selected based on damage observations from large-scale experiments (see Chapter 3) of steel braces subjected to cyclic loading. The three damage states are associated with brace flexural buckling, brace local buckling at its mid-length and finally brace stress loss, i.e., loss of axial force capacity due to fracture at the mid-length of the brace. These failure modes are shown in Figure 4.1. It should be noted that steel braces that fail in a brittle manner at their ends due to premature fracture are not part of this investigation.

### 4.2.1 $DS_1$ Brace Flexural Buckling

Brace flexural buckling corresponds to the first occurrence of axial force strength deterioration of a steel brace subjected to compressive stresses. These stresses are typically less than the yield compressive stresses that the steel material is capable of withstanding. During this damage state, the out-of-plane brace deformation is typically less than the brace depth (Tremblay 2002). The story drift ratio (*SDR*) that corresponds to this damage state is either based on values reported by the investigator conducting the experiment or obtained from the fully digitized axial load – brace elongation hysteretic diagram as shown in Figure 4.2. Figure 4.1a shows an example of  $DS_I$  based on a recent experiment by Fell et al. (2009).

### **4.2.2 DS<sub>2</sub> Brace Local Buckling**

This damage state corresponds to a case that a plastic hinge forms at the midpoint of a steel brace when it is subjected to compressive stresses. The steel brace experiences local buckling at this location (see Figure 4.1b). Figure 4.2 illustrates the associated definition of  $DS_2$  on an axial force – brace elongation hysteretic diagram. It should be noted that in case that the associated story drift ratio that local buckling occurred during the experiment was not reported by the investigator, this point was assumed to be at the story drift ratio associated with 40% axial force reduction after global buckling occurred in the component. This value was determined based on experimental reports that did include the story drift ratio that local buckling occurred such as Fell et al. (2009).

### **4.2.3 DS<sub>3</sub> Brace Strength Loss – Loss of Force Capacity**

This damage state corresponds to the case that considerable loss of the tensile force capacity of a steel brace has occurred due to ductile fracture at the midpoint of the brace. Figure 4.2 shows the definition of this damage state on a hysteretic diagram of a steel brace subjected to cyclic loading. This failure mode is triggered by cyclic loading at the point of plastic hinge formation of the steel brace as discussed in  $DS_2$ . The fracture initiates due to low cycle fatigue and then propagates by ductile tearing through the brace cross section. Figure 4.1c illustrates this phenomenon that occurred during cyclic testing of an HSS steel brace (Fell et al. 2009).

Table A.1 (see Appendix A) presents all the information that was gathered as part of this research including the range of the material and geometric parameters discussed

previously. In the last three columns of this table the story drift ratios associated with the three damage states discussed above are documented. The large variability in the reported *SDR* levels with the progression of damage from  $DS_1$  to  $DS_3$  necessitates the use of a probabilistic approach for estimating the probability of reaching or exceeding the three discrete damage states. In many cases, there was no information to establish the *SDR* at which all three damage states took place either because the information from the experimental reports did not include sufficient details for identifying the *SDR* at which the damage states occurred or because the damage state did not occur (e.g., not all the specimens were tested through fracture).

### **4.3 Drift-Based Fragility Curves for Steel Braces**

The steel database that has been discussed in detail in Chapter 3 of this thesis is utilized to develop drift-based fragility curves for performance-based evaluation of concentrically braced frames. These curves estimate the probability of reaching or exceeding the discrete *DSs* as *SDR* increases. The process discussed herein to develop fragility curves for steel braces is general and can be applied to other structural and/or non-structural components (Aslani and Miranda 2005, Garcia and Negrete 2009, Lignos et al. 2010, Ramirez et al. 2012, ATC-58, 2012a,b). The empirical cumulative frequency distribution function for each damage state is obtained by sorting in ascending order the corresponding absolute peak *SDRs* at which  $DS_1$ ,  $DS_2$  and  $DS_3$  are observed from the experiments. The absolute peak *SDR* values are plotted against the computed probability equal to  $(i - 0.5)/n$ , where  $i$  is the position of the peak story drift ratio and  $n$  is the number of the steel brace specimens included in the data subsets used for each damage

state. Figures 4.3, 4.4 and 4.5 show the empirical cumulative distributions for rectangular HSS braces, round HSS, W- and L- shape braces for flexural buckling ( $DS1$ ), local buckling ( $DS2$ ) and fracture ( $DS3$ ), respectively.

In order to characterize the cumulative empirical distribution for each damage state, three different probability distributions were employed to fit the empirical data including the Weibull, Gumbel and lognormal distribution. These distributions were determined based on the maximum likelihood method (Venables and Ripley 2002). The best fit was found by using the lognormal distribution that is fully defined by two statistical parameters that incorporate the central tendency ( $\mu_{SDR}$ ) and dispersion ( $\beta_{\ln SDR}$ ) of each one of the datasets used as follows,

$$P(DS \geq ds_i | SDR = sdr) = \Phi \left[ \frac{\ln(sdr) - \ln(\mu_{SDR})}{\beta_{\ln SDR}} \right] \quad (4.1)$$

In Equation (4.1),  $P(DS \geq ds_i | SDR = sdr)$  is the conditional probability of reaching or exceeding damage state  $i$ , at a story drift ratio ( $sdr$ ) and  $\Phi$  is the standard normal cumulative distribution. In order to verify if the lognormal cumulative distribution adequately characterizes each one of the empirical distributions shown in Figures 4.3, 4.4 and 4.5, a Kolmogorov-Smirnov (K-S) goodness-of-fit test was employed (Benjamin and Cornell 1970). The same figures show a graphical representation of the K-S tests at 5% significance level for the fragility curves developed as part of this research. Since all the data points from the empirical cumulative distributions lie between the two dashed lines for all the cases presented in Figures 4.3 to 4.5, the hypothesis that the assumed

lognormal distribution is acceptable holds true for all three damage states regardless of the steel brace shape.

The statistical parameters that fully define the lognormal cumulative distributions for each subset of steel braces and for the three discrete damage states are summarized in Tables 4.1 to 4.4. From these tables, aleatory and epistemic uncertainties are reflected in the dispersion term  $\beta_{lnSDR}$  of the fragility curves. In this research, four different sources of epistemic uncertainty have been considered including the finite sample uncertainty, the specimen-to-specimen variability, the uncertainty due to the geometric configuration of the steel braces and the uncertainty due to the loading protocol that was used during the individual component experimentation. From the corresponding low values of dispersion that are reported in Tables 4.1 to 4.4 the developed fragility curves shown in Figures 4.3 to 4.5 provide a reliable way to estimate the likelihood of buckling (global and local) and fracture at the midpoint of steel braces if only the peak *SDR* is used as a single engineering demand parameter to characterize damage in steel braced frames.

#### **4.4 Incorporating Other Sources of Uncertainty**

The drift-based fragility curves presented in Section 4.3 include the specimen-to-specimen variability only. However, the three other sources of epistemic uncertainty should be taken into consideration based on the information that has been retrieved from the experimental database. The first one is related to the uncertainty caused from the finite sample size  $n$  data. The accuracy of any mean estimate derived from a finite sample relies on the central limit theorem of probability. For an infinite sample size and for

uncorrelated data, the distribution of sample means will tend to a normal distribution independent of the form of the parent distribution (Laplace 1812, Ross 2003). For the case of uncorrelated finite sample size  $n$  data the rate at which the sample mean converges to the parent distribution mean is fast. The sample mean will converge slower than  $1/\sqrt{n}$  if correlations exist in the data.

The second source of uncertainty is related to the fact that different geometric testing configurations have been used to compile the experimental database that is used as part of this research (see Chapter 3). The third source of uncertainty is related to the fact that the *SDRs* that are reported in Table A.1 (see Appendix A) are associated with peak values of a pre-defined loading protocol (see Aslani and Miranda 2005, Lignos et al. 2010). A steel brace when subjected to a loading protocol can reach any of the three discrete damage states discussed previously during a loading cycle and not necessarily at a pre-defined peak. The finite sample epistemic uncertainty can be considered for each damage state and steel brace structural shape by computing confidence intervals for the standard deviation  $\beta_{\ln SDR}$  based on Crow et al. (1960),

$$\left[ \frac{(n-1) \cdot \beta_{\ln SDR}^2}{X_{a/2, n-1}^2} \right]^{1/2} \text{ and } \left[ \frac{(n-1) \cdot \beta_{\ln SDR}^2}{X_{1-a/2, n-1}^2} \right]^{1/2} \quad (4.2)$$

In Equation (4.2),  $X_{a/2, n-1}$  and  $X_{(1-a)/2, n-1}$  are the inverses of the  $X^2$  distribution having  $n-1$  degrees of freedom and a probability of occurrence of  $a/2$  and  $(1-a)/2$ , respectively. All sources of epistemic uncertainty discussed in this section were taken into consideration in the central tendency  $\mu_{SDR}$  of the SDR associated to each damage state by

approximating  $\mu_{SDR}$  as discussed in Crow et al. (1960),

$$\left(\mu_{SDR} - \frac{SDR\mu_{SDR}}{2}\right) \cdot \exp\left[\pm z_{a/2} \cdot \frac{\beta_{\ln SDR}}{\sqrt{n}}\right] \quad (4.3)$$

In Equation (4.3)  $z_{a/2}$  is the value in the standard normal distribution such that the probability of a random deviation numerically greater than  $z_{a/2}$  is  $a$  and  $n$  is the data sample size. Tables 4.5 to 4.8 summarize the effects of epistemic uncertainty on the lognormal cumulative distributions for each one of the three discrete damage states and the structural shape used per brace for a 90% confidence interval. Figure 4.6 also demonstrates the influence of the additional sources of epistemic uncertainty on the fragility curves for  $DS_3$  for HSS, round HSS, W-shape and L-shape braces. This figure essentially includes the envelope of shifted fragilities for  $DS_3$  that Tables 4.5 to 4.8 summarize for the four main types of steel braces. These plots are particularly useful for computing the probability of being or exceeding  $DS_3$  if  $SDR$  is used as a single engineering demand parameter to characterize earthquake damage in concentrically braced frame. For instance, there is a 50% probability that round HSS braces fracture at midpoint at a story drift ratio between 2.33% and 3.25% (see Figure 4.6b). Moreover, the probability of exceedence of a damage state such as fracture can be shifted. From the same figure, the probability of exceeding  $DS_3$  varies from 11.8% to 41% when a round HSS steel brace is subjected to a 2% story drift ratio, while including only specimen-to-specimen variability indicates that there is only a probability of 26.5% for the same story drift ratio.

#### 4.4.1 Influence of the Material Type on the Fragility Curves

This section discusses the influence of the material type of a steel brace on the fragility curves for the three discrete damage states discussed in Section 4.2. From this investigation, the angle (L) braces are excluded. The reason is that these braces have been fabricated by either A36 or SS400 steel. These two steel types have the same nominal yield stress [235MPa (36ksi)]. Therefore the influence of the material type on L-shape braces is not visible. The process discussed in Section 4.2 is used to develop the drift-based fragility curves for different material types for HSS, round HSS and W-shape steel braces. Figures 4.7, 4.8 and 4.9 illustrate the fragility curves for these three steel brace shapes for  $DS_1$ ,  $DS_2$  and  $DS_3$ , respectively. From Figure 4.7, it is observed that the higher the yield stress of a steel brace the larger the story drift ratio that global buckling occurs. For instance, from Figure 4.7a, a HSS brace fabricated by A500 Gr.B steel ( $f_{y,nominal} = 345\text{MPa}$ ) in average buckles globally at a  $\mu_{SDR} = 0.39\%$  compared to a HSS brace that is fabricated by S235 JRH steel ( $f_{y,nominal} = 235\text{MPa}$ ). The latter buckles globally in average at a  $\mu_{SDR} = 0.32\%$ . Similar findings are observed from Figures 4.7b and 4.7c when the influence of the steel material is examined on the fragility curves for round HSS and W-shape braces, respectively. Looking at local buckling from Figure 4.8 that shows the influence of the steel material on the fragility curves for  $DS_2$  for HSS, round HSS and W-shape braces, it is observed that in average a higher strength steel brace buckles locally at its midpoint at a larger story drift ratio compared to a lower steel strength brace.

The influence of the steel material on the fragilities for the fracture damage state ( $DS_3$ ) of the steel braces is the opposite compared to the one observed for  $DS_1$  and  $DS_2$ . This can

be seen in Figure 4.9. From this figure, a steel brace fabricated by higher yield stress steel will typically fracture at a lower story drift ratio than a steel brace fabricated by a lower yield stress steel. For instance, HSS steel braces (see Figure 4.9a) fabricated by A500Gr.B ( $f_{y,nominal} = 345\text{MPa}$ ) fracture in average at about  $\mu_{SDR} = 1.5\%$  compared to HSS braces fabricated by SS235 JRH steel ( $f_{y,nominal} = 235\text{MPa}$ ) that fracture in average at about  $\mu_{SDR} = 2.3\%$ . This issue is attributed to the fabrication process that is typically necessary to achieve higher yield stresses. The fabrication process typically involves alloying or quenching and tempering (see Van Vlack 1980). These processes typically reduce the maximum elongation at fracture and the length of the plastic plateau of a stress strain curve of a steel material. From Figure 4.9c, the material influence on the fragility curves for  $DS_3$  diminishes for W-shape steel braces. However, it is believed that this occurs due to the small sample of W-shape braces that are available in the literature.

#### 4.4.2 Influence of the Global Slenderness Ratio on the Fragility Curves

This section discusses the influence of the global slenderness ratio ( $KL/r$ ) on the fragility curves for the four main brace shapes discussed in this chapter. For this reason, dual parameter fragility curves have been developed for  $DS_1$ ,  $DS_2$  and  $DS_3$ . To develop these distributions a joint lognormal cumulative distribution is employed. The story drift ratio  $SDR$  associated with each one of the damage states  $DS_1$ ,  $DS_2$ ,  $DS_3$  is assumed to be jointly lognormal with  $KL/r$ . In order to construct a joint lognormal cumulative distribution, the 2x2 covariance matrix needs to be constructed. However, the cross correlation of  $SDR$  with respect to  $KL/r$  is almost zero based on the data sample that we have available regardless of the steel brace shape. This indicates that these two variables can be treated

as statistically independent. Therefore, the joint lognormal distribution can be written as follows based on the total probability theorem,

$$P\left(DS \geq ds_i | SDR = sdr \ \& \ \frac{KL}{r} = kl/r\right) = \Phi\left[\frac{\ln(sdr) - \ln(\mu_{SDR})}{\beta_{\ln SDR}}\right] \Phi\left[\frac{\ln(kl/r) - \ln(\mu_{KL/r})}{\beta_{\ln KL/r}}\right] \quad (4.4)$$

The mean  $\mu$  and standard deviation  $\beta$  of the two distributions is estimated with the method of the maximum likelihood. Figures 4.10, 4.11 and 4.12 show the dual parameter fragility curves for  $DS_1$ ,  $DS_2$  and  $DS_3$ , respectively, for the four basic steel brace shapes discussed in this chapter. From these figures, a number of findings are summarized:

- In general, L-shape braces typically buckle globally at a lower story drift ratio for the same  $KL/r$  ratio compared to the other three steel brace shapes. This is attributed to the fact that L-shape braces are susceptible to lateral torsional buckling.
- The effect of  $KL/r$  on  $DS_1$  (global buckling) is important regardless of the steel brace shape since a steel brace will typically buckle in flexure rapidly for  $KL/r$  ratios larger than 100. Therefore, the limit of  $KL/r < 100$  that is employed by seismic requirements (AISC 2010, CSA-S16, 2009) is satisfactory.
- The effect of  $KL/r$  on  $DS_3$  (fracture) diminishes regardless of the steel brace shape. This is to be expected since this damage state occurs after local buckling occurs at the midpoint of a steel brace. Therefore, the local slenderness of the cross section controls the post-buckling behaviour of a steel brace. This important finding is further explained in Chapter 5 (see Sections 5.5, 5.6 and 5.7 for HSS, round HSS and W-shape steel braces, respectively) and has been confirmed by a recent

experimental study by Fell et al. (2009).

- W-shape braces would typically fracture at a larger story drift ratio followed by round HSS, followed by HSS and finally followed by L-shape braces. This indicates that in average, for the same loading history, the fracture life of W-shape steel braces is larger compared to the other shape steel braces.

## 4.5 Summary

This chapter summarizes the development of drift-based and dual parameter fragility curves that characterize three discrete damage states observed in HSS, round HSS, W-shape and L-shape braces. These damage states are associated with global buckling, local buckling and fracture at the midpoint of a steel brace. Braces that fail in a brittle manner at their ends due to premature fracture are not part of this investigation. The proposed fragility curves can be used for rapid earthquake damage assessment of steel braced frames in accordance with the next generation of performance-based earthquake evaluation procedures for new and existing buildings. The proposed fragility curves reflect engineering principles. A second set of fragility curves is also developed. This set includes four different sources of epistemic uncertainty. These uncertainties are associated with finite sample, testing configurations, the associated peak values of a pre-defined loading protocol that each damage state is observed and finally the material properties of the steel material. Further investigation related to the material influence on the fragility curves for HSS, round HSS and W-shape steel braces demonstrated that in average, a steel brace fabricated with lower yield stress steel typically buckles globally and locally at a lower story drift ratio compared to an equivalent steel brace fabricated

with higher yield stress steel. However, due to the fabrication process to achieve higher yield stresses for steel, a steel brace fabricated with such material would typically fracture at a lower story drift ratio compared to an equivalent steel brace fabricated with low yield stress steel. Finally, the influence of the global slenderness ratio  $KL/r$  on the three discrete damage states for steel braces is examined through dual parameter fragility curves. The main finding from this investigation is that the effect of  $KL/r$  ratio on  $DS_3$  (fracture) diminishes regardless of the steel brace shape. This is to be expected since this damage state occurs after local buckling occurs at the midpoint of a steel brace. Therefore, local slenderness of the steel brace cross section controls fracture at this location (post-buckling behaviour).

Table 4.1. Statistical parameters for fragility curves for HSS braces

Damage State	HSS			
	$\mu_{SDR}\%$	$m_{SDR}\%$	$\beta_{lnSDR}$	Number of specimens (n)
DS1	0.4	0.41	0.43	116
DS2	1.02	1.05	0.44	112
DS3	1.60	1.60	0.48	104

Table 4.2. Statistical parameters for fragility curves for round HSS braces

Damage State	Round HSS			
	$\mu_{SDR}\%$	$m_{SDR}\%$	$\beta_{lnSDR}$	Number of specimens (n)
DS1	0.41	0.43	0.51	48
DS2	0.96	0.98	0.45	37
DS3	2.75	2.81	0.51	25

Table 4.3. Statistical parameters for fragility curves for W-shape braces

Damage State	W-Shape			
	$\mu_{SDR}\%$	$m_{SDR}\%$	$\beta_{lnSDR}$	Number of specimens (n)
DS1	0.28	0.3	0.58	56
DS2	0.87	1.01	0.54	44
DS3	3.10	3.70	0.41	18

Table 4.4. Statistical parameters for fragility curves for L-shape braces

Damage State	L-Shape			
	$\mu_{SDR}\%$	$m_{SDR}\%$	$\beta_{lnSDR}$	Number of specimens (n)
DS1	0.27	0.26	0.51	23
DS2	0.70	0.72	0.65	22
DS3	1.43	1.23	0.52	5

Table 4.5. Statistical parameters for HSS braces considering all sources of epistemic uncertainty

Damage State	HSS			
	$\mu_{SDR} \%$ 10% CI	$\mu_{SDR} \%$ 90% CI	$\beta_{lnSDR}$ 10% CI	$\beta_{lnSDR}$ 90% CI
DS1	0.43	0.37	0.39	0.48
DS2	1.09	0.95	0.40	0.50
DS3	1.73	1.48	0.43	0.54

Table 4.6. Statistical parameters for round HSS braces considering all sources of epistemic uncertainty

Damage State	Round HSS			
	$\mu_{SDR} \%$ 10% CI	$\mu_{SDR} \%$ 90% CI	$\beta_{lnSDR}$ 10% CI	$\beta_{lnSDR}$ 90% CI
DS1	0.46	0.36	0.44	0.62
DS2	1.08	0.85	0.38	0.56
DS3	3.25	2.33	0.41	0.67

Table 4.7. Statistical parameters for W-shape braces considering all sources of epistemic uncertainty

Damage State	W-Shape			
	$\mu_{SDR} \%$ 10% CI	$\mu_{SDR} \%$ 90% CI	$\beta_{lnSDR}$ 10% CI	$\beta_{lnSDR}$ 90% CI
DS1	0.32	0.25	0.50	0.69
DS2	0.99	0.76	0.46	0.66
DS3	3.63	2.64	0.32	0.57

Table 4.8. Statistical parameters for L-shape braces considering all sources of epistemic uncertainty

Damage State	L-Shape			
	$\mu_{SDR} \%$ 10% CI	$\mu_{SDR} \%$ 90% CI	$\beta_{lnSDR}$ 10% CI	$\beta_{lnSDR}$ 90% CI
DS1	0.32	0.23	0.41	0.68
DS2	0.88	0.56	0.52	0.87
DS3	2.10	0.98	0.34	1.23

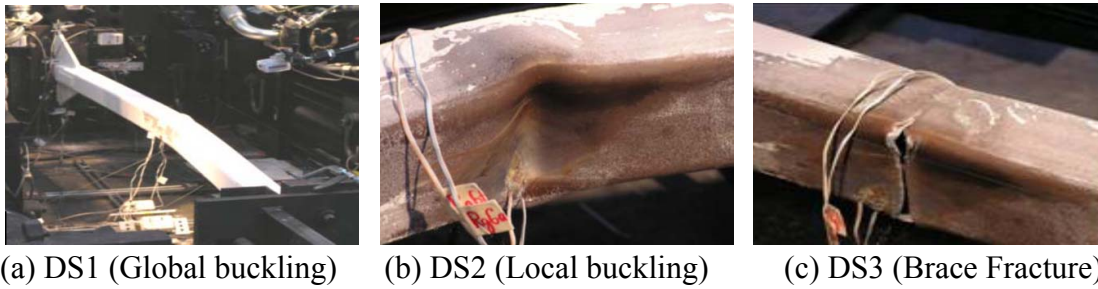


Figure 4.1 Damage stages for steel braces (photos from Fell et al. 2009)

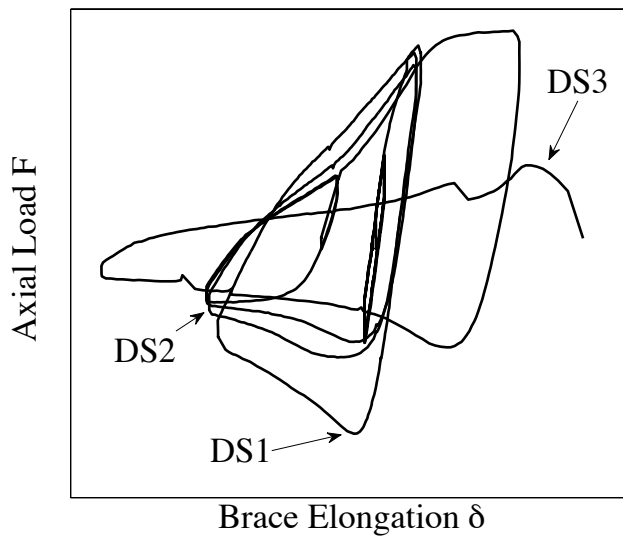
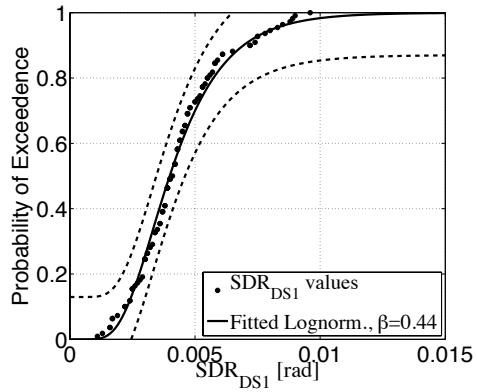
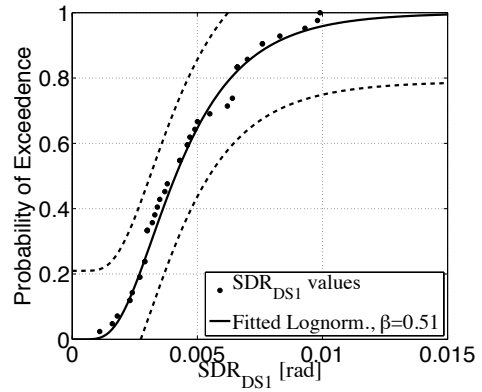


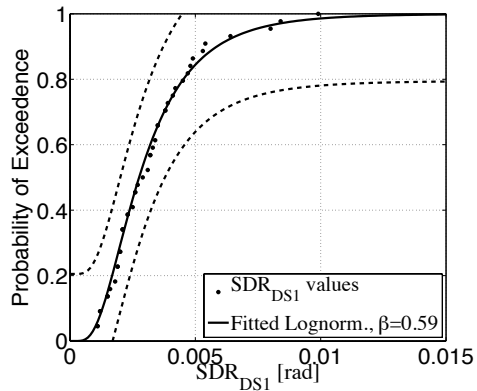
Figure 4.2 Definition of damage states for a typical steel brace



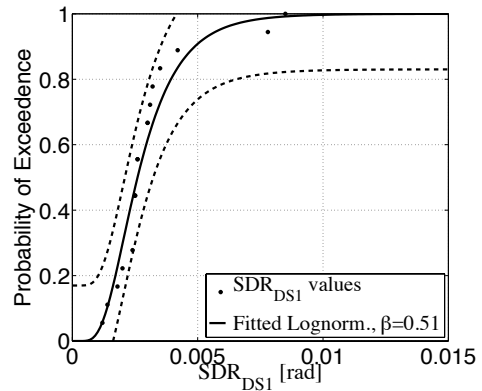
(a) HSS



(b) round HSS

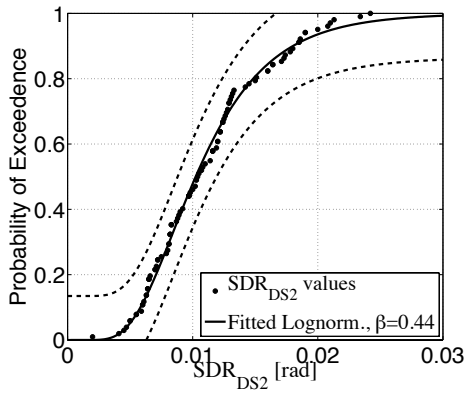


(c) W-shape

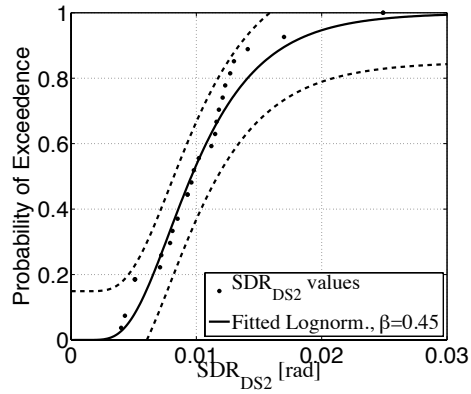


(d) L-shape

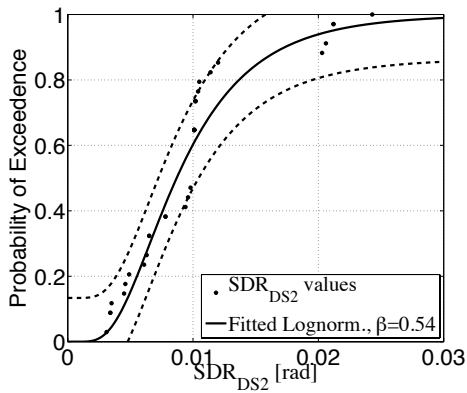
Figure 4.3 Drift-based fragility curves for damage state  $DS1$  for HSS, round HSS, W- and L-shape steel braces



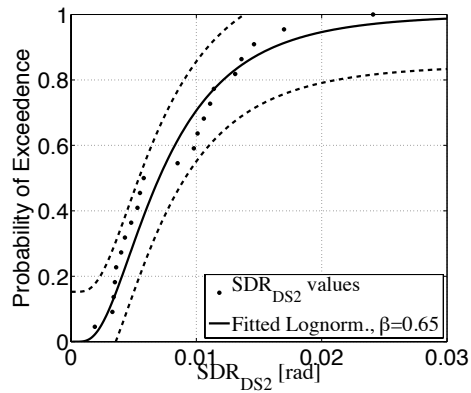
(a) HSS



(b) round HSS

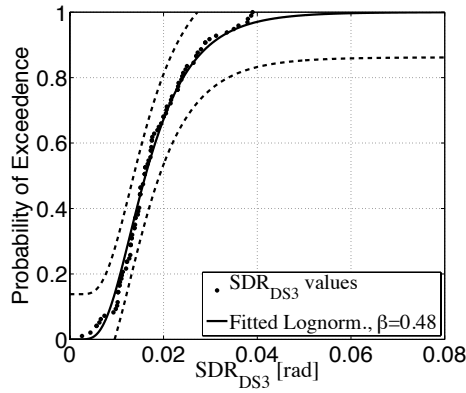


(c) W-shape

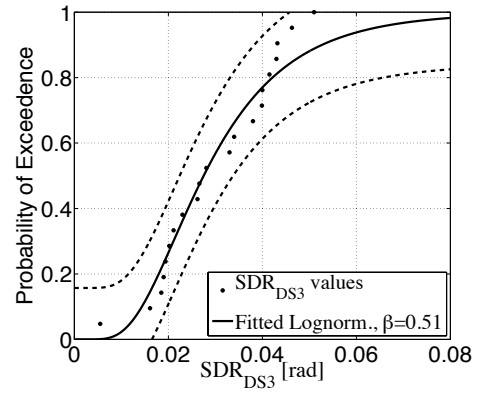


(d) L-shape

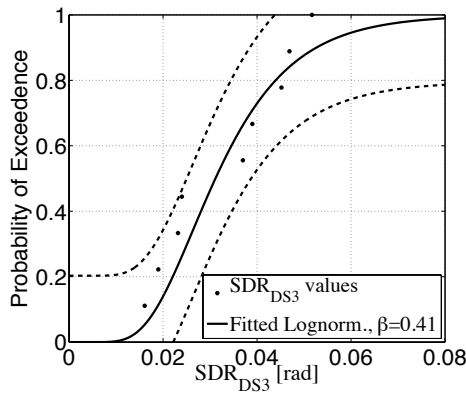
Figure 4.4 Drift-based fragility curves for damage state  $DS_2$  for HSS, round HSS, W- and L-shape steel braces



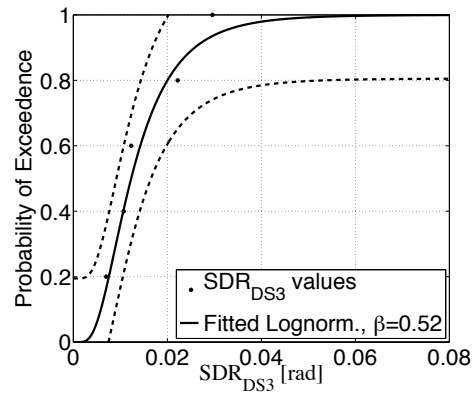
(a) HSS



(b) round HSS

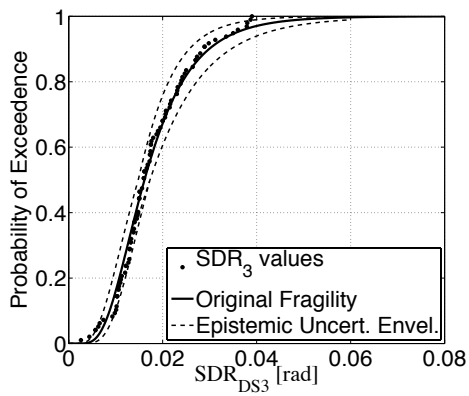


(c) W-shape

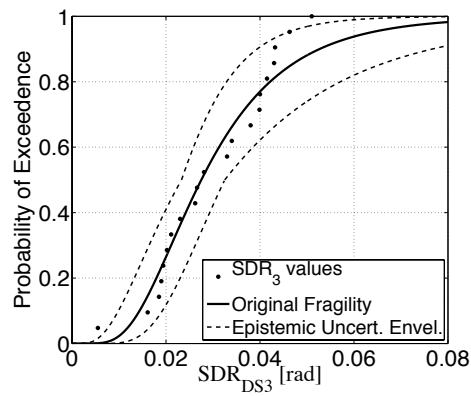


(d) L-shape

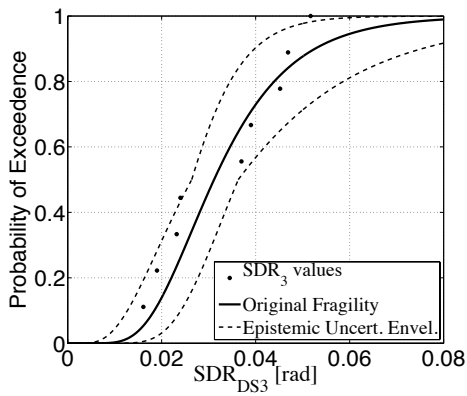
Figure 4.5 Drift-based fragility curves for damage state  $DS3$  for HSS, round HSS, W- and L-shape steel braces



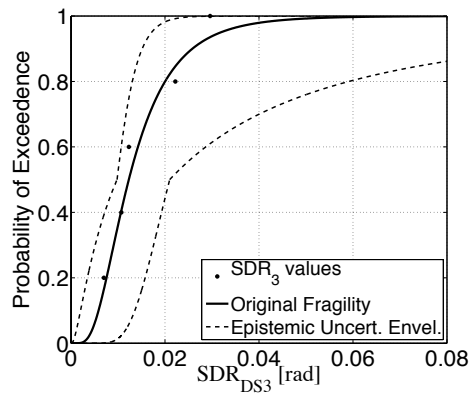
(a) HSS



(b) round HSS

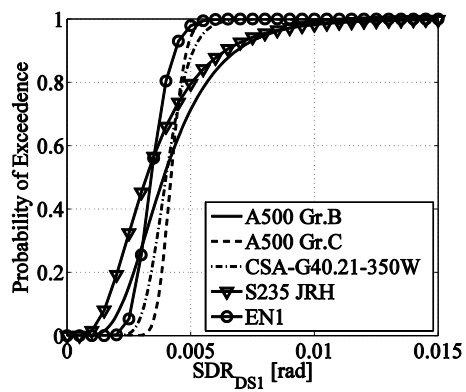


(c) W-shape

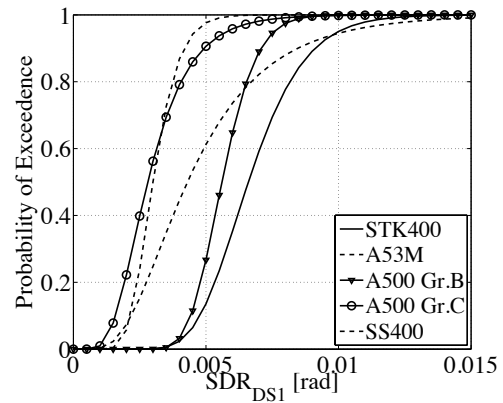


(d) L-shape

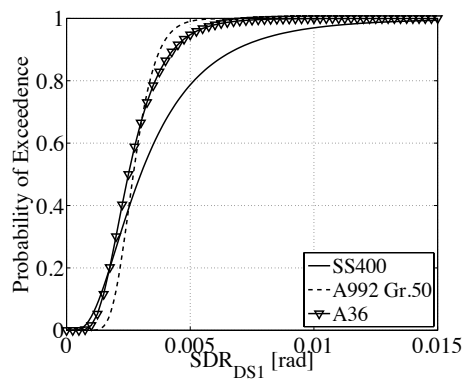
Figure 4.6 Drift-based fragility curves for damage state  $DS3$  for HSS, round HSS, W- and L-shape steel braces including the envelope of epistemic uncertainties on the fragility curves



(a) HSS

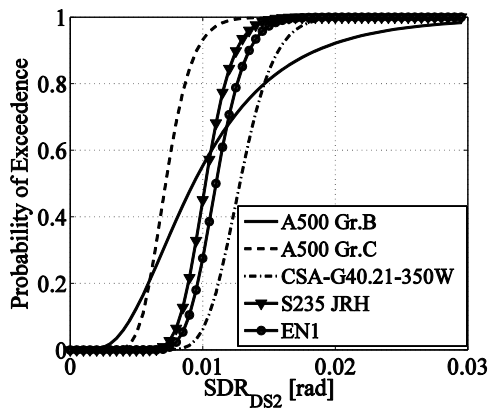


(b) round HSS

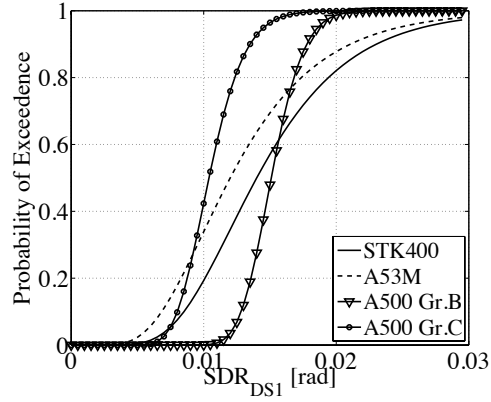


(c) W-shape

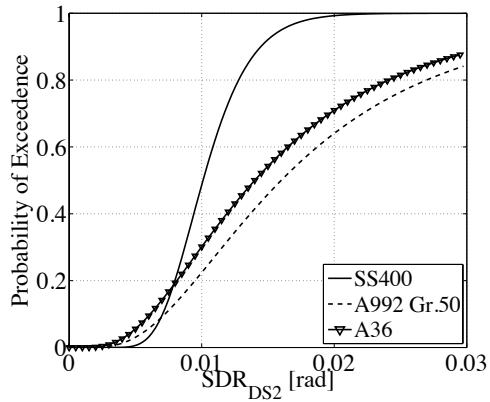
Figure 4.7 Material influence on the drift-based fragility curves for damage state  $DSI$  for HSS, round HSS and W- shape steel braces



(a) HSS

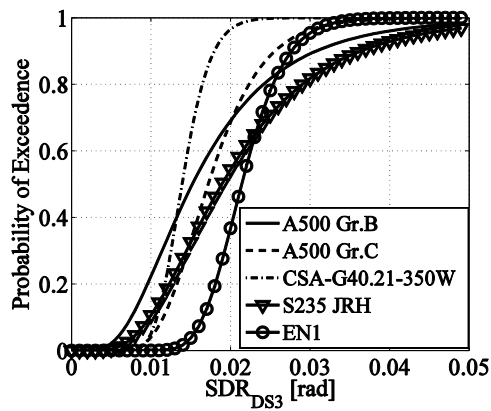


(b) round HSS

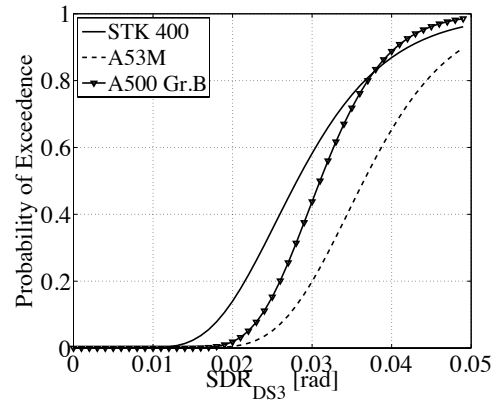


(c) W-shape

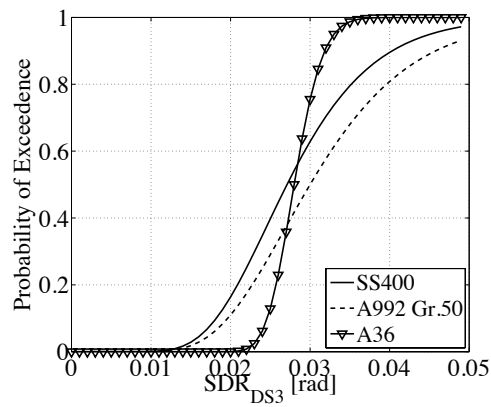
Figure 4.8 Material influence on the drift-based fragility curves for damage state  $DS_2$  for HSS, round HSS and W- shape steel braces



(a) HSS

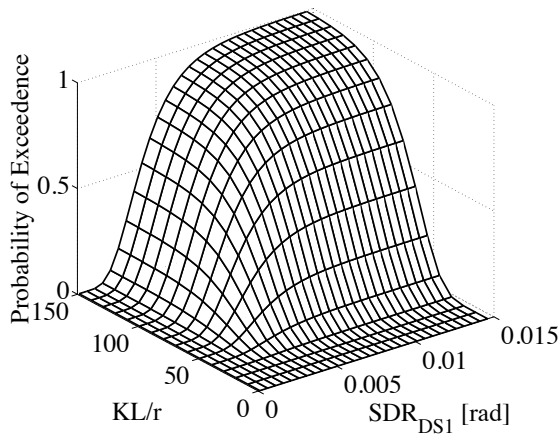


(b) round HSS

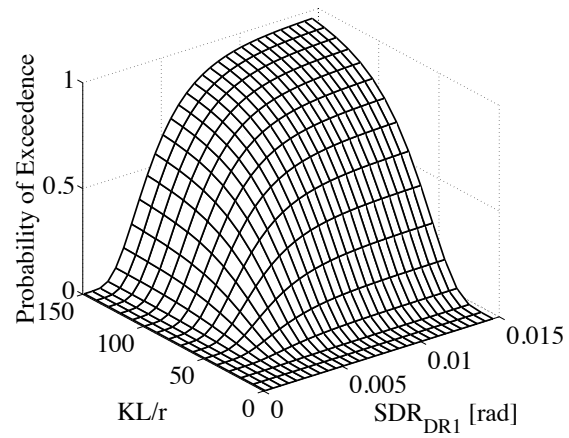


(c) W-shape

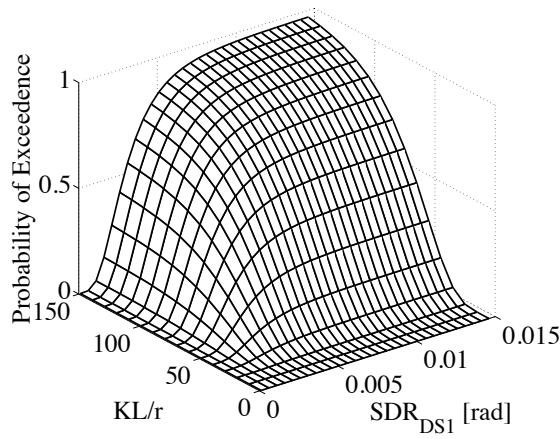
Figure 4.9 Material influence on the drift-based fragility curves for damage state  $DS3$  for HSS, round HSS and W- shape steel braces



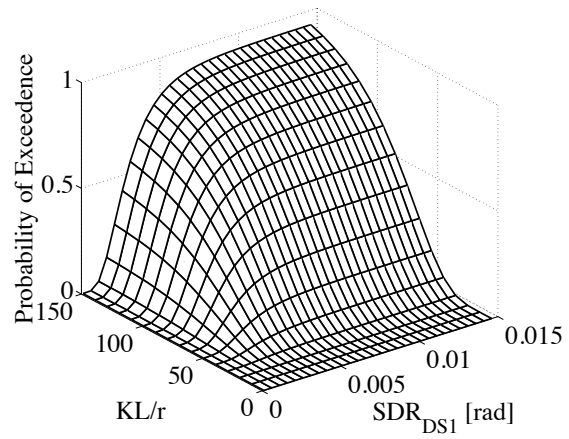
(a) HSS



(b) round HSS

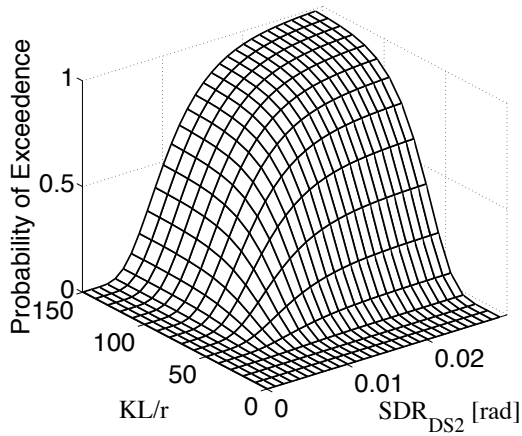


(c) W-shape

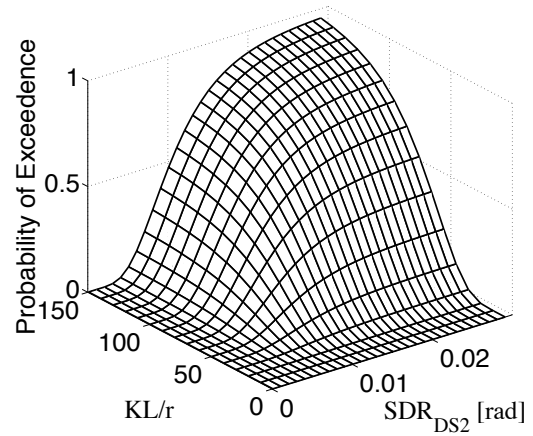


(d) L-shape

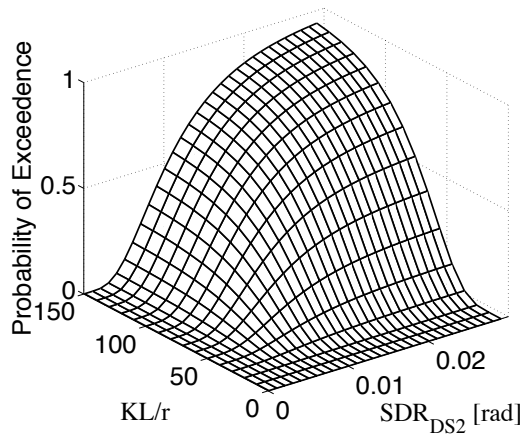
Figure 4.10 Dual parameter fragility curves for damage state  $DS1$  for HSS, round HSS, W- and L-shape steel braces



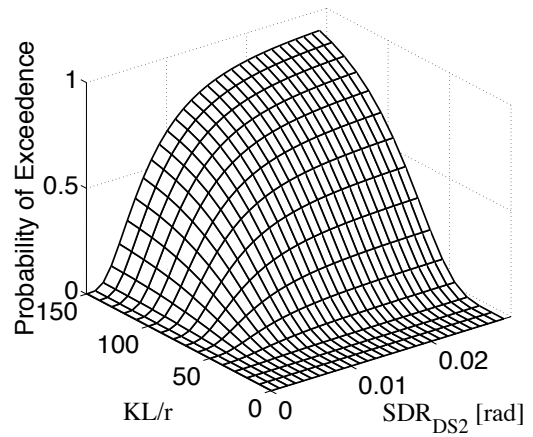
(a) HSS



(b) round HSS

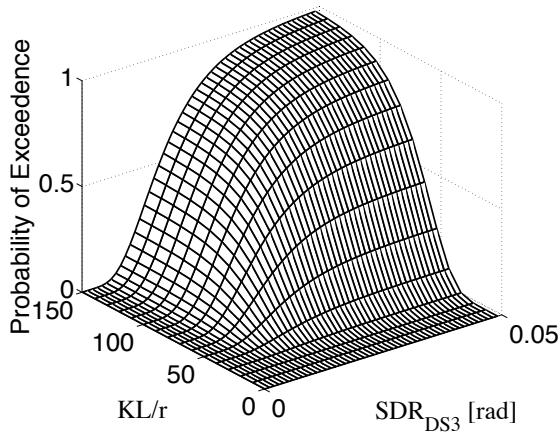


(c) W-shape

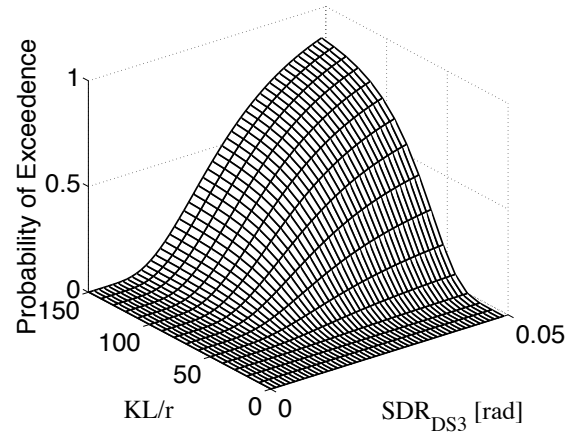


(d) L-shape

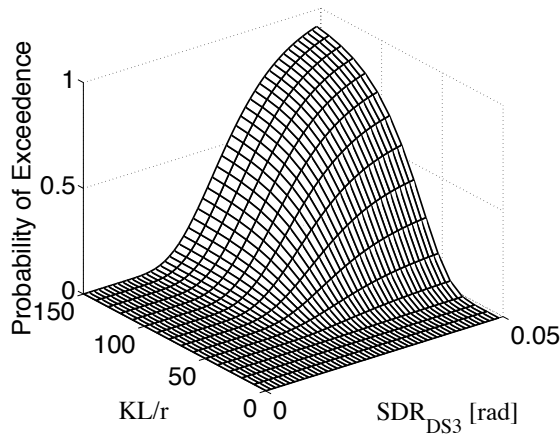
Figure 4.11 Dual parameter fragility curves for damage state  $DS2$  for HSS, round HSS, W- and L-shape steel braces



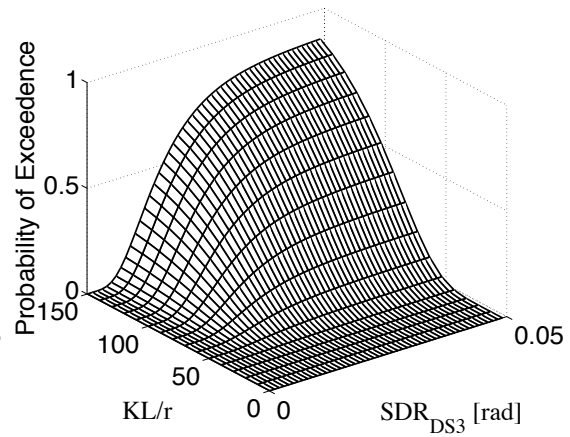
(a) HSS



(b) round HSS



(c) W-shape



(d) L-shape

Figure 4.12 Dual parameter fragility curves for damage state *DS3* for HSS, round HSS, W- and L-shape steel braces

# Chapter 5

## Relationships for Modelling Post-Buckling Behaviour and Fracture of Steel Braces

---

### 5.1 Introduction and Scope

The missing aspect of comprehensive modelling of post-buckling behaviour and fracture due to low cycle fatigue of steel braces is the availability of relationships that associate model parameters that control these deterioration modes with geometric and material properties of the steel braces. A state-of-the-art fibre-based brace component model is extensively calibrated with the digitized axial force – axial displacement hysteretic diagrams that became available from the steel brace database that was presented in Chapter 3. In support of reliable quantification of the collapse capacity of braced frames subjected to earthquakes, relationships and recommendations are proposed for modelling of the post-buckling behaviour and fracture of steel braces due to low cycle fatigue. The proposed relationships are empirical and reflect engineering principles, as they are developed with the use of multivariate regression analysis based on the experimental data that were discussed in Chapter 3.

### 5.2 Description of the Steel Brace Component Model

In order to model the post-buckling behaviour and fracture of a steel brace subjected to

cyclic loading, the brace component model proposed by Uriz (2005) and Uriz and Mahin (2008) is employed in the OpenSees simulation platform (McKenna 1997). This model is based on a force formulation that was originally proposed by Spacone et al. (1996) for reinforced concrete beam columns. This formulation uses a single element to represent the curvature distribution along the length of the brace. Due to its advantages such as proven reliability and robustness of the force formulation approach over other more commonly used displacement-based formulations, the force-based formulation approach is also used for the nonlinear static and dynamic analysis for the case studies discussed in Chapter 6.

The brace component, which is shown in Figure 5.1, is divided into several segments. In this research, the length of the brace is assumed to be equal with its effective length  $L_H$  (from point of inflection to point of inflection). Based on a sensitivity study that was conducted with a smaller subset of the steel brace database, it was found that eight segments are sufficient in order to capture the spread of plasticity along the brace and represent well its curvature. This also agrees with other analytical studies by Hsiao et al. (2012). Hence, the local strains and stresses are adequately represented. A fibre-based approach is used to model the brace cross section. Depending on the cross section, a different discretization process is employed as discussed later in Sections 5.5, 5.6 and 5.7 for rectangular Hollow Structural Section (HSS), round HSS (P) and wide flange (W-) shapes.

A uniaxial engineering stress-strain relationship is assigned to each one of the fiber

elements that are used to discretize the steel brace cross section. It was found that the number of fibers required differs for each cross section shape as discussed later in this chapter. The engineering stress-strain relationship is described with the Menegotto-Pinto model (Menegotto and Pinto, 1973), which is able to capture the Bauschinger effect and the cyclic hardening of the steel material (see Figure 5.1). This material model is fully defined by specifying the yield stress,  $F_y$ , of the material,  $E$ , the modulus of elasticity and  $b$ , the strain-hardening ratio. During the calibration process discussed in the later sections, the measured yield stress,  $F_y$ , from the collected brace tests were used as an input parameter. In case that  $F_y$  is not available, the expected yield stress as defined by AISC-341-10 (2010) provisions ( $R_y$  times  $F_y$ ) is used. For all of the calibrations the modulus of elasticity was assumed to be 200GPa. The strain-hardening ratio  $b$  was set equal to 0.1% for HSS and W- shape braces. For round HSS sections, a  $b=0.5\%$  was found to be more representative. The cyclic response of the Menegotto-Pinto material model is fully defined with a set of three empirical parameters ( $R_0$ ,  $cR_1$  and  $cR_2$ ) that control the transition from the elastic to the plastic branch. It was found that a  $cR_1 = 0.925$  and a  $cR_2 = 0.25$  represent well this transition for all the steel braces that were calibrated. However, the radius  $R_0$  affects the hysteretic response of the individual steel braces and it was considered as part of the calibration procedure. Cyclic hardening is controlled by four isotropic hardening parameters noted as  $a_1$ ,  $a_2$ ,  $a_3$ ,  $a_4$  (Filippou et al. 1983). The parameters  $a_1$  and  $a_3$  were considered as part of the calibration process to obtain a better match between the simulated and experimental hysteretic response of the steel braces. The parameters  $a_2$  and  $a_4$  were set equal to 1.0. The influence of the parameters  $R_0$ ,  $a_1$  and  $a_3$  on the parameter that controls fracture due to low cycle fatigue is discussed in Section

## 5.9.

The Gauss-Lobatto quadratic rule with five integration points at the element ends is used for the numerical integration within each segment. This reduced integration scheme allows for an efficient computation without compromising accuracy.

Global (flexural) buckling is captured with an initial camber (offset), in the mid-length of the brace (see Figure 5.1). Based on a sensitivity study with a number of different steel brace shapes, an initial camber of 0.1% of the brace length was found to adequately capture the flexural buckling load of a brace regardless its shape. This agrees with earlier studies by Uriz (2005) and Agüero et al. (2006).

Note that if different number of segments, fibers and integration points are employed to represent the steel brace, the component behaviour will vary; this issue is one of the drawbacks of fibre-based models compared to physical theory or phenomenological models.

Three different end conditions were observed in the experimental configurations included in the steel brace database (see Figure 3.2). A pin-ended (no rotational resistance), a fixed-fixed (fully restrained) and a semi-rigid configuration due to the flexibility of the gusset plates at the end of a steel brace. The out-of-plane flexibility of the gusset plates may be simulated with a recently proposed model by Hsiao et al. (2012). This model employs a zero-length spring, whose hysteretic behaviour is dictated by empirical

formulae based on experimental data by Roeder et al. (2004). The effect of the end condition assumptions on the hysteretic response of steel braces is discussed in Section 5.8.

As discussed earlier, during the calibrations of the steel brace component model, the effective length  $L_H$  of each steel brace was employed; therefore, pinned conditions were assumed even in the case of steel braces with gusset plates. It was found that when  $L_H$  is used to represent the steel brace length instead of the centerline brace length, the consideration of the out-of-plane flexibility and strength of the gusset plates does not significantly improve the simulated hysteretic response of a steel brace (see Section 5.8).

Fracture due to low cycle fatigue is simulated with the Fatigue material model (Uriz 2005, Uriz et al. 2008), which is already available in the OpenSees simulation platform. The model is based on a linear strain accumulation rule based on a Coffin-Manson relationship (Manson, 1965) in the logarithmic domain as described in Equation 5.1.

$$\varepsilon_i = \varepsilon_0 (N_f)^m \quad (5.1)$$

In this equation,  $\varepsilon_0$  is a material parameter that indicates the strain amplitude  $\varepsilon_i$  at which one complete cycle of an undamaged material will cause fracture. The coefficient  $m$  is a material parameter that relates the sensitivity of the total strain amplitude of the material to the number of cycles to fracture  $N_f$ . Fracture is initiated according to a modified rain-flow-counting rule based on Miner's rule that was developed by Uriz (2005). When

fracture is initiated, the engineering stress in the fibre section drops to zero (see Figure 5.1). The fatigue material model is wrapped around the Menegotto-Pinto material model.

The component model that was described in detail in this section performed well for the purposes of the present research. However, this model has a number of important limitations. The primary one is that the material model that is employed does not capture local buckling of the cross section. For this purpose, detailed Finite Element Models (FEMs) (e.g. Huang and Mahin, 2010) or more recently developed material models (Dhakal and Maekawa 2002, Jin and El-Tawil 2002, Krishnan 2010) may be used instead. Another limitation of the component model is that it ignores a possible distortion of the cross section, which may result in warping of the brace member. These distortions may significantly decrease the stiffness of the member. The warping phenomenon is more common in open channel sections.

### **5.3 Calibrated Case Studies**

A number of experimental studies were selected from the general-purpose steel brace database discussed in Chapter 3 to calibrate the steel brace component model discussed in Section 5.2. Several considerations were employed for the qualification of steel braces to be used as part of the calibration process discussed in Section 5.4. Emphasis is placed on steel braces that experience fracture due to low cycle fatigue at their mid-span, where a plastic hinge occurs. Steel braces that experience net section failures are not part of this investigation. Another consideration is related with the brace slenderness ratio,  $kL/r$ . In particular, steel braces that fail the slenderness limit for axially loaded members,  $kL/r <$

200, suggested by AISC-360-10 (2010) and CISC (2010) are not considered as part of the calibration process.

Tables 5.1 to 5.3 display the refined subset of steel braces per cross section that is used for the calibration studies discussed in the next section. The three subsets of cross sectional shapes that are used are rectangular HSS, round HSS and W- shapes. In summary, these tables include 65 rectangular HSS, 23 round HSS and 18 W- shape steel braces.

## **5.4 Calibration Process**

In order to calibrate the hysteretic response of the steel brace component model discussed in Section 5.2 with the experimental data summarized in Tables 5.1 to 5.3, a systematic approach was developed. Emphasis is placed on the  $\varepsilon_0$  and  $m$  parameters that control the fatigue life of a steel brace. The calibration process of these parameters is based on principles of engineering mechanics and an optimization process that was developed. To facilitate this process, an interactive interface was developed in MATLAB (Mathworks, 2011) programming language. This interface is linked with the OpenSees simulation platform (McKenna 1997). The measured material and geometric properties of each steel brace are directly used as an input into the OpenSees model to define the geometry and uniaxial material model parameters. Section 5.2 summarizes the input model parameters that are fixed including their values for each brace section shape before the optimization process.

Prior to the optimization process, the material model parameter  $R_0$  is manually selected to accurately capture the global buckling load of the steel brace to be calibrated. The range of values that is typically used for this purpose is from 10 to 45 with an increment of 2. Once the parameter  $R_0$  is fixed the parameters  $a_1$  and  $a_3$  are manually calibrated such that the cyclic hardening of the simulated hysteretic response in the positive and negative loading direction matches the experimental response for each brace. These material model parameters typically range from 0.00 to 0.09.

In order to calibrate the two parameters  $\varepsilon_0$  and  $m$  from Equation 5.1 that controls the fatigue life of a steel brace the Mesh Adaptive Search Algorithm (MADS) is used (Abramson et al. 2009). The objective function  $H$ , as shown in Equation 5.2, that is used for the constrained optimization problem is the square root of the sum of the squares of the differences between the simulated  $F_{simul.}$  and experimentally measured  $F_{exp.}$  axial force of the brace for each axial displacement  $\delta_i$  (total of  $N$  points) of the testing loading protocol,

$$H(\varepsilon_0, m) = \sqrt{\sum_{i=1}^N [F_{exp.}(\delta_i) - F_{simul.}(\delta_i)]^2} \quad (5.2)$$

This objective function is non-differentiable and therefore the optimization problem lacks smoothness. However, the advantage of MADS is that it does not use information about the gradient of the objective function to search for an optimal point compared to more traditional optimization algorithms (Levenberg 1944, Lagarias et al. 1998). To efficiently use MADS to facilitate the optimization process, the stopping and tolerance criteria of the

constraint optimization problem were carefully selected. The mesh tolerance of the two parameters to be optimized was limited to 0.01%. The maximum number of successful iterations was bound to 60. This number was found to be conservative based on a systematic study that was conducted with a smaller subset of 22 steel braces.

The main findings from the smaller subset of 22 steel braces discussed above displayed that the material parameter,  $m$ , did not depend on the cross sectional shape, the brace global and local slenderness nor the yield stress of the steel. Figure 5.2 shows the effect of  $kL/r$  and  $w/t$  ratios of HSS steel braces on the parameter  $m$ . Based on a standard  $t$ -test, it was found that none of these two parameters are statistically significant on  $m$  for HSS braces. Similar conclusions were formed for the other two shape types that were considered as part of this evaluation. Therefore  $m$  can be treated as a constant and equal to -0.3. This assumption agrees with earlier findings by Ballio and Castiglioni (1995). They suggested that the parameter  $m$  should constant and equal to -0.45 based on a set of constant displacement amplitude experiments with steel braces. Therefore, the optimization problem can be treated as a single variable problem. Modelling recommendations specific for each cross section type are discussed later. Figures 5.3 to 5.5 show examples of successful calibrations of the simulated versus measured axial force – axial displacement for a variety of steel braces with different geometry, material properties and boundary conditions.

## 5.5 Modelling Recommendations for Rectangular HSS Braces

In this section, recommendations for modelling the post-buckling behaviour and fracture due to low cycle fatigue of rectangular HSS braces are proposed. These recommendations are based on 65 steel braces (see Table 5.1) that meet the requirements discussed in Section 5.3. The parameter  $\varepsilon_0$  that controls fracture is estimated based on multivariate regression analysis (Chatterjee et al. 2000). The parameters  $kL/r$ ,  $w/t$  and  $F_y$  are found to have an effect on the fracture life of a brace. Therefore, in order to understand how the fracture parameter  $\varepsilon_0$  is affected by  $kL/r$ ,  $w/t$  and  $F_y$ , the calibrated  $\varepsilon_0$  values are plotted against each one of these parameters. Trends for the parameter  $\varepsilon_0$  for rectangular HSS braces with respect to the brace slenderness ratio  $kL/r$ ,  $w/t$  ratio and the yield stress  $F_y$  of the steel material are shown in Figures 5.6a to 5.6c. All three parameters are statistically significant with respect to  $\varepsilon_0$  based on a standard  $t$ -test. However, it should be noted that the effect of  $kL/r$  on  $\varepsilon_0$  diminishes since once a plastic hinge forms at the mid-length of a brace the local slenderness controls fracture at the same location. This is discussed in detail later on in this section. A power-law fitting model was found to best describe the experimental data. For this dataset the predictive equation for  $\varepsilon_0$  based on a 95% confidence bound is,

$$\varepsilon_0 = 0.291 \left( \frac{kL}{r} \right)^{-0.484} \left( \frac{w}{t} \right)^{-0.613} \left( \frac{E}{F_y} \right)^{0.3} \quad (5.3)$$

In Equation (5.3), the expected yield stress of the steel brace  $F_y$  is normalized with

respect to the Young's modulus  $E$ . Equation (5.3) is obtained for the following range of parameters:

- $27 \leq kL/r \leq 85$
- $4.20 \leq w/t \leq 30.40$
- $223 \leq F_y \leq 532 \text{ MPa}$

in which,  $kL/r$  is the brace slenderness, where  $k$  is the effective length factor with respect to the axis of buckling,  $L$  is the centerline length of the brace and  $r$  is the radius of gyration with respect to the axis of buckling,  $w/t$  is the width-to-thickness ratio defined per AISC (2010) seismic provisions, where  $w$  is the width of the brace defined as the largest outside dimension of the cross section of the brace minus three times the thickness of the plate,  $t$ .

Table 5.4 summarizes the coefficient of determination  $R^2=0.493$  and the standard error=0.249 of the mean of the regression of the statistical sample of 65 specimens that were used in the multivariate regression analysis. These values indicate a relatively good match between the predicted and calibrated  $\varepsilon_0$  values for rectangular HSS braces. Table 5.5 summarizes the upper and lower bounds of the 95% confidence interval of the coefficients that were estimated per term in Equation (5.3) based on the student distribution. Figure 5.6d illustrates the predicted versus calibrated  $\varepsilon_0$  values based on Equation 5.3. This figure indicates that most of the predicted  $\varepsilon_0$  values are in good agreement with the calibrated  $\varepsilon_0$  values obtained from the individual experiments.

Hsiao et al. (2012) suggested a formula to estimate the maximum strain range ( $Max$

$\varepsilon_{range,pred}$ .) that a brace may undergo prior to fracture based on 47 rectangular HSS steel brace tests. This formula is given as follows,

$$Max \varepsilon_{range,pred} = 0.1435 \left( \frac{kL}{r} \right)^{-0.3} \left( \frac{w}{t} \right)^{-0.4} \left( \frac{E}{F_y} \right)^{0.2} \quad (5.4)$$

In this equation, all of the predictive parameters are defined similarly with Equation 5.3, except for the predicted maximum  $\varepsilon_{range}$  parameter, which is defined as the difference between the maximum and minimum strain that the braces experience at the exterior fiber of the cross section due to cyclic loading prior to fracture. As part of the calibration process discussed earlier these values were also recorded for comparison purposes with Equation (5.4). Figure 5.6e displays how Equation 5.4 predicts the maximum  $\varepsilon_{range}$  of the HSS braces summarized in Table 5.1 versus the calibrated maximum  $\varepsilon_{range}$  that were recorded from each simulation that was carried out. Figures 5.6d and 5.6e demonstrate that two independent calibration procedures that utilize two different brace component models to express fracture of a HSS steel brace yield similar results.

Table 5.6 summarizes the modelling guidelines that are described in this section to model the hysteretic behaviour of rectangular HSS braces as part of steel braced frames subjected to earthquake loading. For the calibration of the brace component model for HSS braces, ten fibers are used along the width of the cross section and four fibers are used through the thickness of the HSS members. It was also found that the parameters  $R_0$ ,  $a_1$  and  $a_3$  are equal to 22, 0.03 and 0.02, respectively. These are average values based on the calibrations of the 65 rectangular HSS steel braces. The effect of these parameters on

the hysteretic response of a rectangular HSS steel brace and on the fracture parameter,  $\varepsilon_0$ , is discussed in Section 5.9.

The exponential coefficients of the predictive parameters of Equation 5.3 suggest that the local slenderness term,  $w/t$ , is the most dominant parameter affecting  $\varepsilon_0$ . To further investigate the effect of local and global slenderness on the fracture of braces, the axial displacement at which the braces experienced fracture (noted as  $\Delta$ ) was also recorded as a part of the calibration process. This value is normalized with the length of the brace ( $L$ ). The term  $\Delta/L$  represents an “equivalent” strain at fracture assuming that the cross section remains uniform. Figure 5.7a and 5.7b display the effect of global and local slenderness ratios on the normalized axial displacement at fracture ( $\Delta/L$ ). The figures suggest that the fracture of braces defined as,  $\Delta/L$ , does not depend on the global slenderness term,  $kL/r$ , and that it strongly depends on the local slenderness term  $w/t$ . Fell et al. (2009, 2010) reached a similar conclusion based on an experimental program of 18 large scale braces with various shapes. This is to be expected since global buckling of steel braces is mostly controlled by the global slenderness; while the post buckling behaviour is mainly determined by the local slenderness of a steel brace. Once a brace experiences global buckling, the spread of plasticity along its cross section at the location of the plastic hinge, controls the post buckling behaviour and subsequently fracture.

For eight HSS braces that are fabricated from stainless steel (Nip et al. 2009) it is found that larger  $a_1$  and  $a_3$  values are typically more representative compared to the rest of the subset. In particular,  $a_1 = a_3 = 0.05$  compared to 0.03 and 0.02 should be used due to the

different hardening mechanism of a stainless steel compared to a carbon steel material. Figure 5.8 illustrates the difference between the stress-strain curves of carbon and stainless steel. The hardening of stainless steel is very gradual compared to carbon steel and the post-yield engineering stress of the material is constantly increasing (BSSA, 2012). Based on the calibrations for 33 steel braces that are fabricated from cold-formed steel material, the equivalent  $a_1$ ,  $a_3$  values can be set equal to zero. This is attributed to the fact that these braces do not exhibit significant cyclic hardening. A strain-hardening ratio  $b=0.1\%$  is found to comply well with all of the rectangular HSS steel braces.

**Effect of predictors on  $\epsilon_0$ :** In order to illustrate the usefulness of the predictive Equation 5.3 quantifying the fracture life of a rectangular HSS brace, a range of rectangular HSS sections has been selected and the effect of various predictors on  $\epsilon_0$  is summarized in Table 5.7. An expected yield stress  $F_y = 460\text{MPa}$  for the CSA-G40.21-350W steel is assumed. The  $w/t$  ratios of the selected HSS sections comply with the AISC-360-10 (2010) and CISC (2010) seismic provisions. This table shows that a stockier rectangular HSS brace has a larger  $\epsilon_0$  compared to a more slender one since the latter buckles locally earlier compared to the former. This observation is confirmed based on experimental evidence (Tremblay et al. 2002).

## 5.6 Modelling Recommendations for Round HSS Braces

This section summarizes the proposed recommendations for modelling the post-buckling behaviour and fracture due to low cycle fatigue of round HSS braces (noted as pipes). The main properties of the 23 braces are summarized in Table 5.2. These braces fractured

at their mid-length after the occurrence of local buckling at the same location. The hysteretic behaviour in terms of axial load-axial deformation between round and rectangular HSS braces is found to be similar. However, round HSS braces typically have a longer fracture life compared to rectangular ones.

Similarly with HSS braces, the  $kL/r$ ,  $D/t$ , where  $D$  is the outer diameter of the cross section of the brace and  $t$  is the thickness of the plate and  $F_y$  parameters are the ones that mostly affect the fracture life of round HSS braces. Figures 5.9a, 5.9b and 5.9c show the effect of  $kL/r$ ,  $D/t$  and  $F_y$  on  $\varepsilon_0$  when these variables are treated as statistically independent. Based on a standard *t-test*, these variables are statistically significant with  $\varepsilon_0$ . However, the effect of  $kL/r$  on the post-buckling behaviour of a round HSS diminishes for similar reasons with HSS braces discussed earlier. In order to take into account the interrelation of the predictive variables, multivariate regression analysis is employed. Similarly, with the HSS braces, a power law predictive equation provides the best fit among other functional forms that were considered. The predictive equation for the parameter  $\varepsilon_0$  based on a 95% confidence bound is given as follows,

$$\varepsilon_0 = 0.748 \left( \frac{kL}{r} \right)^{-0.399} \left( \frac{D}{t} \right)^{-0.628} \left( \frac{E}{F_y} \right)^{0.2} \quad (5.5)$$

In Equation (5.5), the expected yield stress of the steel brace  $F_y$  is normalized with respect to the Young's modulus  $E$ . Equation (5.5) is applicable for the following range of parameters:

- $29 \leq kL/r \leq 128$

- $12.75 \leq D/t \leq 39.91$
- $326 \leq F_y \leq 521 \text{ MPa}$

in which,  $kL/r$  is the brace global slenderness;  $k$  is the effective length factor with respect to the axis of buckling,  $L$  is the centerline length of the brace,  $r$  is the radius of gyration of the cross section,  $D/t$  is the diameter-to-thickness ratio defined by AISC (2010) seismic provisions and  $F_y$  is the measured or expected (in case that the measured is not available) yield stress of the brace.

Table 5.8 summarizes the statistical information in terms of  $R^2$  and standard error of the mean of the sample that was used in the multivariate regression analysis. These values indicate that the predictive equation represents relatively well the calibrated  $\varepsilon_0$  parameters for round HSS braces. Table 5.9 summarizes the coefficients of Equation 5.5 including the standard error for each one of the predictors. The t-statistic is also summarized in the same table for each predictor. These values are used in the Student's  $t$ -test and in the computation of the lower and upper 95% confidence intervals that are also included in the same table. Table 5.9 also summarizes the p-values for each predictor. From these values it can be concluded that the probability of obtaining a  $t$ -statistic at least as extreme as the ones that were observed, assuming the null hypothesis is true, are less than 5% (assumed significance level). Therefore, these values indicate that each predictor is statistically significant with  $\varepsilon_0$ .

Equation (5.5) confirms the expected tendencies of  $\varepsilon_0$  with respect to  $kL/r$ ,  $D/t$  and  $F_y$  based on earlier findings (Tremblay et al. 2002). Figure 5.9d shows the predicted versus

calibrated  $\varepsilon_0$  values for the subset of steel braces that are summarized in Table 5.2. The predicted  $\varepsilon_0$  values are based on Equation 5.5. This figure indicates that the multivariate regression equation reliably predicts the parameter that controls fracture due to low cycle fatigue for round HSS braces. Note that the exponent  $m$  is constant ( $m=-0.3$ ).

Similarly to HSS braces, the exponential coefficients of the predictive parameters of Equation 5.5 suggest that the local slenderness term,  $D/t$ , is the most dominant parameter affecting  $\varepsilon_0$  of round HSS braces. Figure 5.10a and Figure 5.10b display the effect of  $kL/r$  and  $D/t$  on the normalized axial displacement,  $\Delta/L$  at fracture, of round HSS braces, respectively. From these figures it can be seen that there is a stronger tendency between the normalized axial displacement at fracture and local slenderness compared to global slenderness.

Table 5.10 summarizes the modelling recommendations for accurate hysteretic analyses for pipe sections using the component model described in Section 5.2. Similarly with the HSS steel braces, the round HSS braces must be simulated with eight segments along their effective length. 5 integration points are used per segment. Twelve and four fibers around the diameter and through the thickness of the section, respectively, were found to adequately capture the local stresses and strains of the cross section.

The material model parameter  $R_0$  that controls the transition from the elastic to plastic range can be assumed to be 24 based on the average value that is obtained from Table 5.2. The parameters  $a_1$  and  $a_3$  that control the cyclic hardening of a round brace in tension

and compression, respectively, are both equal to 0.02. Similarly with the rectangular HSS braces, for round HSS braces that are fabricated with cold formed steel,  $a_1$  and  $a_3$  should be set to zero due to the smaller cyclic hardening that they exhibit compared to hot rolled steel braces. Finally, a strain-hardening ratio  $b=0.5\%$  was found to be representative for all the calibrations summarized in Table 5.2.

**Effect of predictors on  $\varepsilon_0$ :** In order to display how the regression Equation 5.5 works, typical round HSS braces with three different  $kL/r$  and  $D/t$  values are used to predict the  $\varepsilon_0$  values in Table 5.11. The expected yield stress  $F_y = 460\text{MPa}$  of CSA-G40.21-350W steel is assumed. The  $D/t$  ratios of the selected round HSS braces are of Class 1 (AISC-360-10, CISC, 2010). This table shows that a stockier pipe brace has a larger  $\varepsilon_0$  compared to a more slender one. When compared to HSS braces that have similar local slenderness parameters, pipe braces exhibit a larger fracture life. This is also confirmed with the drift-based fragility curves for round HSS braces that are summarized in Chapter 4.

## 5.7 Modelling Recommendations for W-Shape Braces

The steel braces that are part of the evaluation discussed in this section are of W-shape and have a varying global slenderness ratio between 39 and 153, while their  $b_f/2t_f$  ratios and the  $h/t_w$  ratios vary between 4.19 to 10.20 and 7.99 to 49.40 respectively. The measured yield stress varies between 284 MPa and 414 MPa. A summary of the input component model values for the W-shapes can be found in Table 5.3.

In the case of W-shape braces, the parameters  $kL/r$ ,  $b_f/2t_f$ ,  $h/t_w$ , and  $F_y$  are found to influence the fracture life of W- shape braces the most. Figures 5.11a, 5.11b, 5.11c and 5.11d show the effect of  $kL/r$ ,  $b_f/2t_f$ ,  $h/t_w$  and  $F_y$  on  $\varepsilon_0$ , respectively, when each predictor is treated as an independent variable. To be able to assess the effect of all the parameters on  $\varepsilon_0$ , a multivariate regression analysis is employed. The predictive equation for predicting the parameter  $\varepsilon_0$  for W-shape braces based on a 95% confidence bound is given as follows,

$$\varepsilon_0 = 0.0391 \left( \frac{kL}{r} \right)^{-0.234} \left( \frac{b_f}{2t_f} \right)^{-0.169} \left( \frac{h}{t_w} \right)^{-0.065} \left( \frac{E}{F_y} \right)^{0.351} \quad (5.6)$$

In Equation (5.6), the expected yield stress of the steel brace  $F_y$  is normalized with respect to the Young's modulus  $E$ . Equation (5.6) is obtained for the following range of parameters:

- $39 \leq kL/r \leq 153$
- $4.19 \leq b_f/2t_f \leq 10.20$
- $7.99 \leq h/t_w \leq 49.40$
- $284 \leq F_y \leq 414 \text{ MPa}$

in which,  $kL/r$  is the global brace slenderness;  $k$  is the effective length factor with respect to the axis of buckling,  $L$  is the centerline length of the brace;  $r$  is the radius of gyration with respect to the axis of buckling;  $b_f/2t_f$  and  $h/t_w$  are the local slenderness ratios as defined by AISC (2010) seismic provisions, and  $F_y$  is the measured yield stress of the steel brace (or expected in case that measured is not available). Note that Equation 5.6

considers the influence of the web local slenderness on the fracture life of a W-shape brace. However, the flange local slenderness has a stronger influence on  $\varepsilon_0$  compared to  $h/t_w$  since it is expected that the local instabilities will first be triggered at the flange of the W-shape.

Table 5.12 summarizes the statistical information regarding the multivariate regression analysis in terms of  $R^2$  and standard error of the mean of the sample. These values indicate that Equation 5.6 predicts well the  $\varepsilon_0$  parameter for W- shape braces given their geometric and material properties. Table 5.13 summarizes the coefficients of the predictive Equation 5.6 including the standard error for each one of the predictors. The *t*-*statistic* is also summarized in the same table for each predictor. These values are used in the Student's *t*-test and in the computation of the lower and upper 95% confidence intervals that are also included in the same table. The p-values for each predictor are also included in Table 5.13. These values indicate that each predictor is statistically significant for a 5% significance level.

Equation (5.6) confirms the expected tendencies of  $\varepsilon_0$  with respect to  $kL/r$ ,  $b_f/2t_f$ ,  $h/t_w$  and  $F_y$  based on other shapes in this chapter. Figure 5.11e shows the predicted versus calibrated  $\varepsilon_0$  values for the subset of W-shape braces that are summarized in Table 5.3. The predicted  $\varepsilon_0$  values are based on Equation 5.6. From this figure it can be concluded that the Equation 5.6 predicts well the fracture parameter  $\varepsilon_0$  that controls fracture of W-shape braces due to low cycle fatigue.

In order to investigate the individual effect of global and local slenderness on fracture of W-braces;  $kL/r$ ,  $b_f/2t_f$  and  $h/t_w$  are plotted against the normalized axial displacement,  $\Delta/L$  at fracture in Figures 12a,b and c, respectively. The plots confirm the expected trends where the local slenderness term  $b_f/2t_f$  has the strongest correlation with the normalized displacement at fracture. As mentioned before the flange local slenderness is expected to have a stronger influence on fracture compared to  $h/t_w$  since local instabilities will first be triggered at the flange of the W-shape. As it is the case with rectangular HSS and round HSS braces, the global slenderness term,  $kL/r$ , does have a significant influence on the axial displacement at fracture.

Table 5.14 summarizes the modelling recommendations that are discussed in this section to simulate the hysteretic behaviour of W-braces for the component model that is employed in this research. Eight segments were used to divide the W-shape brace effective length. Five integration points per segment were found to be satisfactory for the calibration process of these braces. To discretize the W-section, six fibers were used along the depth and flange width of the cross section. Two fibers were used through the web and flange thickness. The parameter  $R_0$  may be assumed equal to 20 based on the average value from Table 5.3 from all the W-brace calibrations. The parameters  $a_1$  and  $a_3$  should be 0.01 and 0.02, respectively. Finally, a strain-hardening ratio of  $b=0.1\%$  was found to adequately represent the hysteretic response of W-braces prior to fracture. For the Fatigue material model parameter  $\varepsilon_0$  and  $m$  it is recommended to use Equation 5.6 and a value of -0.3 respectively.

**Effect of predictors on  $\varepsilon_0$ :** In order to display how the regression Equation 5.6 can be employed in analytical models to assess the collapse capacity of steel braced frames using W-shape braces, sample W- sections of different  $kL/r$ ,  $b_f/2t_f$  and  $h/t_w$  values are used to compute  $\varepsilon_0$  values in Table 5.15. The expected yield stress  $F_y = 385\text{MPa}$  of CSA-G40.21-350W steel is assumed for all of the sample braces. The local slenderness ratios of the selected W- sections comply with the AISC-360-10 (2010) and CISC (2010) seismic provisions. This table shows that a stockier W- brace has a larger  $\varepsilon_0$  compared to a more slender one. Both of the local slenderness terms,  $b_f/2t_f$  and  $h/t_w$ , are inverse proportional to  $\varepsilon_0$ . When compared to rectangular HSS and round HSS braces with similar geometric and material parameters, W- braces exhibit a better fracture life. This is also reflected more qualitatively from the drift-based fragility curves for the fracture damage state (see Chapter 4).

## **5.8 Effect of End Conditions on the Hysteretic Behaviour of Steel Braces**

The end conditions of the steel braces have an important effect on their hysteretic behaviour. As discussed earlier, the braces that were collected as part of the steel brace database have three types of end conditions; (a) pin-ended (b) fixed and (c) semi-rigid (i.e., gusset plates). In particular, twelve braces are pin-ended, 19 braces are fixed and 75 braces have been tested with gusset plate connections. The steel braces with fixed boundary conditions have a larger global buckling load than any other brace of the same geometry but with different boundary conditions, due to the fact that the fixed end condition decreases the effective length (i.e. the buckling load increases). The end

conditions also affect the fracture parameter,  $\varepsilon_0$ . A brace with close to rigid end conditions typically has a larger  $\varepsilon_0$  value than a similar brace with pinned conditions. This is attributed to the fact that there is a contribution to the brace energy dissipation from the plastic hinges that form at the fixed ends in addition to the plastic hinge at the brace mid-length location. The steel braces that include gusset plates have a rotational restraint at their ends. This restraint depends on the geometric and material properties of the gusset plates. With larger fixity (and shorter effective length), the brace is stiffer and experiences small out-of-plane deflection, i.e., it sees smaller P-Delta moments at the plastic hinge at mid-length. Brace components employing gusset plates that are very flexible tend to display a similar hysteretic behaviour with pin-ended braces. If the gusset plates have a large out-of-plane rotational stiffness, then the hysteretic response of these braces is similar to that observed in braces with fixed end conditions. In the modelling approach discussed in Section 5.2 (see Figure 5.1) the effective length (from point of inflection to point of inflection) is considered as the brace length. The brace is always modeled pinned at its ends. This approach allows for a simple estimation of the hysteretic response of a brace without having to consider the out-of-plane flexibility and strength of the gusset plates. Hsiao et al. (2012) proposed a practical model to consider the plastic bending strength,  $M_p$ , and out-of-plane stiffness,  $K$ , of a gusset plate connection as part of a steel brace component. These parameters are determined from Equations 5.7, 5.8, respectively,

$$K = \frac{E}{L_{ave}} \left( \frac{W_w t^3}{12} \right) \quad (5.7)$$

$$M_p = \frac{W_w t^2}{6} F_y \quad (5.8)$$

In these equations,  $t$  is the thickness of the gusset plate,  $L_{ave}$  is the average length of the rigid offset from the end of the brace component to the beam-to-column centerline as defined in Hsiao et al. (2012);  $W_w$  is the Whitmore width,  $E$  is the modulus of elasticity of the steel and  $F_y$  is the yield stress of the steel material. Based on the same research study, a strain-hardening ratio of about 1% adequately represents the post-yield stiffness of the gusset plate connection once it is yielded.

The simplified approach that was used herein, in which the effective length between the plastic hinges is used together with pin-ended conditions at the end of a brace is compared to the model suggested by Hsiao et al. (2012). The emphasis is on the effect of the consideration of the gusset plate connection on the global buckling load and the fracture parameter,  $\varepsilon_0$ . Figure 5.13 shows a comparison of the hysteretic response of various brace shapes (rectangular HSS, round HSS and W-shape) with both modelling approaches. As discussed earlier, it is expected that the fracture parameter,  $\varepsilon_0$ , as well as, the global buckling load of the steel braces will increase in the case that the gusset plates are considered. The steel braces that were tested as part of the experimental program by Fell et al. (2009, 2010) are used for illustration purposes. In the case of the HSS1-1 (see Figures 5.13a, b) and P1-1 braces (see Figures 5.13c, d), the global buckling load is increased by 8% and 3%, respectively, after modelling the gusset plate connections at the end of the steel braces. A larger difference between the two modelling approaches is observed in the W1 brace (see Figures 5.13e, f) compared to HSS and P braces. From

these figures, the global buckling load was improved by 57% when the gusset plates were considered as part of the steel brace model. The reason for this improvement in terms of the estimation of the global buckling load is that the W- shape that was used in this test is welded to the gusset plates from both the flanges and the web. This provides a significant out-of-plane rotational resistance to the steel brace. However, the effect of the consideration of the gusset plate connection on the fracture parameter,  $\varepsilon_0$ , is negligible compared to the case that a pinned connection is used since only a 3% increase was observed on the  $\varepsilon_0$  values when the gusset plate connections were considered compared to the effective length approach. This observation holds true regardless the type and size of the steel brace.

## **5.9 Effect of the Material Hardening Parameters on the Hysteretic Behaviour of Steel Braces**

This section investigates the effect of the radius  $R_0$  and the cyclic hardening parameters  $a_1$  and  $a_3$  on  $\varepsilon_0$  that controls fracture initiation at the mid-length of a steel brace due to low cycle fatigue. Note that the parameters  $a_1$  and  $a_3$  control the isotropic hardening of the engineering stress-strain relationship of the steel material (Filippou et al. 1983) in the compression and tension loading directions, respectively. The radius  $R_0$  controls the curvature of the stress-strain curve when yielding occurs in the material. When this parameter is increased, the transition from the elastic to the plastic region in the stress-strain curve is rapid.

It is expected that if the hardening parameters  $a_1$  and  $a_3$  increase, fracture of a steel brace

will occur at an earlier loading cycle. This is due to the fact when larger  $a_1$  and  $a_3$  values are selected (i.e., the steel material hardens more) then more hysteretic energy is dissipated per inelastic cycle. To illustrate this observation, the HSS1-1 steel brace from the experimental program by Fell et al. (2010) is used based on the modelling approach discussed in Section 5.2. Figure 5.14a shows the simulated hysteretic response of this brace for  $a_1 = 0$  and  $a_3 = 0$ . Figure 5.14b shows the simulated hysteretic response of the same brace when  $a_1 = 0.09$  and  $a_3 = 0$ . In this case, due to the increasing rate of cyclic hardening, the amount of hysteretic energy that is dissipated up to loading cycle 6 prior to fracture is equal to the dissipated hysteretic energy that is absorbed up to cycle 7 if  $a_1 = a_3 = 0$ .

An increase of the radius  $R_0$  will result to early brace fracture since the larger the  $R_0$  value the larger the dissipated energy around the buckling load of the first and subsequent compression inelastic cycles of a steel brace. This is confirmed in Figures 5.14c and 5.14d that show the simulated response of nominally identical steel braces with an  $R_0 = 15$  and an  $R_0 = 45$ , respectively.

A parametric study was performed to determine the effect of the parameters  $a_1$ ,  $a_3$  and  $R_0$  on  $\varepsilon_0$  for a range of slenderness ratios,  $kL/r$ . Figure 5.15a shows how the parameter  $\varepsilon_0$  varies with respect to  $a_1$ . For a more compact brace the effect of  $a_1$  on the  $\varepsilon_0$  diminishes compared to a more slender brace. The effect of the parameter  $a_3$  on  $\varepsilon_0$  is important regardless the global slenderness of a steel brace as shown in Figure 5.15b. This should be expected since the post-buckling behaviour of a steel brace is mostly influenced by the

local slenderness of the brace cross sections. It should be pointed out that in these figures while one of the parameters was varied the rest were kept constant for comparison purposes.

Figure 5.15c shows the effect of  $R_0$  on the parameter  $\varepsilon_0$ . This figure shows that regardless of the brace slenderness the parameter  $\varepsilon_0$  becomes almost constant when  $R_0 > 20$ . This observation is consistent with the calibration study that was discussed earlier.

## 5.10 Summary

This chapter summarizes modelling guidelines to accurately simulate the post-buckling hysteretic behaviour and fracture due to low cycle fatigue of three main types of steel including rectangular HSS, round HSS (pipe) and W-shape braces. A state-of-the-art steel brace model has been extensively calibrated and predictive equations that related fracture with geometric and material properties of steel braces are proposed. The effect of the material hardening parameters and the effect of the end conditions of steel braces is also investigated. An important finding is that the effect of the global slenderness ratio  $kL/r$  on fracture due to low cycle fatigue diminishes regardless the steel brace shape. The local slenderness of a brace cross section mostly controls the post-buckling behaviour of steel braces. The predictive equations discussed in this chapter can be employed for the post-fracture evaluation of steel braced frames subjected to earthquake loading.

Table 5.1 Calibrated rectangular HSS specimens

Reference	Spec. ID	$F_y$ [MPa]	$L_{brace}$ [mm]	$kL/r$	$w/t$	$\epsilon_0$	$m$	$R_0$	$cR_1$	$cR_2$	$b$	$a_1$	$a_2$	$a_3$	$a_4$
Han et al. (2007)	S 77-28	394	3572	77	28.30	0.040	-0.30	24	0.93	0.25	0.001	0.09	1.00	0.00	1.00
	S 85-14 A	399	3611	85	13.70	0.032	-0.25	24	0.93	0.25	0.001	0.09	1.00	0.00	1.00
	S 85-14 B	410	3611	85	13.70	0.035	-0.29	24	0.93	0.25	0.001	0.09	1.00	0.00	1.00
	S 85-14 C	408	3611	85	13.70	0.035	-0.29	25	0.93	0.25	0.001	0.00	1.00	0.03	1.00
Shaback and Brown (2003)	1B	421	3452	54	12.90	0.068	-0.30	24	0.93	0.25	0.001	0.09	1.00	0.00	1.00
	2A	442	4040	53	16.00	0.059	-0.31	24	0.93	0.25	0.001	0.09	1.00	0.00	1.00
	3A	461	4456	65	16.80	0.036	-0.30	35	0.93	0.25	0.001	0.09	1.00	0.00	1.00
	3B	421	4446	66	12.90	0.062	-0.30	24	0.93	0.25	0.001	0.09	1.00	0.00	1.00
	3C	461	4414	62	10.40	0.057	-0.23	24	0.93	0.25	0.001	0.09	1.00	0.00	1.00
	4A	442	4944	64	16.00	0.033	-0.30	35	0.93	0.25	0.001	0.09	1.00	0.03	1.00
	4B	442	4914	60	13.00	0.048	-0.31	24	0.93	0.25	0.001	0.09	1.00	0.04	1.00
	HSS6	446	4008	85	10.40	0.028	-0.30	12	0.93	0.25	0.001	0.00	1.00	0.00	1.00
Lehman et al. (2008)	HSS7	446	3792	80	10.40	0.030	-0.30	12	0.93	0.25	0.001	0.00	1.00	0.00	1.00
	HSS12	455	3420	72	10.40	0.044	-0.30	25	0.93	0.25	0.001	0.00	1.00	0.00	1.00
	Specimen 1	426	3429	58	23.50	0.027	-0.30	24	0.93	0.25	0.001	0.09	1.00	0.00	1.00
Lee and Goel (1987)	Specimen 4	400	3480	43	23.50	0.065	-0.30	45	0.93	0.25	0.001	0.00	1.00	0.02	1.00
	Specimen 5	510	3454	77	23.50	0.041	-0.30	35	0.93	0.25	0.001	0.00	1.00	0.02	1.00
	RHS 2	397	4293	40	13.20	0.066	-0.29	15	0.93	0.25	0.001	0.03	1.00	0.00	1.00
Richard (2009)	RHS 4	397	4360	40	17.50	0.048	-0.31	15	0.93	0.25	0.001	0.03	1.00	0.00	1.00
	RHS 10	420	6140	56	24.70	0.026	-0.30	15	0.93	0.25	0.001	0.09	1.00	0.00	1.00
	RHS 12	429	4372	40	24.70	0.031	-0.30	15	0.93	0.25	0.001	0.00	1.00	0.00	1.00
	RHS 13	342	4400	40	30.40	0.036	-0.29	20	0.93	0.25	0.001	0.00	1.00	0.00	1.00
	RHS 19	397	3867	40	13.20	0.057	-0.29	15	0.93	0.25	0.001	0.02	1.00	0.02	1.00
Urriz (2005)	US	418	2912	40	13.00	0.054	-0.27	35	0.93	0.25	0.001	0.01	1.00	0.01	1.00

Table 5.1 Calibrated rectangular HSS specimens (Continued)

Reference	Spec. ID	$F_y$ [MPa]	$L_{brace}$ [mm]	$kl/r$	w/t	$\epsilon_0$	m	$R_0$	cR <sub>1</sub>	cR <sub>2</sub>	b	a <sub>1</sub>	a <sub>2</sub>	a <sub>3</sub>	a <sub>4</sub>
Uriz (2005)	LS	418	2912	40	13.00	0.066	-0.27	35	0.93	0.25	0.001	0.01	1.00	0.03	1.00
	Specimen 1	414	2870	40	13.00	0.061	-0.33	12	0.93	0.25	0.001	0.05	1.00	0.01	1.00
Yang and Mahin (2005)	Specimen 4	414	2870	40	13.00	0.069	-0.35	30	0.93	0.25	0.001	0.00	1.00	0.00	1.00
	Specimen 5	414	2870	40	13.00	0.081	-0.32	20	0.93	0.25	0.001	0.00	1.00	0.00	1.00
	Specimen 7	414	2870	40	13.00	0.062	-0.30	12	0.93	0.25	0.001	0.01	1.00	0.09	1.00
	Specimen 8	414	2870	40	13.00	0.071	-0.30	12	0.93	0.25	0.001	0.06	1.00	0.03	1.00
Haddad et al. (2004)	Specimen 9	414	2870	40	13.00	0.053	-0.30	12	0.93	0.25	0.001	0.06	1.00	0.03	1.00
	Specimen 4	480	3106	66	10.60	0.063	-0.30	25	0.93	0.25	0.001	0.00	1.00	0.02	1.00
	Specimen 5	480	2549	54	10.60	0.084	-0.30	12	0.93	0.25	0.001	0.00	1.00	0.04	1.00
	Specimen 7	480	2318	50	10.60	0.096	-0.30	25	0.93	0.25	0.001	0.00	1.00	0.04	1.00
	Specimen 8	500	3032	68	4.20	0.080	-0.30	12	0.93	0.25	0.001	0.00	1.00	0.00	1.00
	Specimen 9	500	2323	52	9.77	0.055	-0.30	15	0.93	0.25	0.001	0.00	1.00	0.00	1.00
	Specimen 10	500	2308	52	4.20	0.095	-0.30	12	0.93	0.25	0.001	0.00	1.00	0.00	1.00
	HSS1-1	460	2985	77	14.20	0.052	-0.30	18	0.93	0.25	0.001	0.01	1.00	0.01	1.00
	HSS1-2	460	2985	77	14.20	0.044	-0.30	15	0.93	0.25	0.001	0.00	1.00	0.00	1.00
	HSS1-3c	460	2985	77	14.20	0.047	-0.30	18	0.93	0.25	0.001	0.01	1.00	0.01	1.00
Fell et al. (2010)	HSS2-1	499	2985	80	8.50	0.10	-0.30	18	0.93	0.25	0.001	0.00	1.00	0.00	1.00
	HSS2-2c	499	2985	80	8.50	0.090	-0.30	18	0.93	0.25	0.001	0.00	1.00	0.00	1.00
Nip et al. (2009)	60x60x3x2050-CS-HR	458	2050	44	20.00	0.042	-0.30	25	0.93	0.25	0.001	0.00	1.00	0.00	1.00
	40x40x3x2050-CS-HR	478	2050	68	10.30	0.062	-0.30	15	0.93	0.25	0.001	0.00	1.00	0.02	1.00
	40x40x3x1250-CS-HR	478	1250	41	10.30	0.053	-0.30	25	0.93	0.25	0.001	0.00	1.00	0.02	1.00
	60x60x3x2050-CS-CF	361	2050	44	17.00	0.045	-0.30	15	0.93	0.25	0.001	0.00	1.00	0.00	1.00
	40x40x3x1250-CS-CF	451	1250	41	10.30	0.052	-0.30	20	0.93	0.25	0.001	0.00	1.00	0.00	1.00
	60x60x3x2850-SS-CF	483	2850	61	17.00	0.030	-0.30	20	0.93	0.25	0.001	0.00	1.00	0.00	1.00

Table 5.1 Calibrated rectangular HSS specimens (Continued)

Reference	Spec. ID	$F_y$ [MPa]	$L_{prace}$ [mm]	$kL/r$	$w/t$	$\epsilon_0$	$m$	$R_0$	$cR_1$	$cR_2$	$b$	$a_1$	$a_2$	$a_3$	$a_4$
Nip et al. (2009)	50x50x3x2850-SS-CF	552	2850	74	13.70	0.046	-0.30	15	0.93	0.25	0.001	0.09	1.00	0.02	1.00
	60x60x3x2050-SS-CF	483	2050	44	17.00	0.042	-0.30	18	0.93	0.25	0.001	0.00	1.00	0.05	1.00
	50x50x3x2050-SS-CF	552	2050	53	13.70	0.043	-0.30	18	0.93	0.25	0.001	0.00	1.00	0.09	1.00
	60x40x3x2050-SS-CF	538	2050	64	17.00	0.043	-0.30	18	0.93	0.25	0.001	0.00	1.00	0.07	1.00
	60x60x3x1250-SS-CF	483	1250	27	17.00	0.061	-0.30	40	0.93	0.25	0.001	0.00	1.00	0.05	1.00
	50x50x3x1250-SS-CF	552	1250	33	13.70	0.055	-0.30	20	0.93	0.25	0.001	0.05	1.00	0.05	1.00
	60x40x3x1250-SS-CF	538	1250	39	17.00	0.055	-0.30	24	0.93	0.25	0.001	0.02	1.00	0.05	1.00
	CyIS1-40H	280	1100	34	13.00	0.075	-0.30	35	0.93	0.25	0.001	0.00	1.00	1.00	0.03
Goggins et al. (2004)	CyIS5-50H	223	1100	56	18.00	0.065	-0.30	35	0.93	0.25	0.001	0.00	1.00	0.05	1.00
	B1-W1	320	2743	47	14.20	0.095	-0.30	22	0.93	0.25	0.001	0.03	1.00	0.02	1.00
Lai (2012)	B1-E1	320	2743	47	14.20	0.094	-0.30	22	0.93	0.25	0.001	0.03	1.00	0.02	1.00
	B1-W2	386	2469	51	14.20	0.071	-0.30	22	0.93	0.25	0.001	0.03	1.00	0.02	1.00
	B1-E2	386	2469	51	14.20	0.069	-0.30	22	0.93	0.25	0.001	0.03	1.00	0.02	1.00
	B4-W1	405	2743	47	14.20	0.072	-0.30	22	0.93	0.25	0.001	0.03	1.00	0.02	1.00
	B4-E1	405	2743	47	14.20	0.067	-0.30	22	0.93	0.25	0.001	0.03	1.00	0.02	1.00
	B4-W2	427	2469	51	14.20	0.060	-0.30	22	0.93	0.25	0.001	0.03	1.00	0.02	1.00
	B4-E2	427	2469	51	14.20	0.060	-0.30	22	0.93	0.25	0.001	0.03	1.00	0.02	1.00

Table 5.2 Calibrated round HSS specimens

Reference	Spec. ID	$F_y$ [MPa]	$L_{brace}$ [mm]	$kl/r$	$D/t$	$\epsilon_0$	$m$	$R_0$	$cR_1$	$cR_2$	$b$	$a_1$	$a_2$	$a_3$	$a_4$
Fell et al. (2010)	P1-1	326	3010	63	23.04	0.065	-0.30	25	0.93	0.25	0.005	0.04	1.00	0.04	1.00
	P1-2	326	3010	63	23.04	0.072	-0.30	25	0.93	0.25	0.005	0.04	1.00	0.04	1.00
	P1-3	326	3010	63	23.04	0.063	-0.30	25	0.93	0.25	0.005	0.04	1.00	0.06	1.00
	P2-1	372	3010	102	17.30	0.071	-0.30	20	0.93	0.25	0.005	0.05	1.00	0.04	1.00
	P2-2	372	3010	102	17.30	0.063	-0.30	20	0.93	0.25	0.005	0.05	1.00	0.04	1.00
	P2-3	372	3010	102	17.30	0.071	-0.30	20	0.93	0.25	0.005	0.08	1.00	0.04	1.00
Takeuchi and Matsui (2011)	528	349	1622	53	27.81	0.077	-0.30	35	0.93	0.25	0.005	0.00	1.00	0.00	1.00
	721	366	2219	74	21.19	0.085	-0.30	25	0.93	0.25	0.005	0.00	1.00	0.00	1.00
	728	349	2219	73	27.81	0.065	-0.30	35	0.93	0.25	0.005	0.00	1.00	0.03	1.00
	732	357	2219	73	31.79	0.055	-0.30	35	0.93	0.25	0.005	0.00	1.00	0.03	1.00
	1028	349	3135	103	27.81	0.046	-0.30	25	0.93	0.25	0.005	0.00	1.00	0.03	1.00
	1228	353	3135	121	27.14	0.055	-0.30	25	0.93	0.25	0.005	0.00	1.00	0.00	1.00
Richard (2009)	CHS 1	317	5618	40	28.74	0.055	-0.30	15	0.93	0.25	0.005	0.00	1.00	0.00	1.00
	CHS 2	317	7695	60	28.74	0.048	-0.30	15	0.93	0.25	0.005	0.00	1.00	0.00	1.00
Elchalakani et al. (2003)	S7B	379	2820	29	39.91	0.077	-0.30	45	0.93	0.25	0.005	0.00	1.00	0.00	1.00
	S7C	379	2820	29	39.91	0.079	-0.30	15	0.93	0.25	0.005	0.00	1.00	0.00	1.00
Christopoulos et al. (2008)	Specimen 1	521	4260	128	12.75	0.065	-0.30	18	0.93	0.25	0.005	0.00	1.00	0.00	1.00
	Specimen 3	473	6147	111	12.92	0.095	-0.30	18	0.93	0.25	0.005	0.00	1.00	0.00	1.00
	Specimen 4	431	6160	85	13.69	0.088	-0.30	20	0.93	0.25	0.005	0.00	1.00	0.04	1.00
	PSD-1	382	2565	42	26.25	0.076	-0.30	20	0.93	0.25	0.005	0.02	1.00	0.01	1.00
Lai (2012)	PSD-2	434	2565	45	17.68	0.100	-0.30	18	0.93	0.25	0.005	0.00	1.00	0.00	1.00
	B2-W1	470	2743	55	12.90	0.099	-0.30	24	0.93	0.25	0.005	0.02	1.00	0.02	1.00
	B2-E1	470	2743	55	12.90	0.095	-0.30	24	0.93	0.25	0.005	0.02	1.00	0.02	1.00

Table 5.3 Calibrated W- specimens

Reference	Spec. ID	$F_y$ [MPa]	$L_{brace}$ [mm]	$kL/r$	$b_f/2t_f$	$h/t_w$	$\epsilon_0$	$m$	$R_0$	$cR_1$	$cR_2$	$b$	$a_1$	$a_2$	$a_3$	$a_4$
Fell et al. (2010)	W1	414	3010	153	7.53	49.40	0.075	-0.30	20	0.93	0.25	0.001	0.04	1.00	0.00	1.00
	W2	414	3010	153	7.53	49.40	0.058	-0.30	25	0.93	0.25	0.001	0.00	1.00	0.00	1.00
	W3	414	3010	153	7.53	49.40	0.072	-0.30	20	0.93	0.25	0.001	0.04	1.00	0.02	1.00
Richard (2009)	W1	360	4178	40	10.20	25.90	0.081	-0.30	15	0.93	0.25	0.001	0.00	1.00	0.03	1.00
	W4	377	5120	60	9.92	24.90	0.080	-0.30	15	0.93	0.25	0.001	0.00	1.00	0.03	1.00
	W6	360	4413	60	5.86	14.80	0.081	-0.30	20	0.93	0.25	0.001	0.00	1.00	0.00	1.00
Wakabayashi et al. (1977)	SIC1	284	985	39	4.19	7.99	0.087	-0.30	20	0.93	0.25	0.001	0.00	1.00	0.00	1.00
	SIC2	284	1970	79	4.19	7.99	0.085	-0.30	20	0.93	0.25	0.001	0.00	1.00	0.00	1.00
Leowardi and Walpone (1996)	W1	315	2416	80	8.10	21.09	0.088	-0.30	18	0.93	0.25	0.001	0.00	1.00	0.03	1.00
	W2	315	1652	60	8.10	21.09	0.095	-0.30	18	0.93	0.25	0.001	0.00	1.00	0.03	1.00
	W3	315	3056	40	8.10	21.09	0.105	-0.30	25	0.93	0.25	0.001	0.00	1.00	0.03	1.00
Lai (2012)	B3-W1	372	2743	67	7.03	22.30	0.087	-0.30	20	0.93	0.25	0.001	0.01	1.00	0.02	1.00
	WF1	335	3470	79	7.14	21.60	0.060	-0.30	20	0.93	0.25	0.001	0.01	1.00	0.02	1.00
Lumpkin (2009)	WF2	335	3612	83	7.14	21.60	0.068	-0.30	20	0.93	0.25	0.001	0.01	1.00	0.02	1.00
	W1	345	3222	74	7.14	21.60	0.065	-0.30	20	0.93	0.25	0.001	0.01	1.00	0.02	1.00
Clark (2009)	W2	345	3222	74	7.14	21.60	0.071	-0.30	20	0.93	0.25	0.001	0.01	1.00	0.02	1.00
	W3	345	3146	72	7.14	21.60	0.069	-0.30	20	0.93	0.25	0.001	0.01	1.00	0.02	1.00
	W4	345	3146	72	7.14	21.60	0.066	-0.30	20	0.93	0.25	0.001	0.01	1.00	0.02	1.00
	W4	345	3146	72	7.14	21.60	0.066	-0.30	20	0.93	0.25	0.001	0.01	1.00	0.02	1.00

Table 5.4 Regression statistics for rectangular HSS braces

Regression Statistics	
<b>R<sup>2</sup></b>	0.493
<b>Standard Error</b>	0.249
<b>Observations</b>	65

Table 5.5 Statistics for the coefficients of the regression analysis for rectangular HSS braces

	Coefficients	Standard Error	<i>t</i> Stat	<i>P</i> -value	Lower 95%	Upper 95%
<b>Intercept</b>	0.291	0.551	-2.242	0.029	-2.335	-0.134
<b><i>kL/r</i></b>	-0.485	0.114	-4.262	0.000	-0.712	-0.257
<b><i>w/t</i></b>	-0.613	0.093	-6.573	0.000	-0.800	-0.427

Table 5.6 Summary of modelling guidelines for rectangular HSS braces

Level	Modelling Parameter	Recommendation
Brace component	Number of segments along the length	8
	Number of integration points	5
Section	Number of fibers along <i>w</i>	10
	Number of fibers through the thickness <i>t</i>	4
Steel Material (Menegotto-Pinto)	<i>b</i>	0.001
	<i>R<sub>0</sub></i>	22
	<i>a<sub>1</sub></i>	0.03
	<i>a<sub>2</sub></i>	1.00
	<i>a<sub>3</sub></i>	0.02
	<i>a<sub>4</sub></i>	1.00
Fatigue Material	<i>ε<sub>0</sub></i>	Equation 5.3
	<i>m</i>	-0.30

Table 5.7 Fracture parameter  $\epsilon_0$  for various HSS braces based on Equation 5.3

Section Size	<i>kL/r</i>	<i>w/t</i>	<b>F<sub>v</sub> [MPa]</b>	<b>ε<sub>0</sub></b>
102x102x6.4	30	14.2	460	0.068
102x102x6.4	50	14.2	460	0.053
102x102x6.4	80	14.2	460	0.042
254x254x9.5	30	24.7	460	0.048
254x254x9.5	50	24.7	460	0.038
254x254x9.5	80	24.7	460	0.030

Table 5.8 Regression statistics for round HSS braces

Regression Statistics	
<b>R<sup>2</sup></b>	0.636
<b>Standard Error</b>	0.146
<b>Observations</b>	23

Table 5.9 Statistics for the coefficients of the regression analysis for round HSS braces

	Coefficients	Standard Error	<i>t</i> Stat	<i>P</i> -value	Lower 95%	Upper 95%
<b>Intercept</b>	0.748	0.592	-0.490	0.629	-1.525	0.945
<b><i>kL/r</i></b>	-0.399	0.086	-4.654	0.000	-0.578	-0.220
<b><i>D/t</i></b>	-0.628	0.102	-6.133	0.000	-0.842	-0.415

Table 5.10 Summary of modelling guidelines for round HSS braces

Level	Modelling Parameter	Recommendation
Brace component	Number of segments along the length	8
	Number of integration points	5
Section	Number of fibers along <i>D</i>	12
	Number of fibers through the thickness <i>t</i>	4
Steel Material (Menegotto-Pinto)	<i>b</i>	0.005
	<i>R</i> <sub>0</sub>	24
	<i>a</i> <sub>1</sub>	0.02
	<i>a</i> <sub>2</sub>	1.00
	<i>a</i> <sub>3</sub>	0.02
	<i>a</i> <sub>4</sub>	1.00
Fatigue Material	<i>ε</i> <sub>0</sub>	Equation 5.5
	<i>m</i>	-0.30

Table 5.11 Fracture parameter  $\epsilon_0$  for various round HSS braces based on Equation 5.5

Section Size	<i>kL/r</i>	<i>D/t</i>	<i>F<sub>y</sub></i> (MPa)	$\epsilon_0$
Pipe127STD	30	21.6	460	0.094
Pipe127STD	50	21.6	460	0.077
Pipe127STD	80	21.6	460	0.064
Pipe76STD	30	16.2	460	0.113
Pipe76STD	50	16.2	460	0.092
Pipe76STD	80	16.2	460	0.076

Table 5.12 Regression statistics for W- braces

Regression Statistics	
<b>R<sup>2</sup></b>	0.592
<b>Standard Error</b>	0.161
<b>Observations</b>	18

Table 5.13 Statistics for the coefficients of the regression analysis for W- braces

	Coefficients	Standard Error	t Stat	P-value	Lower 95%	Upper 95%
<b>Intercept</b>	0.0391	0.431	-3.912	0.054	-1.314	-0.213
<b><i>kL/r</i></b>	-0.234	0.121	-3.231	0.000	-2.314	-0.012
<b><i>b<sub>f</sub>/2t<sub>f</sub></i></b>	-0.169	0.143	-1.234	0.000	-0.851	-0.051
<b><i>h/t<sub>w</sub></i></b>	-0.065	0.151	-1.031	0.000	-0.741	0.100

Table 5.14 Summary of modelling guidelines for W- braces

Level	Modelling Parameter	Recommendation
Brace component	Number of segments along the length	8
	Number of integration points	5
Section	Number of fibers along <i>b<sub>f</sub></i> and <i>h<sub>w</sub></i>	6
	Number of fibers through the thickness <i>t<sub>f</sub></i> and <i>t<sub>w</sub></i>	2
Steel Material (Menegotto-Pinto)	<i>b</i>	0.001
	<i>R<sub>0</sub></i>	20
	<i>a<sub>1</sub></i>	0.01
	<i>a<sub>2</sub></i>	1.00
	<i>a<sub>3</sub></i>	0.02
	<i>a<sub>4</sub></i>	1.00
Fatigue Material	<i>ε<sub>0</sub></i>	Equation 5.6
	<i>m</i>	-0.30

Table 5.15 Fracture parameter  $\epsilon_0$  for various W- braces based on Equation 5.6

Section Size	<i>kL/r</i>	<i>b<sub>f</sub>/2t<sub>f</sub></i>	<i>h/t<sub>w</sub></i>	<b>F<sub>y</sub> (MPa)</b>	<b>ε<sub>0</sub></b>
W310x24	30	7.53	49.40	385	0.078
W310x24	60	7.53	49.40	385	0.066
W310x24	90	7.53	49.40	385	0.061
W200x42	30	7.03	22.30	385	0.084
W200x42	60	7.03	22.30	385	0.071
W200x42	90	7.03	22.30	385	0.065

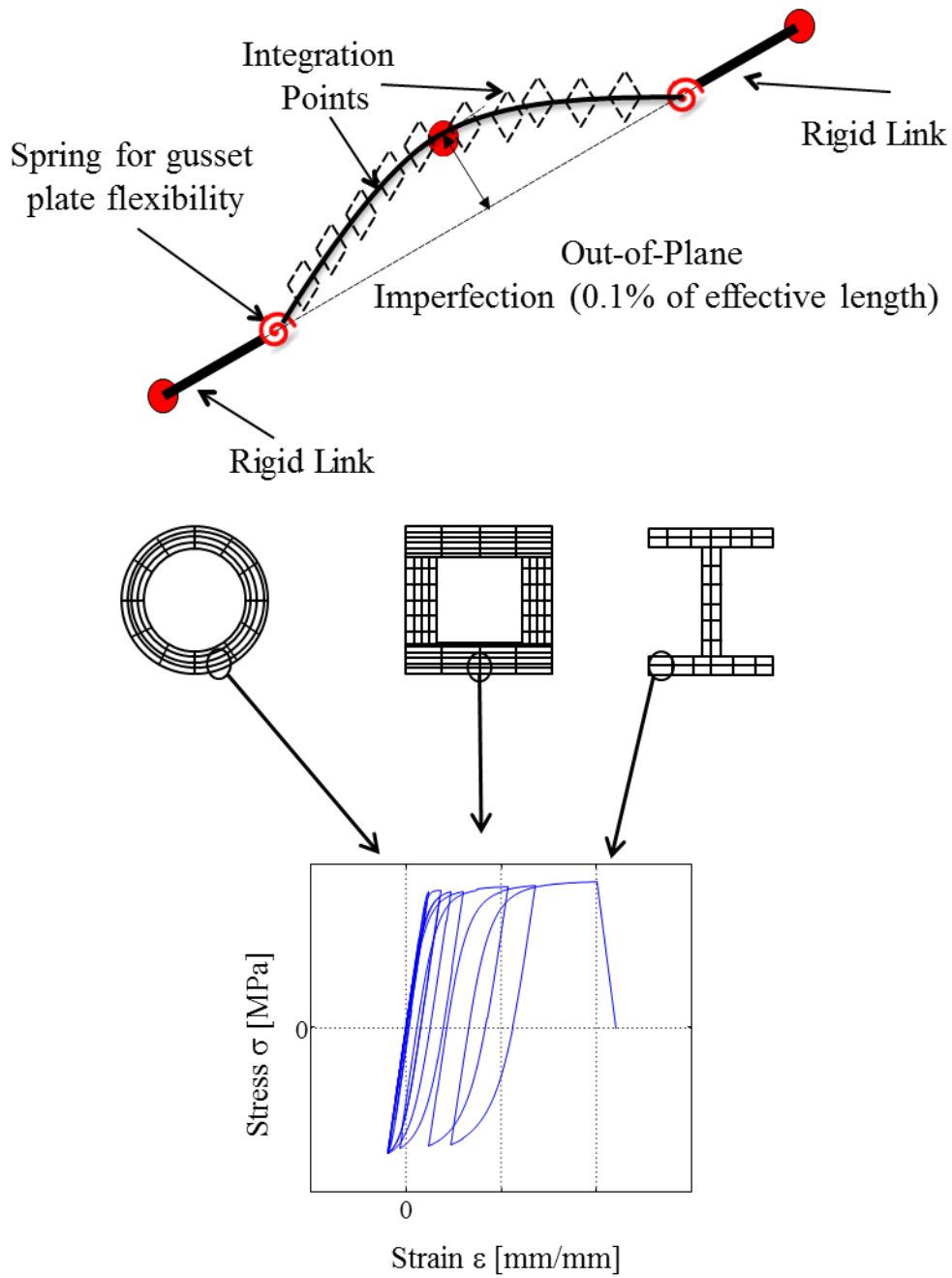


Figure 5.1 Description of the steel brace component model

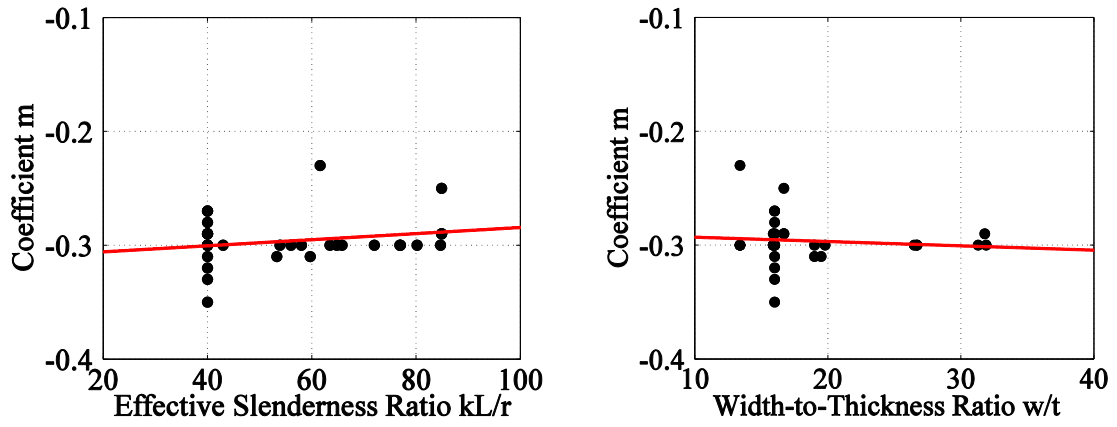


Figure 5.2 Effect of  $kL/r$  and  $w/t$  on the parameter  $m$

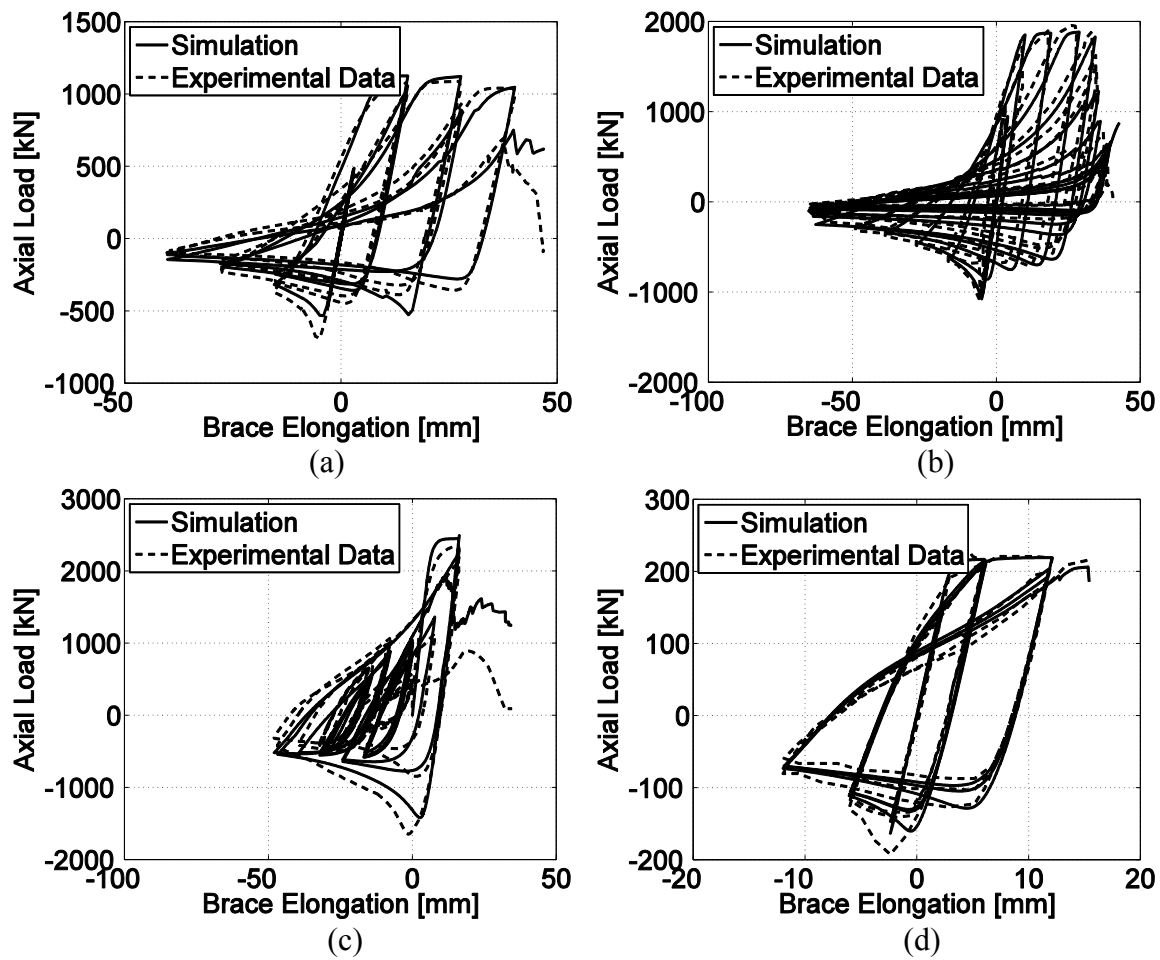


Figure 5.3 Sample calibrated rectangular HSS specimens: (a) 102x102x6.4 (Fell et al. 2010), (b) 127x127x8 (Haddad et al. 2004), (c) 152.4x152.4x9.5 (Yang and Mahin, 2005), (d) 40x40x3 (Nip et al. 2009)

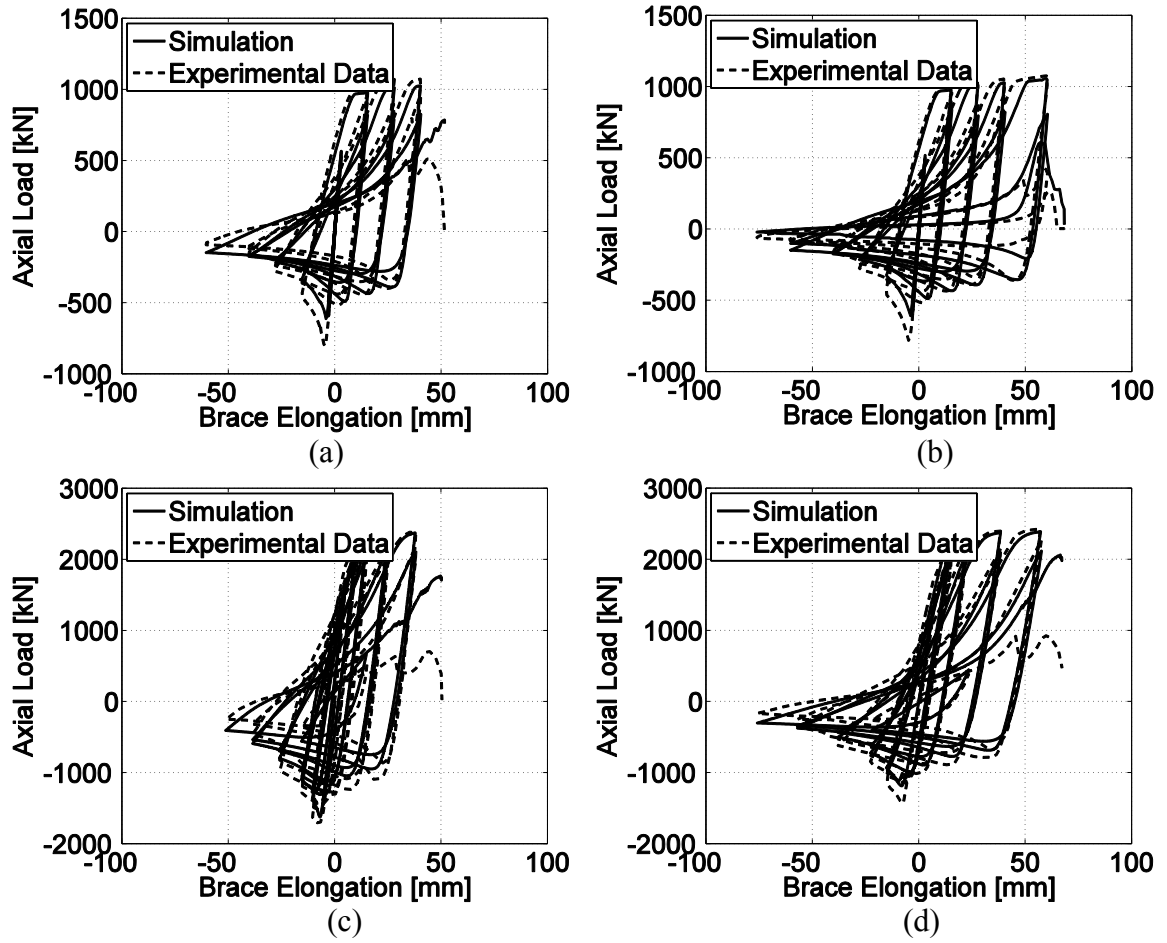


Figure 5.4 Sample calibrated round HSS specimens: (a) 141x6.4 (Fell et al. 2010), (b) 141x6.4 (Fell et al. 2010), (c) 273x9.5 (Richard, 2009), (d) 273x9.5 (Richard, 2009)

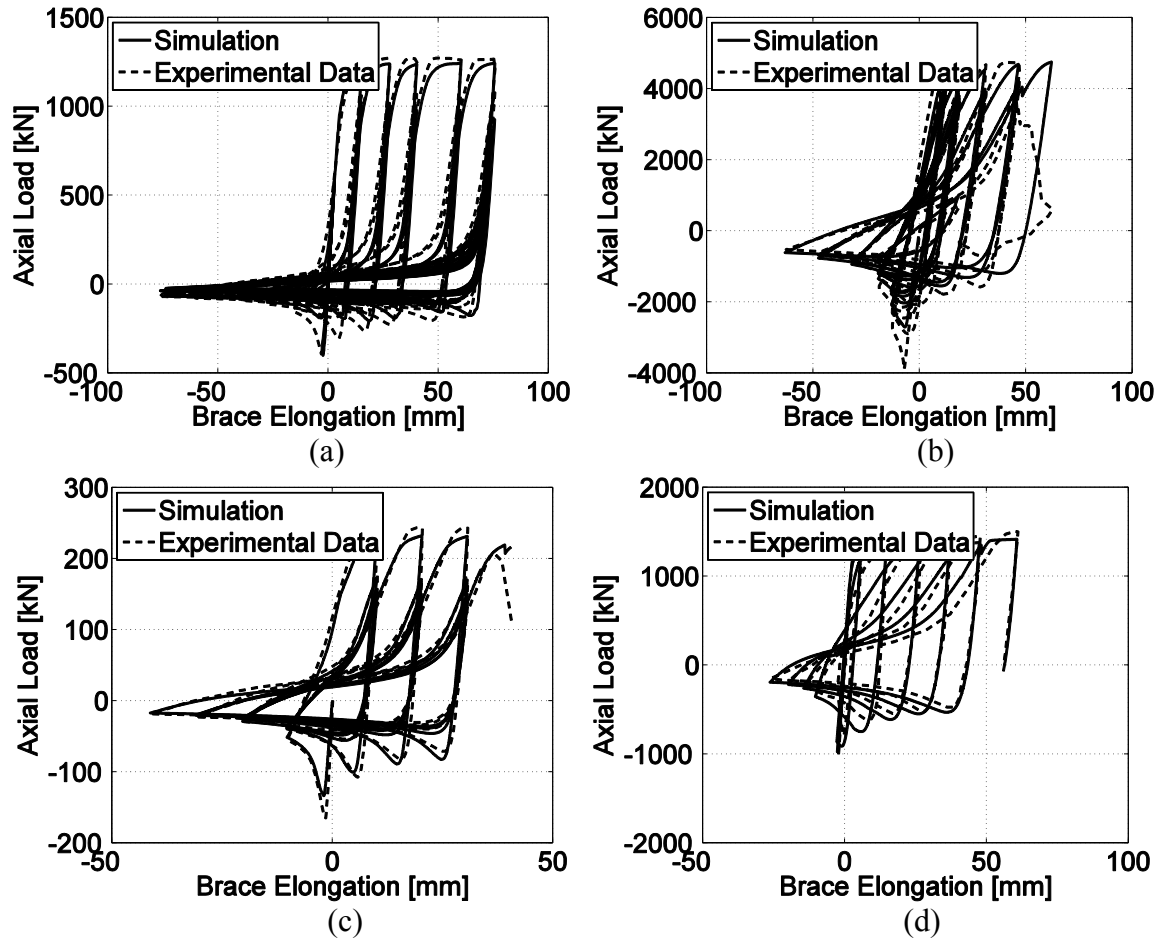


Figure 5.5 Sample calibrated W-shape specimens: (a) W310x24 (Fell et al. 2010) , (b) W310x97 (Richard, 2009), (c) 50x50x6x6 (Wakabayashi et al. 1977), (d) 150UC30 (Leowardi and Walpone, 1996)

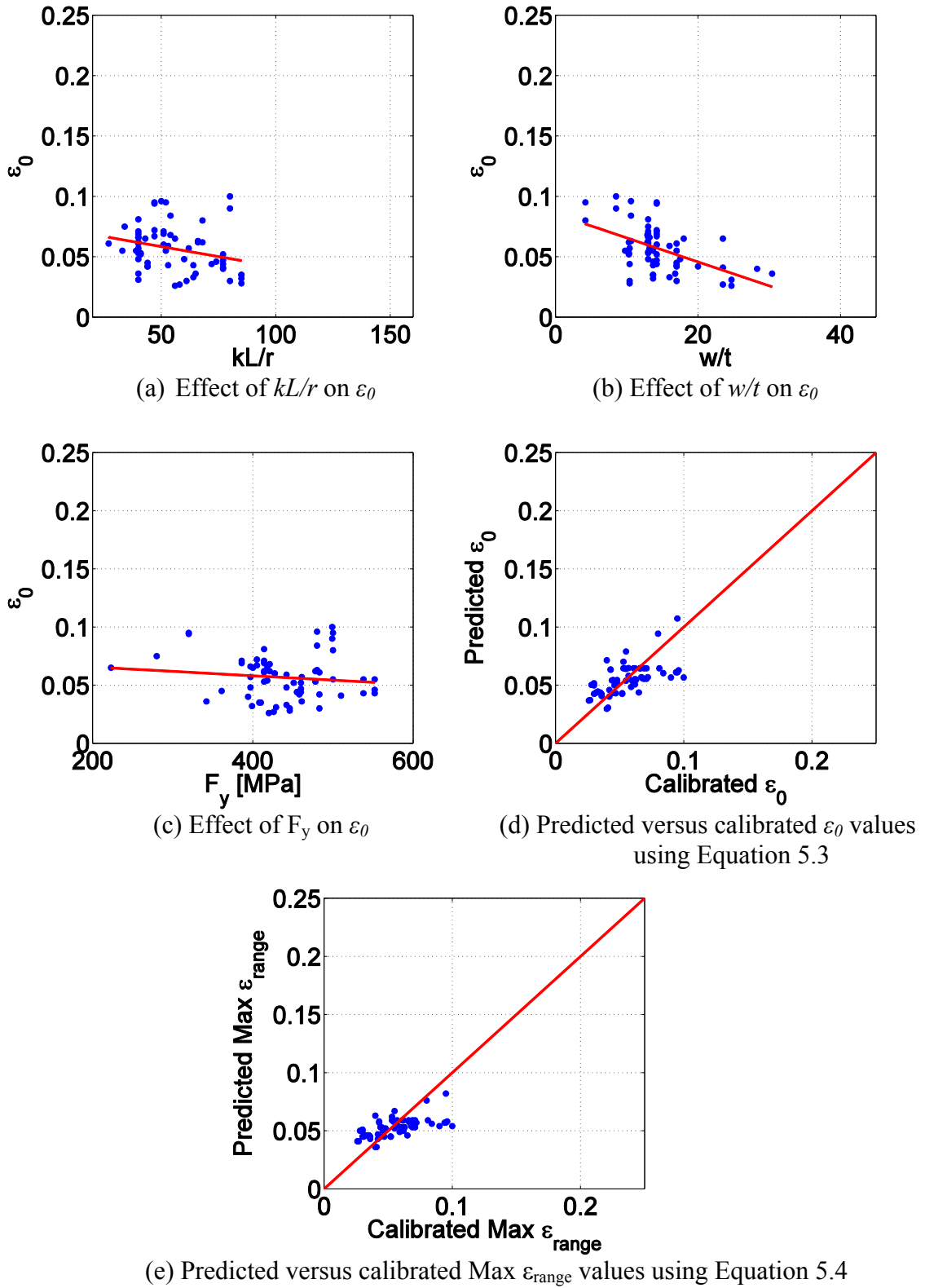


Figure 5.6 Individual trends and regression equations for rectangular HSS sections

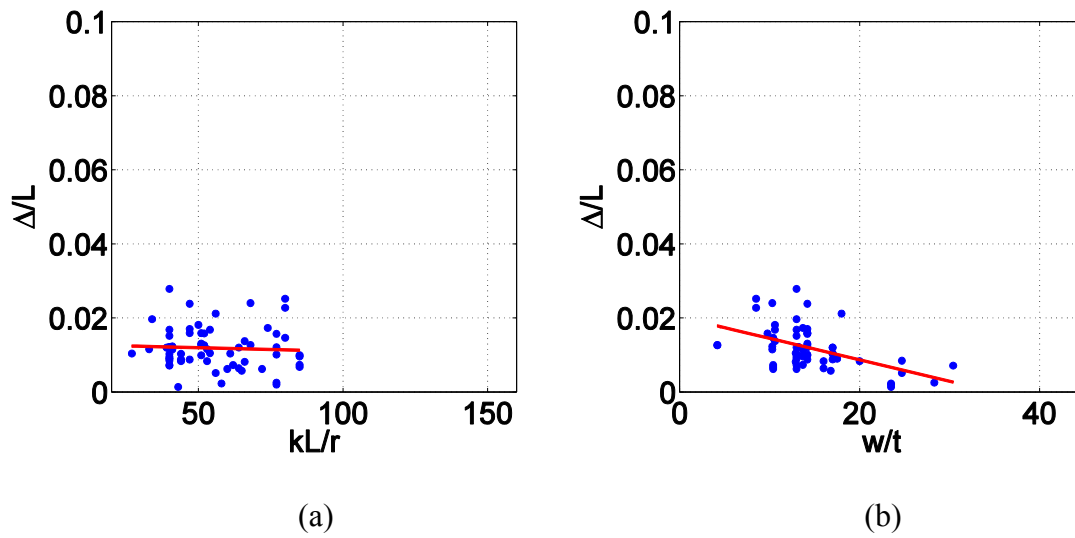


Figure 5.7 Effect of geometric parameters on the normalized axial displacement at fracture for rectangular HSS sections; (a)  $kL/r$  (b)  $w/t$

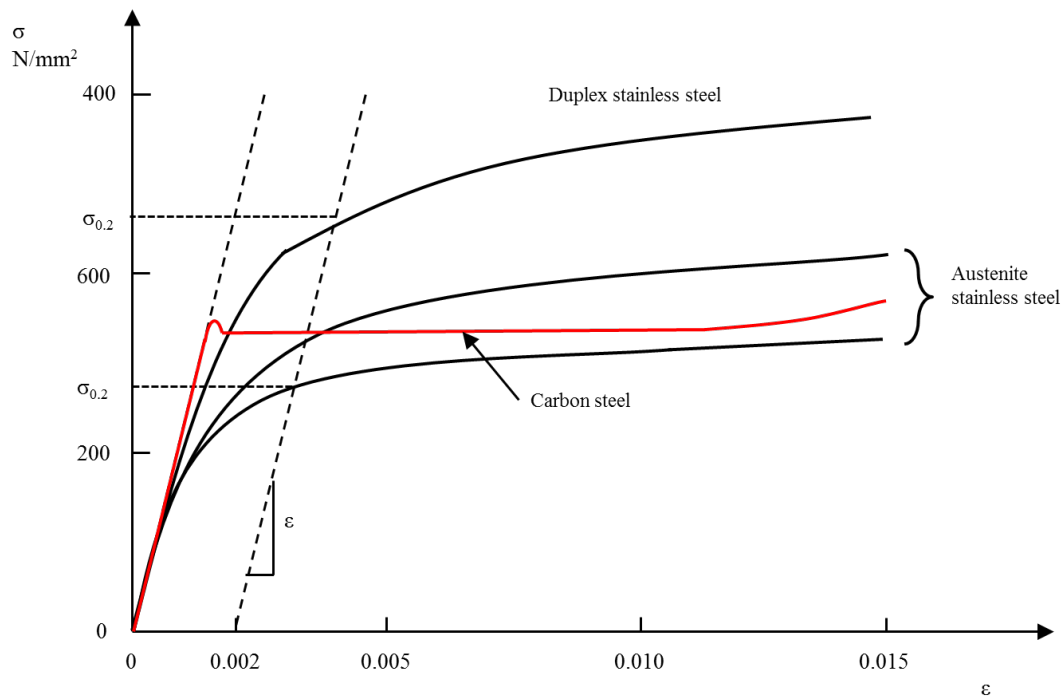


Figure 5.8 Stress-strain curves of carbon steel and stainless steel (BSSA, 2012)

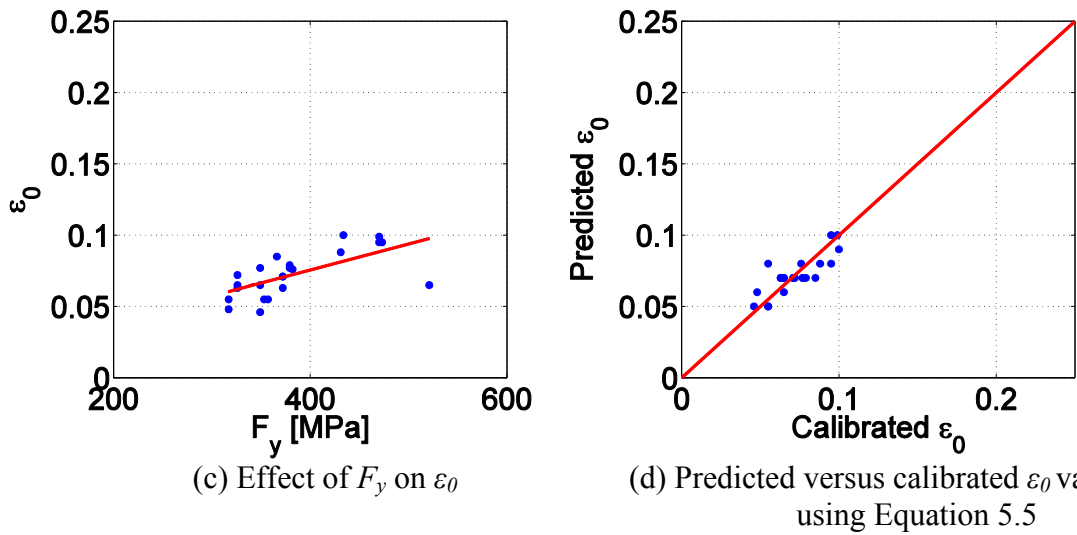
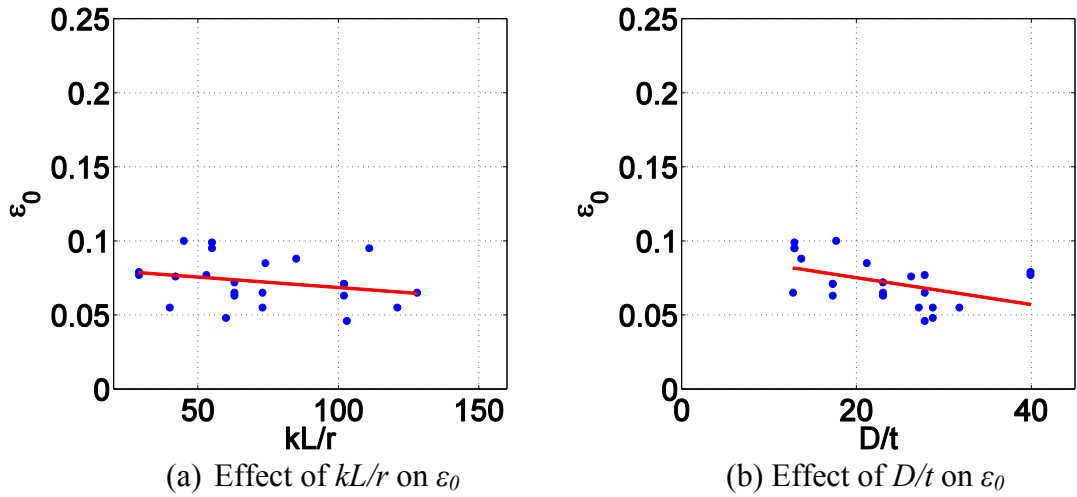


Figure 5.9 Individual trends and regression equations for round HSS braces

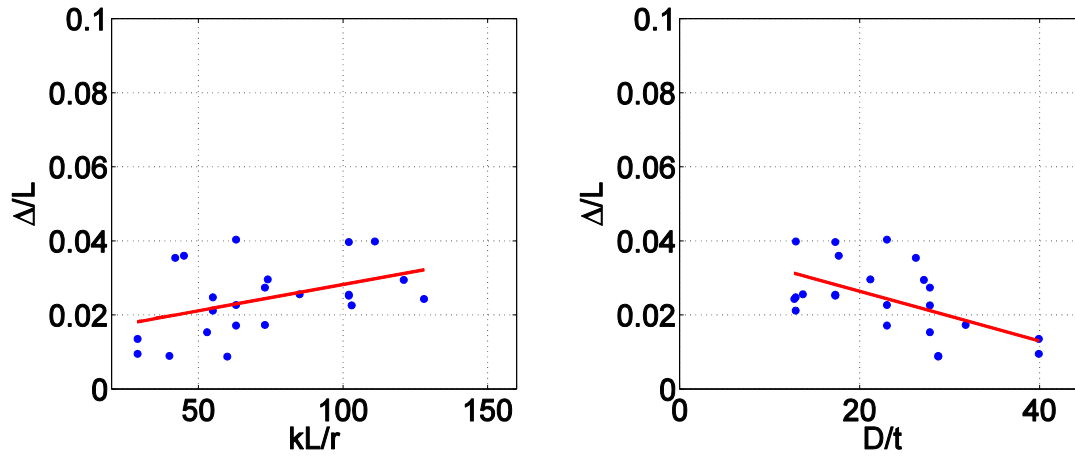


Figure 5.10 Effect of geometric parameters on the normalized axial displacement at fracture for round HSS sections; (a)  $kL/r$  and (b)  $D/t$

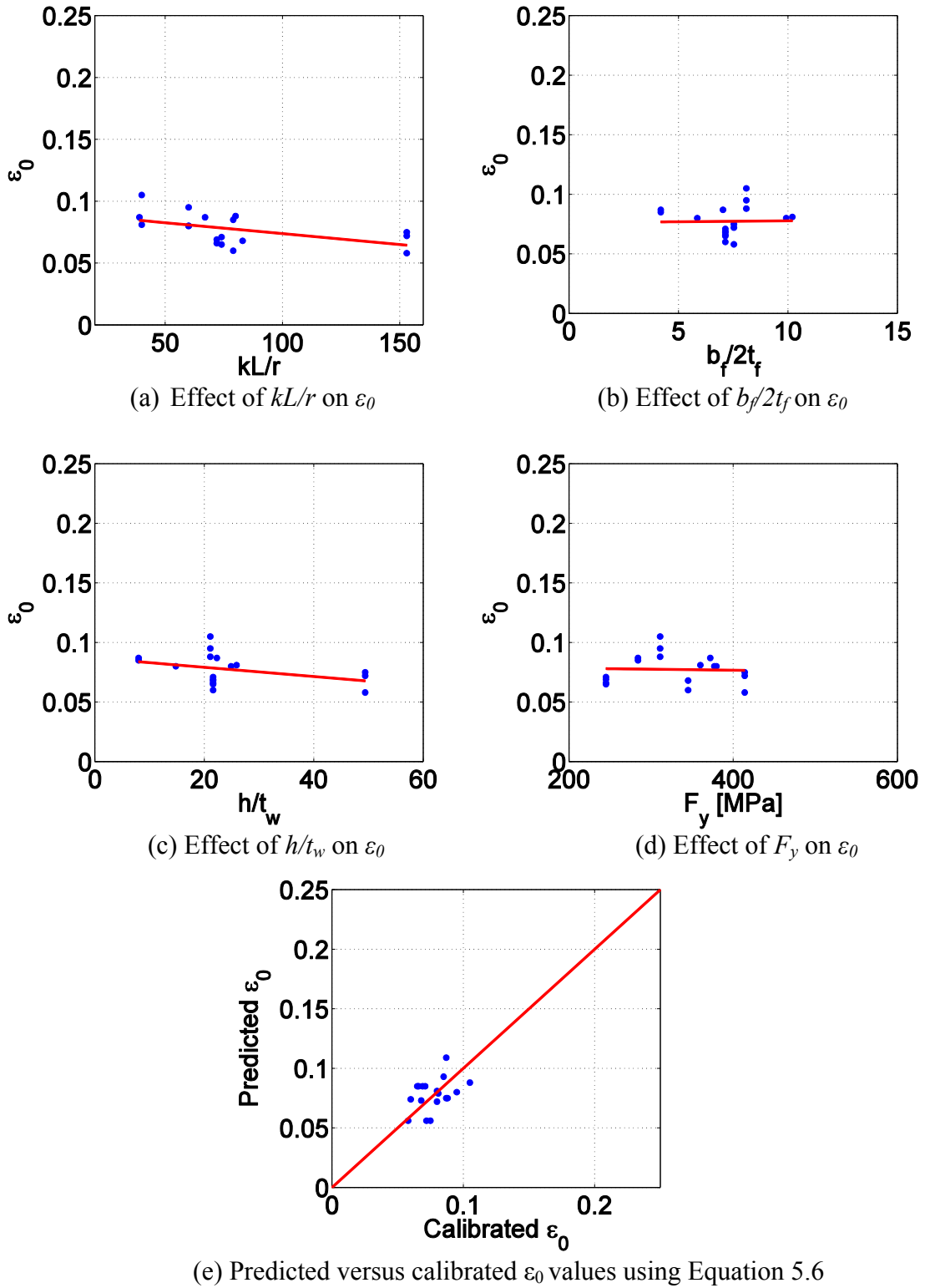


Figure 5.11 Individual trends and regression equations for W- sections

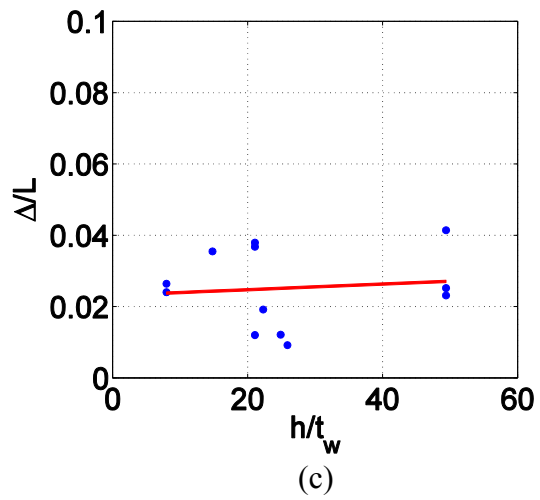
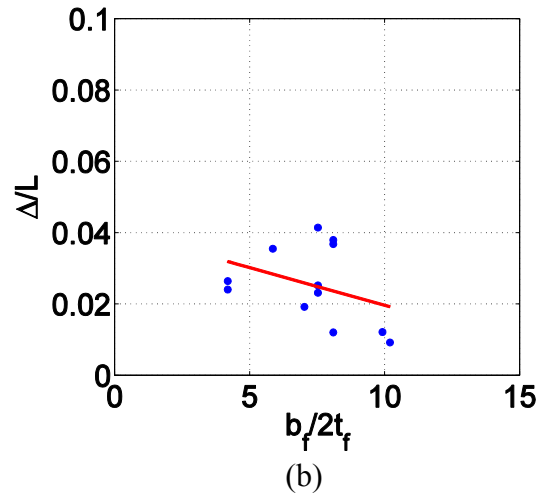
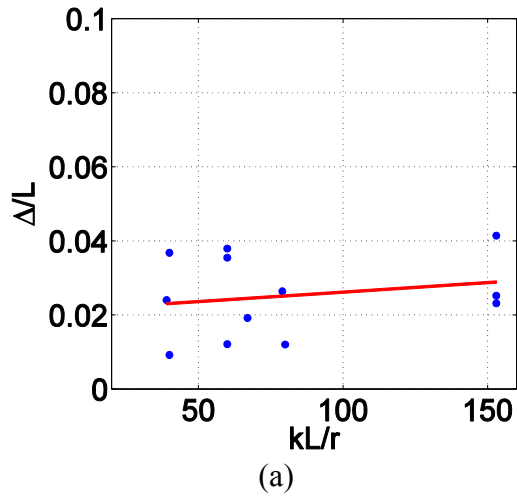


Figure 5.12 Effect of geometric parameters on the normalized axial displacement at fracture for round W- sections; (a)  $kL/r$ , (b)  $b_f/2t_f$  and (c)  $h/t_w$

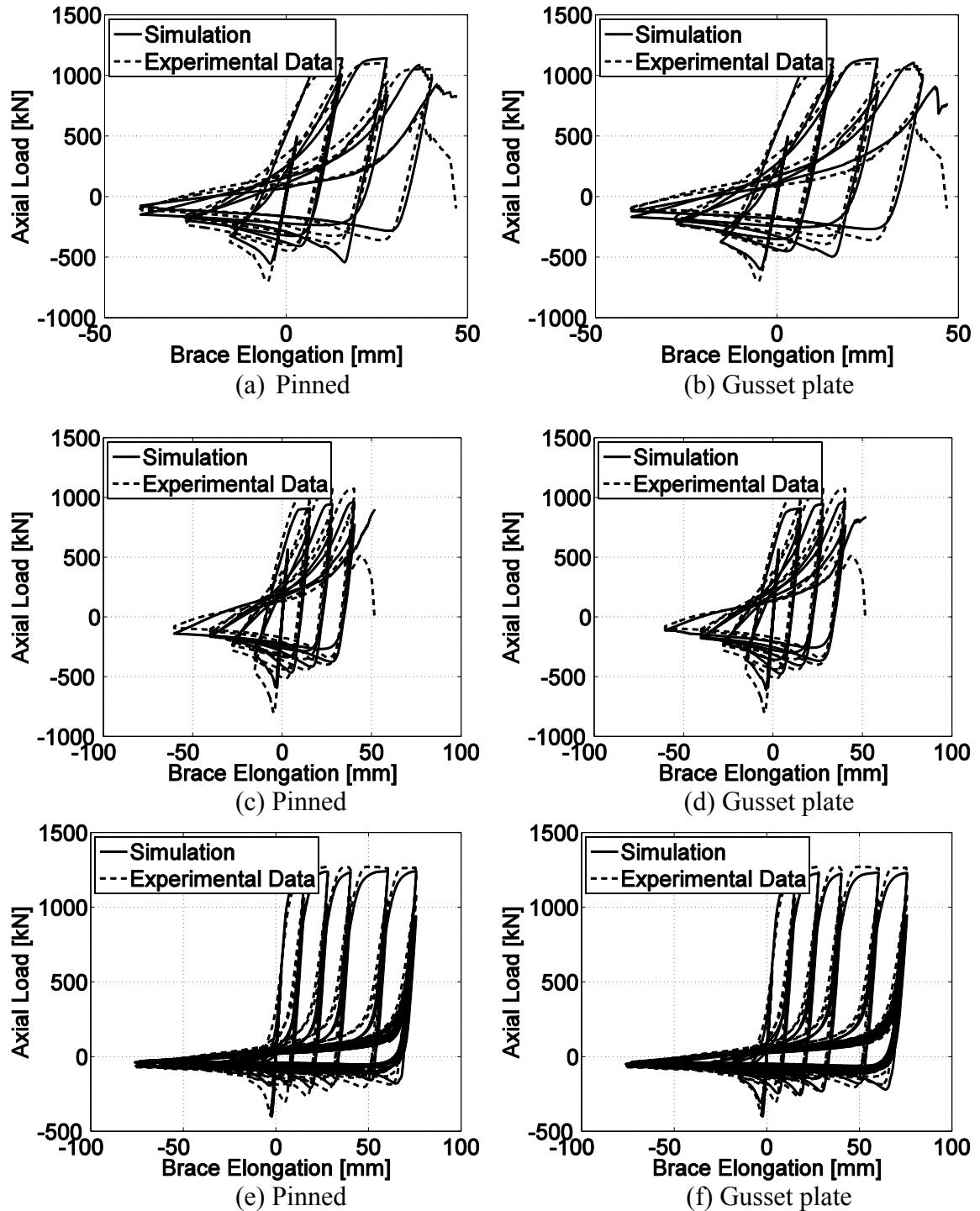


Figure 5.13 Effect of modelling gusset plates on the hysteretic behaviour of steel braces: (a) 102x102x6.4 (Fell et al. 2010); (b) 102x102x6.4 (Fell et al. 2010); (c) 141x6.4 (Fell et al. 2010); (d) 141x6.4 (Fell et al. 2010); (e) W310x24 (Fell et al. 2010); (f) W310x24 (Fell et al. 2010)

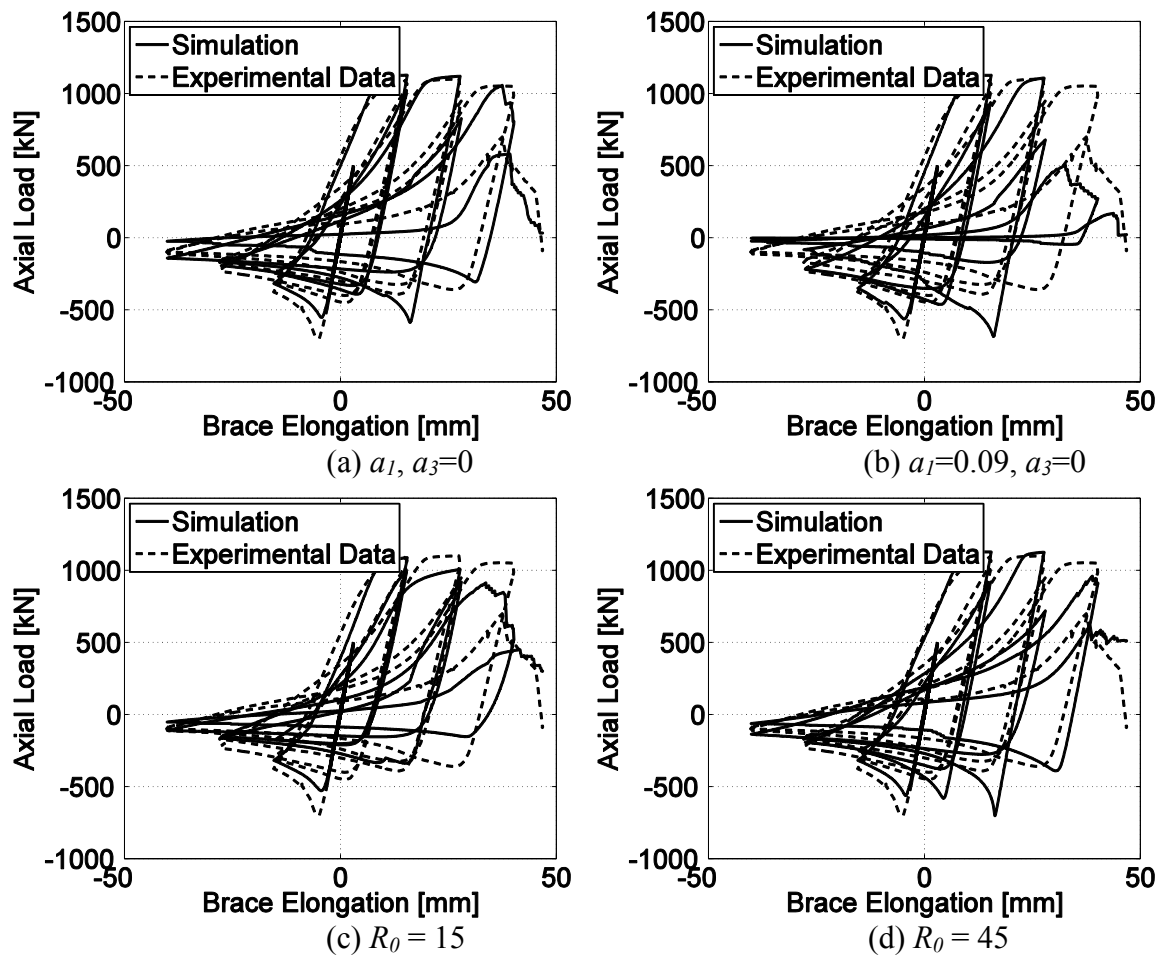


Figure 5.14 Effect of  $a_1$ ,  $a_3$  and  $R_0$  on the hysteretic behaviour of a steel brace: (a) 102x102x6.4 (Fell et al. 2010); (b) 102x102x6.4 (Fell et al. 2010); (c) 102x102x6.4 (Fell et al. 2010); (d) 102x102x6.4 (Fell et al. 2010)

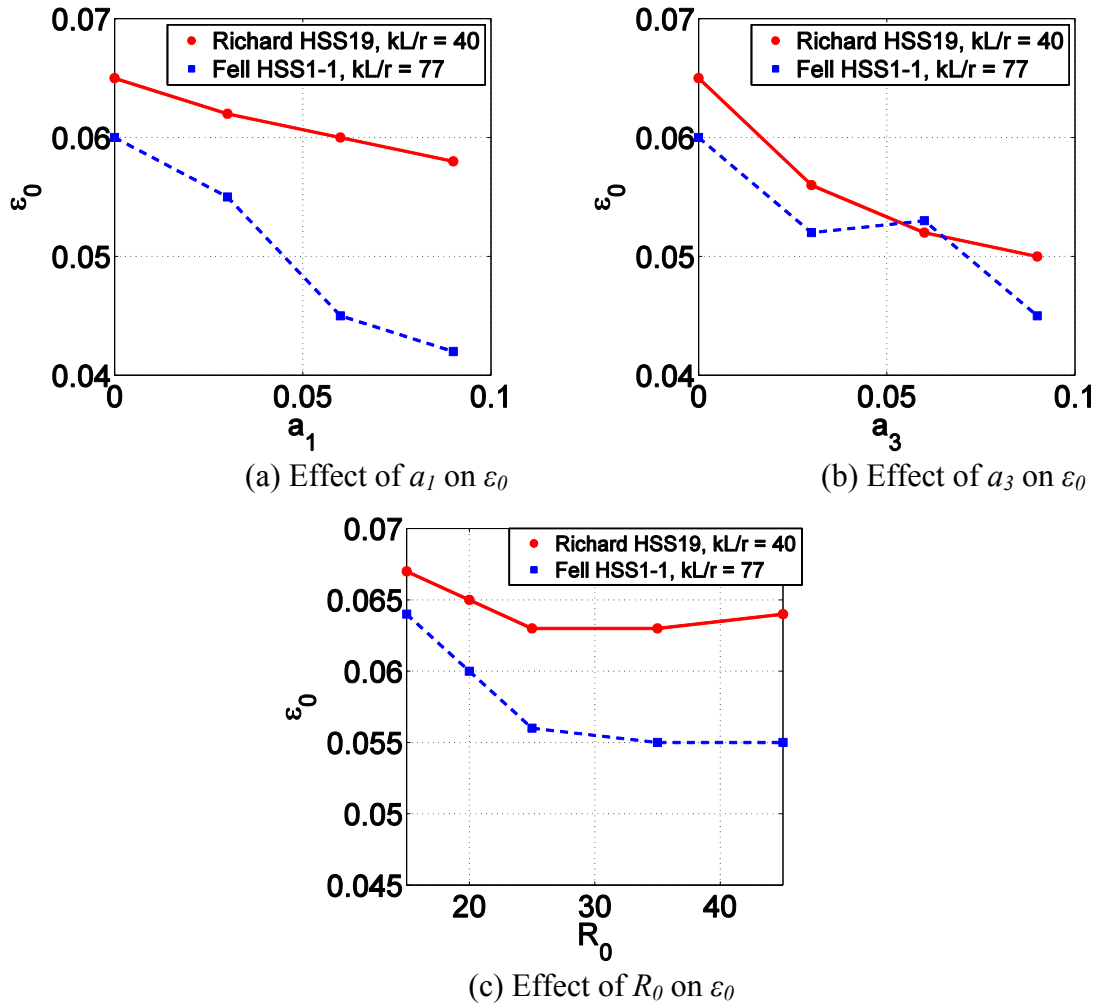


Figure 5.15 Effect of  $a_1$ ,  $a_3$ ,  $R_0$  on the fracture parameter  $\varepsilon_0$  of steel braces



# Chapter 6

## Case Studies

---

### 6.1 Introduction

This chapter summarizes two major case studies that have been used to evaluate the capability of modelling the post-fracture behaviour of concentrically braced frames (CBFs) subjected to earthquake excitations. The emphasis is on the development of a computational framework that reliably estimates the collapse capacity of CBFs during extreme earthquakes. The first case study that is used as a benchmark is a one-bay, two-story Special Concentrically Braced Frame (SCBF) that was tested under static cyclic loading at the University of California at Berkeley. The second case study is a one-bay, 12-story SCBF that has been designed in California based on AISC (2005) seismic design provisions. The proposed computational framework for collapse assessment of CBFs explicitly considers strength and stiffness deterioration of other structural components of CBFs; therefore dynamic collapse can be traced explicitly without the use of non-simulated collapse criteria. In particular, emphasis is placed on deterioration modelling of steel beams and columns and the gusset plate beam-to-column connections. Special emphasis is made on the damping assumption to be used for dynamic analyses of braced frames and the implication of negative stiffness on the seismic performance of these frames.

## 6.2 Description of the Benchmark 2-Story SCBF

The one-bay, two-story Special Concentric Braced Frame (SCBF) is designed and built in accordance with the AISC Seismic Design Provisions (AISC 1997) and the Load and Resistance Factor Design (LFRD) (AISC 1993) as discussed in Uriz (2005). Figure 6.1 shows the basic dimensions of the prototype CBF. Its total height is 5.8 meters (19ft) and its bay width is 6.1 meters (20ft). The first story of the test frame is 3.0 meters (10ft) tall and the upper story is 2.8 meters (9ft) tall suggesting that the frame is a nearly full-scale representation of the prototype design (Uriz 2005). A chevron configuration bracing system employing square HSS braces of ASTM A500 GR.B steel is used as the lateral load resisting system. The beams and columns of the frame are W-shape members of ASTM 992 and ASTM 572 Grade 50 steel, respectively. Connection details are designed based on AISC (1993, 1997) provisions. The gusset plate connections are determined using the uniform force method (AISC 1993) and designed to allow for a fold line formation equal to twice the thickness of the gusset plate. The steel braces are reinforced with steel plates in the gusset plate connection region in order to prevent premature fractures at the reduced net section. Beam-to-column connections are detailed assuming pinned end conditions. Lack of a floor slab resulted in a lateral support of the beams for out-of-plane deformations at the ends of the members. The locations of the lateral support are marked in Figure 6.1. Section and material properties of the members employed in the frame are displayed in Table 6.1 and Table 6.2, respectively. Figure 6.2 displays a photograph of the SCBF as built prior to the execution of the experimental program.

The frame shown in Figure 6.1 was tested with a 6700kN (1500kips) horizontal actuator

that was attached at the top beam of the test frame (see Figures 6.1 and 6.2). The standard AISC static-cyclic symmetric loading protocol was employed for the quasi-static test. Figure 6.3 displays this loading protocol in terms of roof drift ratio versus the number of loading cycles. More information about the test frame and loading conditions can be found in Uriz (2005).

### **6.3 Summary of the Experimental Results**

Based on the experimental results of the earlier study by Uriz (2005), points A and B, that are marked in Figure 6.3 and correspond to a roof drift ratio of 0.76%, are the points at which both braces in the lower story experience global buckling. A significant drop in lateral force resistance of the test frame is observed in the first story of the test frame. This can be seen in Figure 6.4 that shows the base shear versus first story drift ratio (SDR) of the test frame. Based on the drift-based fragility curves that were developed in Chapter 4, at this level of story drift ratio, which corresponds to 1.20% at the first story, global buckling of the rectangular HSS braces is expected to occur with almost 100% probability of exceedence. From the same figure, Points C and D are associated with the occurrence of the initial and the complete fracture of the lower story south brace of the test frame. Similarly, points E and F are associated with the initial and the complete fracture of the lower story north brace of the same frame. The first story drift ratio when fracture of these braces occurred was 2.50%. When compared with the drift-based fragility curves for rectangular HSS brace fracture, this drift ratio corresponds to 80% probability of fracture at the steel braces that are located in the first story. These simple calculations demonstrate the effectiveness of the drift-based fragility curves that were

presented in Chapter 4 as a tool for rapid damage assessment of steel braced frames.

After the occurrence of fracture of both steel braces in the first story of the test frame, the lateral stiffness of the test frame decreased rapidly. This can be seen in Figure 6.4 that shows the base shear versus  $SDR_1$  of the test frame. From this figure, the reserved capacity of the test frame after fracture of both braces occurred is attributed to the frame action associated with the steel columns and the gusset plate beam-to-column connections. The axial load-displacement hysteretic diagrams for both braces of the first story of the test frame are shown in Figure 6.5. After fracture occurred at the lower story braces, a first story collapse mechanism was developed due to the formation of plastic hinges at the first story columns of the test frame. When  $SDR_1$  became 8%, ductile tearing occurred at the first story column flanges as shown in Figure 6.6. Points G and H shown in Figures 6.3 and 6.4 are associated with start of ductile tearing of the north and south first story columns of the test frame. Note that the steel braces in the second story of the SCBF did not experience global buckling. The test stopped one loading cycle after ductile tearing occurred at the flanges of the lower story columns of the test frame.

## **6.4 Analytical Model for the Concentrically Braced Frame**

A 2-dimensional (2-D) analytical model is built in OpenSees (McKenna 1997) in order to simulate the seismic performance of the SCBF discussed in Section 6.3. The ability of this model to simulate fracture of the steel braces due to low cycle fatigue is validated with the quasi-static loading protocol that was discussed in the previous section. The same analytical model is then employed for further investigations. Therefore, a pushover

analysis is conducted based on a triangular lateral load pattern. Finally, the collapse capacity of the same frame is evaluated through Incremental Dynamic Analysis (IDA) as discussed in Vamvatsikos and Cornell (2002).

Figure 6.7 shows an overview of the proposed analytical model of the 2-story CBF. Strength and stiffness deterioration of various structural components of the SCBF is considered. In particular, the steel columns and beams are modeled with elastic elements with concentrated plasticity springs at their ends. These springs utilize the bilinear modified Ibarra-Medina-Krawinkler (IMK) deterioration model (Ibarra et al. 2005, Lignos and Krawinkler 2011). This model captures cyclic deterioration in strength and stiffness of these structural components. The parameters that determine the behaviour of these springs are determined based on multivariate regression equations developed by Lignos and Krawinkler (2011) and have been adopted by ATC-72 (ATC/PEER 2010) modelling guidelines for structural systems. Figure 6.8 shows an example of a typical calibration of the hysteretic response of the modified IMK model in comparison with the deduced moment rotation diagram of a steel beam (Taejin et al. 2000). The modified IMK model does not capture axial force-bending moment (P-M) interaction. However, for stocky columns, such as the ones used as part of the design of the test frame (see Figure 6.1), this effect is less critical since these members tend to deteriorate less in strength due to their short web (Lignos and Krawinkler 2011). This can be observed in Figure 6.9 that shows the hysteretic response of a stocky column (W14x176), which is subjected to 35% axial load ratio (Newell and Uang 2008). In the same figure, the calibrated hysteretic response of the modified IMK model is superimposed. The

comparison with the experimental data demonstrates that this model is able to represent fairly well the behaviour of such components.

The gusset plate beam-to-column shear connections of the test frame are modeled with the pinching version of the modified IMK model, which was implemented in OpenSees for this purpose (Lignos and Krawinkler, 2012). The properties of these springs are calibrated based on experimental data from Liu and Astanteh (2000, 2004). More recent experimental data on the cyclic behaviour of gusset plate beam-to-column shear connections have become available by Stoakes and Fahnestock (2011, 2012). This experimental data can also serve for the same purpose. Figure 6.10 displays an example of the hysteretic moment-rotation behaviour of the modified IMK model with pinching hysteretic response. This model is fully defined with the elastic stiffness  $K_e$  of the gusset plate beam-to-column connection, the effective bending yield strength  $M_y$ , the pre-capping  $\theta_p$  and post-capping  $\theta_{pc}$  rotation capacities of the component. A residual strength factor  $\kappa$  is also needed to full define the backbone curve of the component in the presence of residual strength. Pinching is controlled by two parameters that define the strength and the displacement that pinching occurs. The modified IMK model is able to capture the deterioration in strength, post-capping strength, unloading stiffness and reloading stiffness based on a parameter  $\lambda$  that defines the reference energy dissipation capacity of a gusset plate beam-to-column connection. More information about the modified IMK model can be found in Lignos and Krawinkler (2011, 2012b).

The flexibility and strength of the gusset plates are modeled with concentrated plasticity

springs that are placed between the physical ends of the braces and the rigid offsets that represent the rest of the gusset plates. These springs utilize the Menegotto-Pinto (1973) material model. The flexural stiffness and strength of these springs is determined with the proposed relationships by Hsiao et al. (2012) (see Section 5.8).

The steel braces are modeled with the approach discussed in Chapter 5 (see Section 5.5). The parameter  $\varepsilon_0$  that is used to model fracture due to low-cycle fatigue is determined based on the multivariate regression Equation 5.3 (see Section 5.5). The determined fracture parameters  $\varepsilon_0$  and  $m$  used for all the steel braces are 0.064 and -0.3, respectively, given their  $kL/r$  and  $w/t$  ratios and their measured yield stress. The parameters  $a_1$ ,  $a_3$  and  $R_0$  for the Steel02 material are selected based on Table 5.6. The number of selected fibers to discretize the HSS cross section is also based on the same table. The results of these analyses are discussed in the next sections.

## **6.5 Results and Discussion**

### **6.5.1 Static-cyclic analysis**

The modelling approach that is discussed throughout this thesis resulted in a satisfactory performance in determining the global and local cyclic response of the test frame and its braces (see Section 6.3). The loading protocol shown in Figure 6.3 is applied to the analytical model of the test frame. Figure 6.4 shows a comparison of the base shear versus story  $SDR_1$  as predicted with the analytical model of the test frame and the experimental data. The strength and stiffness degradation of the test frame due to fracture of the braces are predicted fairly accurately (points E, D). The reserved capacity of the

test frame after fracture of both first story braces is also predicted fairly well. Note that the post-fracture behaviour of the test frame is primarily attributed to the frame action only, which is a combination of the column and gusset plate beam-to-column connection strengths.

Figure 6.5 shows the hysteretic response of the north and south steel braces in the first story of the test frame as predicted by the analytical model. In the same figure we have superimposed the experimental results for the same braces. The maximum compressive load and axial deformation that brace global buckling occur is predicted fairly well for both braces. From the same figure it can be seen that the loading cycle that fracture occurs at the mid-length of each brace is also predicted. This demonstrates the effectiveness of the proposed predictive equations discussed in Chapter 5 for fracture modelling of steel braces that fail at their mid-length.

The test stopped once ductile tearing occurred at the top of the first story columns (see Figure 6.6) due to large plastic deformations that occurred upon the fracture of the braces at the same location (Uriz, 2005). The proposed analytical model of the test frame is able to simulate these phenomena as illustrated in Figure 6.11a. This figure shows the moment-rotation of the south steel column at the base of the analytical model. From this figure it can be seen that strength deterioration occurs at about 5% plastic deformation, which is consistent with the test observations. Figure 6.11b shows the moment rotation at the top of the same column. The same conclusions can be found.

### 6.5.2 Pushover Analysis

A pushover analysis (Krawinkler and Seneviratna 1998) is also conducted with the same frame, assuming a lateral load pattern determined by the equivalent lateral force procedure (IBC, 2003). P- $\Delta$  effects are considered in the analysis with a presence of a leaning column. Due to similitude 1000kN per story was assumed to represent gravity loading.

Figure 6.12 shows the pushover analysis in terms of base shear versus roof drift ratio (defined as the roof displacement normalized by the total height of the test frame). Figure 6.13 shows the base shear versus first story drift ratio obtained from the same pushover analysis. From these two figures it can be concluded that a first story collapse mechanism forms since the plastic deformation is concentrated at the first story. In the same figures, point A represents the point that global buckling of the south lower story brace occurs. Point B represents the formation of plastic hinges at the top and bottom of the first story columns. The upper story beam, columns and braces remained elastic during the pushover analysis. These results confirm the first story collapse mechanism that formed during the quasi-static loading protocol that was used during the experimental program discussed in Section 6.3. In Figures 6.12 and 6.13 we have also superimposed the same results without the consideration of P- $\Delta$  effects. A comparison of the two curves (noted as P- $\Delta$  and No P- $\Delta$ ) shows that the strength deterioration of the structural components of the test frame is significant compared to the geometric effects that are associated with the vertical load applied to the 2-story SCBF.

### **6.5.3 Collapse Assessment of CBFs through Incremental Dynamic Analysis: Rayleigh Damping with Initial Stiffness Proportional Damping Assumption**

In this section, Incremental Dynamic Analysis (IDA) is conducted to assess the collapse capacity of the 2-story SCBF. A set of 40 ground motions, compiled by Medina and Krawinkler (2003) is used in order to conduct the analysis. These ground motions represent ordinary records with a Magnitude  $6.5 < M < 6.9$  and a distance  $13 < R < 40\text{km}$  from the rapture zone. Table 6.3 displays a summary of the main characteristics of the selected ground motions to be used in IDA. The 5% damped spectral acceleration at the first mode period of the test frame  $S_a(T_1, 5\%)$  is used as an Intensity Measure (*IM*) to scale incrementally the ground motions. This IM has been widely used in the past in a number of similar studies (Vamvatsikos and Cornell 2002; Medina and Krawinkler, 2003, Ibarra and Krawinkler 2005, Zareian and Krawinkler 2007, Lignos and Krawinkler 2012b).

In order to conduct the nonlinear response analysis a  $\zeta=2\%$  Rayleigh damping approximation at the first and second mode of the 2-story SCBF is used to simulate viscous damping. The first and second modes of the 2-story CBF frame are 0.30sec, and 0.1sec, respectively. The stiffness proportional part of the Rayleigh damping matrix is based on the initial stiffness of the SCBF. This assumption is commonly used in commercially available software.

A time-variant integrator has been developed and implemented in the OpenSees simulation platform that guarantees numerical convergence of the equation of motion

particularly at large deformations. The numerical stability of this integrator and its reliability to compute the response history of frame structures through collapse has been validated with recent small and full-scale collapse experiments (Lignos et al. 2011, 2013, Suita et al. 2008). Figure 6.14 displays the IDA curves of the 2-story SCBF in terms of IM versus maximum SDR. Note that when the individual curves become flat, dynamic instability occurs, i.e., dynamic collapse is simulated explicitly (Lignos et al. 2011). However, from the same figure, for some of the ground motions the 2-story CBF has an unexpectedly large collapse capacity. Two of those cases are highlighted in Figure 6.14 with a dashed line. Note that often times in IDA it is expected that when the intensity of the ground motion increases, at some point, the maximum SDR to decrease for a short term because the collapse direction of the frame changes. This has been shown analytically (Ibarra et al. 2002, 2005) and experimentally (Lignos et al. 2011). This phenomenon is noted as “resurrection from death” and can be seen on Figure 6.14 in the green dashed-dotted curve. The resurrection can only occur once since the structure will either collapse in one loading direction or the other. Therefore, when the two red dashed curves on Figure 6.14 are examined, this resurrection phenomenon is observed multiple times; this results in an unexpectedly large collapse capacity of the 2-story CBF. Therefore, a force “holds” the 2-story CBF from collapsing. The same observation is confirmed from the collapse fragility curve of the same frame that is shown in Figure 6.15. Based on this figure, the 2-story CBF has a median collapse capacity of 1.98g and a standard deviation of 0.38.

In order to examine the unexpected behaviour observed in the IDA results, a closer look

of individual nonlinear response history analyses near collapse is necessary. For this reason, results from the Canoga Park record from the 1994 Northridge earthquake are examined. The ground motion has been scaled by a factor two compared to the unscaled record.

Figure 6.16 displays the story drift histories during the Canoga Park record. Plastic deformations are concentrated in the first story of the SCBF. The upper story remains elastic. This is consistent based on the quasi-static and pushover analyses that were conducted prior to IDAs in terms of the location of the collapse mechanism of the 2-story SCBF. Figure 6.17 shows the base shear versus storySDR<sub>1</sub> of the frame. From this figure, when the frame deteriorates in strength (at about 2% radians) and essentially is in its negative stiffness region near the verge of collapse when it unloads at about 6% radians, its unloading stiffness is not close to straight line as one would expect for an ordinary steel structure. The observed energy dissipation towards the end of the ground motion implies that high velocity forces have been developed in the frame. Similar observations can be done from Figure 6.18 that shows the hysteretic response of the steel braces of the 2-story SCBF. The upper story braces remained elastic. However, even after fracture, the bottom story braces maintain strength, which is inconsistent with experimental observations. The original assumption that the stiffness proportional part of the Rayleigh damping matrix is proportional to the initial stiffness of the 2-story SCBF needs to be further examined since this is the primary reason that produces artificial damping forces once the steel braces in the first story of the SCBF fracture. Since the steel braces of the 2-story SCBF primarily provide its lateral load resistance, once these components

fracture, a large decrease of the lateral stiffness of the SCBF occurs. If the assumption of initial stiffness proportional damping is used, this decrease of stiffness is not captured on the Rayleigh damping matrix of the frame; therefore, large artificial damping forces are produced (Charney, 2008). This can be further explained from Equation 6.1 that describes the basic formulation of the damping forces based on the Rayleigh damping assumption. In this equation, the vector  $F_d$  represents the viscous damping forces of the 2-story SCBF in the equation of motion. These forces are equal to the product of the Rayleigh damping  $[C]$  multiplied by the relative velocity histories  $V(t)$  of the dynamic degrees of freedom of the SCBF. Based on the Rayleigh damping approximation, the damping matrix  $[C]$  is proportional to the stiffness matrix  $[K]$  and the mass matrix  $[M]$  of the SCBF. If the stiffness term  $[K]$  is not updated with the current stiffness of the SCBF during the response history, the generated damping forces will not be realistic. Following the change in state of steel braces after fracture occurs, large viscous damping forces are generated based on the initial stiffness matrix of the SCBF. These forces are the product of the post-event deformational velocities multiplied by the initial stiffness and by the stiffness proportional coefficient  $a_1$  as defined based on Rayleigh damping.

$$F_d = [C] \cdot V(t) = (a_0[M] + a_1[K]) \cdot V(t) \quad (6.1)$$

In order to address this issue, the stiffness proportional part of the Rayleigh damping matrix is modified and is computed based on the current stiffness of the SCBF. The findings from these analyses are presented in the next section.

#### **6.5.4 Collapse Assessment of CBFs through Incremental Dynamic Analysis: Rayleigh Damping with Current Stiffness Proportional Damping Assumption**

In order to be able to assess the effect of the modified damping assumption on the collapse capacity of the SCBF, a non-linear response history analysis is conducted with the same frame and the Canoga Park record that was previously used. The story drift ratio histories during the ground motion are presented in Figure 6.19. This figure suggests that a first story collapse mechanism forms in the 2-story SCBF, which is similar with the results from Figure 6.16. However, when we look at the base shear versus story SDR1 of the same frame (see Figure 6.20), once the steel braces fracture, the framing action solely contributes to the lateral resistance of the 2-story SCBF and when the first story displacements become large the SCBF collapses. The collapse point is the one associated with zero base shear. This is a consistent definition of collapse with findings from recent small and full-scale collapse tests (Lignos et al. 2007, 2013, Suita et al. 2008). Note that the unexpected behaviour due to high velocity forces has diminished indicating that the primary reason is the modified damping assumption. Looking at the hysteretic response of the steel braces of the first story of the SCBF, it can be seen that once these braces fracture, their axial resistance remains at zero. A synthesis of the results presented in Figures 6.16, 6.17, 6.19 and 6.20 demonstrate that the commonly employed drift-based non-simulated collapse criteria (FEMA P695) that are typically employed to trace dynamic collapse of structural systems may lead to significant errors. Collapse should be traced based on a combination of criteria that associate large story drift ratios and the shear resistance of the individual stories of a frame structure at the corresponding drifts.

After re-visiting the Rayleigh damping assumption, incremental dynamic analysis is repeated with the set of 40 ground motions that were previously discussed. Figure 6.22 displays the IDA curves in terms of IM versus maximum SDRs. A comparison between these curves and the ones from Figure 6.14 suggest that the unexpected large collapse capacities observed in some of the IDA curves due to the initial stiffness proportional Rayleigh damping assumption are not observed anymore. This can also be seen from the collapse fragility curve of the same frame that is shown in Figure 6.23. Note that the median collapse capacity of the 2-story SCBF is 1.17g based on the same figure. When compared to median collapse capacity of the same frame from Figure 6.15, a reduction of about 41% is notable. This very important finding, suggests that if the commonly employed damping models that are widely used in nonlinear response history analysis of structural systems are based on their initial stiffness the collapse capacity of these systems can be largely overestimated.

## **6.6 Description of the 12-Story SCBF**

In this section, the computational framework for collapse assessment of CBFs is employed to compute the collapse capacity of a 12-story steel building with Special Concentrically Braced Frames (SCBFs) in both loading directions. The building is designed in accordance with the AISC Seismic Design Provisions (AISC 2005) as discussed in NIST (2010). The same building is part of a number of archetype buildings that were used in the NIST (2010) study to evaluate the FEMA P695 methodology for quantification of seismic performance factors for buildings that utilize braced frames and

other widely used lateral resisting systems such as special moment resisting frames and shear walls. The plan view and elevation of the archetype SCBF can be seen in Figures 6.24 and 6.25, respectively. The total height of the SCBF is 55.2m (180ft). The typical story height of the SCBF is 4.6m (15ft) and its bay width is 9.1m (30ft). An alternating chevron bracing configuration employing round HSS braces of ASTM A500 grade B steel is used as the lateral load resisting system as shown in Figure 6.25. These braces are reinforced in the net section area in order to avoid net section fractures. The beams and columns of the SCBF are W-shape members of ASTM 992 steel. Gusset plate connection details were not provided for the original archetype building. However, a detailed design of these connections is done herein. The gusset plates are fabricated with ASTM A572 Gr. 50 steel and typical corner and middle gusset plate designs are shown in Figure 6.26 and 6.27, respectively. The gusset plates were designed using the guidelines suggested by Lehman et al. (2008) and allow for an elliptical gusset plate clearance equal to eight times the thickness of the gusset plate. The thicknesses of the gusset plates are assumed to be 19mm. For this design pinned end connections are assumed for the beam-to-column connections. Section sizes and material properties of the structural members employed in the frame are summarized in Tables 6.4 and Table 6.5, respectively. Based on the gravity loads summarized on Table 6.6, the seismic weight of a typical floor and the roof of the frame is 8770kN (1971kips) and 6740kN (1515kips) respectively, and the total gravity weight of the frame is 30500kN (6858 kips).

## **6.7 Analytical model of the 12-Story SCBF**

The SCBF in the east-west loading direction is modeled in OpenSees. The modelling

approach that is employed for the steel braces has been extensively discussed in Section 5.6. The parameter  $\varepsilon_0$  that determines the fracture life of each steel brace of the 12-story SCBF is computed based on the multivariate regression Equation 5.5. The modelling recommendations for round HSS braces, which are summarized in Table 5.10, are employed for the steel braces discretization and nonlinear material input characterization.

Cyclic deterioration in strength and stiffness of steel beams, columns and gusset plate beam-to-column connections of the 12-story SCBF are modeled with the modified IMK model in a similar fashion with the 2-story SCBF that is discussed in Section 6.4. Panel zone shear distortion is explicitly considered with a parallelogram model that is able to deform in shear and a trilinear spring that is defined based on the Krawinkler (1978) model. The same approach has been successfully implemented in the past to investigate the influence of the panel zone hysteretic behavior on the dynamic response of steel moment resisting frames (Gupta and Krawinkler 1999).

The first three mode periods of the 12-story SCBF are 1.93sec, 0.62sec and 0.34sec, respectively. These periods are consistent with the original design that is summarized in NIST (2010).

## **6.8 Performance Evaluation**

A preliminary performance evaluation of the 12-story SCBF is conducted based on a nonlinear static analysis (pushover) based on a triangular lateral load pattern. Figure 6.28 shows the normalized base shear  $V$  with respect to the seismic weight  $W$  of the 12-story

SCBF versus the roof drift ratio. The design base shear of the frame is  $V/W = 0.073$ . Therefore, the overstrength of the 12-story SCBF frame is 1.64. This value is consistent with the corresponding values reported in NIST (2010) for the same SCBF.

Based on the triangular load pattern that is applied as a lateral load on the 12-story SCBF, the frame forms a local collapse mechanism that is concentrated over three stories including the fourth, fifth and sixth stories. Once the steel braces in these stories buckle, plastic deformations are concentrated in the same stories. However, since higher mode effects are neglected in pushover analysis and due to other shortcomings of the nonlinear static procedures (see Krawinkler and Seneviratna 1998, NIST 2010) nonlinear response history analysis needs to be conducted.

The collapse capacity of the 12-story SCBF is computed with the set of 40 “ordinary” ground motions that are summarized in Table 6.3. It is important to note that in California, where this frame has been designed, near-fault ground motions with forward directivity may control the long return period hazard of the seismic region. These ground motions have different frequency characteristics than the set of 40 records that are summarized in Table 6.3. However, the purpose of this research is to illustrate the proposed computational framework for collapse evaluation of braced frames. For this reason, the same set of ordinary ground motions is used at all hazard levels of intensity. Incremental dynamic analysis (Vamvatsikos and Cornell 2002) is used in order to determine the collapse capacity of the SCBF. Note that  $\zeta=2\%$  Rayleigh damping is assigned at the first and fifth mode of the SCBF. These modes are used in order to

capture the 90% of the seismic model mass of the 12-story SCBF. The stiffness proportional part of the Rayleigh damping matrix is based on the current stiffness of the SCBF that is computed per integration step during each ground motion for the same reasons summarized in the previous section. The IDA plots are shown in Figure 6.29 in which the 5% spectral acceleration at the first mode period of the structure is plotted versus the maximum story drift ratios of the 12-story SCBF.

The collapse safety of the 12-story SCBF can be evaluated using the collapse fragility curves that describe the probability of collapse of the SCBF as a function of the 5% first mode spectral acceleration of the SCBF. Figure 6.30 shows the counted collapse fragility curve (dotted points) based on the computed collapse intensities from the individual ground motions. This fragility curve is computed by treating the collapse capacity data as a random sample, i.e., equally likely outcomes. In the same figure, a lognormal distribution is fitted to the counted fragility curve. The median collapse capacity of the 12-story SCBF is 0.61g and the standard deviation  $\beta_{ln} = 0.61$ . Note that historically, this value is typically about 0.40 (Ibarra and Krawinkler 2002, Zareian and Krawinkler 2007, FEMA P695). However, the larger variability in the collapse capacity of the 12-story SCBF is attributed to the fact that once a set of steel braces that belong to a particular story fracture, plastic deformations localize in this story. Therefore, there are many more different collapse mechanisms that the SCBF is susceptible to compared to a special moment resisting frame.

## 6.9 Mean Annual Frequency of Collapse

In this section the collapse fragility curve of the 12-story SCBF is combined with the

seismic hazard curve at the design site, which gives the mean annual frequency of exceeding ground motion intensities at the site. The collapse risk assessment of the 12-story SCBF is seen through the mean annual frequency of collapse ( $\lambda_c$ ). Calculating  $\lambda_c$  involves integrating the collapse fragility curve of the 12-story SCBF over the seismic hazard curve at the design site based on the equation (Medina and Krawinkler 2002, Ibarra and Krawinkler 2005, Eads et al. 2012),

$$\lambda_c = \int_0^{\infty} P(C|im) \cdot |d\lambda_{IM}(im)| \quad (6.2)$$

In Equation 6.2,  $P(C|im)$  is the probability that the 12-story SCBF will collapse when subjected to an earthquake with ground motion intensity  $im$ ;  $\lambda_{IM}$  is the mean annual frequency of exceedence of the ground motion intensity  $im$ .

The Bulk Mail Center (33.996°N, -118.162°W) located in the downtown area of Los Angeles, California in the U.S is selected as the design site to compute the site-specific seismic hazard curve. This site represents a high seismicity urban area in California (Eads et al. 2012). The seismic hazard curve for  $S_a(T, 5\%)$  of the 12-story SCBF is obtained from the Ground Motion Parameter Calculator available from the United States Geological Survey (USGS, 2011). Since the USGS hazard curves correspond to the border of NEHRP site classes B and C, a site amplification factor of 1.5 is used to modify the curve for site class D. Figure 6.31 shows the seismic hazard curve at the site, which is computed based on interpolation of the hazard curves for  $T=1.0\text{sec}$  and  $T=2.0\text{sec}$  available from the USGS website. Equation 6.2 is used to compute  $\lambda_c$  by fitting a fourth-

order polynomial in log-log space to the points in the seismic hazard curve (see Figure 6.32). Therefore,  $\lambda_c = 5.5 \times 10^{-4}$ . This value corresponds to a 2.7% probability of collapse in 50 years for the same frame. This value is consistent but slightly larger than the corresponding values (1 to 1.5% probabilities of collapse in 50 years) of code-compliant steel special moment resisting frames and reinforced concrete moment frames obtained in earlier studies (Ibarra and Krawinkler 2005, Haselton and Deierlein 2006, Eads et al. 2012). This indicates that concentrically braced frames may have lower collapse capacities than it is believed since they are susceptible to local story collapse mechanisms once the steel braces in these stories fracture. This is confirmed for the 12-story SCBF from the large record-to-record variability of its collapse capacities ( $\sigma_{ln}=0.55$ ) compared to a typical dispersion  $\sigma_{ln}=0.35$  to 0.40 that has been historically documented for steel MRFs. The authors reached to similar findings after evaluating a 2-story SCBF designed in the same location (Lignos et al. 2012). Further analytical investigations should be conducted to confirm this finding.

## 6.10 Summary

In this chapter, the collapse assessment of a 2-story and a 12-story SCBF is evaluated through incremental dynamic analysis and collapse fragility curves. A framework is presented for reliable collapse assessment of braced frames that accounts for the strength and stiffness deterioration of various components of these frames. Modelling guidelines for post-buckling behaviour and fracture of steel braces discussed in Chapter 5 are found to provide satisfactory results when they are evaluated with a benchmark experimental study of a 2-story SCBF that was tested quasi-statically through complete fracture of its

steel braces.

Based on rigorous nonlinear response history analysis of the two case studies presented in this chapter, it is found that the commonly employed damping assumption that the stiffness part of the Rayleigh damping matrix is proportional to the initial stiffness of a structural system creates large artificial damping forces in particular when stiffness degradation occurs in braced frames due to fracture of their braces. The damping assumption that the stiffness part of the damping matrix is proportional to the current stiffness of the frame produces more realistic damping forces and it should be used for collapse assessment of structural systems with large changes of their global stiffness matrix during the earthquake history. Lastly, the collapse risk of the 12-story SCBF is further evaluated through the mean annual frequency of collapse for a highly seismic region and it is found that its collapse capacity is lower than expected, due to the formation of local story collapse mechanisms. This finding requires further investigation.

Table 6.1 Section properties of the various members of the 2-story SCBF

<b>Member</b>	<b>A (mm<sup>2</sup>)</b>	<b>I<sub>x</sub>/10<sup>6</sup> (mm<sup>4</sup>)</b>	<b>Z<sub>x</sub>/10<sup>6</sup> (mm<sup>3</sup>)</b>	<b>Material</b>
Column (W250x67)	8580	103	900	A992/A572, Gr. 50
Beam (W610x174)	22200	1470	5360	A992/A572, Gr. 50
Brace (HSS152.4x152.4x9.5)	4890	16.4	259	A500 Gr. B
Gusset Plate	-	-	-	A572 Gr. 50
Net Section Reinforcing Plate	-	-	-	A36

Table 6.2 Material properties of the various members of the 2-story SCBF

<b>Member</b>	<b>Average F<sub>y</sub> (MPa)</b>	<b>Average F<sub>u</sub> (MPa)</b>	<b>% Elongation</b>
Column (W250x67)	385	508	23.9
Beam (W610x174)	400	514	26.0
Brace (HSS152.4x152.4x9.5)	418	454	36.0
Base Plate	379	558	17.0
Gusset Plate	386	538	20.0
Net Section Reinforcing Plate	331	476	33.5

Table 6.3 Selected ground motions for collapse assessment of the 2-story SCBF

Record No.	Earthquake Event	Record Name ID	No. of Data Points	Time Step dt [sec]	PGA [g]
1	Loma Prieta	LP89agw	8000	0.005	0.172
2	Loma Prieta	LP89cap	7990	0.005	0.443
3	Loma Prieta	LP89g03	7985	0.005	0.367
4	Loma Prieta	LP89g04	7990	0.005	0.212
5	Loma Prieta	LP89gmr	7990	0.005	0.226
6	Loma Prieta	LP89hch	7815	0.005	0.247
7	Loma Prieta	LP89hda	7925	0.005	0.279
8	Loma Prieta	LP89svl	7850	0.005	0.207
9	Northridge	NR94cnp	2495	0.010	0.420
10	Northridge	NR94far	2995	0.010	0.273
11	Northridge	NR94fle	2995	0.010	0.240
12	Northridge	NR94glp	2995	0.010	0.206
13	Northridge	NR94hol	2000	0.020	0.231
14	Northridge	NR94nya	2995	0.010	0.159
15	Northridge	NR94stc	2995	0.010	0.368
16	San Fernando	SF71pel	2800	0.010	0.174
17	Superstition Hills	SH87bra	2210	0.010	0.156
18	Superstition Hills	SH87icc	8000	0.005	0.358
19	Superstition Hills	SH87pls	2220	0.010	0.186
20	Superstition Hills	SH87wsm	8000	0.005	0.172
21	Imperial Valley	IV79cal	7905	0.005	0.078
22	Imperial Valley	IV79chi	4000	0.010	0.270
23	Imperial Valley	IV79e01	7805	0.005	0.139
24	Imperial Valley	IV79e12	7800	0.005	0.116
25	Imperial Valley	IV79e13	7900	0.005	0.139
26	Imperial Valley	IV79qkp	8000	0.005	0.309
27	Imperial Valley	IV79wsm	7995	0.005	0.110
28	Loma Prieta	LP89hvr	7990	0.005	0.134
29	Loma Prieta	LP89sjw	7990	0.005	0.112
30	Loma Prieta	LP89slc	7915	0.005	0.194
31	Northridge	NR94cen	2995	0.010	0.322
32	Northridge	NR94lh1	1600	0.020	0.087
33	Northridge	NR94lv2	1600	0.020	0.063
34	Northridge	NR94pic	4000	0.010	0.186
35	Northridge	NR94ver	2995	0.010	0.153
36	Imperial Valley	IV79cmp	3600	0.010	0.186
37	Imperial Valley	IV79nil	7995	0.005	0.109
38	Imperial Valley	IV79pls	3745	0.005	0.057
39	Northridge	NR94lv6	1600	0.020	0.178
40	Northridge	NR94stn	3155	0.010	0.474

Table 6.4 Member sizes of the various members of the 12-story SCBF

Story	Columns	Braces	Beams
12	W12x45	HSS6-5/8x0.312	W18x55
11	W12x45	HSS6-5/8x0.312	W18x35
10	W14x99	HSS8-3/4x0.312	W18x60
9	W14x99	HSS8-3/4x0.312	W18x35
8	W14x193	HSS10x0.375	W18x65
7	W14x193	HSS10x0.375	W18x35
6	W14x283	HSS10x0.375	W18x65
5	W14x283	HSS10x0.375	W18x35
4	W14x398	HSS9-5/8x0.5	W18x71
3	W14x398	HSS9-5/8x0.5	W18x35
2	W14x550	HSS9-5/8x0.5	W18x71
1	W14x550	HSS9-5/8x0.5	W18x35

Table 6.5 Material properties of the various members of the 12-story SCBF

Member	Average $F_y$ (ksi)	Average $F_u$ (ksi)
Beams and Columns	50	65
Braces	46	58
Gusset Plate	50	65

Table 6.6 Specified gravity loads of the 12-story SCBF

Component	Gravity Load (kPa)
Roof	3.21
Typical Floor	4.07
Live (roof)	0.96
Live (typ. floor)	2.39
Cladding	0.72

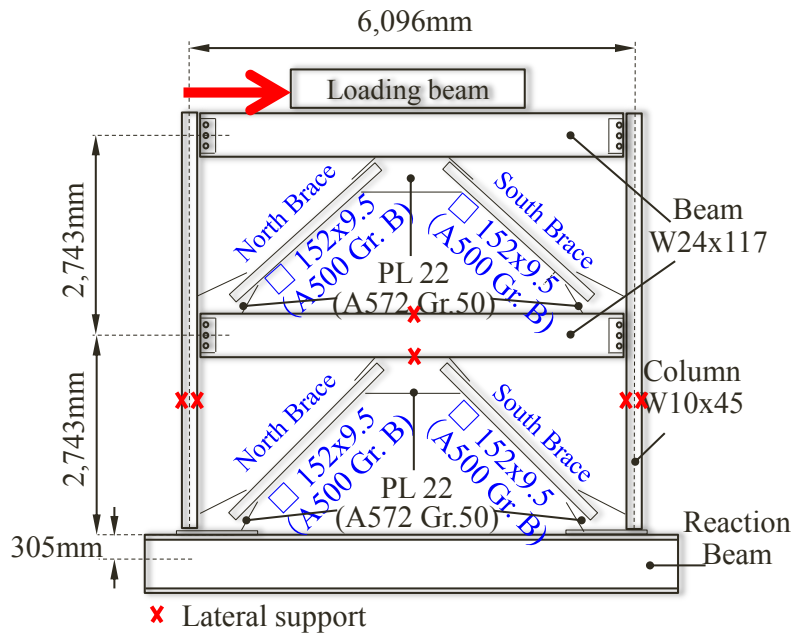


Figure 6.1 Geometry and the member sizes of the 2-story SCBF



Figure 6.2 Photograph of the SCBF as built (Uriz 2005)

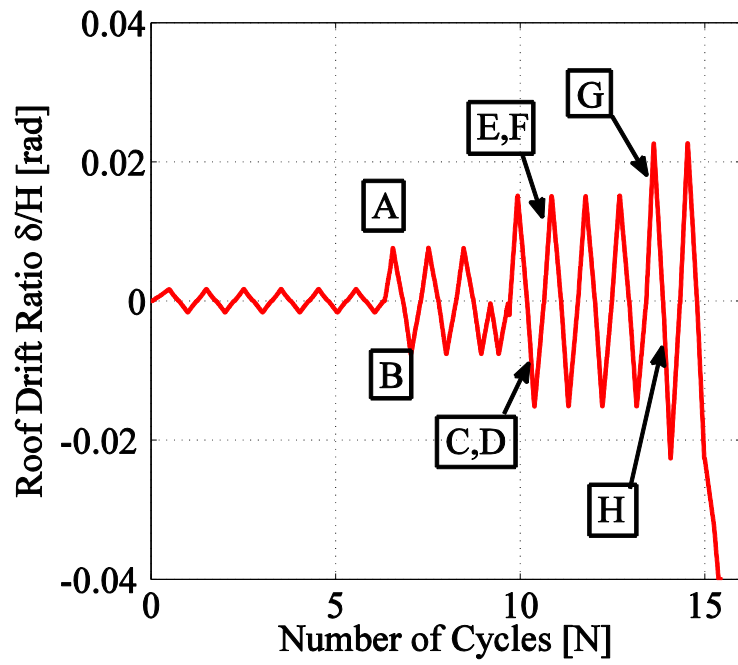


Figure 6.3 Loading protocol of the experimental study

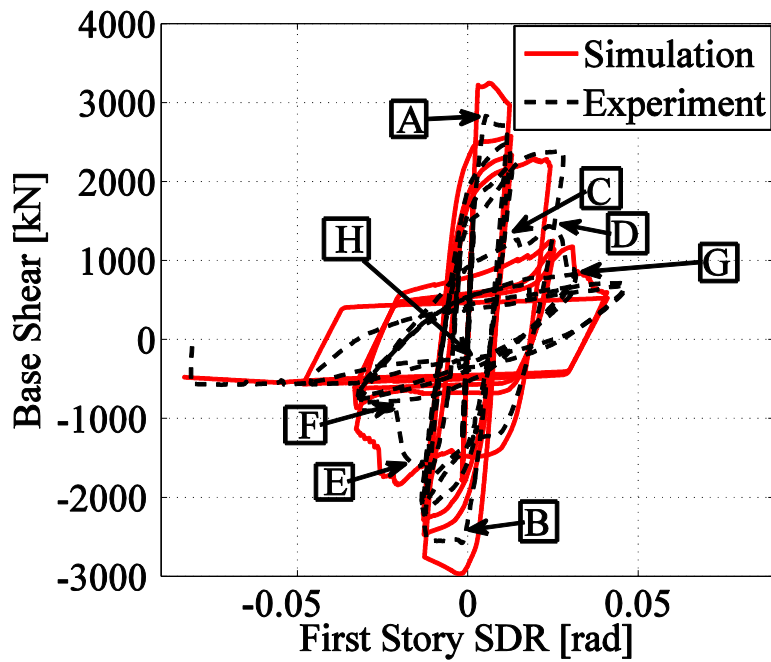


Figure 6.4 Base shear versus first story drift ratio of the 2-story SCBF

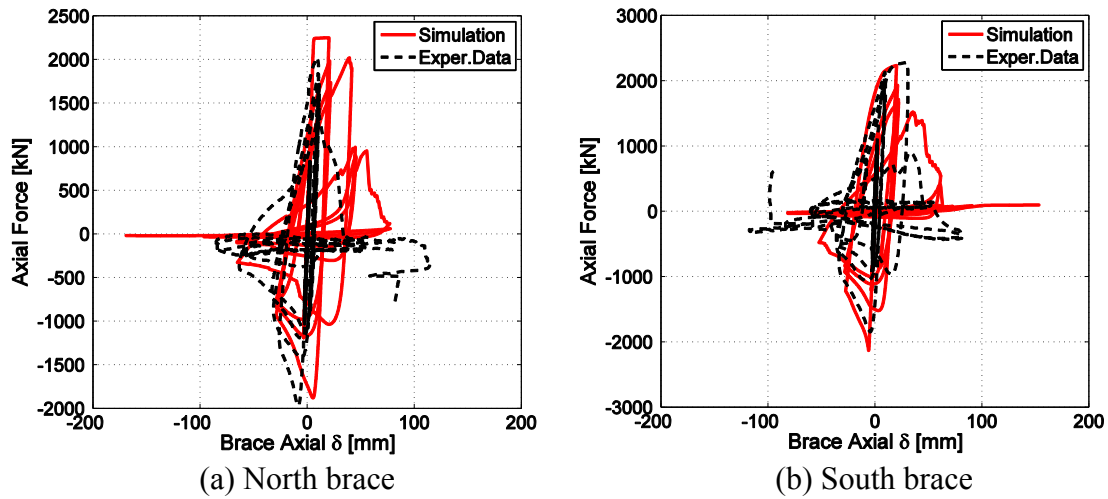


Figure 6.5 Axial force versus axial deformation of the lower story braces of the 2-story SCBF



Figure 6.6 Ductile tearing of the north lower story column of the 2-story SCBF (Uriz, 2005)

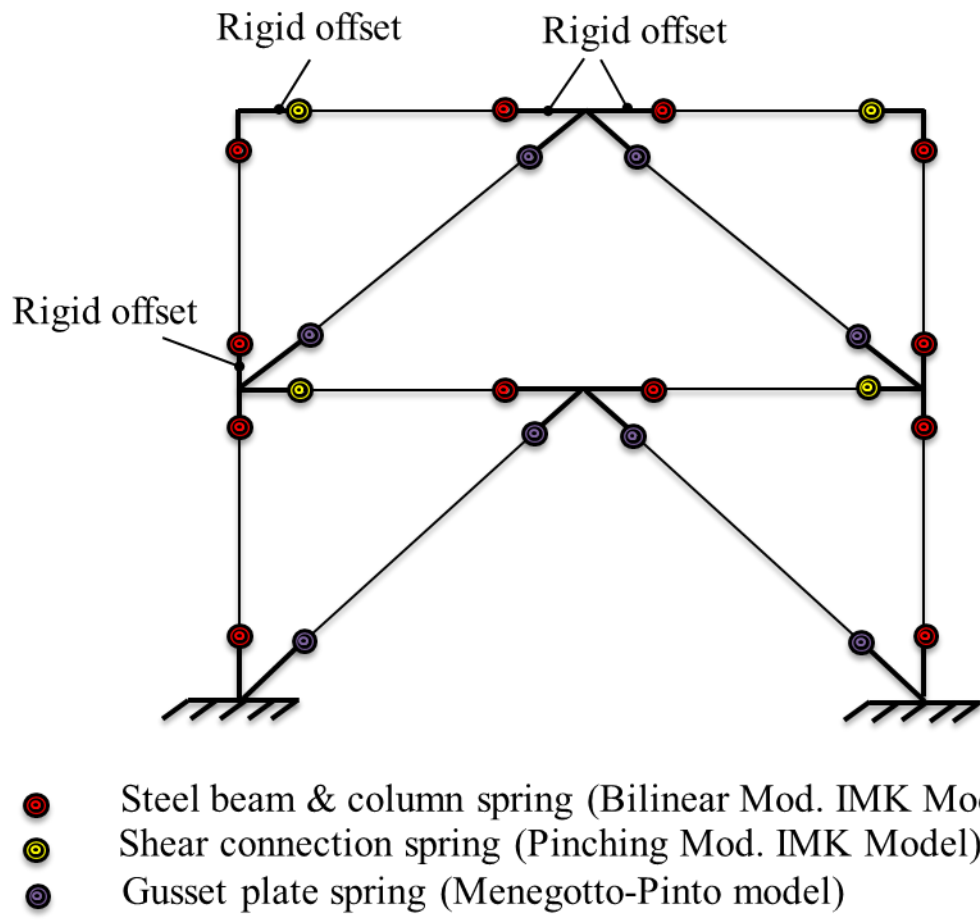


Figure 6.7 Overview of the analytical model of the 2-story SCBF

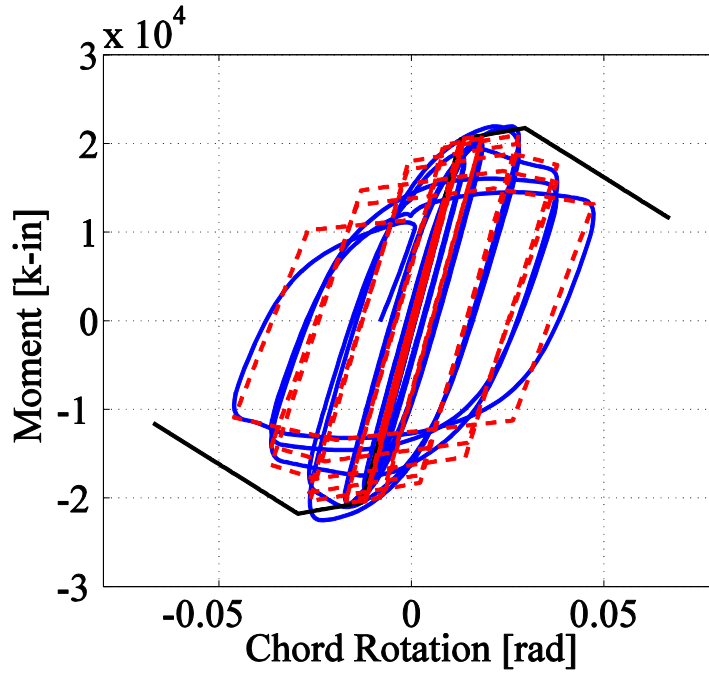


Figure 6.8 Calibration of the IMK deterioration model for steel beams (data from Taejin et al. 2000)

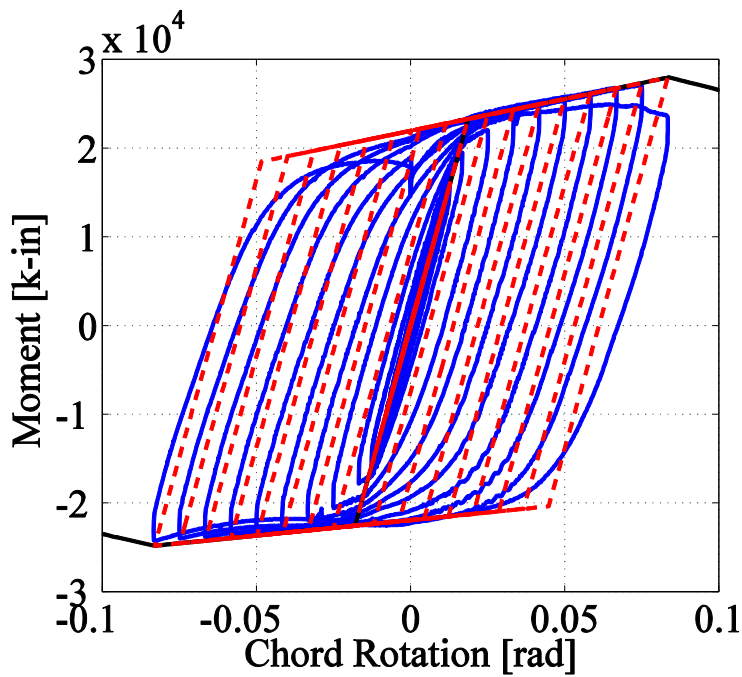


Figure 6.9 Calibration of the IMK deterioration model for steel columns (data from Newell and Uang 2008)

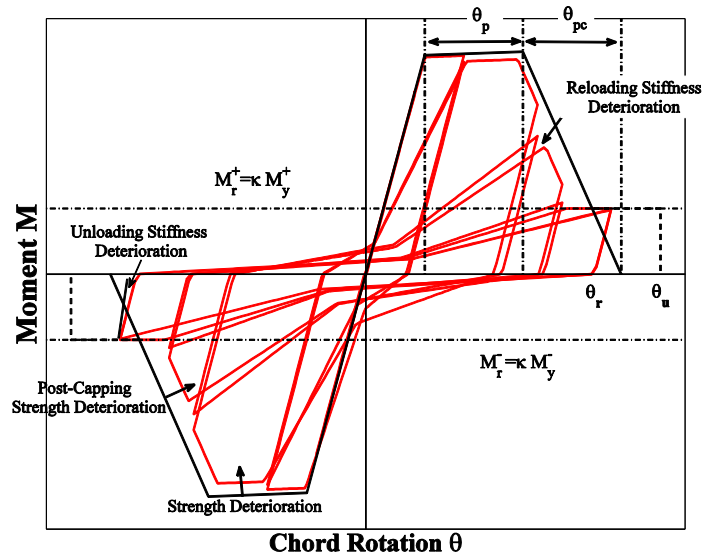


Figure 6.10 Typical hysteretic behaviour of the modified IMK model with pinching hysteretic response

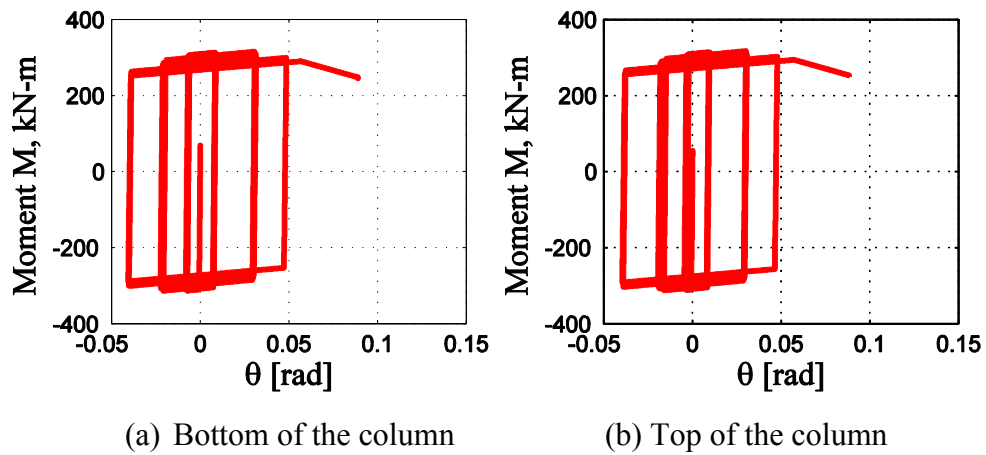


Figure 6.11 Moment - rotation diagram for the south lower story column of the 2-story SCBF

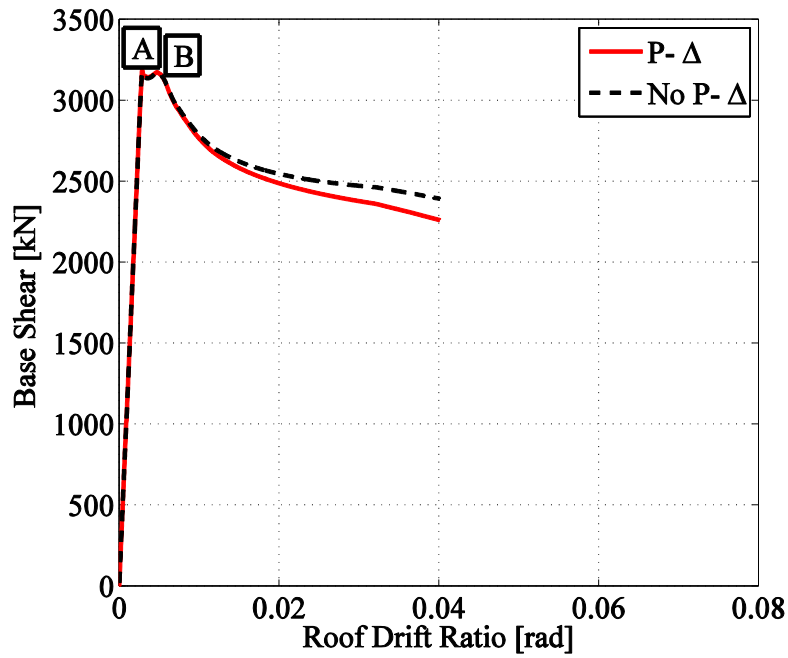


Figure 6.12 Base shear versus roof drift ratio of the 2-story SCBF based on pushover analysis

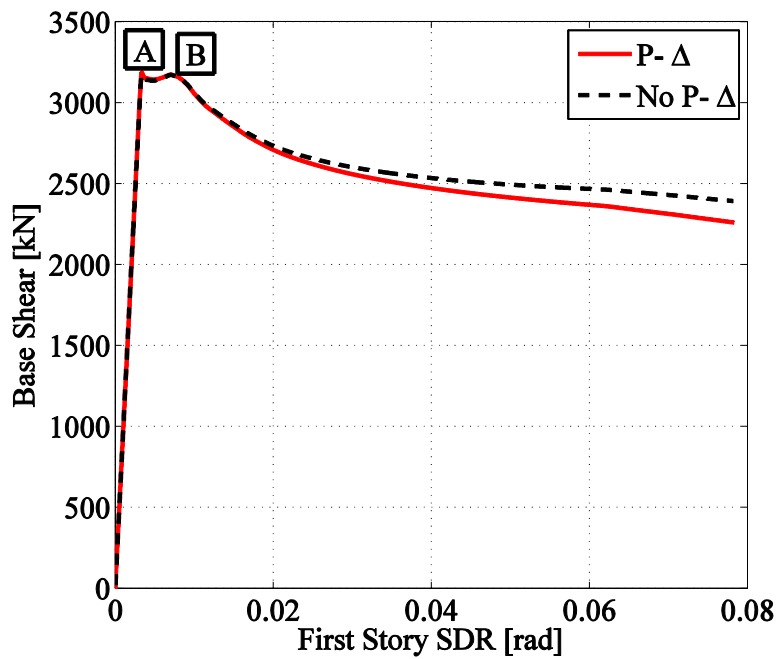


Figure 6.13 Base shear versus first story SDR of the 2-story SCBF based on pushover analysis

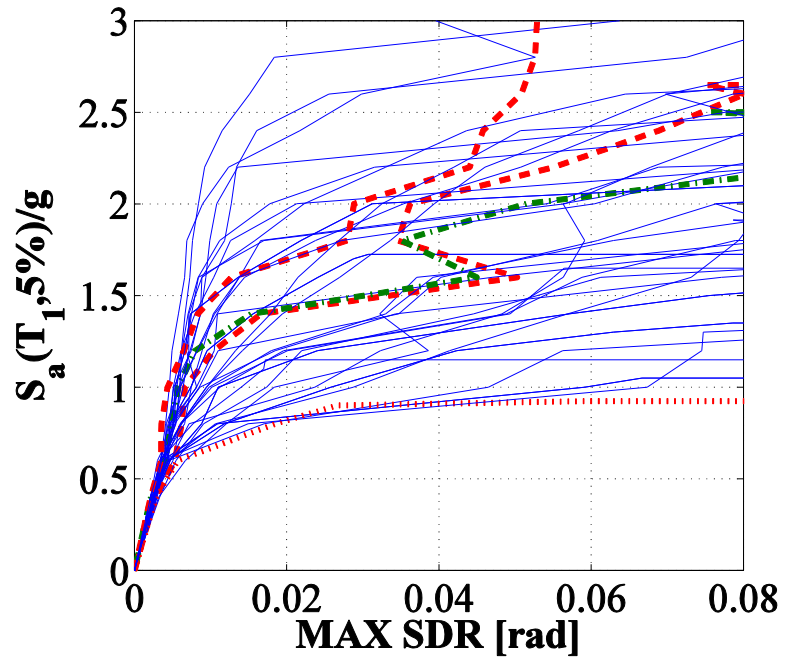


Figure 6.14 IDA curves of the 2-story SCBF (Rayleigh damping using initial stiffness approximation)

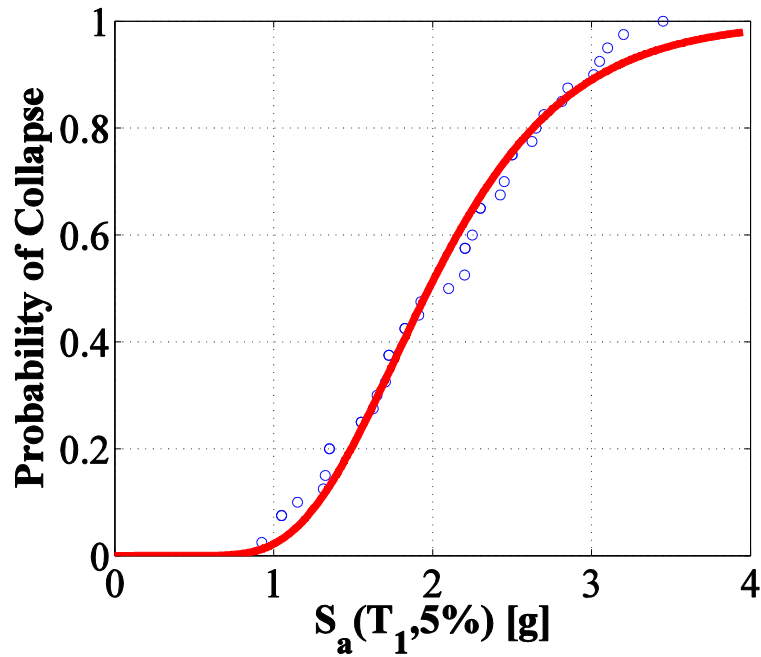


Figure 6.15 Collapse fragility curve of the 2-story SCBF (Rayleigh damping using initial stiffness approximation)

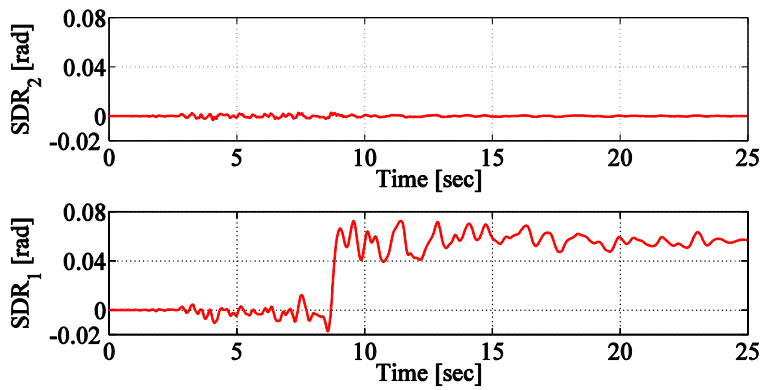


Figure 6.16 Story drift ratio histories of the 2-story SCBF during the Canoga Park record from the Northridge 1994 earthquake (Rayleigh damping using initial stiffness approximation)

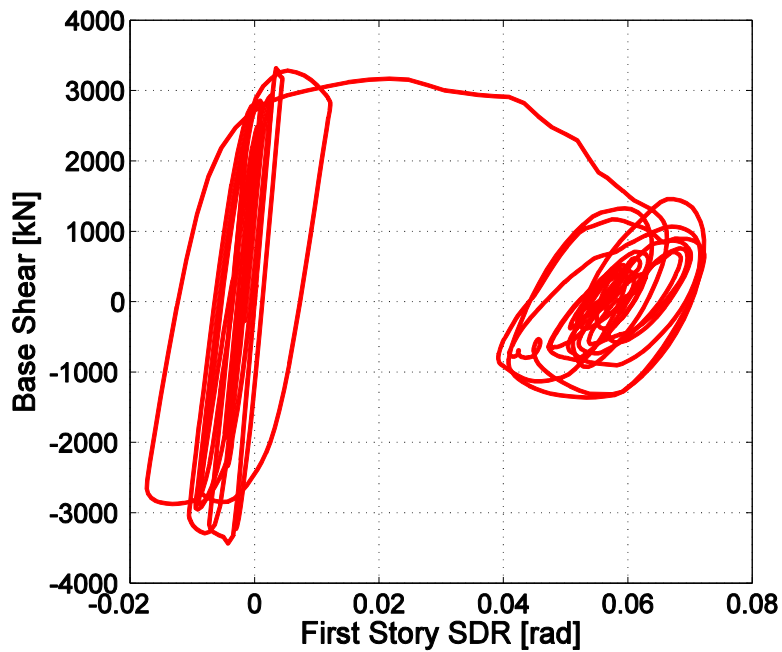


Figure 6.17 Base shear versus first story SDR of the 2-story SCBF during the Canoga Park record from the Northridge 1994 earthquake (Rayleigh damping using initial stiffness approximation)

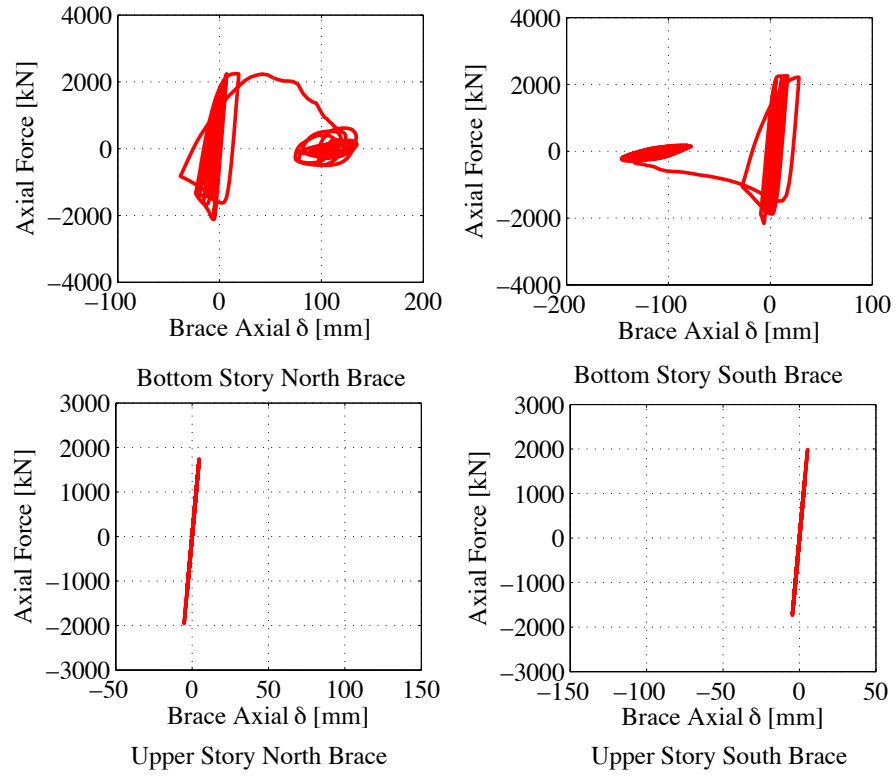


Figure 6.18 Brace hysteretic response of the 2-story SCBF during the Canoga Park record from the Northridge 1994 earthquake (Rayleigh damping using initial stiffness approximation)

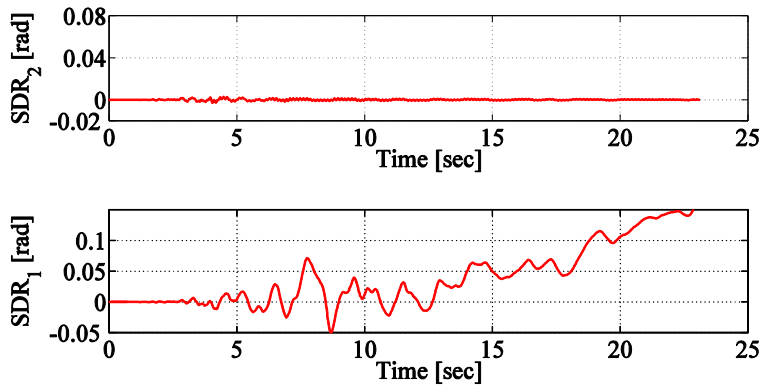


Figure 6.19 Story drift histories of the 2-story SCBF during the Canoga Park record from the Northridge 1994 earthquake (Rayleigh damping using current stiffness approximation)

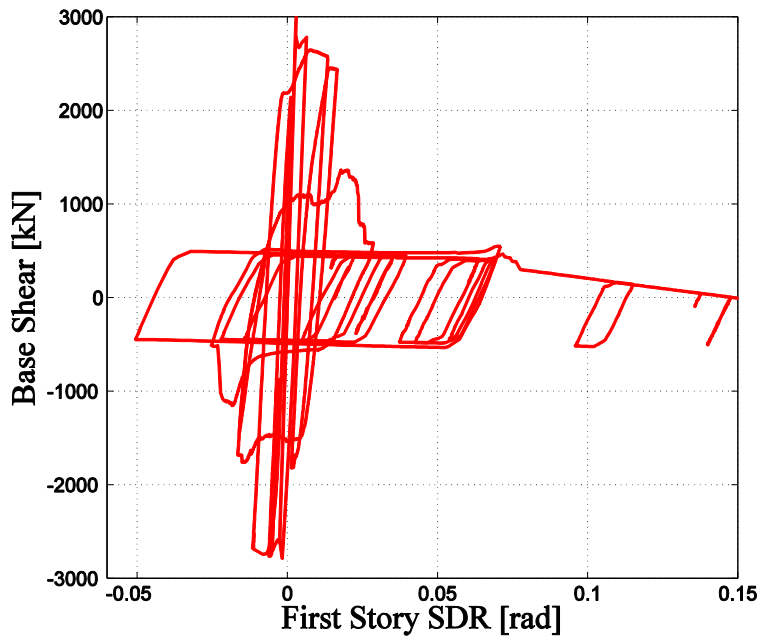


Figure 6.20 Base shear versus first story SDR of the 2-story SCBF during the Canoga Park record from the Northridge 1994 earthquake (Rayleigh damping using current stiffness approximation)

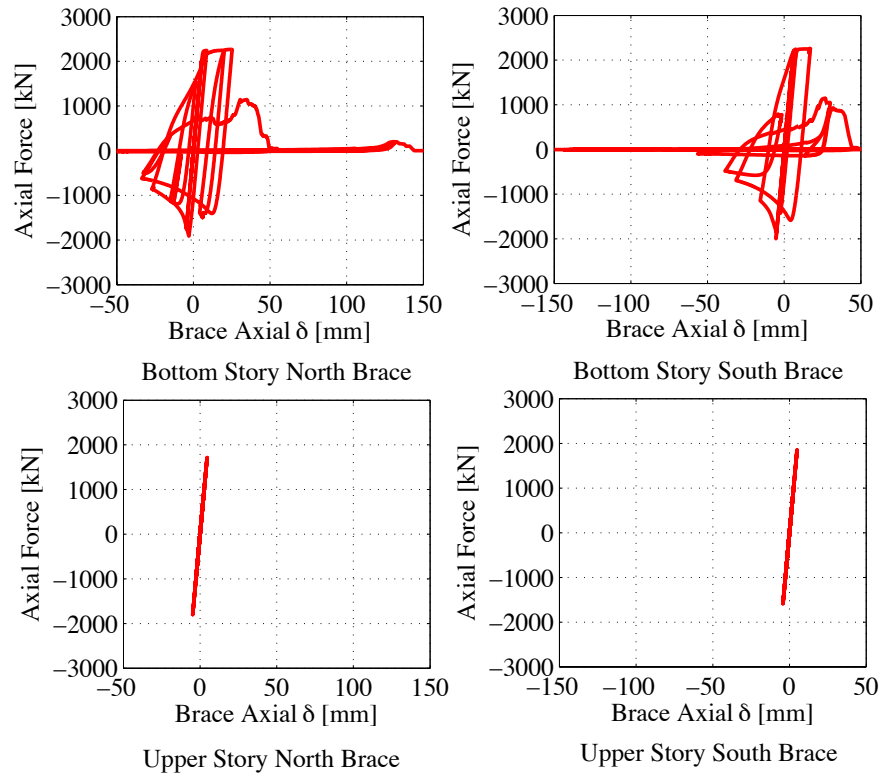


Figure 6.21 Brace hysteretic response of the 2-story SCBF during the Canoga Park record from the Northridge 1994 earthquake (Rayleigh damping using current stiffness approximation)

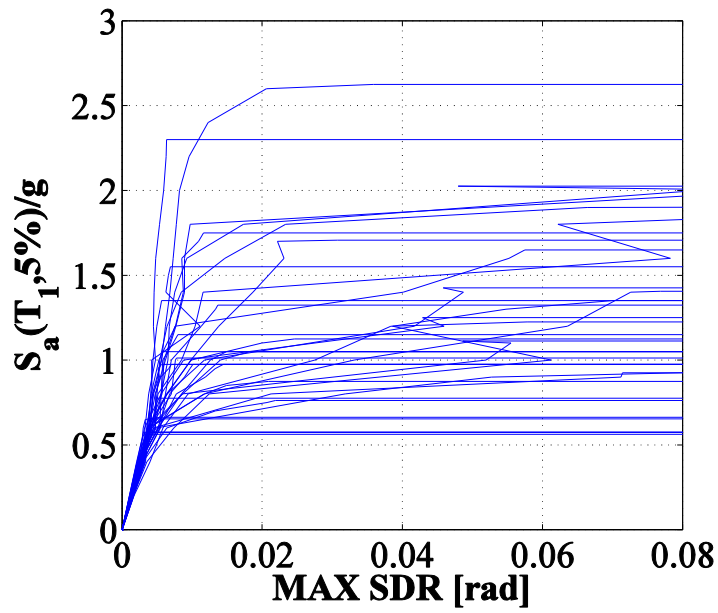


Figure 6.22 IDA curves of the 2-story SCBF (Rayleigh damping using current stiffness approximation)

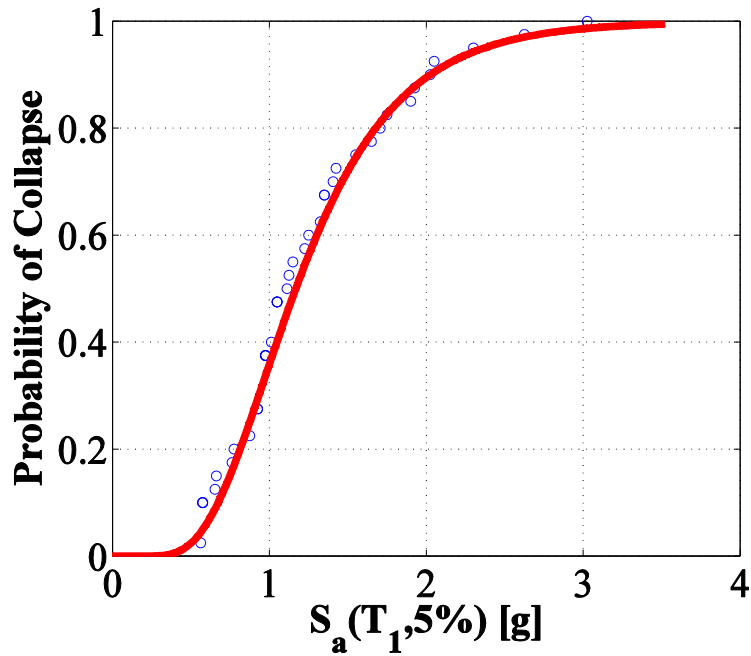


Figure 6.23 Collapse fragility curve of the 2-story SCBF (Rayleigh damping using current stiffness approximation)

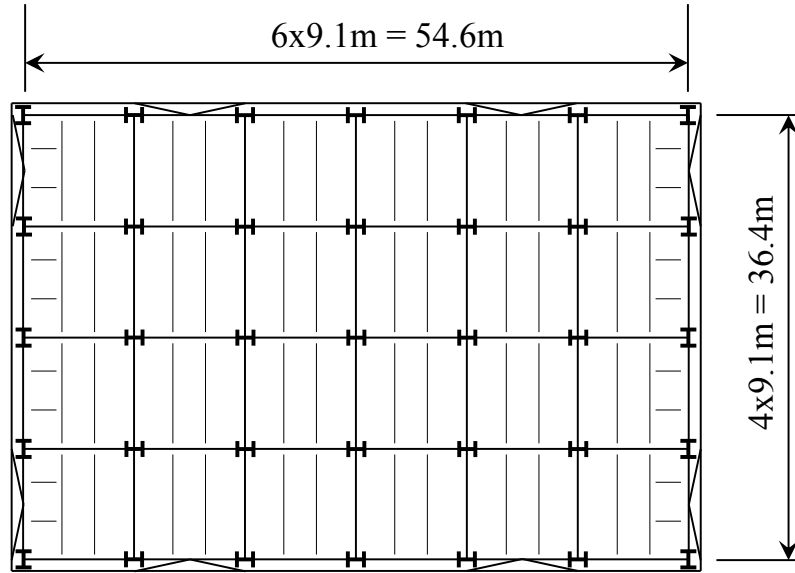


Figure 6.24 Plan view of the 12-story SCBF

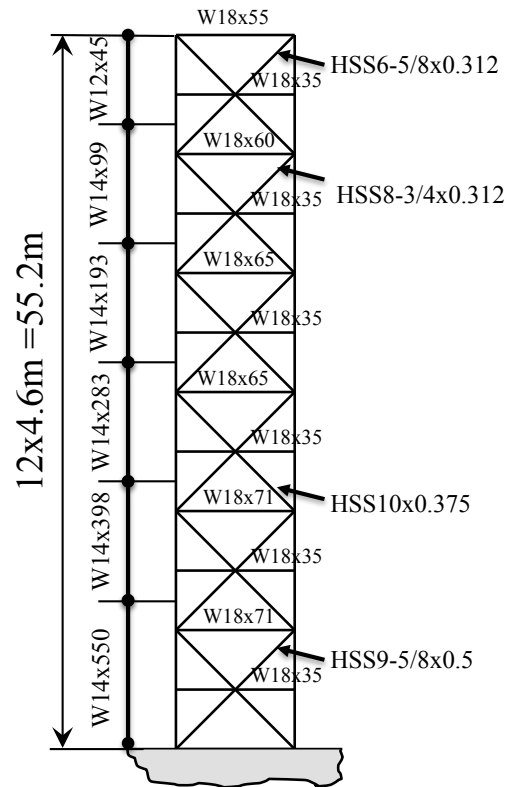


Figure 6.25 Elevation view of the 12-story SCBF

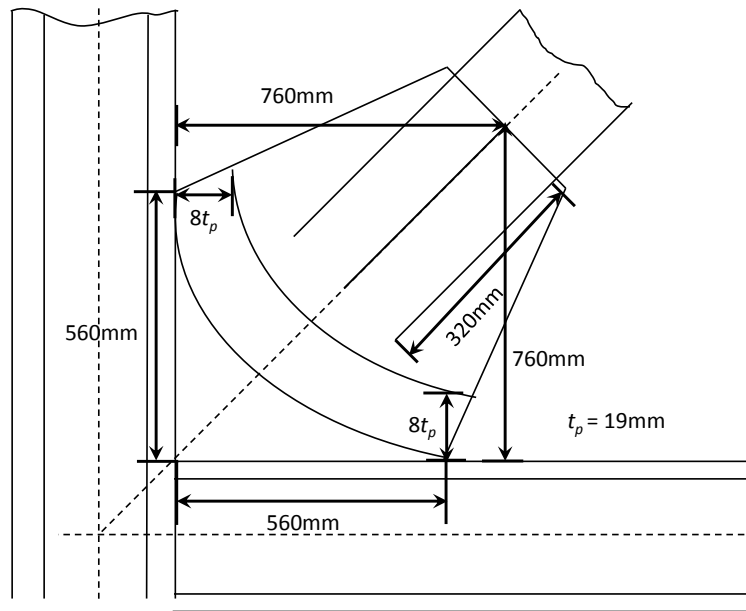


Figure 6.26 Typical corner gusset plate design of the 12-story SCBF

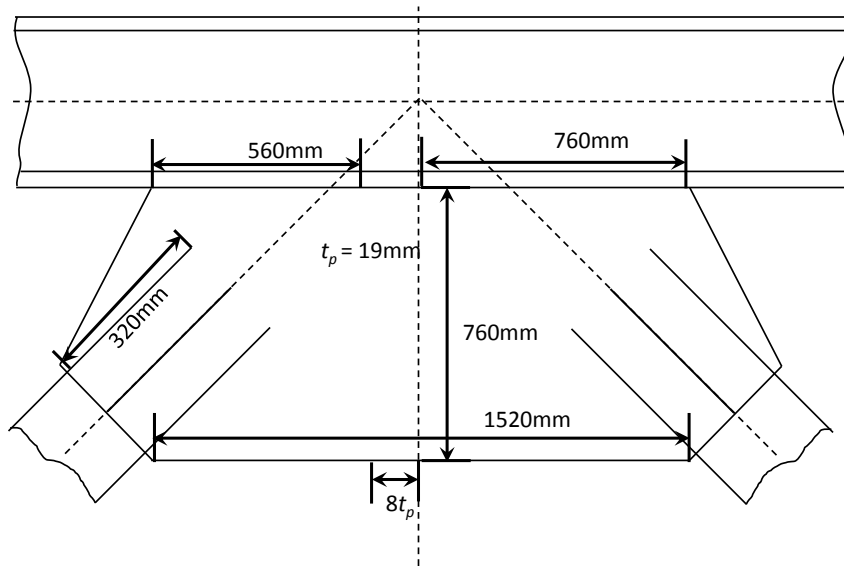


Figure 6.27 Typical middle gusset plate design of the 12-story SCBF

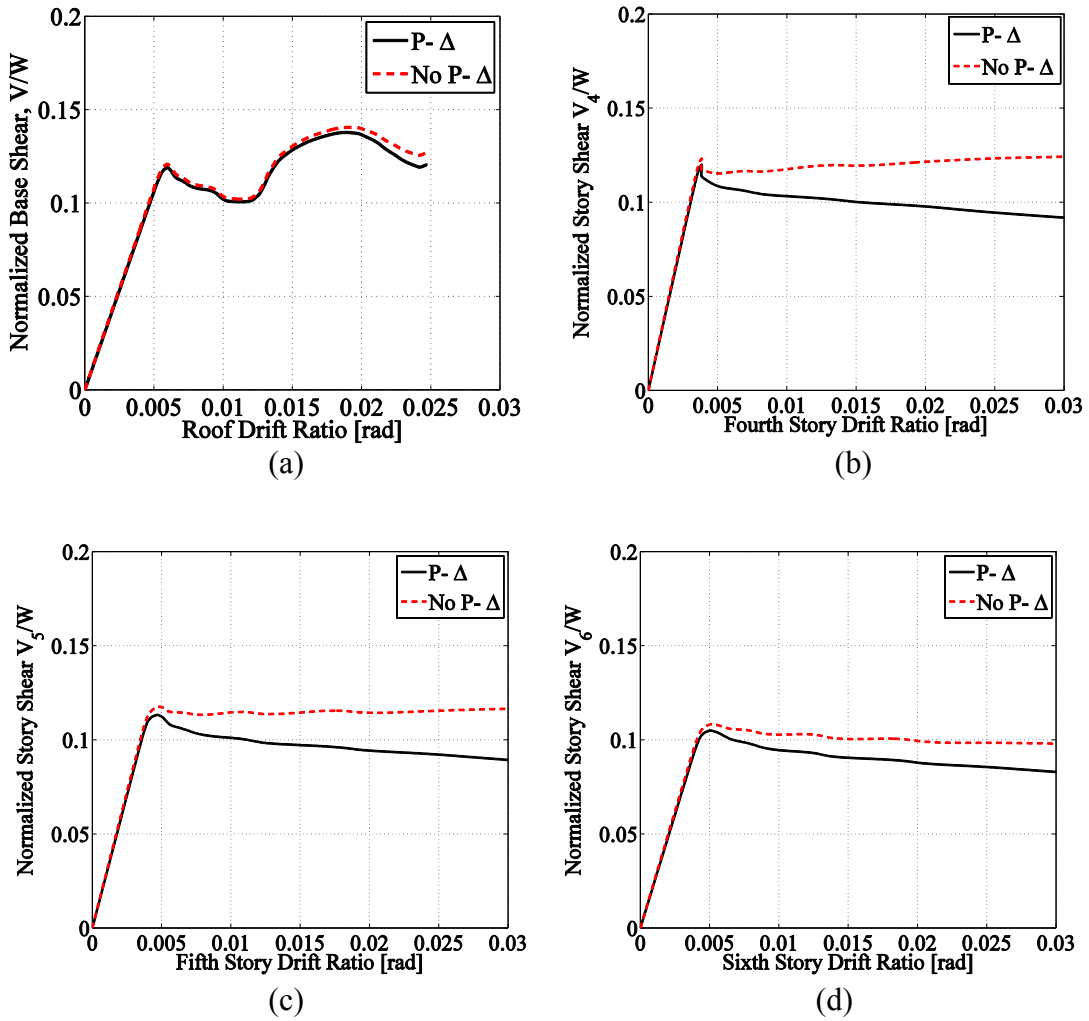


Figure 6.28 Pushover curves for 12-story SCBF based on a triangular lateral load pattern

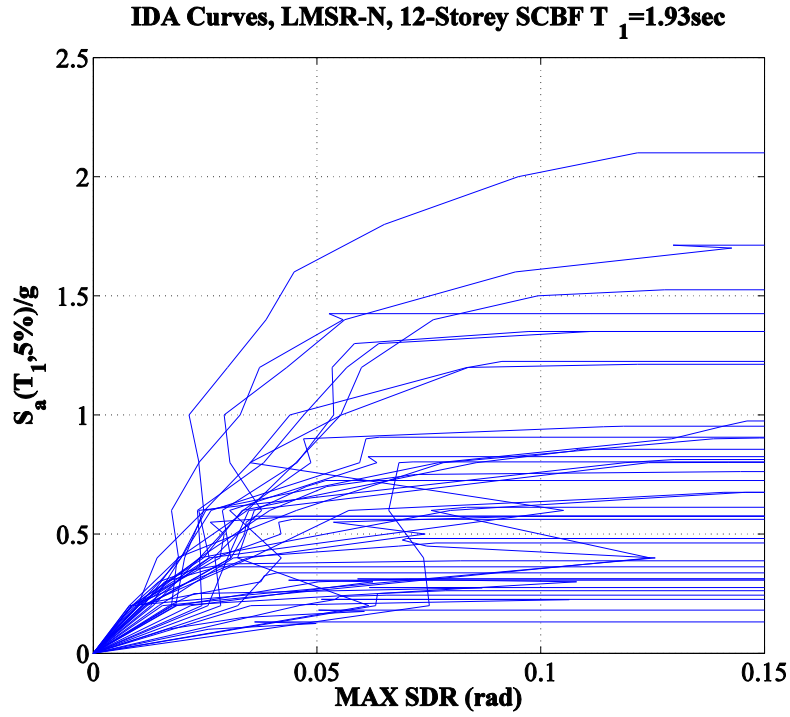


Figure 6.29 IDA curves of the 12-story SCBF (Rayleigh damping using current stiffness approximation)

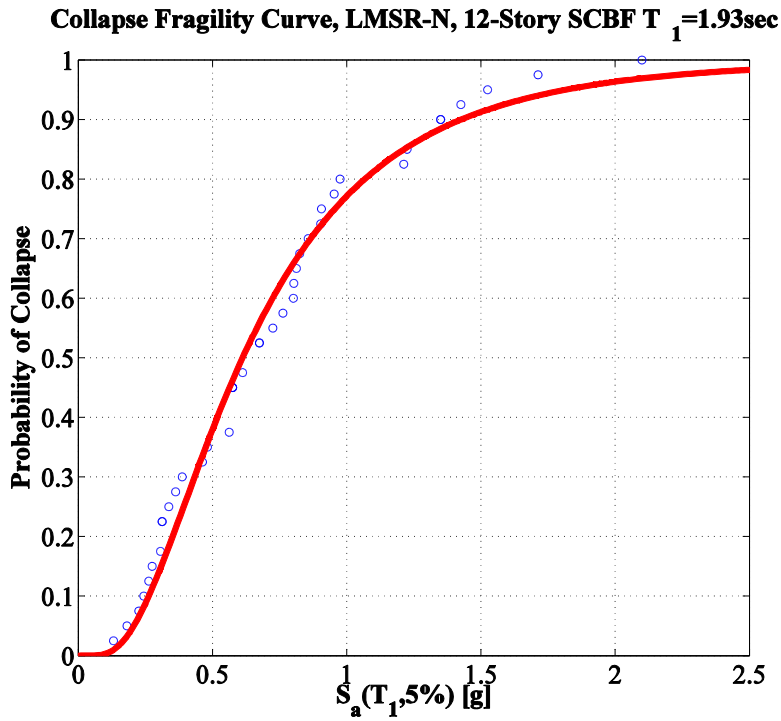


Figure 6.30 Collapse fragility curve of the 12-story SCBF (Rayleigh damping using current stiffness approximation)

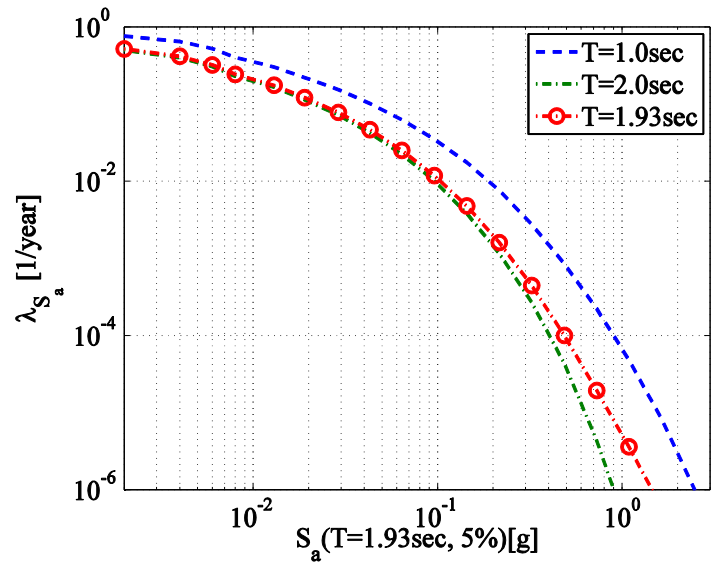


Figure 6.31 Seismic hazard curve for Bulk Mail Center, downtown Los Angeles, CA

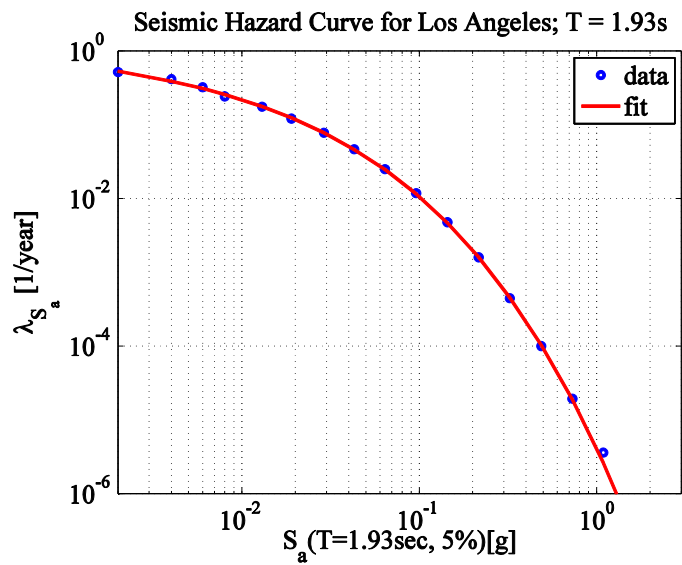


Figure 6.32 Fitted seismic hazard curve for Bulk Mail Center, downtown Los Angeles, CA



# Chapter 7

## Conclusions

---

The main objectives of this research are to develop performance-based evaluation techniques for rapid earthquake assessment of Concentrically Braced Frames (CBFs) designed in seismic regions and to develop a computational framework for reliable collapse assessment of CBFs that explicitly considers strength and stiffness deterioration of various structural components. This chapter summarizes the main contributions of this research.

### **7.1 Development of a Steel Brace Database**

A steel brace database consisting of 317 steel brace experiments has been developed. This database includes detailed information regarding the geometric and material properties of various steel brace shapes categorized in a consistent format. Of particular interest are the axial load-displacement relationships of the collected steel braces that were obtained during quasi-static cyclic and/or monotonic testing. Most of these relationships were digitized and can be used for refinement and validation of numerical models that simulate the hysteretic response of steel braces through fracture due to low cycle fatigue. The collected braces are classified within the section ductility limits based on the CISC and AISC seismic design provisions. The main findings after evaluating the steel braces included in the database are summarized as follows:

- The AISC-341-10 provisions represent adequately the measured yield stresses of various steel braces in the database for all 14 different material grades included in the database. It is recommended that the CSA-S16-09 provisions should include a similar distinction in terms of material properties when computing the probable yield stress of a steel braces. It should be stated that in part the observed differences between the presently employed provisions and the measured material properties from the various brace components are attributed to (1) various shapes and (2) fabrication processes during time and region.
- Based on a comparison of the measured steel brace compressive strengths and the ones computed according to the CSA-S16-09 and AISC-341-10 design guidelines it is concluded that the brace compressive strengths are represented well based on AISC-341-10 since in these guidelines there is a material grade distinction to compute the probable compressive stresses of the steel braces.

## **7.2 Development of Drift-Based and Dual-Parameter Fragility Curves for Discrete Damage States of Steel Braces**

Rapid estimation of structural damage of concentrically braced frames is evaluated through drift-based fragility curves for three discrete damage states of rectangular HSS, round HSS, W- and L- shape braces. These damage states are associated with flexural (global buckling), local buckling and fracture at the mid-length of these members. It should be noted that other failure modes associated with net section fracture or failures associated with the gusset plate connections are not addressed as part of this evaluation.

The methodology for developing drift-based fragility curves is based on a rigorous statistical procedure that was developed and it includes uncertainties related to material, brace shape, loading protocol and geometric configurations of the collected steel braces.

The main findings are summarized as follows:

- Rectangular HSS braces buckle in flexure at a 0.40% story drift ratio. Similarly, round HSS, W- and L-shape braces buckle globally at 0.41%, 0.28%, 0.27%, respectively. In terms of inelastic buckling at mid-length of the steel braces, the corresponding values for rectangular HSS, round HSS, W- and L-shape braces are 1.02%, 0.96%, 0.87%, 0.70% respectively.
- In terms of brace fracture, the corresponding average story drift ratios are 1.60%, 2.75%, 3.10% and 1.43% for rectangular HSS, round HSS, W- and L-shape braces, respectively. This implies that W-shape braces have in average a better fatigue life overall compared to the other three shapes followed by the round HSS braces.
- L- shape braces have the worst performance against global buckling, local buckling and fracture because of the fact that they are susceptible to lateral-torsional buckling, which is known to accelerate local buckling and to shorten the fracture life of a brace component.
- The steel material grade used for the bracing members has a significant effect on the post-buckling behaviour of braces. Braces of lower strength steel grades tend to fracture later than steel braces of higher strength steel.

- Based on dual-parameter fragility curves (drift and global slenderness,  $kL/r$ ) it is found that the effect of global slenderness of steel braces diminishes once these have buckled in flexure.

### **7.3 Modelling Guidelines for Inelastic Buckling and Fracture of Steel Braces**

A state-of-the-art analytical model that is able to simulate the hysteretic behaviour of steel braces from the onset of global buckling through fracture due to low-cycle fatigue was extensively calibrated with the axial load-axial displacement hysteretic diagrams of the collected experimental data. The calibration process was facilitated with an optimization scheme that was developed. Based on multivariate regression analysis, predictive equations for modelling fracture due to low-cycle fatigue are proposed for rectangular HSS round HSS and W-shape braces. These equations relate the geometric and material properties of steel braces with the fracture index of the analytical model that represents the steel braces. The proposed relationships for modelling inelastic buckling and fracture of steel braces reflect engineering principles. The main findings are summarized as follows:

- The local slenderness of steel braces has the largest effect on the post-buckling behaviour and fracture life of steel braces. This is demonstrated both from the analytical model fracture index and an equivalent strain index computed at fracture based on the collected experimental data.
- The effect of global slenderness  $kL/r$  on the fracture life of steel braces diminishes regardless of the brace shape once local buckling forms in the brace cross-section.

This confirms similar findings from the drift-based fragility curves that characterize steel brace damage associated with fracture.

- On average, W- shape braces have a longer fracture life than rectangular HSS and round HSS braces.

## **7.4 Collapse Assessment of Concentrically Braced Frames**

The proposed modelling guidelines for inelastic buckling and fracture of steel braces are validated with a benchmark test of a 2-story CBF that was tested in the past quasi-statically through complete failure of its steel braces. A computational framework to perform collapse assessment of CBFs was presented. This framework suggests how to model strength and stiffness deterioration of various structural components of CBFs. In particular, emphasis was placed on steel columns that are part of local story collapse mechanisms once the steel braces fracture. Cyclic deterioration of gusset plate beam-to-column connections is also considered as part of the proposed computational framework.

Collapse assessment of CBFs is conducted through Incremental Dynamic Analysis (IDA) with a set of 40 ordinary ground motions that represent the seismic hazard of an urban region in California. A Two and 12-story CBF frame structures are used for this purpose. Special emphasis is made on the drawbacks of the commonly used damping assumption that the stiffness proportional part of the Rayleigh damping matrix is proportional to the initial stiffness of a structural system. These case studies revealed that:

- For a reliable collapse assessment of CBFs it is important to account for the strength and stiffness deterioration of all of the components in the CBFs including fracture of the steel braces.
- The initial stiffness proportional damping assumption creates large artificial damping forces after large stiffness changes occur in CBFs due flexural buckling and subsequently fracture of their steel braces. Following the change in state of steel braces after fracture occurs, large viscous damping forces are generated based on the initial stiffness of CBFs. These forces are the product of the post-event deformational velocities multiplied by the initial stiffness and by the stiffness proportional coefficient.
- When the stiffness proportional part of the Rayleigh damping matrix is based on the current stiffness state of CBFs, the viscous damping forces to be expected in CBFs are more realistic compared to the case that the initial stiffness approximation is employed. This is a fundamental finding for frame structures that reach their negative stiffness path once strength deterioration of their structural components occurs due to seismic loading. The implication is that an initial stiffness approximation will typically overestimate the collapse capacities of CBFs.

## **7.5 Suggestions for Future Work**

Areas for future research on the collapse assessment of CBFs subjected to earthquake loading include the following:

- Development of a comprehensive physical theory model for steel braces that is not sensitive to the discretization of the steel brace cross section and can be easily used by engineering professionals.
- Development of 3-dimensional steel brace models that are able to capture explicitly local instabilities such as local buckling and at the same time can be efficiently used in frame analysis programs for large-scale parametric studies with CBFs.
- Development of new damping models that reliably represent the change of viscous damping forces of CBFs and other lateral resisting systems that deteriorate in strength and stiffness during an earthquake.
- Design and execution of experimental studies on steel braces with emphasis on the effect of the loading protocol on the fracture life of these braces. In particular, a loading protocol with few inelastic cycles followed by a large pulse would better reflect the inelastic displacement demands that a steel brace would undergo during a severe ground motion.
- Numerical simulation studies with a range of CBF archetype buildings that will include the effect of modelling uncertainties on their seismic performance through dynamic collapse.



# List of References

---

Aboosaber, M., and Hines, E.M. (2011), "Modeling reserve system performance for low-ductility braced frames," *Report No. TUSSR-2011/1*, Tufts University Structural Systems Research, Tufts University, Medford, MA.

Abramson, M., Audet, C., Chrissis, J., and Walston, J. (2009), "Mesh adaptive direct search algorithms for mixed variable optimization," *Opt. Lett.* **3** (1), pp. 35-47.

Aguero, A., Izvernari, C., and Tremblay, R. (2006), "Modelling of the seismic response of concentrically braced steel frames using the OpenSees analysis environment," *International Journal of Advanced Steel Construction*, **2** (3), pp. 242-274.

ASCE (2005), "ASCE Standard Minimum Design Loads for Buildings and Other Structures," ASCE 7-05, American Society of Civil Engineers, Reston, VA.

AISC (1989), "Specification for structural steel buildings- allowable stress design and plastic design," American Institute of Steel Construction AISC, Chicago, Illinois.

AISC (1993), "Load and resistance factor design LRFD," American Institute of Steel Construction AISC, Chicago, Illinois.

AISC (1997), "Seismic provisions for structural steel buildings," American Institute of Steel Construction AISC, Chicago, Illinois.

AISC (2005), "Seismic provisions for structural steel buildings," American Institute of Steel Construction AISC, Chicago, Illinois.

AISC (2010a), "Seismic provisions for structural steel buildings," ANSI/AISC 341-10, American Institute of Steel Construction AISC, Chicago, Illinois.

AISC (2010b), "Specification for structural steel buildings," ANSI/AISC 360-10, American Institute of Steel Construction AISC, Chicago, Illinois.

AIJ (1995), "Reconnaissance report on damage to steel building structures observed from the 1995 Hyogoken-Nanbu Earthquake," The Kinki Branch of the Architectural Institute of Japan, Steel Committee, Osaka, Japan.

Aslani, F., Goel, S.C., and Peixin, X. (1987), "Effect of stitch spacing on the cyclic behavior of built-up bracing members," *Report No. UMEE 87-8*, Department of Civil Engineering, University of Michigan, Ann Arbor, MI.

Aslani, H., and Miranda, E. (2005), "Probabilistic earthquake loss estimation and loss

disaggregation in buildings,” *Report No. 157*, John. A. Blume Earthquake Engineering Research Center, Stanford University, Stanford, CA.

ASTM (2010), “A370-12 Standard Test Methods and Definitions for Mechanical Testing of Steel Products,” American Society for Testing and Materials, West Conshohocken, PA.

Archambault, M. (1995), “Étude du comportement séismique des contreventement ductiles en X avec profilés tubulaires en acier,” *M.Sc. Thesis*, Department of Civil, Geological and Mining Engineering, Montreal Polytechnic, Montreal, QC.

ATC-58 (2012a), “Guidelines for Seismic Performance Assessment of Buildings, Volume 1-Methodology,” Applied Technology Council, Redwood City, CA.

ATC-58 (2012b), “Guidelines for Seismic Performance Assessment of Buildings, Volume 2-Implementation Guide,” Applied Technology Council, Redwood City, CA.

Ballio, G., and Perotti, F. (1987), “Cyclic behavior of axially loaded members: numerical simulation and experimental verification,” *Journal of Constructional Steel Research*, **7** (1), pp. 3-41.

Ballio, G., and Castiglioni, C. A. (1995), "A unified approach for the design of steel structures under low and/or high cycle fatigue," *Journal of Constructional Steel Research*, **34** (1), 75-101.

Bara, C.I. (2007), “The seismic behaviour of steel braces with large sections,” *M.Sc. Thesis*, Department of Civil, Geological and Mining Engineering, Montreal Polytechnic, Montreal, QC.

Benjamin, J., and Cornell, C.A. (1970), *Probability, statistics and decision for civil engineers*, McGraw-Hill, New York.

Black, R.G., Wenger, W.A.B. and Popov, E.P. (1980), “Inelastic buckling of steel strut under cyclic load reversals,” *Report No. UCB/EERC-80/40*, Earthquake Engineering Research Center, University of California, Berkeley, CA.

BSSA (2012), “Comparison of structural design in stainless steel and carbon steel,” BSSA, <http://www.bssa.org.uk/topics.php?article=125>.

Calik, E.E. (2007), “Development of a physical theory model for the simulation of hysteretic behavior of steel braces,” *M.Sc. Thesis*, Middle East Technical University, Ankara, Turkey.

CISC (2010), “Handbook of Steel Construction,” Canadian Institute of Steel Construction, 10<sup>th</sup> Edition, Toronto, ON.

Charney, F. (2008). "Unintended consequences of modeling damping in structures", *J., Struct., Eng.*, ASCE, **134** (4), pp. 581-592.

Chatterjee, S., Hadi, A.S., Price, B. (2000), "Regression analysis by example," 3<sup>rd</sup> Edition, John Wiley and Sons Inc., New York, NY.

Chen, Y., and Clough, R.W. (1980), "Shaking table test of a nine-story k-braced steel frame," *Report No. CE 299*, Department of Civil Engineering, University of California, Berkeley, CA.

Chen, C., Lai, J., and Mahin, S.A. (2008), "Seismic performance assessment of concentrically braced steel frame buildings," *Proceedings, 14th World Conference on Earthquake Engineering*, October 2008, Beijing, China.

Christopoulos, C., Packer, J.A., Tremblay, R., and de Oliveria, C. (2008), "Quasi-static cyclic testing of individual full-scale circular steel tubular braces equipped with cast connex high-strength connectors," *Publication No. 2008-01*, Department of Civil Engineering, University of Toronto, Toronto, ON.

Clark, K.A. (2009), "Experimental performance of multi-story X-braced SCBF systems," *M.Sc. Thesis*, Department of Civil and Environmental Engineering, University of Washington, Seattle, WA.

Crow, E.L., Davis, F.A., and Maxfield, M.W. (1960), *Statistics manual*, Dover, New York.

CSA (2005), "CAN/CSA-S16-01 limit states design of steel structures," Canadian Standard Association, Rexdale, ON.

CSA (2005), "S16S1-05 supplement no.1 to CAN/CSA-S16-01, limit states design of steel structures," Canadian Standard Association, Rexdale, ON.

CSA (2009), "CAN/CSA-S16-09 limit states design of steel structures," Canadian Standard Association, Rexdale, ON.

Dhakar, R. P. and Maekwa, K. (2002), "Path-dependent cyclic stress-strain relationship of reinforcing bar including buckling," *Engineering Structures*, Elsevier, **24** (12), pp. 1383-1396.

Davaran, A. and Adelzadeh, M. (2009), "An improved non-linear physical modeling method for brace elements," *Scientia Iranica*, Sharif University of Technology, **16** (1), pp. 58-64.

Davaran, A. and Far, N.E. (2009), "An inelastic model for low cycle fatigue prediction in steel braces," *Journal of Constructional Steel Research*, **65** (3), pp. 523-530.

Eads, L., Miranda, E., Krawinkler, H., and Lignos, D.G. (2012), "An efficient method for estimating the collapse risk of structures in seismic regions", *Earthquake Engineering and Structural Dynamics*, EESD, doi: 10.1002/eqe.2191 (in press).

Eckert, T. (2009), "Effect of modifying brace slenderness in concentrically braced frames," *M.Sc. Thesis*, Department of Civil and Environmental Engineering, University of Pittsburgh, Pittsburgh, PA.

Elchalakani, M., Zhao, X. and Grzebieta, R. (2003), "Tests of cold-formed circular tubular braces under cyclic axial loading," *Journal of Structural Engineering*, ASCE, **129** (4), pp. 507-514.

Eurocode 8 (1998), "Design provisions for earthquake resistant structures."

Fadare, D.A., Fadara, T.G., and Akanbi, O.Y. (2011), "Effect of heat treatment on mechanical properties and microstructure of NST 37-2 steel," *Journal of Minerals & Materials Characterization & Engineering*, JMMCE, **10** (3), pp. 299-308.

Fell, B.V., Kanvinde, A.M., Deierlein, G.G., and Myers, A.T. (2009), "Experimental investigation of inelastic cyclic buckling and fracture of steel braces," *Journal of Structural Engineering*, ASCE, **135** (1), pp. 19-32.

Fell, B.V., Kanvinde, A.M., and Deierlein, G.G. (2010), "Large-scale testing and simulation of earthquake induced ultra low cycle fatigue in bracing members subjected to cyclic inelastic buckling," *Report No. 172*, John. A. Blume Earthquake Engineering Research Center, Stanford University, Stanford, CA.

FEMA P695 (2009). "Quantification of building seismic performance factors", *Rep. FEMA P695*, Federal Emergency Management Agency, Washington, D.C.

Filiatrault, A., and Tremblay, R. (1998), "Design of tension-only concentrically braced steel frames for seismic induced impact loading," *Engineering Structures*, Elsevier, **20** (12), pp. 1087-1096.

Filippou, F.C., Popov, E.P., and Bertero, V.V. (1983), "Effects of bond deterioration on hysteretic behavior of reinforced concrete joints". *Report No. UCB/EERC 83-19*, Earthquake Engineering Research Center, University of California at Berkeley, Berkeley, CA.

Fukuta, T., Nishiyama, I., Yamanouchi, H., and Kato, B. (1989), "Seismic performance of steel frames with inverted V braces," *Journal of Structural Engineering*, ASCE, **115** (8), pp. 2016-2028.

Gan, W. (1996), "Earthquake response of steel braces and braced steel frames," *Ph.D. Thesis*, California Institute of Technology, Pasadena, CA.

Garcia, J.R., Negrete, M. (2009), "Drift-based fragility assessment of confined masonry walls in seismic zones," *Journal of Engineering Structures*, Vol. **31** (1), pp. 170-181.

Ghanaat, Y. (1980), "Study of X-braced steel frame structures under earthquake simulation," *Report No. UCB/EERC-80/08*, Earthquake Engineering Research Center, University of California, Berkeley, CA.

Ghanaat, Y., and Clough, R.W. (1982), "Shaking table tests of a tubular steel frame model," *Report No. UCB/EERC-82/02*, Earthquake Engineering Research Center, University of California, Berkeley, CA.

Goggins J.M. (2004), "Earthquake resistant hollow and filled steel braces," *Ph.D. Thesis*, Trinity College, University of Dublin, Dublin, Ireland.

Gugerli, H., and Goel, S.C. (1982), "Inelastic cyclic behavior of steel bracing members," *Report No. UMEE 82R1*, Department of Civil Engineering, University of Michigan, Ann Arbor, MI.

Gupta, A., and Krawinkler, H. (1999), "Prediction of seismic demands for SMRFs with ductile connections and elements," SAC Background Document, *Report No. SAC/BD-99/06*, SAC Joint Venture, Sacramento, CA.

Haddad, M.A. (2004), "Design of concentrically braced steel frames for earthquakes," *Ph.D. Thesis*, Department of Civil Engineering, University of Calgary, Calgary, AB.

Han, S., Kim, W.T. and Foutch, D.A. (2007), "Seismic behavior of HSS bracing members according to width-thickness ratio under symmetric cyclic loading," *Journal of Structural Engineering*, ASCE, **133** (2), pp. 264-273.

Haselton, C.B., and Deierlein G.G., (2006), "Assessing seismic collapse safety of modern reinforced concrete moment frame buildings," *Report No. TR 156*, John. A. Blume Earthquake Engineering Research Center, Stanford University, Stanford, CA.

Higginbotham, A.B. (1973), "The inelastic cyclic behavior of axially-loaded steel members," *Ph.D. Dissertation*, Department of Civil Engineering, University of Michigan, Ann Arbor, MI.

Hines, E.M., Baise, L.G. and Swift, S.S. (2011), "Ground Motion Suite Selection for Eastern North America," *Journal of Structural Engineering*, ASCE, **137** (3), pp. 358-366.

Hsiao, P., Lehman, D.E., and Roeder, C.W. (2012a), "Improved analytical model for special concentrically braced frames," *Journal of Constructional Steel Research*, Elsevier, **73**, pp. 80-84.

Hsiao, P.C., Lehman, D.E., and Roeder, C.W. (2012b). "A model to simulate special concentrically braced frames beyond fracture", *Earthquake Engineering and Structural*

*Dynamics*, EESD, doi: 10.1002/eqe.2202 (in press).

Huang, Y., and Mahin, S.A. (2010), "Simulating the inelastic seismic behavior of steel braced frames including the effects of low-cycle fatigue," *Report No. PEER 2010/104*, Pacific Earthquake Engineering Research Center, University of California at Berkeley, Berkeley, CA.

Huber, A.W., and Ketter, R.L. (1952), "Experimental results of the influence of residual stress on column strength," *Report 220A.6*, Fritz Engineering Laboratory, Lehigh University, Bethlehem, PA.

Huber, A.W. (1956), "Summary of important findings on residual stress and compressive properties of rolled WF columns," *Report 220A.23*, Fritz Engineering Laboratory, Lehigh University, Bethlehem, PA.

Ibarra, L.F., Medina, R., and Krawinkler, H., (2002), "Collapse assessment of deteriorating SDOF systems," *Proc. 12<sup>th</sup> European Conference on Earthquake Engineering*, London, U.K.

Ibarra, L.F., and Krawinkler, H., (2004), "Global collapse of deteriorating MDOF systems," *Proc. 13<sup>th</sup> World Conference on Earthquake Engineering*, Vancouver, B.C., Canada.

Ibarra, L.F., Medina R., and Krawinkler, H., (2005), "Hysteretic models that incorporate strength and stiffness deterioration," *Earthquake Engineering and Structural Dynamics*, Wiley, **34** (12), pp. 1489-1511.

IBC, (2003), "International building code," International Code Council (ICC), Falls Church, VA.

Ikeda, K., and Mahin, S.A. (1986), "Cyclic response of steel braces," *Journal of Structural Engineering*, ASCE, **112** (2), pp. 342-361.

Ikeda, K., Mahin, S.A., and Dermizakis, S.N. (1984), "Phenomenological modeling of steel braces under cyclic loading," *Report No. UCB/EERC-84/09*, Earthquake Engineering Research Center, University of California, Berkeley, CA.

Jain, A.K., Goel, S.C., and Hanson, R.D. (1978), "Hysteresis behavior of bracing members and seismic response of braced frames with different proportions," *Report No. UMEME 78R3*, Department of Civil Engineering, University of Michigan, Ann Arbor, MI.

Jin, J., and El-Tawil, S. (2003), "Inelastic cyclic model for steel braces," *Journal of Engineering Mechanics*, ASCE, **129** (5), pp. 548-557.

Kanvinde, A., and Deierlein, G.G. (2004), "Micromechanical simulation of earthquake induced fractures in steel structures," *Report No. TR145*, John A. Blume Center, Stanford

University, Stanford, CA.

Khatib, I.F., Mahin, S.A., and Pister, K.S. (1988), "Seismic behavior of concentrically braced steel frames," *Report No. UCB/EERC-88/01*, Earthquake Engineering Research Center, University of California, Berkeley, CA.

Krawinkler, H., Bertero, V.V., and Popov, E.P. (1971), "Inelastic behavior of steel beam-to-column subassemblages," *Report No. EERC 71/07*, Earthquake Engineering Research Center, University of California, Berkeley, CA.

Krawinkler, H. (1978), "Shear in beam-column joints in seismic design of steel frames," *Engineering Journal*, AISC, **15** (3), pp. 82-91.

Krawinkler, H., and Seneviratna, G.D.P.K. (1998), "Pros and cons of a pushover analysis for seismic performance evaluation," *Journal of Engineering Structures*, Elsevier, **20** (4-6), pp. 452-464.

Krawinkler, H., Gupta, A., Median, R., and Luco, N. (2000), "Loading histories for seismic performance testing of SMRF Components and Assemblies," SAC Joint Venture, *Report No. SAC/BD-00/10*.

Krishnan, S. (2003), "FRAME3D—A program for three-dimensional nonlinear time-history analysis of steel buildings: User guide," *Technical Rep. No. EERL 2003-03*, Earthquake Engineering Research Laboratory, California Institute of Technology, Pasadena, CA.

Krishnan, S. (2009), "FRAME3D V2.0—A program for the three-dimensional nonlinear time-history analysis of steel structures: User's guide," *Technical Rep. No. EERL 2009-04*, Earthquake Engineering Research Laboratory, California Institute of Technology, Pasadena, CA.

Krishnan, S. (2010), "The modified elastofiber element for steel slender column and brace modeling," *Journal of Structural Engineering*, ASCE, **136** (11), pp. 1350-1366.

Lagarias, J.C., Reeds, J.A., Wright, M.H., and Wright, P.E. (1998), "Convergence properties of the Nelder-Mead simplex method in low dimensions," *SIAM Journal of Optimization*, **9** (1), pp. 112-147.

Lai, J., Chen, C., and Mahin, S.A. (2010), "Experimental and analytical performance of concentrically braced steel frames," *Structures Congress*, ASCE, Orlando, FL.

Lai, J. (2012), "Experimental and Analytical Studies on the Seismic Behavior of Conventional and Hybrid Braced Frames," *Ph.D. Dissertation*, University of California at Berkeley, Berkeley, CA.

Laplace, P. (1812), *Theorie Analytique des Probabilites*, Courcier.

Lee, S., and Goel, S.C. (1987), "Seismic behavior of hollow and concrete-filled square tubular bracing members," *Report No. UMEE 87-11*, Department of Civil Engineering, University of Michigan, Ann Arbor, MI.

Lee, K., and Bruneau, M. (2005), "Energy dissipation of compression members in concentrically braced frames: review of experimental data," *Journal of Structural Engineering*, ASCE, **131** (4), pp. 552-559.

Lehman, D.E., and Roeder, C.W. (2008), "Improved seismic design of concentrically braced frames and gusset plate connections," *Structures Congress*, ASCE, Vancouver, BC.

Lehman, D.E., Roeder, C.W., Herman, D., Johnson, S., and Kotulka, B. (2008), "Improved seismic performance of gusset plate connections," *Journal of Structural Engineering*, ASCE, **134** (6), pp. 890-901.

Leowardi, S. and Walpole, W. (1996), "Performance of Steel Brace Members," *Report No. ISSN 0110-3326*, University of Cantenbury, New Zealand.

Levenberg, K. (1944), "A method for the solution of certain problems in least-squares," *Quarterly Applied Math.* **2**, pp. 164–168.

Lignos, D.G., and Krawinkler, H. (2007), "A Database in Support of Modeling of Component Deterioration for Collapse Prediction of Steel Frame Structures," *Proceedings ASCE Structures Congress*, ASCE, Long Beach, CA.

Lignos, D.G. and Krawinkler (2012b), "Sidesway collapse of deteriorating structural systems under seismic excitations," *Report No. TB177*, John. A. Blume Earthquake Engineering Research Center, Stanford University, Stanford, CA.

Lignos, D.G., Kolios, D., and Miranda, E. (2010), "Fragility assessment of reduced beam section moment connections," *Journal of Structural Engineering*, ASCE, **136** (9), pp. 1140-1150.

Lignos, D.G., and Krawinkler, H. (2011), "Deterioration modeling of steel components in support of collapse prediction of steel moment frames under earthquake loading," *Journal of Structural Engineering*, ASCE, **137** (11), pp. 1291-1302.

Lignos, D.G., Krawinkler, H., and Whittaker, A. S. (2011), "Prediction and validation of sidesway collapse of two scale models of a 4-story steel moment frame," *Earthquake Engineering and Structural Dynamics*, EESD, **40** (7), pp. 807-825.

Lignos, D.G., and Krawinkler, H. (2012), "Development and utilization of structural component databases for performance-based earthquake engineering," *Journal of Structural Engineering*, ASCE, doi: 10.1061/(ASCE)ST.1943-541X.0000646.

Lignos, D.G., Karamanci, E., and Martin, G. (2012), "A steel database for modeling post-buckling behavior and fracture of concentrically braced frames under earthquakes," Proceedings, 15<sup>th</sup> World Conference of Earthquake Engineering (15WCEE), Lisbon, Portugal, 2012, paper No. 4366.

Lignos, D.G., Hikino, T., Matsuoka, Y., Nakashima, M. (2013). "Collapse assessment of steel moment frames based on E-Defense full-scale shake table collapse tests", *Journal of Structural Engineering*, ASCE, **139** (1), pp. 120-132.

Liu, J., and Astanteh-Asl, A. (2000), "Cyclic testing of simple connections including effects of slab," *Journal of Structural Engineering*, ASCE, **126** (1), pp. 32-39.

Liu, J., and Astanteh-Asl, A. (2004), "Moment-rotation parameters for composite shear tab connections", *Journal of Structural Engineering*, ASCE, **130** (9), pp. 1371-1380.

LSTC (2007), "LS-DYNA," Livermore Software Technology Corporation, CA.

Lumpkin, E.J. (2009), "Enhanced seismic performance of multi-story special concentrically braced frames using a balanced design procedure," *Ph.D. Dissertation*, Department of Civil and Environmental Engineering, University of Washington, Seattle, WA.

Mamaghani, I.H.P., Usami, T., and Mizuno, E. (1996), "Cyclic elastoplastic large displacement behaviour of steel compression members", *Journal of Structural Engineering*, JSCE, **42A**, pp. 135-145.

Manson, S.S. (1965), "Fatigue: A complex subject - some simple approximations," *Experimental Mechanics*, **5** (7), pp. 193-226

Mathworks (2011), "Matlab documentation," <http://www.mathworks.com/access/helpdesk/help/techdoc/matlab.shtml>.

McKenna, F. (1997), "Object oriented finite element programming frameworks for analysis, algorithms and parallel computing," *Ph.D. Dissertation*, University of California at Berkeley, Berkeley, CA.

Medina, R.A., and Krawinkler, H. (2003), "Seismic demands for non-deteriorating structures and their dependence on ground motions", *Report No. 144*, John. A. Blume Earthquake Engineering Research Center, Stanford University, Stanford, CA.

Menegotto, M., and Pinto, P.E. (1973), "Method of analysis for cyclically loaded reinforced concrete plane frames including changes in geometry and non-elastic behavior of elements under combined normal force and bending," *Proceedings, IABSE Symposium on Resistance and Ultimate Deformability of Structures Acted on by Well Defined Repeated Loads*, pp. 15-22.

Nakashima, M., Roeder, C., and Maruoka, Y. (2000), "Steel moment frames for earthquakes in United States and Japan," *Journal of Structural Engineering*, ASCE, **126** (8), pp. 861-868.

NBCC (2005), "National Building Code of Canada," 12<sup>th</sup> ed., National Research Council of Canada, Ottawa, ON.

NEHRP (1997), "Recommended Provisions for the Development of Seismic Regulations for New Buildings (and other Structures)," Building Seismic Safety Council, Washington, D.C.

Newell, J.D., and Uang, C. (2008), "Cyclic behavior of steel wide-flange columns subjected to large drift," *Journal of Structural Engineering*, ASCE, **134** (8), pp. 1334-1342.

Nip, K.H., Gardner, L., and Elghazouli, A.Y. (2010), "Cyclic testing and numerical modeling of carbon steel and stainless steel tubular bracing members," *Engineering Structures*, Elsevier, **32** (2), pp. 424-441.

NIST, (2010). "Evaluation of the FEMA P-695 methodology for quantification of building seismic performance factors, GCR 10-917-8", prepared by the NEHRP consultants Joint Venture for the National Institute of Standards and Technology, Gaithersburg, MD.

Nonaka, T. (1973), "An elastic-plastic analysis of a bar under repeated axial loading," *International Journal of Solids and Structures*, **9** (5), pp. 569.

Okazaki, T., Lignos, D.G., Hikino, T., and Kajiwara, K. (2011), "Dynamic response of a steel concentrically braced frame," *Structures Congress 2011*, ASCE, Las Vegas, NV.

Okazaki, T., Lignos, D.G., Hikino, T., and Kajiwara, K. (2012), "Dynamic response of a chevron concentrically braced frame," *Journal of Structural Engineering*, ASCE, doi: 10.1061/(ASCE)ST.1943-541X.0000679.

Palmer, K., Roeder, C., Okazaki, T., Shield, C., and Lehman, D. (2011), "Three-dimensional tests of two-story, one-bay by one-bay, steel concentric braced frames," *Structures Congress 2011*, ASCE, Las Vegas, NV.

PEER/ATC, (2010). "Modeling and acceptance criteria for seismic design and analysis of tall buildings", Rep. PEER/ATC-72-1, prepared by the Applied Technology Council in cooperation with the Pacific Earthquake Engineering Research Center, Redwood City, CA.

Perotti, F., and Scarlassara, G. P. (1991), "Concentrically braced steel frames under seismic actions: Non-linear behaviour and design coefficients," *Earthquake Engineering*

and *Structural Dynamics*, **20** (5), pp. 409-427.

Popov, E.P., Takanashi, K., and Roeder, C.W. (1976), "Structural steel bracing systems: behavior under cyclic loading," *Report No. EERC 76-17*, Earthquake Engineering Research Center, California Institute of Technology, Pasadena, CA.

Popov, E.P., Zayas, V.A. and Mahin, S.A. (1980), "Cyclic inelastic buckling of tubular steel braces," *Report No. UCB/EERC-0/16*, Earthquake Engineering Research Center, University of California, Berkeley, CA.

Powell, G.H. (1973), "DRAIN-2D user guide," *Report No. EERC 73-22*, Earthquake Engineering Research Center, University of California, Berkeley, CA.

Ramirez, C.M., Lignos, D.G., Miranda, E., and Kolios, D. (2012), "Fragility functions for pre-Northridge welded steel moment-resisting beam-to-column connections," *Journal of Engineering Structures*, Vol. **45**, pp. 574-584.

Richard, J. (2009), "Étude du comportement sismique de bâtiments industriels avec systèmes de contreventement en acier de faible ductilité," *M.Sc. Thesis*, Department of Civil, Geological and Mining Engineering, Montreal Polytechnic, Montreal, QC.

Richards, P.W. (2009), "Seismic column demands in ductile braced frames," *Journal of Structural Engineering*, ASCE, **135** (1), pp. 33-41.

Remennikov, A.M., and Walpole, W.R. (1997), "Modeling the inelastic cyclic behavior of a bracing member for work-hardening material," *International Journal of Solids and Structures*, **34** (27), pp. 491-515.

Roeder, C. W., Lehman, D. E., and Yoo, J. H. (2004), "Performance based seismic design of braced-frame connections," *7th Pacific Structural Steel Conference*, Long Beach, CA.

Shaback, J.B. (2001), "Behaviour of square HSS braces with end connections under reversed cyclic axial loading," *M.Sc. Thesis*, Department of Civil Engineering, University of Calgary, Calgary, AB.

Shaback, J.B., and Brown, T. (2003), "Behaviour of square hollow structural steel braces with end connections under reversed cyclic axial loading," *Canadian Journal of Civil Engineering*, **30** (4), pp. 745-753.

Shiabata, M. (1982), "Analysis of elastic-plastic behavior of a steel brace subjected to repeated axial force," *International Journal of Solids and Structures*, **18** (3), pp. 217-228.

Singh, P. (1977), "Seismic behavior of braces and braced steel frames," *Ph.D. Dissertation*, Department of Civil Engineering, University of Michigan, Ann Arbor, MI.

Spacone, E., Filippou, F.C., and Taucer, F.F. (1996), "Fiber beam-column model for

nonlinear analysis of R/C frames, part I: formulation,” *Earthquake Engineering and Structural Dynamics*, EESD, **25**, pp. 711-725.

Stoakes, C.D., Fahnestock, L.A. (2011). “Cyclic flexural testing of concentrically braced frame beam-column connections”, *J., Struct., Eng.*, ASCE, **137** (7), pp. 739-747.

Stoakes, C.D., and Fahnestock, L.A. (2012), “Cyclic flexural analysis and behavior of beam-column connections with gusset plates,” *Journal of Constructional Steel Research*, **72**, pp. 227-239.

Stoakes, C.D. (2012), “Beam-column connection flexural behavior and seismic collapse performance of concentrically braced frames,” *Ph.D. Dissertation*, Department of Civil Engineering, University of Illinois at Urbana-Champaign, Urbana, IL.

Suita, K., Yamada, S., Tada, M., Kasai, K., Matsuoka, Y., and Shimada, Y. (2008), “Collapse experiment on 4-story steel moment frame: Part 2 detail of collapse behavior,” *Proceedings 14th World Conference on Earthquake Engineering*, Beijing, China.

Taejin, K., Whittaker, A. S., Gilani, A. S., Bertero, V., and Takhirov, S. (2000), “Cover-plate and flange-plate steel moment-resisting connections,” *Journal of Structural Engineering*, ASCE, **137** (11), pp. 474-482.

Takeuchi, T., and Matsui, R. (2011), “Cumulative cyclic deformation capacity of circular tubular braces under local buckling,” *Journal of Structural Engineering*, ASCE, **137** (11), pp. 1311-1318.

Tang, X., and Goel, S.C. (1989), “Brace Fractures and Analysis of Phase I Structure,” *Journal of Structural Engineering*, ASCE, **115** (8), pp. 1960-1976.

Tsuji, B., and Nishino, T. (1988), “Elastic plastic deformation and collapse behavior of braced frames,” *Proceedings of Ninth World Conference on Earthquake Engineering*, Tokyo-Kyoto, Japan.

Tremblay, R., Timler, P., Bruneau, M., and Filiatrault, A. (1995), “Performance of steel structures during the 1994 Northridge earthquake,” *Canadian Journal of Civil Engineering*, NRC, **22**, pp. 338-360.

Tremblay, R. (2002), “Inelastic seismic response of steel bracing members,” *Journal of Constructional Steel Research*, Elsevier, **58**, pp. 665-701.

Tremblay, R., Haddad, M., Martinez, G., Richard, J., and Moffatt, K. (2008), “Inelastic cyclic testing of large size steel bracing members,” *Proceedings, 14th World Conference on Earthquake Engineering*, October 2008, Beijing, China.

Uriz, P. (2005), “Towards earthquake resistant design of concentrically braced steel structures,” *Ph.D. Dissertation*, Department of Civil and Environmental Engineering, University of California, Berkeley, CA.

Uriz, P., and Mahin, S.A., (2008), "Towards earthquake resistant design of concentrically braced steel structures," *Report No. PEER 2008/08*, Pacific Earthquake Engineering Research Center, University of California at Berkeley, Berkeley, CA.

Uriz, P., Filippou, F.C., Mahin, S.A. (2008). "Model for cyclic inelastic buckling of steel braces," *J., Struct., Eng.*, ASCE, **134** (4), pp. 619-628.

USGS (2011), "Java ground motion parameter calculator," Version 5.1.0., United States Geological Survey, <http://earthquake.usgs.gov/hazards/designmaps/javacalc.php>.

Vamvastikos, D., and Cornell, C.A. (2002), "Incremental dynamic analysis," *Earthquake Engineering and Structural Dynamics*, EESD, **31** (4), pp. 491-514.

Venables, W.N., and Ripley, B.D. (2002), *Modern applied statistics with S*, 4th Ed., Springer, New York.

Victorsson, V.K. (2011), "The reliability of capacity-designed components in seismic resistant systems," *Ph.D. Dissertation*, Department of Civil and Environmental Engineering, Stanford University, Stanford, CA.

Van Vlack, L.H. (1980), "Elements of materials science and engineering," Reading Massachusetts: Addison-Wesley.

Wakabayashi, M., Nonaka, T., Nakamura, T., Morino, S., and Yoshida, N. (1973), "Experimental studies on the behavior of steel bars under repeated axial loading," *Disaster Prevention Research Institute Annuals*, Kyoto University, **16B**, pp. 113-125.

Wakabayashi, M., Nakamura, S., and Yoshida, N. (1977), "Experimental studies on the elastic-plastic behavior of steel braced frames under repeated horizontal loading. Part 1 experiments of braces with an H-shaped cross section in a frame," *Bulletin of the Disaster Prevention Research Institute*, Kyoto University, **27** (3), pp. 121-154.

Wakabayashi, M., Nakamura, S., and Yoshida, N. (1980a), "Experimental studies on the elastic-plastic behavior of steel braced frames under repeated horizontal loading. Part 2 experiments of braces composed of steel circular tubes, angle-shapes, flat bars or round bars," *Bulletin of the Disaster Prevention Research Institute*, Kyoto University, **29** (3), pp. 99-127.

Wakabayashi, M., Nakamura, S., and Yoshida, N. (1980b), "Experimental studies on the elastic-plastic behavior of steel braced frames under repeated horizontal loading. Part 3 experiments of one story-one bay braced frames," *Bulletin of the Disaster Prevention Research Institute*, Kyoto University, **29** (4), pp. 143-164.

Walpole, W. R. (1996), "Behaviour of cold-formed steel RHS members under cyclic loading," Department of Civil Engineering, University of Canterbury, Christchurch, New

Zealand.

Yamanouchi, H., Midorikawa, M., Nishiyama, I., and Hirose, M. (1985), "Experimental results on a K-braced steel structure under seismic loading utilizing large-scale test facilities," *Proceedings The Sixth Joint Technical Coordinating Committee Meeting*, The U.S.-Japan Cooperative Research Program.

Yang, F., and Mahin, S.A. (2005), "Limiting net section failure in slotted HSS braces," *Steel TIPS Report*.

Yang, C.S. (2006), "Performance evaluation of innovative steel braced frames," *Ph.D. Dissertation*, Department of Civil and Environmental Engineering, University of California, Berkeley, CA.

Yu, W., and LaBoube, R.A. (2010), "Cold-Formed Steel Design," Fourth Edition, John Wiley & Sons, Inc., Hoboken, NJ.

Zareian, F., and Krawinkler, H. (2007), "Sensitivity of collapse potential of buildings to variations in structural systems and structural parameters," *Structures Congress*, ASCE, Long Beach, CA.

Zayas, V.A., Popov, E.P. and Mahin, S.A. (1980), "Cyclic inelastic buckling of tubular steel braces," *Report No. UCB/EERC-80/16*, Earthquake Engineering Research Center, University of California, Berkeley, CA.

# Appendix A

## Steel Brace Database

---

### Steel Brace Database

This appendix includes the complete steel brace database that is developed to be able to reach the research goals of this thesis. The database includes information about the geometric and material properties of the 317 brace specimens that are discussed extensively in Chapters 2 and 3.

The first column of Table A.1 is used for identification purposes for each specimen included in the steel brace database. The second and third columns of the same table include the citation of the experimental studies of the deduced data. The next column indicates the cross sectional shape of each brace. The following two columns summarize the steel grade of the individual braces including their measured yield strength,  $f_{y,m}$ . The N/R fields in these columns indicate that either the steel grade or the measured yield strength is not provided. The brace slenderness  $kL/r$  and  $\lambda_c$  as defined in Chapter 3 are listed in the next two columns. The length of the brace  $L_{brace}$  is, in mm, the length of the brace specimens (see Chapter 3). The width-to-thickness ratios,  $w/t$ , for all brace specimens, or the  $D/t$  ratio in round HSS sections, are calculated in accordance to AISC (2010) guidelines. For W-, WT-, channel and angle shapes the listed local slenderness ratio,  $w/t$ , is the  $b/t_f$  ratio where  $b$  is the effective flange length and the  $t_f$  is the flange

thickness as defined in AISC (2010). The last three columns in the database contain the story drift ratios (in radians) for the three damage states that are of concern in this thesis as defined in Chapter 4. The N/A fields in these columns indicate that the respective damage state is not observed for the brace component.

Table A.1. Steel brace database

ID	Investigator	Specimen ID	Shape	Steel Brace Cross Section	Material Designation	$f_{y,m}$ [Mpa]	kL/r	$\lambda_c$	$L_{brace}$ [mm]	w/t (or D/t)	IDRDS1 [% rad]	IDRDS2 [% rad]	IDRDS3 [% rad]
1		HSS1-1	HSS	HSS102x102x6.4	ASTM A500 Grade B	460	77	1.18	2985	14.2	0.30	1.85	2.70
2		HSS1-2	HSS	HSS102x102x6.4	ASTM A500 Grade B	460	77	1.18	2985	14.2	1.00	2.50	0.30
3		HSS1-3c	HSS	HSS102x102x6.4	ASTM A500 Grade B	460	77	1.18	2985	14.2	0.30	2.10	2.80
4		HSS1-4	HSS	HSS102x102x6.4	ASTM A500 Grade B	460	77	1.18	2985	14.2	0.40	2.70	3.80
5		HSS1-5	HSS	HSS102x102x6.4	ASTM A500 Grade B	460	77	1.18	2985	14.2	0.90	7.90	2.00
6		HSS1-6	HSS	HSS102x102x6.4	ASTM A500 Grade B	460	77	1.18	2985	14.2	0.35	1.90	2.50
7		HSS2-1	HSS	HSS102x102x9.5	ASTM A500 Grade B	499	80	1.27	2985	8.5	0.30	1.50	3.60
8		HSS2-2c	HSS	HSS102x102x9.5	ASTM A500 Grade B	499	80	1.27	2985	8.5	0.30	1.80	2.70
9		P1-1	Pipe	Pipe127STD	ASTM A53 Grade B	326	63	0.81	3010	21.6	0.30	2.70	2.30
10	Fell et al. (2010)	P1-2	Pipe	Pipe127STD	ASTM A53 Grade B	326	63	0.81	3010	21.6	0.30	2.70	3.30
11		P1-3	Pipe	Pipe127STD	ASTM A53 Grade B	326	63	0.81	3010	21.6	6.80	3.50	3.40
12		P1-4	Pipe	Pipe127STD	ASTM A53 Grade B	326	63	0.81	3010	21.6	N/A	N/A	6.50
13		P2-1	Pipe	Pipe76STD	ASTM A53 Grade B	372	102	1.40	3010	16.2	0.30	2.50	4.00
14		P2-2	Pipe	Pipe76STD	ASTM A53 Grade B	372	102	1.40	3010	16.2	0.30	2.50	3.80
15		P2-3	Pipe	Pipe76STD	ASTM A53 Grade B	372	102	1.40	3010	16.2	7.00	1.30	4.30
16		P2-4	Pipe	Pipe76STD	ASTM A53 Grade B	372	102	1.40	3010	16.2	N/A	N/A	5.10
17		W1	W	W310x24	ASTM A992	414	153	2.22	3010	7.5	0.20	2.43	5.00
18		W2	W	W310x24	ASTM A992	414	153	2.22	3010	7.5	1.30	5.90	2.40
19		W3	W	W310x24	ASTM A992	414	153	2.22	3010	7.5	7.20	0.34	3.90
20		528	Pipe	89.1x3.2	STK400 (JIS G3444)	349	53	0.70	1622	28.0	0.70	1.41	2.81
21		532	Pipe	89.1x2.8	STK400 (JIS G3444)	357	53	0.71	1622	32.0	0.98	0.98	2.11
22	Takeuchi and Matsui (2011)	721	Pipe	89.1x4.2	STK400 (JIS G3444)	366	74	1.01	2219	21.0	0.46	1.70	2.62
23		728	Pipe	89.1x3.2	STK400 (JIS G3444)	349	73	0.97	2219	28.0	0.46	0.93	4.63
24		732	Pipe	89.1x2.8	STK400 (JIS G3444)	357	73	0.98	2219	32.0	0.93	0.93	1.85
25		1021	Pipe	89.1x4.2	STK400 (JIS G3444)	366	104	1.42	3135	21.0	0.66	2.49	4.15
26		1028	Pipe	89.1x3.2	STK400 (JIS G3444)	349	103	1.37	3135	28.0	0.66	2.66	4.32

Table A.1. Steel braced Database (Continued)

ID	Investigator	Specimen ID	Shape	Steel Brace Cross Section	Material Designation	$f_{y,m}$ [Mpa]	$kL/r$	$\lambda_c$	$L_{brace}$ [mm]	w/t (or D/f)	IDRDS1 [% rad]	IDRDS2 [% rad]	IDRDS3 [% rad]
27	Takeuchi and Matsui (2011)	1032	Pipe	89.1x2.8	STK400 (JIS G3444)	357	103	1.38	3135	32.0	0.66	1.16	2.66
28		1228	Pipe	76.3x2.8	STK400 (JIS G3444)	353	121	1.62	3135	27.0	0.83	2.49	3.99
29	Han et al. (2007)	S 77-28	HSS	100x100x3.2	ASTM A500 Grade B	394	77	1.09	3572	28.3	0.30	0.59	0.57
30		S 90-22	HSS	100x100x4	ASTM A500 Grade B	411	80	1.16	3630	22.0	N/A	N/A	N/A
31		S 82-19	HSS	100x100x4.5	ASTM A500 Grade B	421	82	1.20	3650	19.2	N/A	N/A	N/A
32		S 70-18	HSS	125x125x6	ASTM A500 Grade B	405	70	1.01	3600	17.8	N/A	N/A	N/A
33		S 85-14 A	HSS	100x100x6	ASTM A500 Grade B	399	85	1.21	3611	13.7	0.17	1.10	1.39
34		S 85-14 B	HSS	100x100x6	ASTM A500 Grade B	410	85	1.22	3611	13.7	0.08	0.97	1.75
35		S 85-14 C	HSS	100x100x6	ASTM A500 Grade B	408	85	1.22	3611	13.7	0.06	1.02	1.74
36		S 69-11	HSS	125x125x9	ASTM A500 Grade B	402	69	0.98	3573	10.9	N/A	N/A	N/A
37		S 90-8 A	HSS	100x100x9	ASTM A500 Grade B	425	90	1.33	3611	8.1	0.11	N/A	0.66
38		S 90-8 B	HSS	100x100x9	ASTM A500 Grade B	392	90	1.27	3611	8.1	0.05	N/A	0.57
39	S 90-8 C	HSS	100x100x9	ASTM A500 Grade B	395	90	1.28	3611	8.1	0.02	N/A	0.63	
40	Shaback and Brown (2003)	1A	HSS	127x127x6.4	G40.21M 350W Class C	461	52	0.80	3450	16.8	0.46	1.74	N/A
41		1B	HSS	127x127x8.0	G40.21M 350W Class C	421	54	0.79	3452	12.9	0.45	1.60	1.60
42		2A	HSS	152x152x8.0	G40.21M 350W Class C	442	53	0.80	4040	16.0	0.45	1.07	1.07
43		2B	HSS	152x152x9.5	G40.21M 350W Class C	442	52	0.78	4028	13.0	0.53	1.22	1.22
44		3A	HSS	127x127x6.4	G40.21M 350W Class C	461	65	0.99	4456	16.8	0.31	1.73	1.73
45		3B	HSS	127x127x8.0	G40.21M 350W Class C	421	66	0.96	4446	12.9	0.38	1.30	1.30
46		3C	HSS	127x127x9.5	G40.21M 350W Class C	461	62	0.94	4414	10.4	0.39	1.27	1.27
47		4A	HSS	152x152x8.0	G40.21M 350W Class C	442	64	0.95	4944	16.0	0.37	1.33	1.33
48		4B	HSS	152x152x9.5	G40.21M 350W Class C	442	60	0.89	4914	13.0	0.39	1.22	1.22
49		Strut-1	W	W200X31	ASTM A36	279	120	1.43	3810	6.6	0.11	0.31	N/A
50	Black et al. (1980)	Strut-2	W	W150X37	ASTM A36	291	40	0.49	1550	6.6	0.23	0.65	N/A
51		Strut-3	W	W150X30	ASTM A36	277	80	0.95	3070	8.2	0.21	0.78	N/A
52		Strut-4	W	W150X30	ASTM A36	277	80	0.95	3070	8.2	0.21	0.35	N/A

Table A.1. Steel brace database (Continued)

ID	Investigator	Specimen ID	Shape	Steel Brace Cross Section	Material Designation	$f_{y,m}$ [Mpa]	kL/r	$\lambda_c$	$L_{brace}$ [mm]	w/t (or D/t)	IDRDS1 [% rad]	IDRDS2 [% rad]	IDRDS3 [% rad]
53	Black et al. (1980)	Strut-5	W	W150X30	ASTM A36	277	80	0.95	3070	8.2	0.21	0.46	N/A
54		Strut-6	W	W150X24	ASTM A36	308	120	1.50	2950	5.0	0.11	0.34	N/A
55		Strut-7	W	W150x24	ASTM A36	345	40	0.53	1480	5.0	0.38	0.63	N/A
56		Strut-8	Angle	L152x89x9.5	ASTM A36	281	80	0.96	2830	15.9	0.18	0.35	N/A
57		Strut-9	Angle	L127x89x9.5	ASTM A36	301	40	0.49	1480	13.4	0.10	0.34	N/A
58		Strut-10	Angle	L102x89x9.5	ASTM A36	287	120	1.45	3810	10.7	N/A	N/A	N/A
59		Strut-11	Channel	C200x17	ASTM A36	245	120	1.34	3000	5.8	0.05	0.36	N/A
60		Strut-12	WT	WT125x33.5	ASTM A36	272	80	0.94	2540	6.5	0.13	0.39	N/A
61		Strut-13	WT	WT205x33.5	ASTM A36	288	80	0.97	3190	6.2	0.16	0.31	N/A
62		Strut-14	Pipe	Pipe102STD	ASTM A53 Grade B	327	80	1.03	3070	17.7	0.23	0.43	N/A
63		Strut-15	Pipe	Pipe102STD	ASTM A53 Grade B	327	80	1.03	3070	17.7	0.18	0.79	N/A
64		Strut-16	Pipe	Pipe102XS	ASTM A53 Grade B	165	80	0.73	3010	13.3	0.09	0.40	N/A
65		Strut-17	HSS	102x102x6.4	ASTM A501 Hot Rolled	407	80	1.15	3050	12.9	0.22	0.92	N/A
66		Strut-18	HSS	102x102x13	ASTM A501 Hot Rolled	565	80	1.35	2760	4.8	0.16	0.47	N/A
67		Strut-19	W	W150X30	ASTM A36	277	40	0.47	2190	8.2	0.27	0.96	N/A
68		Strut-20	Angle	L152x89x9.5	ASTM A36	281	80	0.96	4040	15.9	0.14	0.33	N/A
69		Strut-21	Pipe	Pipe102 X-Strong	ASTM A53 Grade B	165	80	0.73	2190	12.6	0.47	N/A	N/A
70		Strut-22	HSS	102x102x13	ASTM A501 Hot Rolled	565	80	1.35	3950	4.8	0.29	0.66	N/A
71		Strut-23	W	127x127x9.1	ASTM A36	246	80	0.89	3660	11.0	0.26	0.45	N/A
72		Strut-24	Pipe	Pipe89STD	ASTM A53 Grade B	319	80	1.02	3890	16.2	0.24	0.51	N/A
73		HSS1	HSS	HSS127x127x9.5	ASTM A500 Grade B	483	72	1.13	3417	10.4	0.17	0.41	1.30
74		HSS2	HSS	HSS127x127x9.5	ASTM A500 Grade B	483	85	1.33	4008	10.4	0.27	0.70	1.50
75		HSS3	HSS	HSS127x127x9.5	ASTM A500 Grade B	483	85	1.33	4008	10.4	0.30	0.70	1.30
76		HSS4	HSS	HSS127x127x9.5	ASTM A500 Grade B	505	83	1.32	3904	10.4	0.25	0.65	1.40
77	HSS5	HSS	HSS127x127x9.5	ASTM A500 Grade B	505	85	1.35	4008	10.4	0.31	0.72	1.40	
78	HSS6	HSS	HSS127x127x9.5	ASTM A500 Grade B	446	85	1.27	4008	10.4	0.47	0.83	1.72	

Table A.1. Steel brace database (Continued)

ID	Investigator	Specimen ID	Shape	Steel Brace Cross Section	Material Designation	$f_{u,m}$ [Mpa]	kL/r	$\lambda_c$	$l_{brace}$ [mm]	w/t (or D/t)	IDRDS1 [% rad]	IDRDS2 [% rad]	IDRDS3 [% rad]
79	Lehman et al. (2008)	HSS7	HSS	HSS127x127x9.5	ASTM A500 Grade B	446	80	1.21	3792	10.4	0.54	1.00	1.10
80		HSS8	HSS	HSS127x127x9.5	ASTM A500 Grade B	446	87	1.31	4121	10.4	0.42	0.80	1.50
81		HSS9	HSS	HSS127x127x9.5	ASTM A500 Grade B	446	85	1.27	4008	10.4	0.39	0.50	1.32
82		HSS10	HSS	HSS127x127x9.5	ASTM A500 Grade B	454	84	1.28	3990	10.4	0.43	0.65	1.50
83		HSS11	HSS	HSS127x127x9.5	ASTM A500 Grade B	454	80	1.22	3792	10.4	0.96	0.20	1.06
84		HSS12	HSS	HSS127x127x9.5	ASTM A500 Grade B	455	72	1.09	3420	10.4	0.47	0.71	1.20
85		HSS13	HSS	HSS127x127x9.5	ASTM A500 Grade B	455	80	1.21	3790	10.4	0.42	0.60	2.05
86		HSS14	HSS	HSS127x127x9.5	ASTM A500 Grade B	N/R	84	1.06	4005	10.4	0.44	1.08	1.90
87		HSS15	HSS	HSS127x127x9.5	ASTM A500 Grade B	N/R	86	1.09	4116	10.4	0.44	0.83	1.87
88		HSS16	HSS	HSS127x127x9.5	ASTM A500 Grade B	N/R	70	0.88	3334	10.4	0.16	0.45	2.30
89		HSS17	HSS	HSS127x127x9.5	ASTM A500 Grade B	N/R	84	1.06	3994	10.4	0.51	0.63	2.15
90		HSS18	HSS	HSS127x127x9.5	ASTM A500 Grade B	505	81	1.30	4008	10.4	0.38	0.64	1.50
91		HSS19	HSS	HSS127x127x9.5	ASTM A500 Grade B	N/R	85	1.07	4005	10.4	0.34	0.65	1.80
92		HSS20	HSS	HSS127x127x9.5	ASTM A500 Grade B	N/R	72	0.91	4005	10.4	N/A	N/A	1.60
93		HSS21	HSS	HSS127x127x9.5	ASTM A500 Grade B	N/R	81	1.02	4005	10.4	0.40	0.75	1.48
94		HSS22	HSS	HSS127x127x9.5	ASTM A500 Grade B	N/R	84	1.06	3994	10.4	0.25	0.5	1.38
95		HSS23	W	W150x37	ASTM A500 Grade B	N/R	104	1.31	4031	6.6	0.38	0.49	2.32
96		HSS24	HSS	HSS127x127x9.5	ASTM A500 Grade B	N/R	69	0.87	4005	10.4	0.39	0.63	2.00
97		HSS25	HSS	HSS127x127x9.5	ASTM A500 Grade B	N/R	49	0.62	3778	10.4	0.53	0.72	1.11
98		HSS26	HSS	HSS127x127x9.5	ASTM A500 Grade B	N/R	50	0.63	3778	10.4	0.33	N/A	0.74
99		HSS27	HSS	HSS127x127x9.5	ASTM A500 Grade B	N/R	85	1.07	4012	10.4	N/A	N/A	N/A
100		HSS28	HSS	HSS127x127x9.5	ASTM A500 Grade B	N/R	82	1.03	3861	10.4	0.34	0.55	1.46
101		HSS29	Channel	2-MCI50X17.9	ASTM A36 Annealed ASTM AISI 1020	N/R	218	2.46	4020	6.2	N/A	N/A	N/A
102		Zayas et al. (1980)	Strut 1	Pipe	100.8x2.1	214	54	0.56	1404	48.0	0.27	0.51	N/A
103			Strut 2	Pipe	102.3x3.1	1020	214	54	0.56	1404	33.0	0.27	0.51

Table A.1. Steel brace database (Continued)

ID	Investigator	Specimen ID	Shape	Steel Brace Cross Section	Material Designation	$f_{y,m}$ [Mpa]	$kL/r$	$\lambda_c$	$L_{brace}$ [mm]	w/t (or D/t)	IDRDS1 [% rad]	IDRDS2 [% rad]	IDRDS3 [% rad]
104	Zayas et al. (1980)	Strut 3	Pipe	100.8x2.1	ASTM A513 1020	634	54	0.97	1404	44.0	0.43	0.71	N/A
105		Strut 4	Pipe	102.3x3.1	Annealed ASTM A513 1020	510	54	0.87	1404	33.0	0.50	N/A	0.55
106		Strut 5	Pipe	100.8x2.1	Annealed ASTM A513 1020	214	25	0.26	1784	48.0	0.62	0.81	N/A
107		Strut 6	Pipe	102.3x3.1	Annealed ASTM A513 1020	214	25	0.26	1784	33.0	0.43	1.02	N/A
108		Specimen 1	HSS	HSS127x127x4.8	ASTM-A500	426	58	0.85	3429	23.5	0.37	1.25	0.44
109		Specimen 2	HSS	HSS127x127x4.8	ASTM-A500	430	35	0.52	3429	23.5	0.58	1.31	0.26
110	Lee and Goel (1987)	Specimen 3	HSS	HSS127x127x4.8 & 4xL25x25x4.8	ASTM-A500	426	32	0.47	3429	23.5	0.53	1.22	1.06
111		Specimen 4	HSS	HSS102x102x3.2	ASTM-A500	400	43	0.61	3480	23.5	0.44	1.90	1.32
112		Specimen 5	HSS	HSS102x102x6.4	ASTM-A500	510	77	1.24	3454	23.5	0.37	1.85	1.01
113		Specimen 6	HSS	HSS102x102x6.4	ASTM-A500	510	45	0.72	3480	23.5	0.58	1.78	1.02
114		Specimen 7	HSS	HSS102x102x6.4	ASTM-A500	510	45	0.72	3480	23.5	0.43	1.26	0.57
115		1	HSS	25.4x25.4x2.67	ASTM A570-Grade C	263	57	0.66	461	6.5	0.37	1.28	N/A
116		2A	HSS	25.4x25.4x2.67	ASTM A570-Grade C	263	53	0.61	461	6.5	N/A	N/A	N/A
117	2B	HSS	25.4x25.4x2.67	ASTM A570-Grade C	392	53	0.75	461	6.5	N/A	N/A	N/A	
118	3	HSS	25.4x25.4x2.67	ASTM A570-Grade C	263	34	0.39	461	6.5	N/A	N/A	N/A	
119	4	HSS	25.4x25.4x2.67	ASTM A570-Grade C	263	30	0.35	512	6.5	0.78	1.60	N/A	
120	5	HSS	25.4x25.4x2.67	ASTM A570-Grade C	263	30	0.35	512	6.5	N/A	N/A	N/A	
121	6	HSS	25.4x25.4x2.67	ASTM A570-Grade C	263	94	1.08	790	6.5	0.19	1.45	N/A	
122	7A	HSS	25.4x25.4x2.67	ASTM A570-Grade C	263	81	0.93	777	6.5	N/A	N/A	N/A	
123	7B	HSS	25.4x25.4x2.67	ASTM A570-Grade C	392	81	1.14	777	6.5	N/A	N/A	N/A	
124	8	HSS	25.4x25.4x2.67	ASTM A570-Grade C	263	54	0.62	803	6.5	N/A	N/A	N/A	
125	9	HSS	25.4x25.4x2.67	ASTM A570-Grade C	263	50	0.58	853	6.5	0.40	N/A	N/A	
126	10	HSS	25.4x25.4x2.67	ASTM A570-Grade C	263	50	0.58	853	6.5	N/A	N/A	N/A	
127	11	HSS	25.4x25.4x2.67	ASTM A570-Grade C	263	140	1.62	1264	6.5	N/A	N/A	N/A	

Table A.1. Steel brace database (Continued)

ID	Investigator	Specimen ID	Shape	Steel Brace Cross Section	Material Designation	$f_{m}$ [Mpa]	kL/r	$\lambda_c$	$L_{brace}$ [mm]	w/t (or D/t)	IDRDS1 [% rad]	IDRDS2 [% rad]	IDRDS3 [% rad]	
128	Jain et al. (1978)	12A	HSS	25.4x25.4x2.67	ASTM A570-Grade C	263	115	1.33	1219	6.5	0.25	N/A	N/A	
129		12B	HSS	25.4x25.4x2.67	ASTM A570-Grade C	392	115	1.62	1219	6.5	N/A	N/A	N/A	
130		13	HSS	25.4x25.4x2.67	ASTM A570-Grade C	263	84	0.97	1314	6.5	N/A	N/A	N/A	
131		14	HSS	25.4x25.4x2.67	ASTM A570-Grade C	263	80	0.92	1365	6.5	N/A	N/A	N/A	
132		15	HSS	25.4x25.4x2.67	ASTM A570-Grade C	263	80	0.92	1365	6.5	0.34	1.32	N/A	N/A
133		16	HSS	25.4x25.4x2.67	ASTM A570-Grade C	263	57	0.66	461	6.5	0.74	3.25	N/A	N/A
134		17	HSS	25.4x25.4x2.67	ASTM A570-Grade C	263	34	0.39	461	6.5	N/A	N/A	N/A	N/A
135		18	HSS	25.4x25.4x2.67	ASTM A570-Grade C	263	92	1.06	803	6.5	N/A	N/A	N/A	N/A
136		19	HSS	25.4x25.4x2.67	ASTM A570-Grade C	263	54	0.62	803	6.5	0.32	1.42	1.51	N/A
137		20	HSS	25.4x25.4x2.67	ASTM A570-Grade C	263	134	1.55	1219	6.5	N/A	N/A	N/A	N/A
138		21	HSS	25.4x25.4x2.67	ASTM A570-Grade C	263	78	0.90	1219	6.5	N/A	N/A	N/A	N/A
139		1L	Angle	L25.4x25.4x6.4	M1020- hot rolled	365	85	1.16	846	4.0	N/A	N/A	N/A	N/A
140		2L	Angle	L25.4x25.4x6.4	M1020- hot rolled	365	120	1.63	1194	4.0	0.25	N/A	N/A	N/A
141		3L	Angle	L37.7x37.7x3.18	M1020- hot rolled	352	85	1.13	1295	12.0	0.26	N/A	N/A	N/A
142		4L	Angle	L31.8x31.8x3.18	M1020- hot rolled	372	120	1.65	1486	10.0	0.25	N/A	N/A	N/A
143		5L	Angle	L25.4x25.4x6.4	M1020- hot rolled	365	85	1.16	846	4.0	0.42	1.06	N/A	N/A
144		6L	Angle	L25.4x25.4x6.4	M1020- hot rolled	365	120	1.63	1194	4.0	0.20	1.46	N/A	N/A
145		7L	Angle	L37.7x37.7x3.18	M1020- hot rolled	352	85	1.13	1295	12.0	0.31	1.70	N/A	N/A
146		8L	Angle	L31.8x31.8x3.18	M1020- hot rolled	372	120	1.65	1486	10.0	0.24	1.11	N/A	N/A
147		A1	Angle	2 L89x64x6.4	ASTM A36	323	130	1.66	3251	14.0	N/A	0.48	1.23	N/A
148	A2	Angle	2 L89x64x6.4	ASTM A36	323	130	1.66	3251	14.0	N/A	0.19	0.70	N/A	
149	A3	Angle	2 L89x64x9.5	ASTM A36	323	117	1.50	3175	9.3	N/A	1.36	1.07	N/A	
150	A4	Angle	2 L89x64x9.5	ASTM A36	323	117	1.50	3175	9.3	0.07	0.55	N/A	N/A	
151	A5	Angle	2 L89x64x9.5	ASTM A36	315	117	1.48	3175	9.3	0.09	0.58	N/A	N/A	
152	C1	Channel	2 C130x10	ASTM A36	365	50	0.68	3405	5.5	N/A	N/A	N/A	N/A	
153	C2	Channel	2 C100X8	ASTM A36	317	50	0.63	3059	5.9	N/A	N/A	N/A	N/A	

Table A.1. Steel brace database (Continued)

ID	Investigator	Specimen ID	Shape	Steel Brace Cross Section	Material Designation	$f_{y,m}$ [Mpa]	kL/r	$\lambda_c$	$L_{brace}$ [mm]	w/t (or D/t)	IDRDS1 [% rad]	IDRDS2 [% rad]	IDRDS3 [% rad]
154	Aslani et al. (1987)	C3	Channel	2 C100X8	ASTM A36	N/R	50	0.56	3059	5.9	N/A	N/A	N/A
155		1	HSS	152x152x8	G40.21-M350W	467	65	0.99	4850	13.8	0.39	1.03	1.03
156		2	HSS	152x152x8	G40.21-M350W	467	65	0.99	4850	13.8	0.26	1.20	N/A
157		3	HSS	152x152x8	G40.21-M350W	467	65	0.99	4850	13.8	0.34	1.24	1.03
158		4	HSS	127x127x8	G40.21-M350W	480	66	1.03	4350	10.6	0.28	1.24	1.61
159	Haddad et al. (2004)	5	HSS	127x127x8	G40.21-M350W	480	54	0.85	4350	10.6	0.48	1.29	1.61
160		6	HSS	127x127x8	G40.21-M350W	480	50	0.78	4350	10.6	0.50	N/A	N/A
161		7	HSS	127x127x8	G40.21-M350W	480	50	0.78	3050	10.6	0.50	1.51	2.16
162		8	HSS	127x127x13	G40.21-M350W	500	68	1.08	4350	4.2	0.43	1.24	1.75
163		9	HSS	127x127x13	G40.21-M350W	500	52	0.83	4350	4.2	0.45	1.29	1.29
164		10	HSS	127x127x13	G40.21-M350W	500	52	0.83	3450	4.2	0.39	1.86	1.45
165		RHS 2	HSS	254x254x16	ASTM A500 Grade C	397	40	0.57	4293	13.2	0.48	0.97	2.42
166		RHS 4	HSS	254x254x13	ASTM A500 Grade C	397	40	0.57	4360	17.5	0.47	0.90	1.68
167		RHS 10	HSS	254x254x9.5	ASTM A500 Grade C	420	56	0.82	6140	24.7	0.42	0.60	1.13
168		RHS 12	HSS	254x254x9.5	ASTM A500 Grade C	429	40	0.59	4372	24.7	0.41	0.64	1.56
169		RHS 13	HSS	254x254x8	ASTM A500 Grade C	342	40	0.53	4400	30.4	0.36	0.61	1.51
170	Richard (2009)	RHS 14	HSS	254x254x8	ASTM A500 Grade C	342	40	0.53	4840	30.4	0.43	0.55	1.38
171		RHS 19	HSS	152X152X9.5	ASTM A500 Grade C	397	60	0.85	3867	13.2	0.36	0.89	2.98
172		CHS 1	Pipe	273x9.5	ASTM A500 Grade C	317	40	0.51	5618	30.7	0.35	1.12	1.94
173		CHS 2	Pipe	273x9.5	ASTM A500 Grade C	317	60	0.76	7695	30.7	0.23	0.72	1.90
174		W1	W	W360x134	ASTM A992	360	40	0.54	5758	10.3	0.23	0.65	1.61
175		W4	W	W310x97	ASTM A992	377	60	0.83	6746	9.9	0.25	0.61	1.90
176		W6	W	W250x115	ASTM A992	N/R	60	0.79	5981	5.9	0.29	0.78	4.69
177	Goggins et al. (2004)	CylIS1-40H	HSS	40x40x2.5	cold-formed S235JRH	280	34	0.40	1100	13.0	0.57	1.64	3.79
178		CylIS4-20H	HSS	20x20x2.0	cold-formed S235JRH	222	75	0.80	1100	7.0	0.32	1.64	N/A
179		CylIS5-50H	HSS	50x25x2.5	cold-formed S235JRH	223	56	0.60	1100	18.0	0.47	1.71	3.50

Table A.1. Steel brace database (Continued)

ID	Investigator	Specimen ID	Shape	Steel Brace Cross Section	Material Designation	$f_{y,m}$ [Mpa]	kL/r	$\lambda_c$	$L_{brace}$ [mm]	w/t (or D/t)	IDRDS1 [% rad]	IDRDS2 [% rad]	IDRDS3 [% rad]
180	Goggins et al. (2004)	CyLS1-40H	HSS	40x40x2.5	cold-formed S235JRH	343	99	1.30	3300	14.0	0.22	0.81	N/A
181		CyLS2-40H	HSS	40x40x2.5	cold-formed S235JRH	346	98	1.30	3300	14.0	0.24	0.82	N/A
182		CyLS3-40H	HSS	40x40x2.5	cold-formed S235JRH	352	97	1.30	3300	14.0	0.22	0.82	N/A
183		CyLS4-20H	HSS	20x20x2.0	cold-formed S235JRH	471	200	3.09	3300	8.0	N/A	N/A	0.98
184		CyLS5-20H	HSS	20x20x2.0	cold-formed S235JRH	481	192	3.00	3300	8.0	N/A	N/A	0.93
185		CyLS6-20H	HSS	20x20x2.0	cold-formed S235JRH	475	193	3.00	3300	8.0	N/A	N/A	1.03
186		CyLS7-50H	HSS	50x25x2.5	cold-formed S235JRH	298	155	1.90	3300	18.0	0.24	0.79	N/A
187		CyLS8-50H	HSS	50x25x2.5	cold-formed S235JRH	487	134	2.10	3300	18.0	0.13	0.82	N/A
188	CyLS9-50H	HSS	50x25x2.5	cold-formed S235JRH	495	133	2.10	3300	18.0	0.17	0.81	N/A	
189	Elchalakani et al. (2003)	S7A	Pipe	139.7x3.5	AS 1163 grade C350L0 (ASTM 500)	379	29	0.40	2820	39.9	0.66	N/A	6.95
190		S7B	Pipe	139.7x3.5	AS 1163 grade C350L0 (ASTM 500)	379	29	0.40	2820	39.9	0.64	1.18	2.02
191		S7C	Pipe	139.7x3.5	AS 1163 grade C350L0 (ASTM 500)	379	29	0.40	2820	39.9	0.76	1.21	N/A
192	Yang and Mahin (2005)	Specimen 1	HSS	152.4x152.4x9.5	A500 Grade B	414	51	0.74	2108	13.0	0.25	N/A	3.12
193		Specimen 2	HSS	152.4x152.4x9.5	A500 Grade B	414	51	0.74	2108	13.0	0.75	N/A	2.89
194		Specimen 3	HSS	152.4x152.4x9.5	A500 Grade B	414	51	0.74	2108	13.0	0.83	0.97	2.73
195		Specimen 4	HSS	152.4x152.4x9.5	A500 Grade B	414	51	0.74	2108	13.0	0.72	N/A	6.75
196		Specimen 5	HSS	152.4x152.4x9.5	A500 Grade B	414	51	0.74	2108	13.0	0.88	2.42	3.90
197		Specimen 6	HSS	152.4x152.4x9.5	A500 Grade B	414	51	0.74	2108	13.0	N/A	N/A	N/A
198		Specimen 7	HSS	152.4x152.4x9.5	A500 Grade B	414	51	0.74	2108	13.0	N/A	N/A	N/A
199		Specimen 8	HSS	152.4x152.4x9.5	A500 Grade B	414	51	0.74	2108	13.0	N/A	N/A	N/A
200	Specimen 9	HSS	152.4x152.4x9.5	A500 Grade B	414	51	0.74	2108	13.0	N/A	N/A	N/A	
201	Christopoulos et al. (2008)	Specimen 1	Pipe	102x8	ASTM A500 Grade C	521	128	2.08	4293	13.8	0.11	0.85	N/A
202		Specimen 2	Pipe	141x9.5	ASTM A500 Grade C	N/R	141	1.86	6617	16.0	0.29	0.96	N/A
203		Specimen 3	Pipe	168x13	ASTM A500 Grade C	473	111	1.72	6147	14.3	0.37	1.23	N/A
204		Specimen 4	Pipe	219x16	ASTM A500 Grade C	431	85	1.26	6160	14.8	0.49	1.27	N/A

Table A.1. Steel brace database (Continued)

ID	Investigator	Specimen ID	Shape	Steel Brace Cross Section	Material Designation	$f_{y,m}$ [Mpa]	kL/r	$\lambda_c$	$L_{brace}$ [mm]	w/t (or D/t)	IDRDS1 [% rad]	IDRDS2 [% rad]	IDRDS3 [% rad]
205	Christopoulos et al. (2008)	PSD-1	Pipe	168x6.4	ASTM A 500 Grade C	382	42	0.58	2565	26.3	0.29	N/A	N/A
206		PSD-2	Pipe	168x9.5	ASTM A 500 Grade C	434	45	0.67	2565	17.7	0.33	6.12	N/A
207	Wakabayashi et al. (1977)	SIM 1	W	50x50x6x6	Annealed SS 41-Grade	284	39	0.47	985	4.2	0.48	N/A	N/A
208		SIC 1	W	50x50x6x6	Annealed SS 41-Grade	284	40	0.47	985	4.2	0.49	1.02	N/A
209		SIM 2	W	50x50x6x6	Annealed SS 41-Grade	284	79	0.94	1972	4.2	0.16	N/A	N/A
210		SIC 2	W	50x50x6x6	Annealed SS 41-Grade	284	79	0.95	1970	4.2	0.15	1.02	4.52
211		SIM 3	W	50x50x6x6	Annealed SS 41-Grade	252	121	1.37	2970	4.2	0.05	N/A	N/A
212		SIC 3	W	50x50x6x6	Annealed SS 41-Grade	252	121	1.37	2972	4.2	0.12	1.14	N/A
213		SOM1	W	50x50x6x6	Annealed SS 41-Grade	284	39	0.47	990	4.2	0.45	N/A	N/A
214		SOC 1	W	50x50x6x6	Annealed SS 41-Grade	284	40	0.48	989	4.2	0.35	2.03	N/A
215		SOM 2	W	50x50x6x6	Annealed SS 41-Grade	284	79	0.95	1968	4.2	0.19	N/A	N/A
216		SOC 2	W	50x50x6x6	Annealed SS 41-Grade	284	79	0.94	1970	4.2	0.15	1.02	N/A
217		SOM 3	W	50x50x6x6	Annealed SS 41-Grade	252	121	1.37	2968	4.2	0.12	N/A	N/A
218		SOC 3	W	50x50x6x6	Annealed SS 41-Grade	252	121	1.36	2968	4.2	0.18	1.01	N/A
219	Wakabayashi et al. (1977)	DIM 1	W	50x50x6x6	Annealed SS 41-Grade	284	23	0.27	990	4.2	0.41	N/A	N/A
220		DIC 1-D1	W	50x50x6x6	Annealed SS 41-Grade	284	22	0.27	988	4.2	0.99	2.12	6.35
221		DIC 1-D2	W	50x50x6x6	Annealed SS 41-Grade	284	22	0.27	988	4.2	N/A	N/A	N/A
222		DIM 2	W	50x50x6x6	Annealed SS 41-Grade	284	44	0.53	1977	4.2	0.84	N/A	N/A
223		DIC 2-D1	W	50x50x6x6	Annealed SS 41-Grade	284	44	0.53	1979	4.2	0.35	1.04	3.70
224		DIC 2-D2	W	50x50x6x6	Annealed SS 41-Grade	284	44	0.53	1983	4.2	N/A	N/A	N/A
225		DIM 3	W	50x50x6x6	Annealed SS 41-Grade	252	67	0.76	2963	4.2	0.42	N/A	N/A
226		DIC 3-D1	W	50x50x6x6	Annealed SS 41-Grade	252	68	0.77	2968	4.2	0.26	0.94	N/A
227		DIC 3-D2	W	50x50x6x6	Annealed SS 41-Grade	252	68	0.77	2964	4.2	N/A	N/A	N/A
228		DOM 1	W	50x50x6x6	Annealed SS 41-Grade	284	28	0.33	989	4.2	0.80	N/A	N/A
229		DOC 1-D1	W	50x50x6x6	Annealed SS 41-Grade	284	28	0.34	992	4.2	0.54	2.06	N/A
230		DOC 1-D2	W	50x50x6x6	Annealed SS 41-Grade	284	28	0.34	993	4.2	N/A	N/A	N/A

Table A.1. Steel brace database (Continued)

ID	Investigator	Specimen ID	Shape	Steel Brace Cross Section	Material Designation	$f_{cm}$ [Mpa]	$kL/r$	$\lambda_c$	$L_{brace}$ [mm]	w/t (or D/t)	IDRDS1 [% rad]	IDRDS2 [% rad]	IDRDS3 [% rad]
231	Wakabayashi et al. (1977)	DOM 2	W	50x50x6x6	Annealed SS 41-Grade	284	56	0.67	1981	4.2	0.53	N/A	N/A
232		DOC 2-D1	W	50x50x6x6	Annealed SS 41-Grade	284	56	0.67	1978	4.2	0.33	1.01	N/A
233		DOC 2-D2	W	50x50x6x6	Annealed SS 41-Grade	284	56	0.67	1982	4.2	N/A	N/A	N/A
234		DOM 3	W	50x50x6x6	Annealed SS 41-Grade	252	84	0.95	2968	4.2	0.47	N/A	N/A
235		DOC 3-D1	W	50x50x6x6	Annealed SS 41-Grade	252	84	0.95	2973	4.2	0.32	0.98	N/A
236		DOC 3-D1	W	50x50x6x6	Annealed SS 41-Grade	252	84	0.95	2969	4.2	N/A	N/A	N/A
237		SPM 1	Pipe	43x3.48	JIS-STK 41	421	38	0.55	987	12.4	0.99	N/A	N/A
238		SPC 1	Pipe	43x3.47	JIS-STK 41	421	38	0.55	993	12.4	0.32	1.15	N/A
239		SPM 3	Pipe	42.9x3.45	JIS-STK 41	421	109	1.59	2970	12.4	0.10	N/A	N/A
240		SPC 3	Pipe	42.9x3.45	JIS-STK 41	421	109	1.59	2969	12.4	0.16	N/A	1.61
241		DPM 1	Pipe	43x3.47	JIS-STK 41	421	36	0.52	985	12.4	0.76	2.99	N/A
242		DPC 1-1	Pipe	43x3.46	JIS-STK 41	421	36	0.52	983	12.4	0.55	2.03	N/A
243		DPC 1-2	Pipe	43x3.46	JIS-STK 41	421	36	0.52	983	12.4	N/A	N/A	N/A
244		DPM 2	Pipe	42.8x3.49	JIS-STK 41	421	71	1.04	1976	12.3	0.43	N/A	N/A
245		DPM 3-1	Pipe	43x3.48	JIS-STK 41	421	107	1.56	2965	12.4	0.38	N/A	N/A
246		DPM 3-2	Pipe	43x3.48	JIS-STK 41	421	107	1.56	2965	12.4	N/A	N/A	N/A
247	Wakabayashi et al. (1980a)	DPC 3-1	Pipe	43x3.43	JIS-STK 41	421	107	1.56	2968	12.5	0.34	N/A	N/A
248		DPC 3-2	Pipe	43x3.43	JIS-STK 41	421	107	1.56	2968	12.5	N/A	N/A	N/A
249		SAM 1	Angle	49.7x3.88	JIS-SS41	348	42	0.55	998	12.8	0.30	0.85	N/A
250		SAC 1	Angle	50.1x3.91	JIS-SS41	348	42	0.55	995	12.8	0.26	1.31	N/A
251		SAM 3	Angle	49.7x3.77	JIS-SS41	348	106	1.41	2962	13.2	0.12	0.40	N/A
252		SAM 3	Angle	50.1x3.81	JIS-SS41	348	106	1.41	2972	13.2	0.06	1.14	N/A
253		DAM 1-1	Angle	49.9x3.89	JIS-SS41	348	34	0.45	993	12.8	0.78	N/A	N/A
254		DAM 1-2	Angle	49.9x3.89	JIS-SS41	348	34	0.45	993	12.8	N/A	N/A	N/A
255		DAC 1-1	Angle	49.9x3.89	JIS-SS41	348	34	0.45	995	12.8	0.85	2.41	N/A
256		DAC 1-2	Angle	49.9x3.89	JIS-SS41	348	34	0.45	995	12.8	N/A	N/A	N/A

Table A.1. Steel brace database (Continued)

ID	Investigator	Specimen ID	Shape	Steel Brace Cross Section	Material Designation	$f_{y,m}$ [Mpa]	$kL/r$	$\lambda_c$	$L_{brace}$ [mm]	w/t (or D/t)	IDRDS1 [% rad]	IDRDS2 [% rad]	IDRDS3 [% rad]
257		DAM 2-1	Angle	49.9x3.76	JIS-SS41	348	53	0.70	987	13.3	0.32	0.43	N/A
258		DAM 2-2	Angle	49.9x3.76	JIS-SS41	348	53	0.70	987	13.3	N/A	N/A	N/A
259		DAC 2-1	Angle	50x3.8	JIS-SS41	348	53	0.70	1983	13.2	0.30	1.01	2.22
260	Wakabayashi et al. (1980a)	DAC 2-2	Angle	50x3.8	JIS-SS41	348	53	0.70	1983	13.2	N/A	N/A	N/A
261		DAM 3	Angle	50.4x3.89	JIS-SS41	348	83	1.11	2971	13.0	0.25	0.53	2.96
262		DAC 3-1	Angle	50x3.89	JIS-SS41	348	83	1.11	2969	12.9	0.35	0.98	N/A
263		DAC 3-2	Angle	50x3.89	JIS-SS41	348	83	1.11	2969	12.9	N/A	N/A	N/A
264		BFSI	W	50x50x6x6	Hot Rolled JIS SS 41	270	36	0.42	1980	4.2	0.19	1.01	N/A
265		BFSO	W	50x50x6x6	Hot Rolled JIS SS 41	270	36	0.42	1980	4.2	0.20	1.01	N/A
266	Wakabayashi et al. (1980b)	BFDI-D1	W	50x50x6x6	Hot Rolled JIS SS 41	270	36	0.42	1980	4.2	0.39	1.01	N/A
267		BFDI-D2	W	50x50x6x6	Hot Rolled JIS SS 41	270	36	0.42	1980	4.2	N/A	N/A	N/A
268		BEDO	W	50x50x6x6	Hot Rolled JIS SS 41	270	56	0.65	1980	4.2	0.34	1.01	N/A
269		BEDO	W	50x50x6x6	Hot Rolled JIS SS 41	270	56	0.65	1980	4.2	N/A	N/A	N/A
270		US	HSS	HSS152X152x9.5	ASTM A500 Grade B	418	42	0.62	2915	13.0	0.55	2.13	2.38
271	Uriz (2005)	UN	HSS	HSS152X152x9.5	ASTM A500 Grade B	418	42	0.62	2915	13.0	N/A	N/A	N/A
272		LS	HSS	HSS152X152x9.5	ASTM A500 Grade B	418	42	0.62	2915	13.0	0.42	2.34	2.89
273		LN	HSS	HSS152X152x9.5	ASTM A500 Grade B	418	42	0.62	2915	13.0	N/A	N/A	N/A
274		60x60x3x205 0-CS-HR	HSS	60x60x3	Grade S355 J2H	458	44	0.67	2050	17.0	0.65	0.83	1.66
275		40x40x3x205 0-CS-HR	HSS	40x40x3	Grade S355 J2H	478	68	1.05	2050	10.3	0.56	0.98	3.87
276	Nip et al. (2009)	40x40x3x125 0-CS-HR	HSS	40x40x3	Grade S355 J2H	478	41	0.64	1250	10.3	0.58	0.97	2.47
277		60x60x3x205 0-CS-CF	HSS	60x60x3	Grade S235 JRH	361	44	0.59	2050	17.0	0.61	0.88	1.76
278		40x40x4x205 0-CS-CF	HSS	40x40x4	Grade S235 JRH	410	69	1.00	2050	9.3	0.43	0.87	N/A
279		40x40x3x205 0-CS-CF	HSS	40x40x3	Grade S235 JRH	451	68	1.02	2050	10.3	0.46	1.16	N/A

Table A.1. Steel brace database (Continued)

ID	Investigator	Specimen ID	Shape	Steel Brace Cross Section	Material Designation	$f_{cm}$ [Mpa]	$kL/r$	$\lambda_c$	$L_{brace}$ [mm]	w/t (or D/t)	IDRDS1 [% rad]	IDRDS2 [% rad]	IDRDS3 [% rad]	
280	Nip et al. (2009)	40x40x3x125 0-CS-CF	HSS	40x40x3	Grade S235 JRH	451	41	0.62	1250	10.3	0.75	1.16	2.30	
281		60x60x3x285 0-SS-CF	HSS	60x60x3	Grade EN 1.4301	483	61	0.96	2850	17.0	0.52	1.03	1.73	
282		50x50x3x285 0-SS-CF	HSS	50x50x3	Grade EN 1.4301	552	74	1.24	2850	13.7	0.55	1.14	3.35	
283		60x40x3x285 0-SS-CF	HSS	60x40x3	Grade EN 1.4301	538	89	1.48	2850	17.0	0.59	1.20	N/A	
284		60x60x3x205 0-SS-CF	HSS	60x60x3	Grade EN 1.4301	483	44	0.69	2050	17.0	0.72	1.04	2.06	
285		50x50x3x205 0-SS-CF	HSS	50x50x3	Grade EN 1.4301	552	53	0.89	2050	13.7	0.80	1.16	2.31	
286		60x40x3x205 0-SS-CF	HSS	60x40x3	Grade EN 1.4301	538	64	1.06	2050	17.0	0.61	1.19	2.18	
287		60x60x3x125 0-SS-CF	HSS	60x60x3	Grade EN 1.4301	483	27	0.42	1250	17.0	0.85	1.05	2.07	
288		50x50x3x125 0-SS-CF	HSS	50x50x3	Grade EN 1.4301	552	33	0.45	1250	13.7	1.19	2.08	1.60	
289		60x40x3x125 0-SS-CF	HSS	60x40x3	Grade EN 1.4301	538	39	0.65	1250	17.0	0.89	2.00	1.95	
290		Leowardi and Walpole (1996)	W1	W	150 UC 30	AS3679.1-300	311	80	1.00	2416	8.1	0.64	1.20	7.30
291			W2	W	150 UC 30	AS3679.1-300	311	60	0.75	1652	8.1	0.32	2.12	6.82
292			W3	W	150 UC 30	AS3679.1-300	311	40	0.50	3056	8.1	0.31	1.05	5.17
293		Walpole (1996)	T1	HSS	N/R	N/R	449	80	1.21	2064	N/R	0.47	1.10	2.92
294	T2		HSS	N/R	N/R	449	60	0.90	1388	N/R	0.69	1.15	2.95	
295	T3		HSS	N/R	N/R	449	40	0.60	2704	N/R	0.54	1.11	1.48	
296	Lai (2012)	B1-W1	HSS	152.4x152.4x9.5	ASTM A500 Grade B	320	47	0.60	2743	14.2	0.74	1.67	2.22	
297		B1-E1	HSS	152.4x152.4x9.5	ASTM A500 Grade B	320	47	0.60	2743	14.2	0.93	1.85	2.96	
298		B1-W2	HSS	127x127x8.0	ASTM A500 Grade B	386	51	0.71	2469	14.2	0.41	1.64	2.06	
299		B1-E2	HSS	127x127x8.0	ASTM A500 Grade B	386	51	0.71	2469	14.2	0.41	1.64	2.06	
300		B2-W1	Pipe	152.4x12.7	ASTM A500 Grade B	470	55	0.85	2743	12.9	0.56	1.11	2.41	
301	B2-E1	Pipe	152.4x12.7	ASTM A500 Grade B	470	55	0.85	2743	12.9	0.37	1.85	2.77		

Table A.1. Steel brace database (Continued)

ID	Investigator	Specimen ID	Shape	Steel Brace Cross Section	Material Designation	$f_{y,m}$ [Mpa]	kL/r	$\lambda_c$	$L_{brace}$ [mm]	w/t (or D/t)	IDRDS1 [% rad]	IDRDS2 [% rad]	IDRDS3 [% rad]
302	Lai (2012)	B2-W2	Pipe	127x12.7	ASTM A500 Grade B	454	60	0.91	2469	10.8	0.51	1.22	N/A
303		B2-E2	Pipe	127x12.7	ASTM A500 Grade B	454	60	0.91	2469	10.8	0.51	1.64	N/A
304		B3-W1	W	W200x42	ASTM A992	372	67	0.92	2743	7.0	0.37	1.30	3.52
305		B3-E1	W	W200x42	ASTM A992	372	67	0.92	2743	7.0	0.50	1.40	N/A
306		B3-W2	W	W200x31	ASTM A992	373	77	1.06	2469	7.0	0.50	1.33	N/A
307		B3-E2	W	W200x31	ASTM A992	373	77	1.06	2469	7.0	0.50	1.74	N/A
308		B4-W1	HSS	152.4x152.4x9.5	ASTM A500 Grade B	405	47	0.67	2743	14.2	0.56	1.20	2.22
309		B4-E1	HSS	152.4x152.4x9.5	ASTM A500 Grade B	405	47	0.67	2743	14.2	0.74	2.22	1.48
310		B4-W2	HSS	127x127x8.0	ASTM A500 Grade B	427	51	0.75	2469	14.2	0.62	2.12	2.47
311		B4-E2	HSS	127x127x8.0	ASTM A500 Grade B	427	51	0.75	2469	14.2	0.62	1.34	2.47
312	Lumpkin (2009)	WF1	W	175x175x7.5x11	ASTM A36	335	79	1.03	3470	7.1	0.39	1.99	3.45
313		WF2	W	175x175x7.5x11	ASTM A36	335	83	1.08	3612	7.1	0.38	2.12	3.50
314	Clark (2009)	W1	W	175x175x7.5x11	ASTM A992	345	74	0.98	3222	7.1	0.43	2.13	2.98
315		W2	W	175x175x7.5x11	ASTM A992	345	74	0.98	3222	7.1	0.42	2.13	2.99
316		W3	W	175x175x7.5x11	ASTM A992	345	72	0.95	3146	7.1	0.43	2.13	3.42
317		W4	W	175x175x7.5x11	ASTM A992	345	72	0.95	3146	7.1	0.43	2.13	3.42